UNIVERSITÀ DEGLI STUDI DI PALERMO
Scienze Molecolari e Biomolecolari
Dipartimento di Scienze e Tecnologie Biologiche Chimiche e Farmaceutiche (STEBICEF)
Settore Scientifico Disciplinare - SSD:CHIM/08

Synthesis and biological evaluation of new 1,2,4-oxadiazole derivatives of Topsentin

IL DOTTORE
Dott.ssa DANIELA CARBONE

IL COORDINATORE
Chiar.ma Prof.ssa PATRIZIA DIANA

IL TUTOR
Chiar.ma Prof.ssa PATRIZIA DIANA

IL CO TUTOR
Preg.ma Dott.ssa BARBARA PARRINO

CICLO XXXI
ANNO CONSEGUIMENTO TITOLO 2019

INDEX

1. INTRODUCTION **1**

1.1. Bioactive marine natural products: an overview 1

1.2. Marine Alkaloids as antitumor and antibacterial agents 3

1.2.1 Pyridoacridine Alkaloids 3

1.2.2 Pyrrole Alkaloids 10

1.2.3 Pyridine Alkaloids 16

1.2.4 Isoquinoline Alkaloids 18

1.2.5 Guanidine Alkaloids 19

1.2.6 Aminoimidazole Alkaloids 20

1.2.7 Macrocyclic Alkaloids 21

1.2.8 Steroidal Alkaloids 22

1.2.9 Indole Alkaloids 26

2. AIM OF THE STUDY **37**

3. CHEMISTRY SECTION **38**

4. BIOLOGY SECTION **53**

4.1 Anti-biofilm activity 53

4.2 Anti-proliferative activity 56

4.3 Effect on cell apoptosis 70

4.4 Effect on cell cycle 74

4.5 Anti-migration activity 75

4.6 Gene expression profiling of epithelial-mesenchymal transition by real-time PCR 84

5. EXPERIMENTAL SECTION **91**

5.1. Chemistry 91

5.2. Biology 136

5.2.1 Inhibition of biofilm formation assay 136

5.2.2 Viability assay *in vitro* 137

5.2.3 Cell apoptosis analysis 138

5.2.4 Cell cycle analysis 138

5.2.5 Wound healing assay 139

5.2.6 Gene expression analysis 139

6. REFERENCES **141**

7. SUPPORTING INFORMATION **153**

7.1 Representative cell apoptosis spectra 153
7.2 Cell cycle spectra 162

1. INTRODUCTION

1.1 Bioactive marine natural products: an overview

During the past decades, the technological progress made possible the extension of research to marine organisms, leading to the isolation of different substances that often exhibit such unusual and complex molecular architectures, never identified in terrestrial organisms, to suggest the existence of a distinguished "Chemistry of the Sea".

It is known that most of the microorganisms have produced very different classes of chemicals, through distant biosynthetic pathways, and that such strong chemical variations seem to be related to the their natural environment rather than to the microorganisms themselves.[1]

So far, more compounds have been isolated or extracted from marine organisms, such as molluscs (2%), algae (9%), echinoderms (6%), tunicates (6%), bryozoans (1%), sponges (37%), coelenterates (21%) and microorganisms, including bacteria, microalgae and fungi (18%) (Figure 1).[2,3]

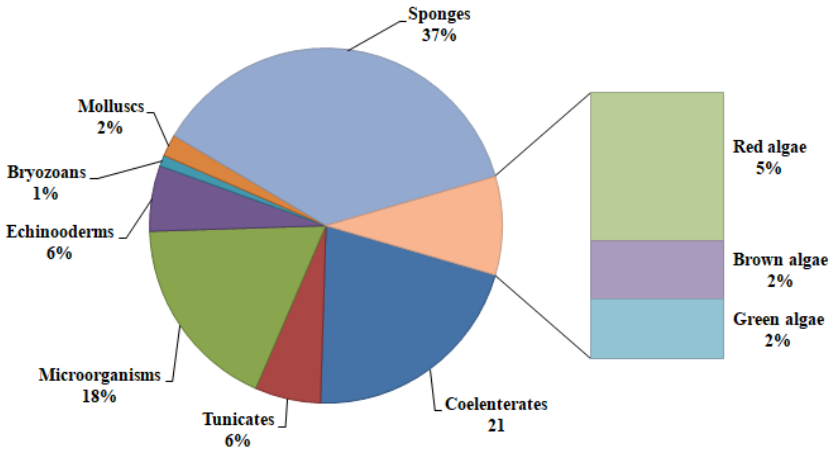

Figure 1. Distribution of marine natural products

In the last 50 years, 9220 papers have reported the isolation of 24662 new compounds from marine organisms.[4] These numerous bioactive compounds have been described as indole alkaloids,[5,6] polycyclic diamine alkaloids,[7] steroid dimers,[8] manzamines,[9,10] long-chain polyols and polyethers from symbiotic marine algae,[11] b-carboline alkaloids,[12] peptides,[13] diterpenoids,[14] sesquiterpenoids,[15] sesterterpenoids,[16] spongiane diterpenoids,[17] furanosesterterpenoids,[18] and macrolide haterumalides and biselides[19].

Thus, marine ecosystems are considered a plentiful resource in terms of bioactive substances, secondary metabolites with potential clinical applications, which are an inexhaustible source of compounds usable as a lead for the synthesis of new molecules of pharmaceutical interest.

As far as their pharmacology applications, marine bioactive compounds have been used mainly because of their antiviral, anticancer, antibacterial, antifungal, anti-inflammatory activities (Figure 2).[20]

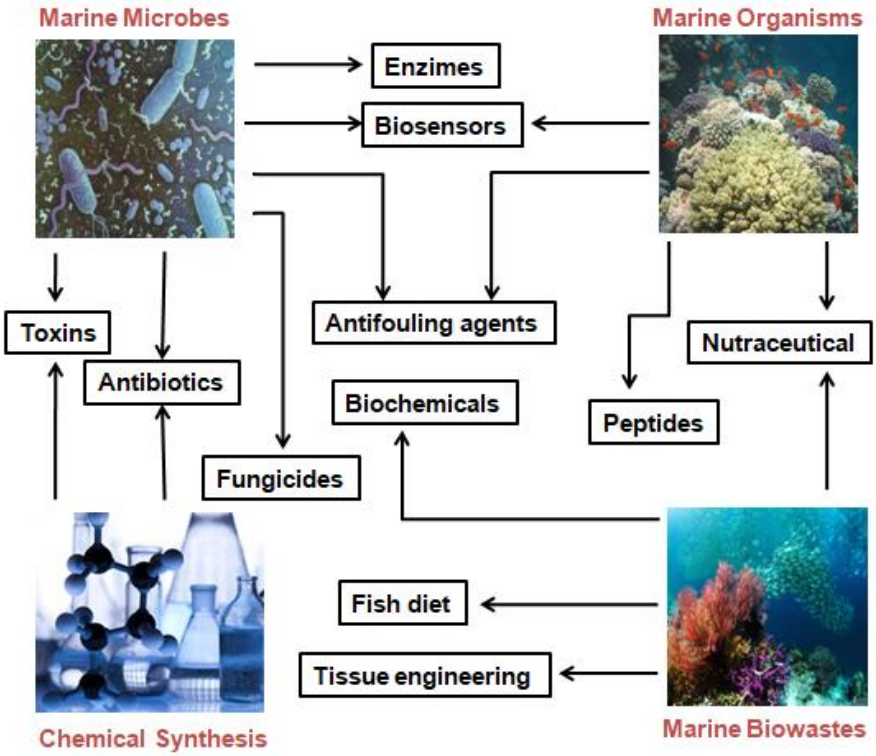

Figure 2. Marine drugs biological activities

It was hypothesized that the activities found by these secondary metabolites, produced by marine sponges, or organisms without armor and therefore without mechanical defense against external enemies, are the result of an evolutionary process during which these species develop a very sophisticated series of biochemical mechanisms, suitable for the protection of the species, as defense strategies against predation and the proliferation of competitive species.[21–25]

Thanks to this chemical barrier capacity, they are able to defend themselves against the attacks of viruses, bacteria and fungi, offering us a wide range of possible anti-pathogens.[26]

Marine organisms have developed specialized features and they have produced characteristic secondary metabolites that are often without parallel in their terrestrial counterparts.[27] This is partly due to the difference in the chemical-physical nature of the two environments. Higher pressures, lower temperatures, lack of light, under low levels of oxygen, high ionic concentrations present in the sea and restricted vital spaces that make microorganisms very competitive and complex, can explain the biosynthesis of highly functionalized and unusual molecules originating from marine organisms, that are essential for survival.[28]

Among these marine organisms, marine sponges have been considered as a drug treasure house concerning the great biological activities of their secondary metabolites. Despite only 243 new compounds were discovered in 2013, a noteworthy decrease compared to previous years (19% and 33% less than in 2011 and 2012, respectively), and although few sponge-derived products are approved as drugs, sponges remain the dominant phylum for the discovery of a huge number of new compounds with interesting pharmacological activities.[4,29] Several marine-derived bioactives from marine sponges are already in various stages of clinical development as agents against cancer, microbial infections, viral infections, cardiovascular disorders, inflammation and other diseases. However, in the case of marine organisms drug development is severely thwarted by the limited availability of the respective secondary metabolites, as they are often present only in slight amounts in the spongy tissue. In spite of these difficulties, the abundance of synthetic compounds with similar chemical functional groups and, therefore, limited chemical diversity, has renewed interest in nature as an unfailing source of compounds that can be used as leads for the synthesis of new molecules of pharmaceutical interest. So far, the approach to new drugs through natural products has proved to be one of the most successful strategies for the discovery of new drugs.[30,31]

1.2 Marine Alkaloids as antitumor and antibacterial agents

Marine alkaloids, including pyridoacridine, pyrrole, pyridine, isoquinoline, guanidine, aminoimidazole, macrocyclic, steroidal and indole alkaloids, are a class of marine sponge natural products that show unique promise in the development of new drug leads. In the past few years, some of the isolated marine alkaloids and their derivatives have been synthesized and evaluated for their biological activity, in order to find new lead compounds against cancer and microbial infections.

1.2.1 Pyridoacridine Alkaloids

The chemical structure of pyridoacridine alkaloids **1** is characterized by a polycyclic planar heteroaromatic 11*H*-pyrido[4,3,2,*mn*]acridine system, that allows it to assume a characteristic intense colour. [32] The members of pyridoacridine alkaloid family differ by chemical compositions and conformations, that including different side chains, rings fused to ring C or to acridine nitrogen, bromination at C2 in ring A (rarely) and varied oxidation states (ring D can be partially saturated).[33]

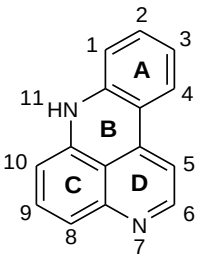

1

Pyridoacridine alkaloids showed cytotoxic activity toward cultures of murine leukemia cells (P388) and inhibitory activity against topoisomerase II, at micromolar level. The cytotoxic activity of this class of compounds is probably due to a highly electron-deficient planar aromatic system that can intercalate DNA, to a topoisomerase II inhibition and to a production of reactive oxygen species, leading to inhibition of cell growth.[34–36] In addition, they reported fungicidal and bactericidal properties,[37–39] inhibition of anti HIV,[40] sarcoplasmic reticulum Ca^{+2} releasing activity and induction of neuronal differentiation.[41,42]

On the basis of their structural variability, pyridoacridines are divided into five main groups namely, tetracyclic (four rings), pentacyclic (five rings), hexacyclic (six rings), heptacyclic (seven rings), and octacyclic (eight rings) alkaloids.

The first pyridoacridine alkaloids isolated from a marine sponge and therefore the first tetracyclic member of this class are cystodytins A-C (**2-4**). The isolation and the following characterization of these compounds have been reported by Kobayashi in 1988.[43] Three years later, in 1991, the same research group reported the isolation of six other novel tetracyclic alkaloids of cystodytin family, cystodytins D-I (**5-10**).[39] The common heterocyclic nucleus of this class of compounds is an iminoquinone substituted at C10 with a 2-amidoethyl (**2-6**) or an O-methyl ether (**7-8**) or O-9-octadecenoate ester (**9-10**) side chain.

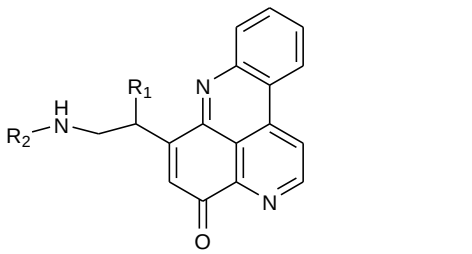

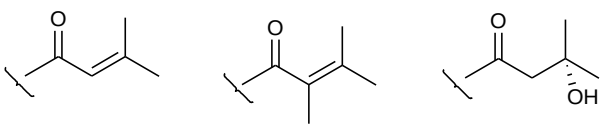

X Y Z

Cystodytin A, 2, R_2 = X, R_1= H
Cystodytin B, 3, R_2 = Y, R_1= H
Cystodytin C, 4, R_2 = Z, R_1=H
Cystodytin D, 5, R_2 = X, R_1=OH
Cystodytin E, 6, R_2 = Y, R_1=OH
Cystodytin F, 7, R_2 = X, R_1=OCH_3
Cystodytin G, 8, R_2 = Y, R_1=OCH_3
Cystodytin H, 9, R_2 = X,
R_1= $OCO(CH_2)_7CH=CH(CH_2)_7CH_3$
Cystodytin I, 10, R_2 = Y,
R_1= $OCO(CH_2)_7CH=CH(CH_2)_7CH_3$

The cystodytins **2**, **3** and **4** showed potent antiproliferative activity against L-1210 lymphoma cells, reporting IC_{50} values of 0.22, 0.22 and 0.24 µg/mL, respectively. Comparable antiproliferative activity was found for cystodytins D-I (**6-11**) against murine L-1210 lymphoma cells, with IC_{50} values of 1.1 (**5** and **6**), 0.068 (**7** and **8**) and 0.080 (**9** and **10**) µg/mL. Furthermore, the cystodytins D-I displayed inhibitory activity *in vitro* against human epidermoid carcinoma KB cells, with IC_{50} values of 1.4 (**5** and **6**), 0.078 (**7** and **8**) and 0.092 (**9** and **10**) µg/mL.[39]

In 1994, a new pyridoacridine alkaloid, cystodytin J (**11**), in addition to the known compounds cystodytin A-I **2-10**, was isolated from the ascidian *Fijian Cystodytes sp.*. It was reported that this compound showed *in vitro* dose-dependent inhibition of proliferation in human colon cancer (HCT) and xrs-6 cells, reporting IC_{50} value of 1.6 and 135.6 µM, respectively. On the basis of the observed topoisomerase II dose- dependent inhibition (IC_{90} value of 8.4 µM), it was hypothesized that the cystodyn J brought about cell death by interfering with nucleic acid structure and function.[44]

In 2002, Appleton *et al*. reported the isolation of cystodytin K **12**, a 12-methoxy derivative of cystodytin J **11**, from the extract of the ascidian *Lissoclinum notti*. Cystodytin K **12** exhibited cytotoxic activity against P-388 murine leukemia cell line with IC_{50} value of 1.3 µM and microbial inhibition against *B. subtilise* at concentration of 120 µg/ml.[45]

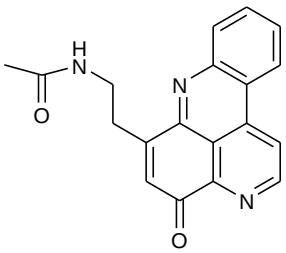

Cystodytin J
11

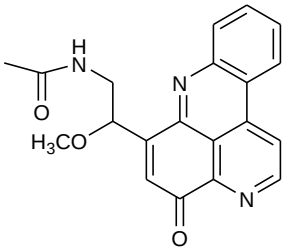

Cystodytin K
12

In 1989, a new tetracyclic alkaloid, diplamine **13,** was isolated from the tunicate *Diplosoma sp*. and was found to be cytotoxic towards L-1210 murine leukemia cells, reporting IC_{50} value of 0.02 µg/mL and also revealed antimicrobial activity against *E. coli* and *S. aureas*. The diplamine **13**, which has the same polycyclic planar heteroaromatic system as the cystodytins, showed citotoxic activity of an order of magnitude more than the cystodytins, indicating that the thio-methyl in C-9 plays an important role in cytotoxicity.[46]

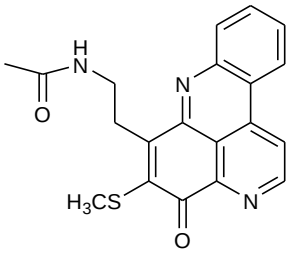

Diplamine
13

Recently, two other tetracyclic alkaloids, isodiplamine **14** and lissoclinidine 1**5**, along with known diplamine **13**, were isolated from an ascidian *Lissoclinum notti*. In order to evaluate their cytotoxic activity, all compounds were tested against murine leukaemia (P-388), human colon tumour (HCT-116) and non-malignant African Green Monkey kidney (BSC-1) cell lines. Diplamine **13** was found to be the most active compound among the three, proving that movement of the thiomethyl group from C-9 (diplamine) to C-5 (isodiplamine) or the cyclization of the thiomethyl group into a benzoxathiole ring (lissoclinidine) decreases cytotoxicity against all the cells.[45]

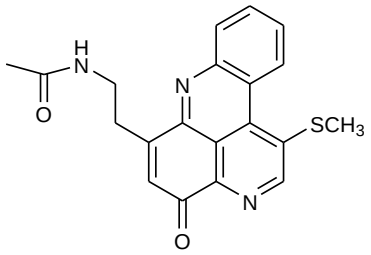

Isodiplamine
14

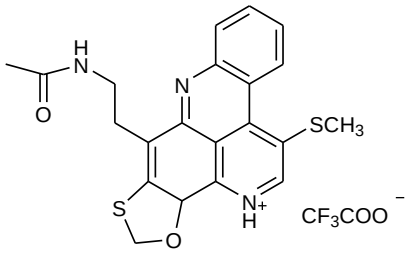

Lissoclinidine
15

In 1988, a first novel pentacyclic alkaloid with significant biological activity, ascididemin **16** was isolated from brown colored tunicate *Didemnum sp.* The structure of the compound was elucidated on the basis of spectroscopic data. Ascididemin **16** exhibited selective cytotoxic activity against L-1210 murine leukemia cells *in vitro*, with IC_{50} value of 0.39 µg/mL, and sarcoplasmic reticulum Ca-releasing activity, more than caffeine, a well-known Ca^{+} releaser.[47] It was also tested *in vitro* at six different concentrations against 12 different human cancer cell lines, including glioblastomas, breast, colon, lung, prostate and bladder cancers. Ascididemin **16** exhibited significant cytotoxic activity, with IC_{50} values ranging from 0.008 µM to 0.9 µM.[48]

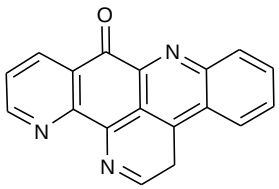

Ascididemin
16

Cystodamine **17** was isolated from a mediterranean ascidian *Cystodytes dellechiajei*. The skeletal structure, determined by spectroscopic analysis, contains a phenanthroline portion fused with a 7-aminopyridine unit. Cystodamine **17** showed cytotoxic activity against CEM human leukemic lymphoblast, with IC_{50} value of 1.0 µg/mL.[49]

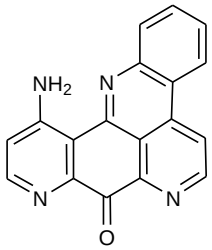

Cystodamine
17

From 1988 to 1994, it was reported the isolation of three new pentacyclic alkaloid, shermilamine A **18**, shermilamine B **19** and shermilamine C **20**. Shermilamine A **18** contains a pentacyclic pyridoacridine thiazinone system; while, shermilamine B **19** is a debromo analogues of shermilamine A **18**.[44,50–52]

In 1998, two other novel shermilamine alkaloids, shermilamines D **21** and E **22** were isolated from the Indian Ocean tunicate *Cystodytes violatinctus*. Among all shermilamine alkaloids, only compound **21** exhibited cytotoxicity against P-388, A-549, HT-29 and MEL-28 cancer cell lines, reporting IC_{50} values of 0.53, 0.27, 2.66 and 0.53 µM, respectively.[53,54]

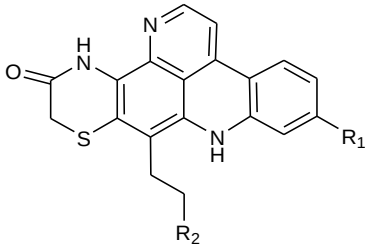

Shermilamine A, 18, R_1 = Br, R_2 = $NHCOCH_3$
Shermilamine B, 19, R_1 = H, R_2 = $NHCOCH_3$
Shermilamine C, 20, R_1 = H, R_2 = $NHCOCH=C(CH_3)_2$

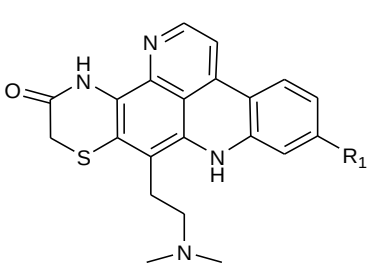

Shermilamine D
21

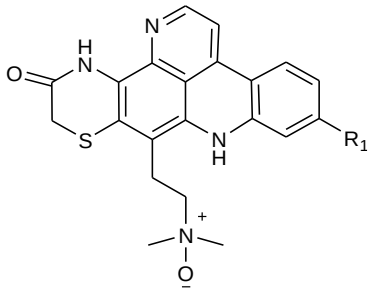

Shermilamine E
22

Davis *et al*. isolated two other new pyridoacridine pentacyclic alkaloids, ecionines A **23** and B **24** from Australian sponge *Ecionemia geodides*, characterized by an imine moiety, that is very rarely found in pyridoacridine class. Both compounds were tested against a panel of human bladder cancer cell lines (TSU-Pr1, TSU-Pr1-B1 and TSU-Pr1-B2) and the superficial bladder cancer cell line 5637. The ecionine A **23** displayed weak cytotoxic effects against all the human bladder cancer cell lines, with IC_{50} values ranging from 3.55 μM to 6.49 μM. On the other hand, the ecionine B **24** showed cytotoxic effect only against the 5637 and TSU-Pr1-B2 cells at 10 μM, reporting cell growth inhibitions of 54% and 51% cells, respectively.[55]

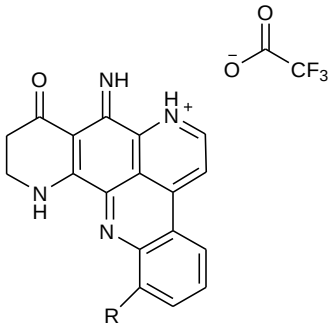

Ecionine A, 23, R =H
Ecionine B, 24, R =OH

So far, the only two pyridoacridine hexacyclic alkaloids, isolated from deep water marine sponges, are cyclodercitin **25** and stellettamine **26**. The sixth ring in cyclodercitin **25** is formally derived by cyclization of the 2-aminoethyl side chain to the acridine nitrogen. The pyridine ring of cyclodercitin **25** is substituted with an N-methyl group, in contrast to unsubstituted pyridine ring of stellettamine **26**. Cyclodercitin **25** showed *in vitro* anti-proliferation activity against P-388 murine leukemia cells, with IC_{50} value of 1.9 μM.[56,57]

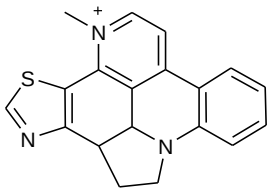

Cyclodercitin
25

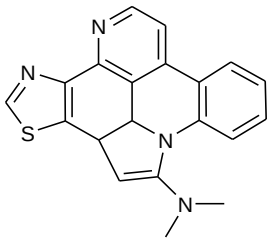

Stellettamine
26

Eilatin **27**, extracted from the Red Sea tunicate *Eudistoma sp*., is the only known heptacyclic pyridoacridine alkaloid of the marine origin. The chemical structure of eilatin has been determined by spectroscopic analysis. The ^{1}H NMR spectrum showed only six aromatic protons that can be associated with the common six protons of the benzodiazaphenanthroline system. While, the ^{13}C NMR spectrum exhibited only 12 carbon lines (six protonated and six unprotonated). Eilatin **27** was found to exhibit antiproliferative activity against HCT human colon cancer cell line with IC_{50} value of 5.3 μM and anti-viral activity against *Human Immunodeficiency Virus* (HIV).[40,50]

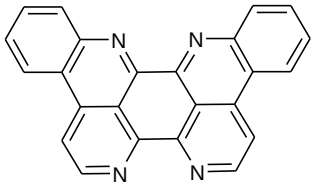

Eilatin
27

Recently, an octacyclic analogue of eilatin **28** was synthesized by Demeunynck *et al.* The antitumor activity of this compound was evaluated against two cancer cell lines, HT-29 (human colon adenocarcinoma) and A-431 (human epithelial carcinoma). At concentration of 5 μM, the compound **28** reduced the A-431 cell proliferation by 25%, but did not show any activity against HT-29 cell line.[58]

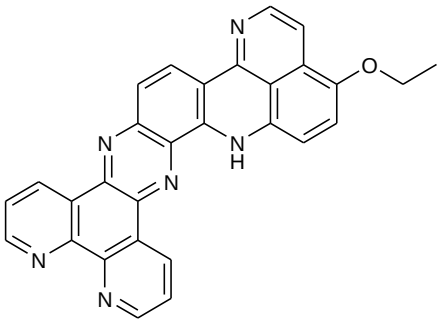

28

1.2.2 Pyrrole Alkaloids

In 1991, the first two pyridine alkaloids were isolated from the marine sponge *Axinella cylindratus* by Kuramoto *et al.*. Cylindradines A **29** and B **30** showed *in vitro* slight cytotoxicity against P-388 murine leukemia cell line, with IC_{50} values of 7.9 and 33 μg/mL, respectively.[59]

Two years later, a novel alkaloid, agelastatin A **31**, isolated from the deep water marine sponge *Agelas dendromorpha,* exhibited significant activity *in vitro* against L-1210 and KB tumor cells, reporting IC_{50} values in the micromolar range (0.033- 0.469 μM). The structure activity relationship (SAR) studies of agelastatin A **31** revealed that the hydroxyl group in C8a and both NH in position 5 and 6 are needed for the biological activity.[60–62]

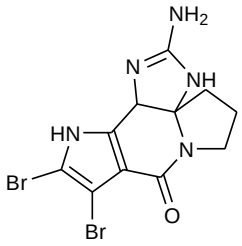

Cylindradines A
29

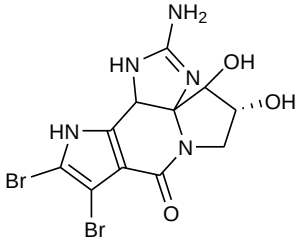

Cylindradines B
30

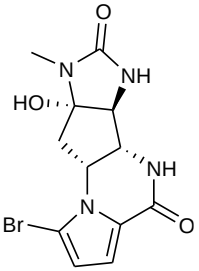

Agelastatin A
31

In the same year, a new pyrrole alkaloid, called clathrodin **32** and isolated from the Caribbean sea sponge *Agelas clathrodes*, reported noteworthy cytotoxic activity against CHO-K1 ovaric ephitelial cells with ED_{50} value of 1.33 μg/mL and potent blocking activity against cholinergic receptors, isolated from frog skeletal muscle, at concentrations of 10^{-7}-10^{-3} M.[63] The tetracyclic pyrrole-imidazole alkaloid, dibromophakellstatin **33**, isolated from the marine sponge *Phakellia mauritiana*, displayed inhibitory activity against a panel of human cancer cell lines: ovary (OVCAR-3), brain (SF-295), kidney (A-498), lung (H-460), colon (KM20L2) and melanoma (SK-MEL-5) with ED_{50} values ranging from 0.11 to 1.5, μg/mL.[64]

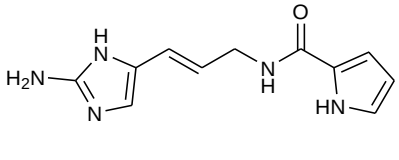

Clathrodin
32

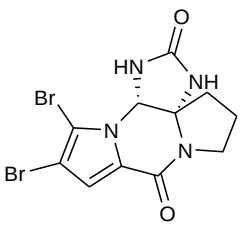

Dibromophakellstatin
33

In 2001, three new pyrrole alkaloids, 3-bromomaleimide **34**, 3,4-dibromomaleimide **35** and 12-chloro-11-hydroxydibromoisophakellin **36** were isolated from the marine sponge *Axinella brevistyla*. All compound showed antifungal activity against the Saccharomyces cerevisiae at <1.0, 30, and 100 µg/disk, respectively, and reported antitumor activity against L1210 cells with IC_{50} values of 1.1, 0.66, and 2.5 µg/mL, respectively.[65]

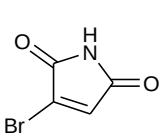

3-Bromomaleimide
34

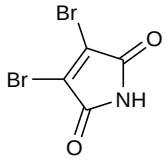

3,4-Dibromomaleimide
35

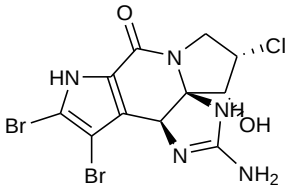

12-Chloro-11-hydroxydibromoisophakellin
36

A new dipyrroloquinone, zyzzyanone A **37**, isolated from the Australian marine sponge *Zyzzya fuliginosa*, showed a mild inhibitory affect against Ehrlich carcinoma cells, with IC_{50} value of 25 µg/mL.[66] One year later, Zyzzyanones B-D (**38-40**), three related dipyrroloquinones, were characterized. As the Zyzzyanone A **37**, Zyzzyanones B-D (**38-40**), pronounced weak cytotoxicity against Ehrlich carcinoma cells with IC_{50} value of 25 µg/mL.[67]

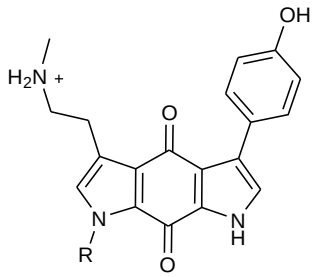

Zyzzyanone A, 37, R = CH_3
Zyzzyanone B, 38, R = H

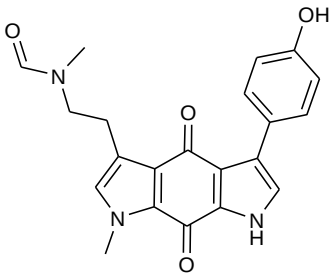

Zyzzyanone C, 39, R = CH_3
Zyzzyanone D, 40, R = H

In 1986, a pyrroloquinoline alkaloid, discorhabdin C **41**, was extracted from red-brown sponge *Latrunculia du*. The skeletal structure of this compound contains a new tetracyclic iminoquinone chromophore with a spiro 2,6- dibromocyclohexadienone.[68]

Two years later, Perry *et al.* isolated other two pyrroloquinoline alkaloid, discorhabdins A **42** and B **43**, from the three species of *Latrunculia* sponge. Discorhabdins A **42**, B **43** and C **41** showed *in vitro*, but not *in vivo*, cytotoxicity against P-388 assays with ED_{50} values of 0.05, 0.1 and 0.03 µg/mL, respectively. The discorhabdins also exhibited antimicrobial and antiviral activity. Discorhabdins C **41** and A **42** reported activity against *Escherichia coli*, *Bacillus subiilis* and

Candida albicans, but not against *Pseudomonas aeruginosa*. While, discorhabdin B **43** was active against *Escherichia coli* and *Bacillus subiilis* but not against *Candida albicans* and *Pseudomonas aeruginosa.*[69]

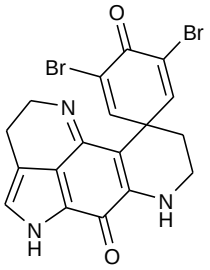

Discorhabdin C
41

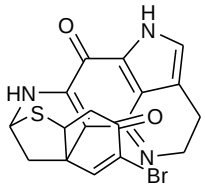

Discorhabdin A
42

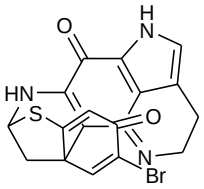

Discorhabdin B
43

In the following years, three other members of discorhabdin family, discorhabdin D **44**, discorhabdins L **45** and I **46** were isolated from *Latrunculia brevis*. Discorhabdin D **44** reported, *in vitro* e *in vivo*, IC_{50} value of 6 µg/mL against P-388 cells. Discorhabdins L **45** and I **46** were tested against a broad panel of 14 tumor cell lines, including prostate (DU-145 and LN-caP), ovary (SK-OV-3, IGROV and IGROV-ET), breast (SK-BR3), melanoma (SK-MEL-28), endothelium (HMEC1), NSCL (A549), leukemia (K562), pancreas (PANC-1) and colon (HT29, LOVO and LOVO-DOX). The HT-29 colon cell line resulted the most sensitive cell line, against which the compounds **45** and **46** reported GI_{50} values of 0.12 and 0.35 µM, respectively.[70]

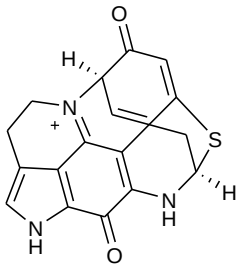

Discorhabdin D
44

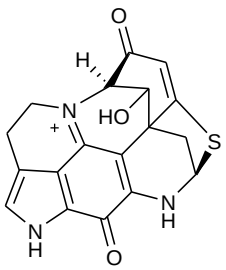

Discorhabdin L
45

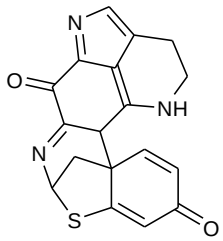

Discorhabdin I
46

In 2005, Lang et *al.* isolated a novel symmetrical alkaloid of discorhabdin family, discorhabdin W **47** from a marine sponge *Latrunculia sp*. The skeletal structure of this compound contains a disulfide link between two discorhabdin units. Discorhabdin W **47** presented *in vitro* potent cytotoxic activity against P-388 cells, reporting IC_{50} value of 0.09 µg/mL.[71]

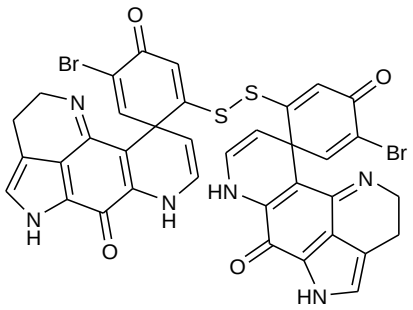

Discorhabdin W
47

Sun *et al.* reported the isolation of three highly functionalized pyrroloquinoline alkaloids, isobatzellines A-D **48-51,** from the sponge *Batzella sp*. Isobatzellines A-D **48-51**, having a pyrrolo[4,3,2-de]quinoline ring system fused with an aminoiminoquinone moiety, were found to exhibit *in vitro* cytotoxicity against P-388 leukemia cell line and moderate antifungal activity against *Candida albicans*. Isobatzellines A, B, C and D reported IC_{50} values against P388 leukemia cells of 0.42, 2.6, 12.6 , 20 μg/mL, respectively; while, against *Candida albicans,* they reported MIC values of 3.1, 25, 50, 25 μg/mL, respectively.[72]

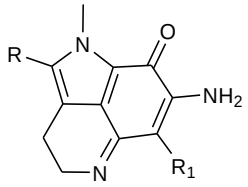

Isobatzelline A, 48, R=SCH_3, R_1=Cl
Isobatzelline B, 49, R=SCH_3, R_1=H
Isobatzelline C, 50, R=H, R_1=Cl
Isobatzelline D, 51, R=H, R_1=H

Radisky *et al.* reported the isolation and the characterization of six novel pyrroloiminoquinone alkaloids, the makaluvamines A-F **52-57** from the Fijian sponge *Zyzzya cf. marsailis*. The makaluvamines A-F **52-57** showed *in vitro* potent cytotoxicity against the human colon tumor cell line HCT-116 (IC_{50} values ranging from 0.17 to 36.2 μM), topoisomerase II sensitive CHO cell line xrs-6 (IC_{50} values ranging from 0.08 to 13.49 μM), and also inhibited the catalytic activity of topoisomerase II. Several *in vivo* studies showed that, against P388 murine leukemia, makaluvamines A **52** and C **54** exhibited only marginal cytotoxicity, while against the human ovarian tumor Ovcar 3 implanted in athymic mice, makaluvamines A **52** and C **54** showed substantial decrease in tumor mass. The antitumor activity of these compounds has been thought to be due a DNA double-stranded breakage, an activity characteristic of topoisomerase II inhibitors.[73]

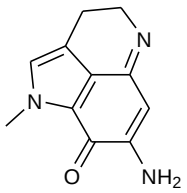

Makaluvamine A
52

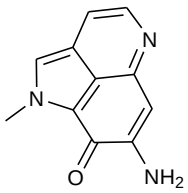

Makaluvamine B
53

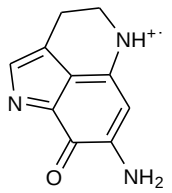

Makaluvamine C
54

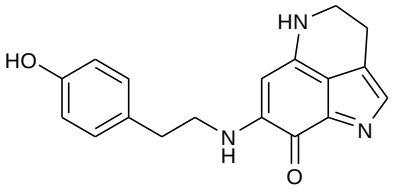

Makaluvamine D
55

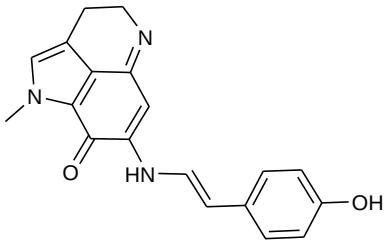

Makaluvamine E
56

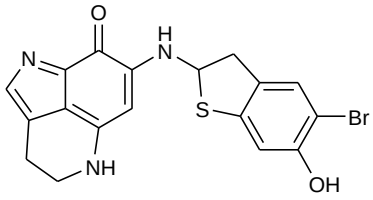

Makaluvamine F
57

In the same year, makaluvamine G **58**, having a discorhabdin-like structure with two additional *N*-methyl groups, was isolated from a sponge of the genus *Histodcnnella*. As other pyrroloiminoquinone-containing compounds, makaluvamine G **58** was found to be cytotoxic against several tumor cell lines, reporting an IC_{50} value of 0.50 µg/mL against P-388 (murine leukemia), A-549 (human non small cell lung cancer), HT-29 (human colon cancer) and MCF-7 (human breast cancer) and an IC_{50} value of 0.35 µg/mL against KB (human oral epidermoid carcinoma). It was also able to inhibit the activity of topoisomerase-I (IC_{50} of 3.0 µM) and RNA, DNA and protein synthesis, with IC_{50} values of 15, 15, 21 µM, respectively.[74]

Four years later, a new alkaloid, makaluvamine N **59** was isolated from the sponge *Zyzzya fuliginosa*. Compound **59** reduced *in vitro* the growth of the HCT-116 human colon tumor cells, with LC_{50} value of 0.6 µg/mL. It also exhibited selective inhibitory activity against topoisomerase II unwinding of pBR-322 at 5 µg/mL, interfering with the breakage-rejoining reaction.[75]

Recently, it was reported the isolation of a new member of makaluvamine family, makulavamine P **60**, from the sponge *Zyzzya cf. Fuliginosa.* The skeletal structure contains a pyrroloiminoquinone unit and a *p*-hydroxyphenethyl moiety. Makulavamine P **60** inhibited *in vitro* growth of the KB tumor cells (64%) with IC_{50} value of 3.2 µg/mL. It also showed a potent inhibition against xanthine oxidase, which is involved in several disease, with IC_{50} value of 16.5 µg/mL. [76]

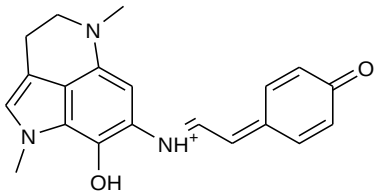

Makaluvamine G
58

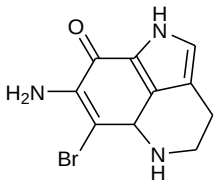

Makaluvamine N
59

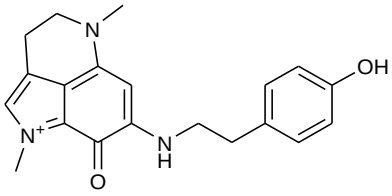

Makaluvamine P
60

In 1996, two other new bispyrroloiminoquinone alkaloids, tsitsikammamine A **61** and the methyl derivative tsitsikammamine B **62**, were isolated from the sponge *Tsitsikamma favus*. The tsitsikammamine A **61** and tsitsikammamine B **62** exhibited antimicrobial activity against *Bacillus subtilis*, cytotoxic activity against murine cell line and antifungal acticity.[76]

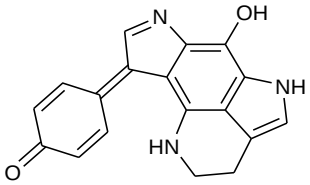

Tsitsikammamine A
61

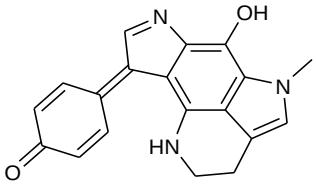

Tsitsikammamine B
62

In 2012, six 4-thiazolidinone derivatives of marine bromopyrrole alkaloids, having a 4,5-dibromopyrrole carboxamide moiety incorporated in to 4-thiazolodinone, were synthesized by Rane *et al.*, to investigate their antibiofilm activity. This new series of compounds was tested against Gram-positive bacteria *S. aureus, S. epidermidis* and *E. faecalis.* The compounds **63** and **64** showed antibiofilm activity against *S. aureus* 3-fold superior to (MIC of 0.78 μg/mL) that of known vancomycin (MIC of 3.125 μg/mL), while activity of compounds **65-68** was 2-fold superior (MIC of 1.56 μg/mL) to that of standard. All compounds (**63-68)** showed the same antibiofilm activity against *S. epidermidis* and moderate antibiofilm activity against *E. faecalis* (MIC ranging from 6.25 to 12.5 μg/mL) of standard vancomycin (MIC of 3.125 μg/mL).[77]

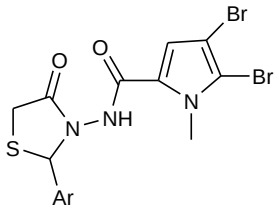

63, Ar=4-methoxyphenyl
64, Ar=4-nitrophenyl
65, Ar=2-hydroxy-4-methoxyphenyl
66, Ar=2,5-dihydroxyphenyl
67, Ar=4-fluorophenyl
68, Ar=4-chlorophenyl

1.2.3 Pyridine Alkaloids

In 1999, Kitamura *et al.* isolated from sponge *Echinoclathria sp.* the first pyridine alkaloids, echinoclathrines A-C **69-71**, characterized by a 4-aryl-2-methylpyridine common unit. Only echinoclathrine A **69** showed slight cytotoxic activity against P-388, A-549 and HT-29 cell lines, with IC_{50} of 10 µg/mL. The other echinoclathrines were found to be inactive.[78]

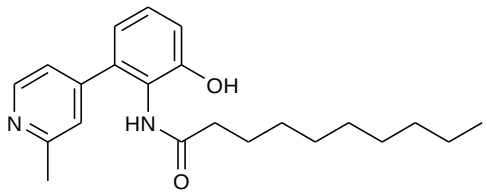

Echinoclathrine A
69

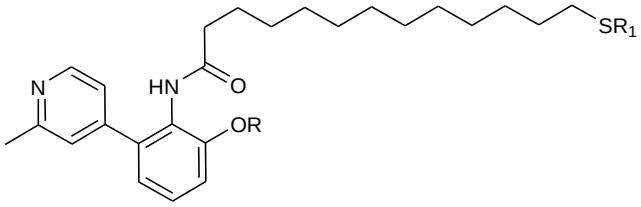

Echinoclathrine B, 70, R=H, R_1=Ac
Echinoclathrine C, 71, R=R_1=H

In the same years, Tsuda *et al.* isolated another pyridine alkaloid, pyrinodemin A **72** from *Amphimedon sp* sponge. The structure of compound contains two 3-alkyl-substituted pyridine rings fused with cis-cyclopent[*c*]isoxazolidine unit. Pyrinodemin A **72** showed potent cytotoxicity *in vitro* against murine leukemia L-1210 and KB epidermoid carcinoma cells, reporting IC_{50} values of 0.058 and 0.5 µg/mL, respectively.[79] Pyrinodemins B-D **73-75**, isolated one years later by Kobayashi *at al*. from *Amphimedon sp*. sponge, showed *in vitro* an inhibitory affect against L-1210 murine leukemia cells with IC_{50} values of 0.07, 0.06 and 0.08 µg/mL, respectively, and against KB epidermoid carcinoma cells, with IC_{50} of 0.5 µg/mL for each compound.[80]

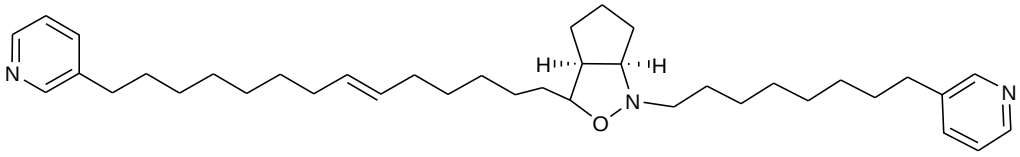

Pyrinodemin A
72

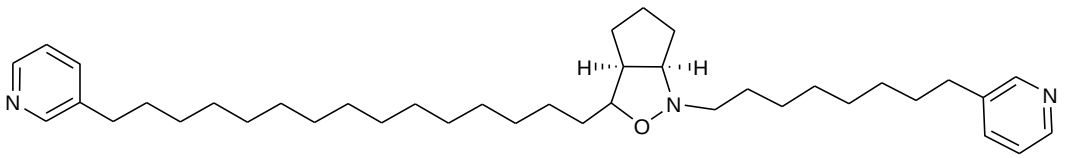

Pyrinodemin B
73

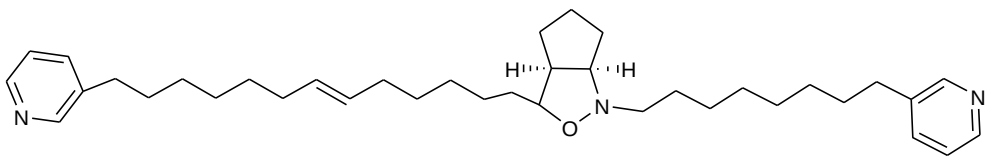

Pyrinodemin C
74

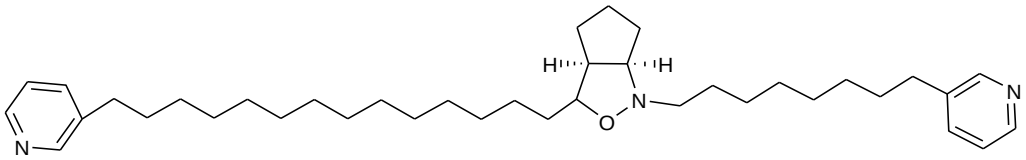

Pyrinodemin D
75

Another pyridine alkaloid, pyrinadine A **76**, isolated from the marine sponge *Cribrochalina sp.*, showed anti-proliferative activity against L-1210 murine leukemia and KB human epidermoid carcinoma cells, with IC_{50} in the micromolar range (1-2 μg/mL).[81]

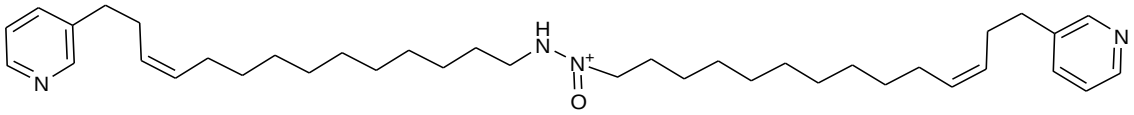

Pyrinadine A
76

Recently, it has been reported the isolation of the first glucosylated alkaloids, amphimedosides A-E **77-81** from a marine sponge *Amphimedon sp.*. Amphimedosides **77-81** were found to be active against P-388 murine leukemia cells, reporting IC_{50} values ranging from 0.45 to 11 μg/mL.[82]

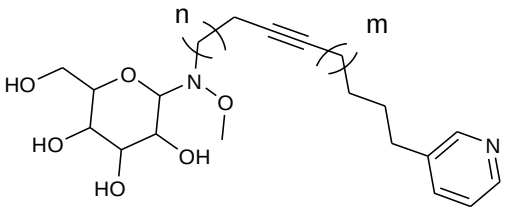

Amphimedoside A, 77, m=3, n=9
Amphimedoside B, 78, m=3, n=7
Amphimedoside C, 79, m=1, n=9

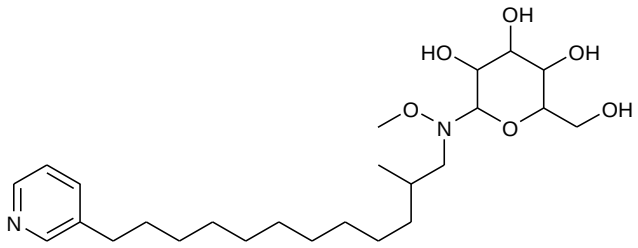

Amphimedoside D
80

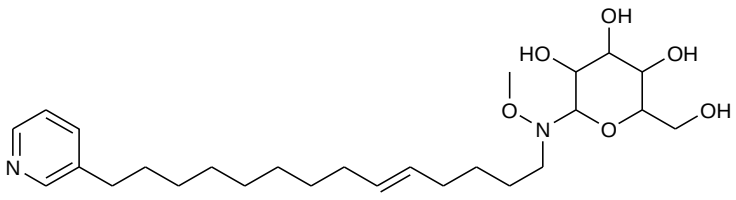

Amphimedoside E
81

1.2.4 Isoquinoline Alkaloids

In 1992, Pettit *et al.* isolated the first two isoquinolinequinones alkaloids, cribrostatin 1 **82** and cribrostatin 2 **83** from a deep blue colored sponge *Cribrochalina sp.*. Tested against NCI-60 cancer cell line panel, cribrostatins 1 and 2 showed selective cytotoxic activity against lymphocytic leukemia cell line (P-388), with ED_{50} values of 1.58 and 2.73 μg/mL, respectively. Cribrostatin 2 also reported activity against opportunistic fungi and a variety of bacteria, including clinical isolates of penicillin- resistant *Neisseria gonorrhoeae* and *Streptococcus pneumoniae*.[83,84] Eight years later, the same research group reported the isolation of cribrostatins 3 **84**, 4 **85** and 5 **86** from the same sponge. Compounds **84-86** were submitted to NCI and their antitumor activity was tested against several cancer cell lines. Mouse leukemia P-388 cell line was found to be the most sensitive to Cribrostatins 3 **84**, 4 **85** and 5 **86** exhibiting ED_{50} values of 2.5, 2.2 and 0.045 μg/mL, respectively. Cribrostatin 3 and cribrostatin 4 showed mean panel GI_{50} values of 4.27 μM and 5.01 μM, respectively. Cribrostatins **84-86** also reported selective antimicrobial activity against penicillin-resistant *Neisseria gonorrhoeae*, with MIC values ranging from 0.39 to 12.5 μM.[84] Cribrostatin 6 **87**, isolated from the same marine sponge *Cribrochalina sp*., was found to be able to inhibit the growth of murine P-388 lymphocytic leukemia, with GI_{50} of 0.29 μg/mL. Among human cancer cell lines, the most sensitive cell line was MCF-7 (GI_{50} of 0.21), followed by SF-268 (GI_{50} of 0.24) and DU-145 (GI_{50} of 0.38). Cribrostatin 6 **87** exhibited antimicrobial activity against several Gram-positive bacteria, such as *Candida albicans* (ATCC 90028) and *Streptococcus pneumoniae* (ATCC 6303), and pathogenic fungi. The only Gram-negative bacterium inhibited was *Neisseria gonorrhoeae*.[83]

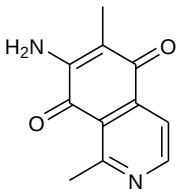

Cribrostatin 1
82

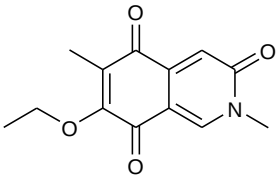

Cribrostatin 2
83

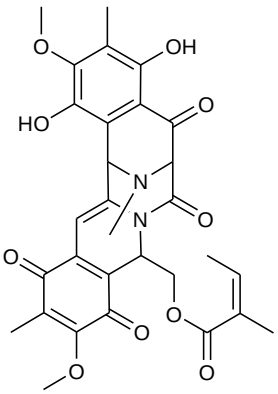

Cribrostatin 4
85

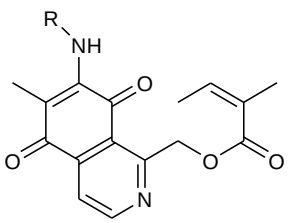

Cribrostatin 3, 84, R=H
Cribrostatin 5, 86, R=CH_3

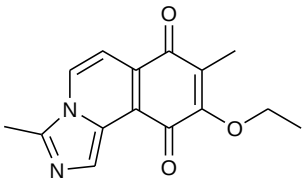

Cribrostatin 6
87

1.2.5 Guanidine Alkaloids

The ptilomycalin A **88** has been the first discovered guanidine alkaloid. It was isolated from the Caribbean sponge *Ptilocaulis spiculifer* and the red sea sponge *Hemimycale sp*. and characterizated by Kashman *et al*., in 1989. The skeletal structure of this compound consists of a linear long-chain fatty acid between a pentacyclic guanidine moiety and a spermidine unit. Ptilomycalin A **88** showed significant cytotoxic activity against P-388, L-1210 and KB cell lines, reporting IC_{50} values of 0.1, 0.4 and 1.3 μM, respectively.[85]

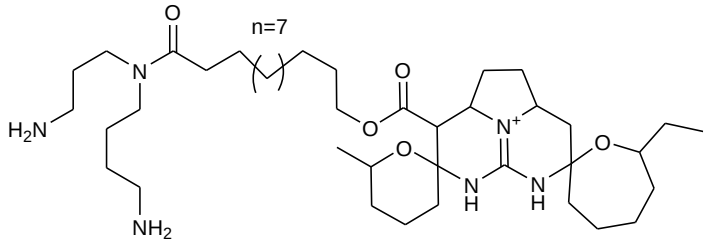

Ptilomycalin A
88

In 2006, seven new tricyclic guanidine alkaloids, netamines A-G **89-95** were extracted from the sponge *Biemna laboutei*. All compounds were tested in order to evaluate their ability to inhibit the proliferation of three human tumor cells: A-549NSCL (non small cell lung cancer), HT-29 (colon cancer) and MDA-MB-231 (breast cancer). Only netamines C **91** and D **92** exhibited antitumor activity against A549 (GI_{50} of 4.3 and 6.6 μM,) HT29 (GI_{50} of 2.4 and 5.3 μM,) and MDA-MB-231 (GI_{50} of 2.6 and 6.3 μM, respectively), whereas other compounds were found to be inactive or slightly toxic.[86]

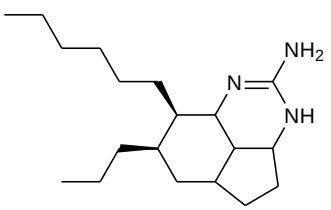

Netamine A
89

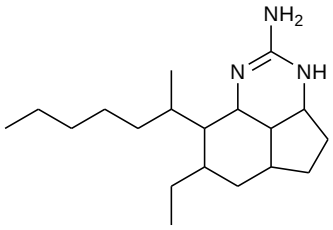

Netamine B
90

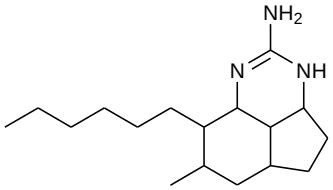

Netamine C
91

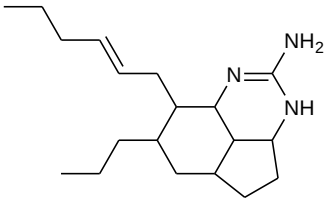

Netamine D
92

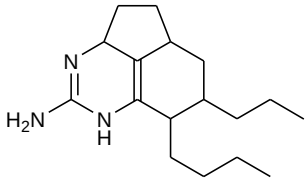

Netamine E
93

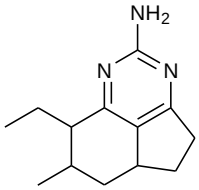

Netamine F
94

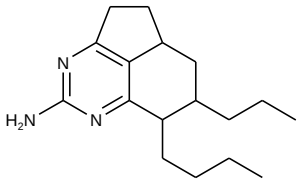

Netamine G
95

1.2.6 Aminoimidazole Alkaloids

In 2007, Ralifo *et al.* reported the isolation and the characterization of two aminoimidazole alkaloids, leucosolenamines A **96** and B **97** from the marine sponge *Leucosolenia sp.*. Leucosolenamine A **96**, containing a 2-aminoimidazole unit funzionalizated at C-4 and C-5 with an *N*,*N*-dimethyl-5,6-diaminopyrimidine-2,4- dione and a benzyl group respectively, exhibited slight cytotoxicity against the C-38 colon adenocarcinoma cell line. Although, the compound **97**, characterized by the same core structure funzionalizated with a 5,6-diamino-1,3-dimethyl-4-(methylimino)-3,4-dihydropyrimidin-2(1*H*)-one moiety at C-4, did not show antitumor activity.[87]
In the same year, Tsukamoto *et al.* isolated two new aminoimidazole alkaloids, naamidines H **98** and I **99** from the marine sponge *Leucetta chagosensis*. Both compounds showed weak antiproliferative activity against HeLa cells, reporting IC_{50} values of 5.6 and 15 μg/mL, respectively.[88]

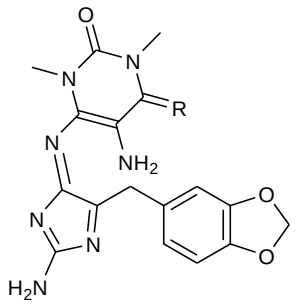

Leucosolenamine A, 96, R=O
Leucosolenamine B, 97, R=NCH_3

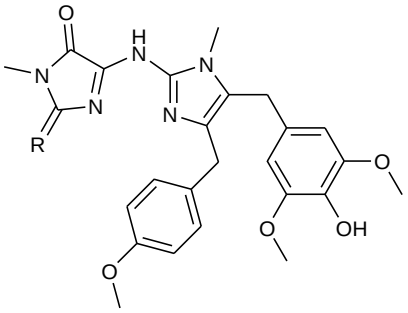

Naamidine H, 98, R=O
Naamidine I, 99, R=NCH_3

In 2017, a new family of 2-aminoimidazole alkaloids, named terrazoanthines A−C **100-102** was isolated from the Tropical Eastern Pacific Zoantharian *Terrazoanthus onoi* and characterized by Guillen *et al.* The skeletal structure of the terrazoanthines A−B contains an unprecedented 6-(imidazol-5-yl)benzo[*d*]imidazole moiety. Finally, as far as their biological activity was concerned, these three compounds were tested in order to evaluate their antimicrobial activity and their cytotoxic activity against the Heg2 human liver cancer cell line, but they were found inactive.[89]

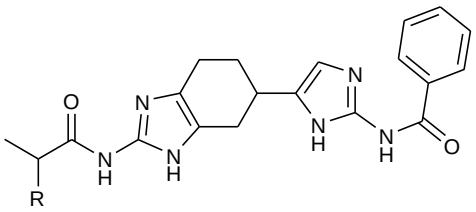

Terrazoanthine A, 100, R=CH_3
Terrazoanthine B, 101, R=H

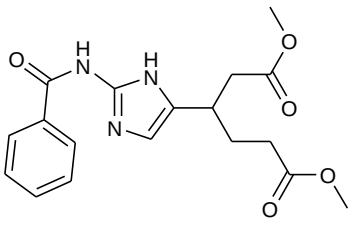

Terrazoanthine C
102

1.2.7 Macrocyclic Alkaloids

Motuporamines A-C **103-105**, macrocyclic alkaloids isolated from the marine sponge *Xestospongia exigua*, showed anti-invasive and anti-angiogenic activity, inhibiting *in vitro* invasion of basement membranes by many tumor cells, including MDA-231 breast carcinoma and PC-3 prostate carcinoma cells. Motuporamine C **105**, the best promising potential anti-cancer compound among motuporamine macrocyclic alkaloids family, induced cytoskeletal changes in

cancer cells and hindered the activation of β1-integrin, leading to inhibition the cell migration and angiogenesis.[90–92]

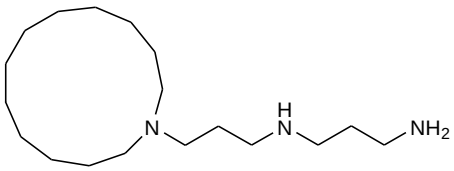

Motuporamine A
103

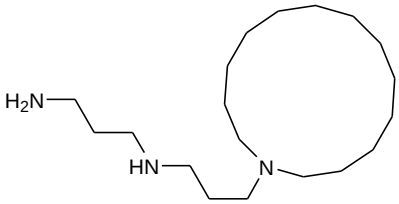

Motuporamine B
104

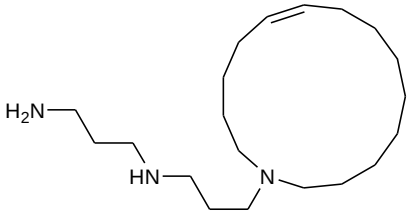

Motuporamine C
105

1.2.8 Steroidal Alkaloids

In 2002, the steroidal alkaloids plakinamine G **106**, plakinamine H **107**, 4-*R*-hydroxydemethylplakinamine B **108** and tetrahydroplakinamine A **109** were isolated from the marine sponge *Corticium sp.* and were tested for cytotoxicity against rat glioma (C6) and murine macrophages (RAW-264) cell lines. Compounds **106** and **109** showed activity only against C6 cells, reporting IC_{50} values of 6.8 and 1.4 µg/mL, respectively. Compounds **107** and **108** were cytotoxic against both cell lines. In particular, the compound **107** showed more activity against C6 cells (IC_{50} of 9.0 µg/mL) than against RAW-264 (IC_{50} of 61 µg/mL), while compound **108** reported greater value of IC_{50} (16.2 µg/mL) against RAW-264 cell line than to C6 cells (IC_{50} of 26.1 µg/mL).[93]

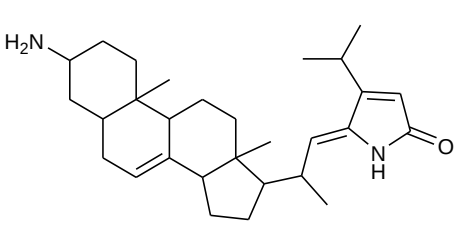

Plakinamine G
106

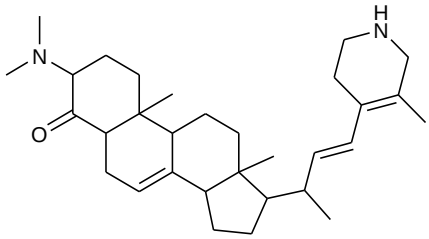

Plakinamine H
107

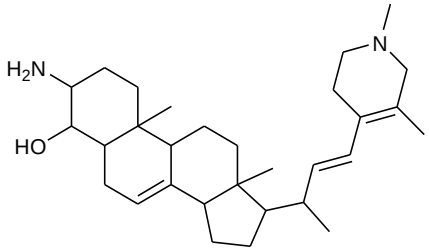

***4R*-hydroxydemethylplakinamine B**
108

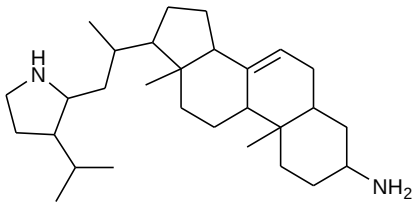

tetrahydroplakinamine A
109

One year later, Ridley *et al.* isolated four other steroidal alkaloids, plakinamines I-K **110**-**112** and dihydroplakinamine K **113** from the same sponge *Corticium niger*. The antitumor activity of all compounds was evaluated against the HCT-116 human colon tumor cell line. Plakinamines I-K **110**-**112** and dihydroplakinamine K **113** reported IC_{50} values of 10.6 μM, 6.1 μM, 1.4 μM and 1.4 μM, respectively. The compounds were also submitted to Bristol-Myers Squib Pharmaceutical Research Institute, in order to evaluate their antitumor activity against eleven other cancer cell lines. Against these cell lines, the compounds **110**-**112** reported IC_{50} mean values ranging from 1.6 μM to 6 μM.[94]

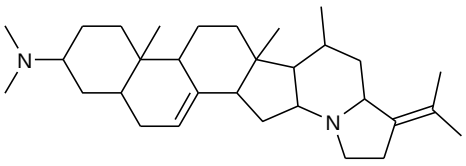

Plakinamine I
110

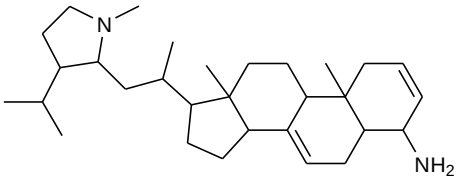

Plakinamine J
111

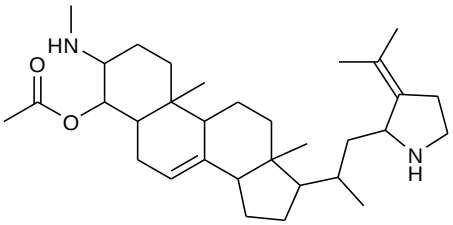

Plakinamine K
112

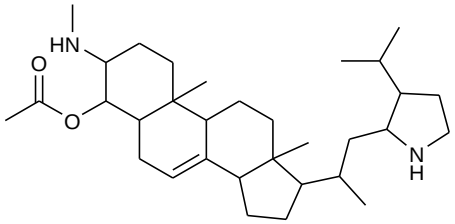

Dihydroplakinamine K
113

In 2014, two other steroidal alkaloids of plakinamine family were extracted from the marine sponge *Corticium niger*, plakinamines N **114** and O **115**. In order to evaluate their antitumor activity, all compounds were submitted to National Cancer Institute and tested against sixty tumor cell lines. They showed selective inhibitory effects against all of the colon cell lines with mean GI_{50} values ranging from 1.4 μM to 11.5 μM. [95]

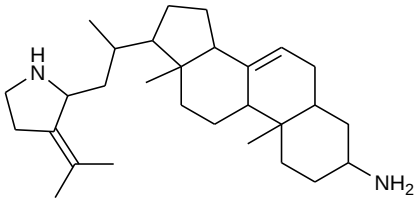

Plakinamine N
114

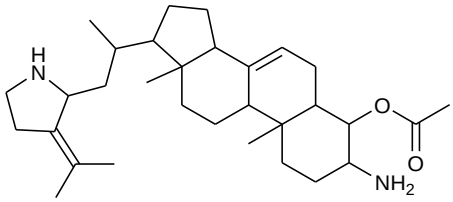

Plakinamine O
115

Cortistatins J-L **116-118,** characterized by an isoquinoline unit, were isolated from the Indonesian marine sponge *Corticium simplex* and tested against HUVEC human umbilical vein endothelial cells, in order to evaluate their anti-proliferative activity. Cortistatin J **116** exhibited potent cytostatic activity, with IC_{50} value of 8 nM, and inhibitory activity against the VEGF/bFGF-inducted migration of HUVEC cells. Whereas, cortistatins K **117** and L **118** were less potent than cortistatin J **116**, reporting IC_{50} values of 40 and 23 nM, respectively.[96]

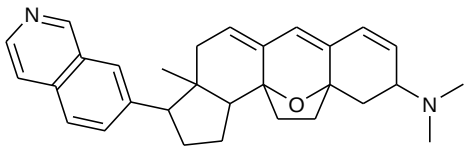

Cortistatin J
116

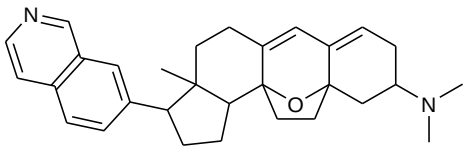

Cortistatin K
117

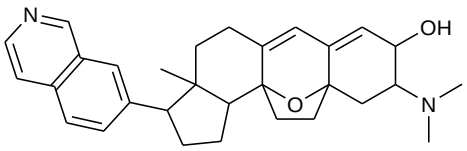

Cortistatin L
118

(+)-Agelasine D **119**, a new steroidal (diterpene) alkaloid extracted from the Indonesian marine sponge *Agelas nakamurai*, was reported to display potent inhibitory effect on Na+/K+-ATPase as well as antibacterial activity against *M. tuberculosis* as well as both aerobes and anaerobes Gram-positive and Gram-negative bacteria. It also exhibited selective cytotoxicity against several cancer cells, including multidrug-resistant cell lines. From the same sponge, two other diterpenoid alkaloids, (-)-agelasine D **120** and (-)-ageloxime D **121** were isolated. These showed antitumor activity against lymphoma cells, eliciting IC_{50} value of 4.03 and 12.5 μM, meaning that presence of the oxime function decreases activity.[97–99] In 2010, Hertiani *et al.* found that (-)-ageloxime D **121** inhibits biofilm formation in *S. epidermidis*, but does not affect bacterial growth. The oxime substituent on C-6' is important for the antibiofilm activity, despite their antitumor activity. On the other hand, the compound **120** exhibited antibacterial activity against the planktonic form of *S. epidermidis* (MIC < 0.0877 lM) but did not inhibit biofilm formation.[100]

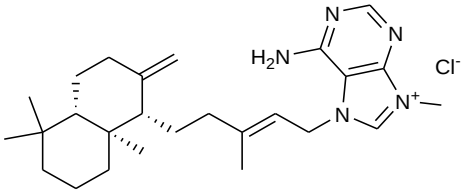

(+)-Agelasine D
119

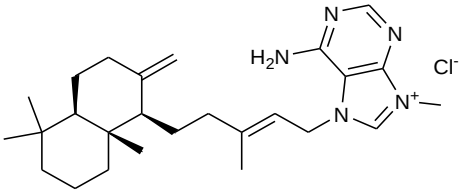

(-)-Agelasine D
120

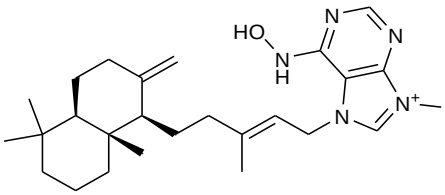

(-)-Ageloxime D
121

1.2.9 Indole Alkaloids

Among all marine alkaloids, bisindole-containing alkaloids have received considerable attention due to their broad spectrum of biological properties such as antitumor, antiviral, antimicrobial and anti-inflammatory.[101–104] The skeletal structure of these compounds is characterized by two indole units connected to each other, through their position 3, by a spacer such as carbocycles, linear chains or heterocycles differently sized.

Among bisindole alkaloids with acyclic spacer, examples are constituted by Hyrtiosin B **122**, isolated from the Japanese marine sponge *Hyrtios erecta*, that has shown cytotoxic activity on human cells of KB epidermoid carcinoma, and by Coscinamides A-C **123-125**, containing an unusual α-keto enamide moiety and extracted from the sponge *Coscinoderma sp.* The coscinamides exhibited only partial cytoprotection against HIV.[105,106]

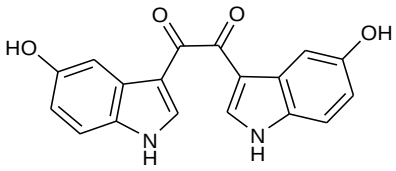

Hyrtiosin B
122

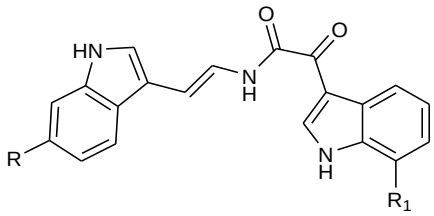

Coscinamide A, 123, R=Br, R_1=H
Coscinamide B, 124, R=R_1=H
Coscinamide C, 125, R=Br, R_1=OH

Asterriquinone **126**, a bisindolic alkaloid characterized by a carbocyclic spacer (quinone) and isolated from *Aspergillus terreus* IFO 6123 as one of intracellular metabolic products, showed an antitumor affect against Ehrlich carcinoma, ascites hepatoma AH13 and mouse P-338 leukemia.[107]

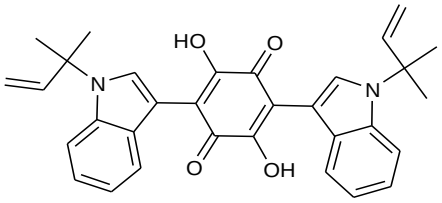

Asterriquinone
126

Dragmacidins, a class of bis-indole alkaloid characterized by different saturated six-membered heterocyclic links, were isolated from deep-water sponges, including *Dragmacidon,*[108] *Halicortex,*[109] *Spongsorites,*[110] *Hexadella*[111] and tunicate *Didemnum Candidum*[112]. Dragmacidin **127** and dragmacidins A-C **128-130**, characterized by a saturated six-membered heterocyclic

piperazine ring, showed several biological activies. Dragmacidin exhibited *in vitro* cytotoxicity, reporting IC_{50} values of 15 μg/mL against P-388 cell line and in the range 1-10 μg/mL against A-549 (human lung), HCT-8 (human colon) and MDAMB (human mammary) cancer cell lines.[113] Dragmacidin A **128** showed *in vitro* antiproliferative activity against L-1210 mouse lymphocytic leukemia cells, with ED_{50} value of 10 mg/mL, whereas dragmacidin B was found to be inactive.[111]

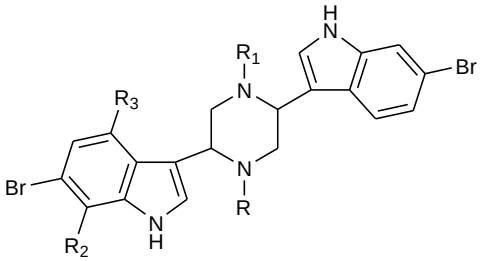

Dragmacidin, 127, R=H, R_1=CH_3, R_2=Br, R_3=OH
Dragmacidin A, 128, R=R_2=R_3=H, R_1=CH_3
Dragmacidin B, 129, R=R_1=CH_3, R_2=R_3=H
Dragmacidin C, 130, R=R_1=R_2=R_3=H

Further, Capon *et al.* reported the isolation of dragmacidin D **131** from a deep water marine sponge *Spongosorites sp.*. Dragmacidin D **131**, a pyrazinone indole alkaloid with a imidazol-2-amine functionalized side chain, was found to be active against human lung tumor cell lines and inhibited *in vitro* growth of the P-388 murine and A-549 with IC_{50} values of 1.4 and 4.5 μg/mL, respectively.

It also inhibited *in vitro* the replication of feline leukemia virus (FeLV), reporting a MIC (minimum inhibitory concentration) value of 6.25 μg/mL. Dragmacidin D showed antimicrobial activity against *Escherichia coli*, *Bacillus subtilis*, *Pseudomonas aeruginosa*, *Candida albicans*, and *Cryptococcus neoformans*, with MIC values of 15.6 μg/mL, 3.1 μg/mL, 62.5 μg/mL, 15.6 μg/mL and 3.9 μg/mL, respectively.[114]

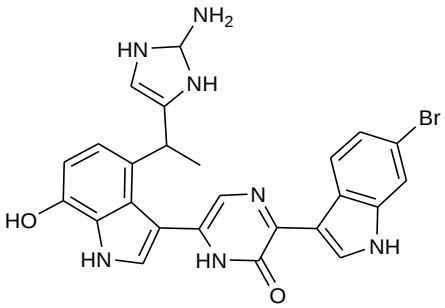

Dragmacidin D
131

In 2000, Riccio and his co-workers isolated a new bromoindole alkaloid, dragmacidin F **132** from a Mediterranean sponge *Halicortex sp*. The carbon skeletal of dragmacidin F **132** is characterized by the same 3-[bromoindole-3-yl]-pyrazin-2-one portion of dragmacidin D and a novel polycyclic carbon framework, derived from cyclization of the 2-aminoimidazole of dragmacidin D. The compound **132** showed *in vitro* antiviral activity against HSV-1 and HIV-1, reporting EC_{50} values of 95.8µM and 0.91µM, respectively.[109]

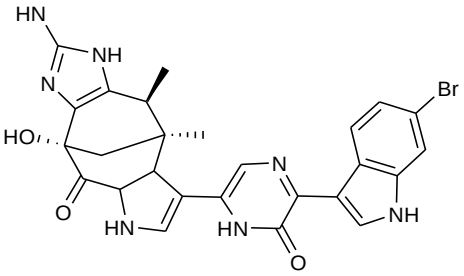

Dragmacidin F
132

In 2017, dragmacidin G **133**, characterized by a pyrazine ring linking the two indole portions, was extracted from a deep-water sponge of the genus *Spongosorites*. It showed antiviral activity against *S. aureus* and *MRSA* with minimum inhibitory concentration (MIC) of 0.62 µg/mL. The anti-mycobacterial activity of the compound **133** was assayed against *M. Tuberculosis*, for which it reported MIC of 21.0 µM with cytotoxicity of 125 µM. Against *Plasmodium falciparum*, it showed a modest inhibition, reporting an IC_{50} value of 6.4 µM. Dragmacidin G **133** exhibited antiproliferative activity against a panel of pancreatic cancer cell lines, including the PANC-1 and MIA PaCa-2 human pancreatic cancer cells, BxPC-3 and ASPC-1 human pancreatic adenocarcinoma cells with IC_{50} values at 72 hours of treatment ranging from 14 µM to 27 µM.[110]

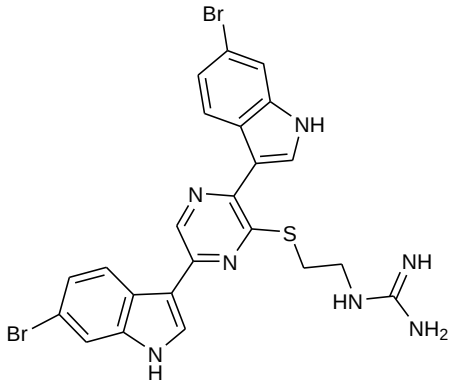

Dragmacidin G
133

In 2007, hyrtinadine A **134**, a new cytotoxic bis-indole alkaloid, having a characteristic 2,5-disubstituted pyrimidine ring between two indole portions, was isolated by Kobayashi *et al.* from Okinawan marine sponge *Hyrtios sp.*. Hyrtinadine A **134** showed *in vitro* potent cytotoxicity against murine leukemia L-1210 and human epidermoid carcinoma KB cells, eliciting IC_{50} values of 1.0 and 3 µg/mL, respectively.[115]

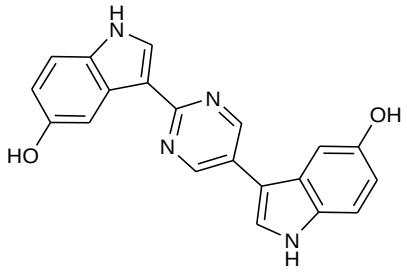

Hyrtinadine A
134

Hamacanthin A **135** and B **136**, two isomeric bisindole alkaloids characterized by a 5,6-dihydro-1(2H)-pyrazinone moiety between two bromoindole portions, were isolated from a deep-water marine sponge *Hamacantha sp.* by Gunasekera *et al.*. Both the hamacanthin A and the B **135-136** showed significant antimicrobial activity against *C. albicans* ATCC 44506, *C. neoformans* ATCC 32045 and *B. subtilis* ATCC 6633, with MIC values ranging from 1.6 to 6.2 µg/ml. Moreover, Hamacanthin A **135** showed potent antibacterial activity against MRSA, with MIC value of 3.12 µg/ml.[116,117]

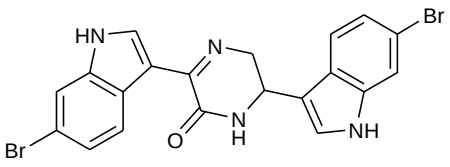

Hamacanthin A
135

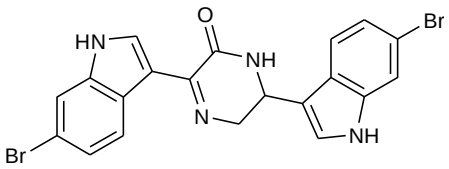

Hamacanthin B
136

In 1991, three new bisindole alkaloids characterized by an imidazole ring between two indole units, nortopsentins A-C **137-139**, were isolated from the Caribbean deep sea sponge *Spongosorites ruetzleri*. The nortopsentins **137-139** exhibited cytotoxic activity against P-388 cells with IC_{50} values of 7.6, 7.8, 1.7 µg/mL, respectively and antifungal activity against *Candida albicans*, reporting MIC values of 3.1, 6.2 and 12.5 µg/mL.[117,118] Nortopsentin A **137** also showed antiplasmodial activity against chloroquine-sensitive (3D7) and chloroquine-resistant (Dd2) *P. falciparum* strains, with IC_{50} values of 460 nM and 580 nM, respectively.[119]

The trimethyl and tetramethyl derivatives of nortopsentin B **140-141**, obtained as $MeSO_4^-$ salt by methylation of nortopsentine B with dimethyl sulfate in the presence of potassium carbonate in acetone, showed *in vitro* better antitumor activity against P-388 cells than their parent compound **138** (0.9 and 0.34 μg/ml).[118]

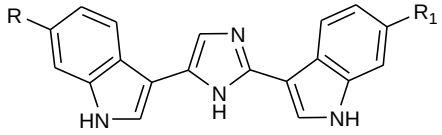

Nortopsentin A, 137, R=R_1=Br
Nortopsentin B, 138, R=Br, R_1=H
Nortopsentin C, 139, R=H, R_1=Br

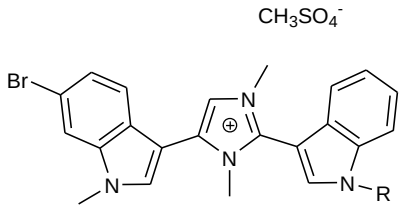

Trimethylnortopsentin B, 140, R=H
Tetramethylnortopsentin B, 141, R=CH_3

In the research group in which I have carried out my PhD, a long and complex project concerning these metabolites have been carried out. In particular, numerous nortopsentin analoguess have been reported in which the central imidazole ring of nortopsentin, a spacer linking the two indolic units, has been replaced by other pentatomic heterocycles, thus obtaining bis-indolyl thiophenes **142**,[120] pyrazoles **143**,[121] isoxazoles **144**,[122] furans **145**,[122] pyrroles **146**,[123] and thiazoles **147**[124]. Most compounds have shown antiproliferative activity on a wide spectrum of human tumour cell lines at GI_{50} values in the micro- and sub-micromolar range.

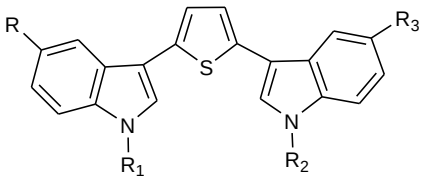

2,5-bis(3'-indolyl)thiophenes
142

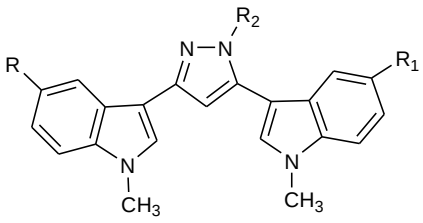

2,5-bis(3'-indolyl)pyrazoles
143

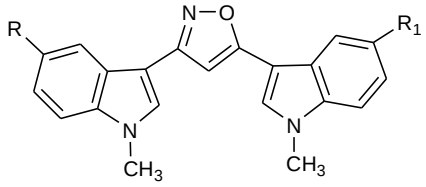

3,5-bis(3'-indolyl)isoxazoles
144

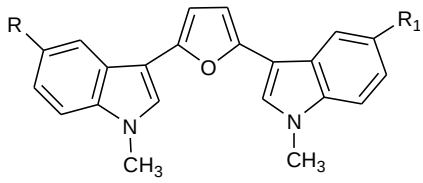

2,5-bis(3'-indolyl)furans
145

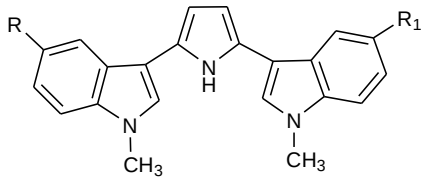

2,5-bis(3'-indolyl)pyrroles
146

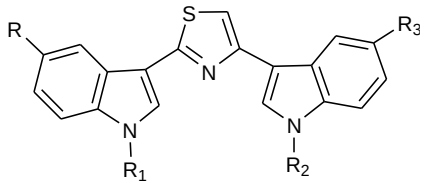

2,5-bis(3'-indolyl)thiazoles
147

Furthermore, in case of thiazole derivatives, several structural manipulations were carried out in one or both of the indole portions, that was substituted by a phenyl or aza-indole moiety (compounds **148-154**).

Almost all the compounds showed significant antitumor activity against several human tumor cell lines at concentrations in the range from micro-to sub-micromolar, with a selective inhibition of kinase-cyclin dependent of type 1 (CDK1) in a time dependent way with IC_{50} values comparable to those of known inhibitors of CDK1, such as roscovitin and purvalanol A.[125–129]

The most active compounds were also tested on cell lines belonging to human tumours of different histological types, such as breast cancer (MDA-MB-231), pancreatic (MiaPaCa-2), prostatic (PC3) and malignant peritoneal mesothelioma (STO), showing a significant reduction in cell growth at IC_{50} values between 4.1 and 25.0 μM, with a particular selectivity towards the cell line of malignant peritoneal mesothelioma (STO). Furthermore, studies on cell cycle progression on STO cells have highlighted a cell cycle arrest in G_2/M phase, with an apoptosis cell death mechanism. Moreover, many thiazole derivatives, especially those belonging to 6-azaindole series **154**, were able to stop the cell cycle progression in G1 phase, inducing morphological changes characteristic of autophagic death, such as cell volume decrease (loss of intracellular liquids for active processes

mediated by membrane pumps), condensation, marginalization and fragmentation of chromatin and formation of cytoplasmic protuberances (blebs), bounded by membrane (exposure of PS) and containing fragments of condensed chromatin and cytoplasmic organelles.[127,128]

Same derivatives of type**151** were also tested against *S. aureus* ATCC 25923, *S. aureus* ATCC 6538 and *P. aeuruginosa* ATCC 15442 to evaluate their ability to inhibit biofilm formation and microbial growth. Initially, in order to assay their antimicrobial activity, the compounds were tested against the planktonic form, but they did not show significant effect on the microbial growth, reporting Minimum Inhibitory Concentrations (MIC) values greater than 100 μg/mL. on the other hand, almost all the compounds were found to be active as inhibitors of biofilm formation, with greater selectivity against staphylococcal biofilm formation of both reference strains , showing IC_{50} values at submicromolar level.[130]

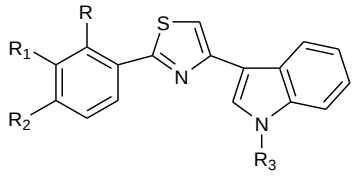

3-(2-phenyl-1,3-thiazol-4-yl)-1*H*-indoles
148

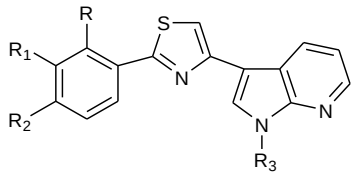

3-(2-phenyl-1,3-thiazol-4-yl)-1*H*-7-azaindoles
149

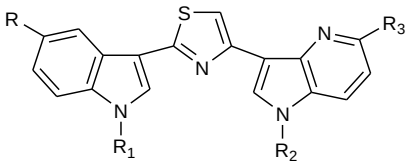

3-[2-(1*H*-indol-3-yl)-1,3-thiazol-4-yl)-1*H*-4-azaindoles
150

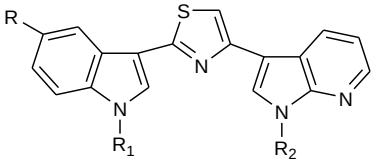

3-[2-(1*H*-indol-3-yl)-1,3-thiazol-4-yl)-1*H*-7-azaindoles
151

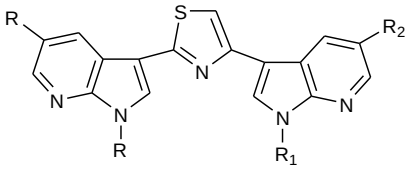

3-3'-(1,3-thiazol-2,4-diyl)bis-1*H*-7-azaindoles
152

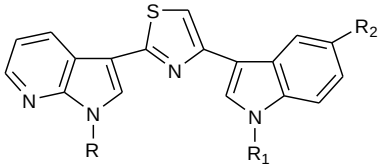

3-[4-(1*H*-indol-3-yl)-(1,3-thiazol-2-yl)-1*H*-7-azaindoles
153

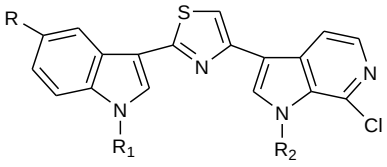

7-chloro-3-[2-(1*H*-indol-3-yl)-1,3-thiazol-4-yl)-1*H*-6-azaindoles
154

In 1987, two other bisindole alkaloids, topsentin **155** and bromotopsentin **156** were extracted from the sponge *Topsentia genitrix*. The structure of the compounds was elucidated on the basis of spectroscopic data, reporting the presence of a 2-acyl imidazole moiety between two indole units with different substitution on benzene rings.[131]

In 1995, Capon *et al.* reported the isolation and the characterization of isobromotopsentin **157** from the deep water sponge *Spongosorites sp*., collected from the coast of southern Australia.[132]

Topsentin **155** showed *in vitro* cytotoxic activity against P-388 murine tumour cells, with IC_{50} value of 3 μg/mL and against several human tumour cells, including HCT-8, A-549, T47D, at concentration of 20 μg/mL. In addition, it exhibited *in vivo* activity against P-388 (T/C 137%, 150 mg/kg) and B16 melanoma (T/C 144%, 37.5 mg/kg). Bromotopsentin **156** was found to be active against human non-small-cell bronchopulmonary cancer cells (NSCLC-N6) and P-388, with an IC_{50} of 12 μg/mL and 7 μg/mL, respectively. Both compounds also exhibited *in vitro* antiviral activity against *HSV-1*, *Vesicular stomatitis virus* (VSV) and the *corona virus A-59*.[118,132–135]

Topsentin and bromotopsentin were also found to be able to bind α_{1a} and α_{1b} adrenergic receptors, which is involved in BPH (benign prostatic hyperplasia) or vascular hypertension, with Ki values ranging from 0.08 to 1.15 μM.[136]

Deoxytopsentin **158** was isolated from the sponge *Hexadella sp.*, collected in Columbia. The skeletal structures of topsentin **155** and deoxytopsentin **158** are the same, except the indole ring which is unsubstituted in case of deoxytopsentin **158**. Deoxytopsentin **158** was found to be active against human bronocopulmanary cancer cells (NSCLC-N6), breast cancer and hepatoma (HepG2), reporting IC_{50} values of 6.3 μg/mL, 10.7 μg/mL and 3.3 μg/mL, respectively. Deoxytopsentin **158** also exhibited potent antibacterial activity against various bacteria, including *Staphylococcus aureus* methicillin-resistant (MRSA), *Bacillus subtilis*, *Micrococcus leuteus*, *Proteus vulgaris* and *Salmonella typhimurium*, with MIC values ranging from 3.12 μg/mL to 12.5 μg/mL.[135,137,138]

In 1999, two other topsentin derivatives were isolated from the sponge *Spongosorites genitrix* and characterized by Shin *et al.*: bromodeoxytopsentin **159** and isobromodeoxytopsentin **160**. They showed moderate cytotoxicity against the human leukemia cell-line K-562, with LC_{50} values of 0.6 and 2.1 μg/mL, respectively.[138,139]

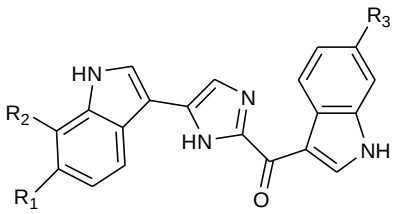

Topsentin, 155, R_1=R_2=H, R_3=OH
Bromotopsentin, 156, R_1=Br, R_2=H, R_3=OH
Isobromotopsentin, 157, R_1=H, R_2=OH, R_3=Br

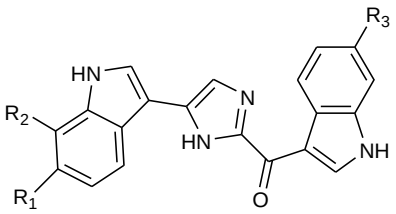

Deoxytopsentin, 158, R_1=R_2=R_3=H
Bromodeoxytopsentin, 159, R_1=Br, R_2=R_3=H
Isobromodeoxytopsentin, 160, R_1=R_2=H, R_3=Br

During a screening for inhibitors of sortase A (SrtA), a membrane enzyme with transpeptidase and protease activity that plays a key role in the anchorage and virulence of Gram-positive bacteria, Shin *et al.* have evaluated the *in vitro* activity of four topsentin alkaloids. Treatment of bacterial strain of *S. aureus* with topsentin analogues reduced the capability of the bacterium to adhere to fibronectin-coated surface in a dose-dependent manner. Bromotopsentin **156**, deoxytopsentin **158**, bromodeoxytopsentin **159**, and isobromodeoxytopsentin **160** showed significant inhibitory activity against SrtA, recording IC_{50} values between 15.67 and 19.44 μg/mL, a result comparable to the known SrtA inhibitor β-sitosterol-3-O-glucopyranoside (18.3 μg/mL). The inhibition of SrtA, an enzyme involved only in the process of bacterial adhesion and virulence, could not suggest an alteration of the growth or proliferation of the bacterium but rather an alteration of the capacity of formation of bacterial biofilms, obtained by aggregation of more bacterial cells that pass from independent cells (planktonic form) to a multi-stratified cellular community (sessile form), responsible for the development of antibiotic-resistance.[138,140]

Bromodeoxytopsentin **159** also exhibited significant inhibitory activity against MRSA pyruvate kinase, an essential enzyme for the bacterial metabolism involved in the production of ATP, at 10 μM and potent selective inhibitory activity against *Staphylococcus aureus* methicillin-resistant (MRSA) pyruvate kinase (PK) *versus* human pyruvate kinase (PK) isoforms at 5 μM.[141]

In order to elucidate the SAR of bisindole alkaloid inhibitors against the MRSA pyruvate kinase (PK), Veale *et al.* synthesized six new dihalogenated analogues of the sponge metabolite deoxytopsentin (**161**-**166**).[142]

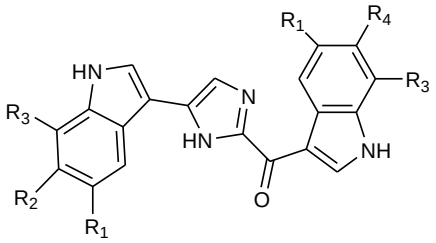

161, R_1=R_3=H, R_2=R_4=Br
162, R_1=R_3=H, R_2=R_4=F
163, R_1=R_3=H, R_2=R_4=Cl
164, R_1=R_3=H, R_2=R_4=I
165, R_1= Br, R_2=R_3=R_4=H
166, R_1=R_2=R_4=H, R_3=Cl

All compounds were tested for their ability to inhibit enzymatic activity against MRSA and human PKs. It is interesting to note that all of the C-6 halogenated analogues **161-164** showed remarkable inhibitory activity against MRSA PK at nanomolar concentrations (1.5-26 nM), displaying activity greater than bromodeoxytopsentin **159,** providing that halogenation of both indole rings is essential for this activity. Interestingly, the bromination at C-5 (**165**) leaded to the unaffected inhibition of MRSA PK, while chlorination at C-7 (**166**) resulted in a decrease of activity. Compounds **161**, **163** and **164** were found to be active against human PK orthologues R and L at concentration of 5 μM. A slight decrease in inhibitory activity against human PKs was observed with the C-5 halogenated analogue **165**; on the other hand, fluorination at C-6 (**162**) and the chlorination at C-7 (**166**) leaded to less activity against human PK.[142]

In 2014, different analogues of topsentin have been synthesized, in which the imidazole ring of topsentin was replaced by a thiazole ring. Biological evaluation of thiazole derivatives **167-173** showed that they presented moderate inhibitory activity against MRSA PK, reporting IC_{50} values ranging from 5.1 to 20 μM. The reduction of the inhibitory activity against the PK, compared with that of topsentin and imidazole analogues of topsentin, could be imputed to either steric hindrance engendered by the sulfur atom, or the replacement of a H-bond donating NH with a H-bond accepting sulfur.[143]

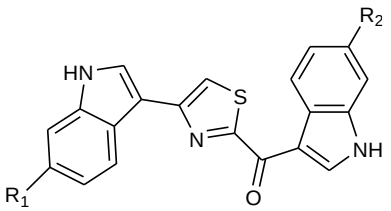

167, R_1=R_2=H
168, R_1=R_2=F
169, R_1=R_2=Cl
170, R_1=R_2=Br
171, R_1=Br, R_2=F
172, R_1=F, R_2=Br
173, R_1=F, R_2=Cl

Recently, it has been synthesized five pyrrole derivatives of topsentin (**174-178**), in which the imidazole moiety of topsentin was replaced by a pyrrole ring as a linker between the two functionalized indole portions.[144]

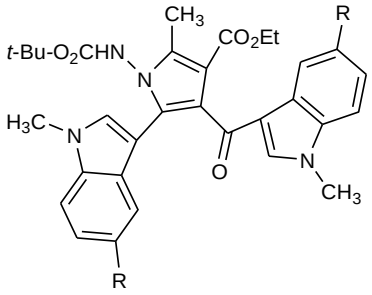

174, R=H
175, R=CH_3
176, R=OCH_3
177, R=Cl
178, R=Br

All pyrrole derivatives **174-178** were submitted to NCI in order to evaluate their antitumor activity and four analogues were selected for a single dose concentration, *in vitro* disease-oriented antitumor screenings against about 60 human tumour cell lines. At the concentration of 10 μM, the compound **178** showed the best result, reporting a growth of −27.31% against the SNB-75 cell line of the CNS cancer sub-panel and 4.73% against the HOP-92 of the non-small cell lung cancer sub-panel.[144]

2. AIM OF THE STUDY

Considering the interesting results shown by topsentin **155** and its analogues and the importance of heterocyclic oxadiazole rings in the drug discovery scenario[145–148], the aim of my PhD project was the synthesis of new biologically active 1,2,4-oxadiazole topsentin analogues. In particular, three new series have been synthesized:

- (1-methyl-1*H*-indol-3-yl)[3-(1-methyl-1*H*-indol-3-yl)-1,2,4-oxadiazol-5-yl]methanones **179** in which two 1-methyl-1*H*-indole rings are linked to the oxadiazole central ring;
- [3-(1*H*-indol-3-yl)-1,2,4-oxadiazol-5-yl](1-methyl-1*H*-indol-3-yl)methanones **180** in which the 1*H*-indole and 1-methyl-1*H*-indol-3-yl-methanone moieties, respectively in position 3 and 5, are linked to the oxadiazole central ring;
- (1-methyl-1*H*-pyrrolo[2,3-b]pyridin-3-yl)-[3-(1-methyl-1*H*-indol-3-yl)-[1,2,4]oxadiazol-5-yl]-methanones **181** in which the 1*H*-indol-3-yl-methanone unit in position 5 of topsentin is replaced by a (1-methyl-1*H*-pyrrolo[2,3-b]pyridin-3-yl)-methanone moiety.

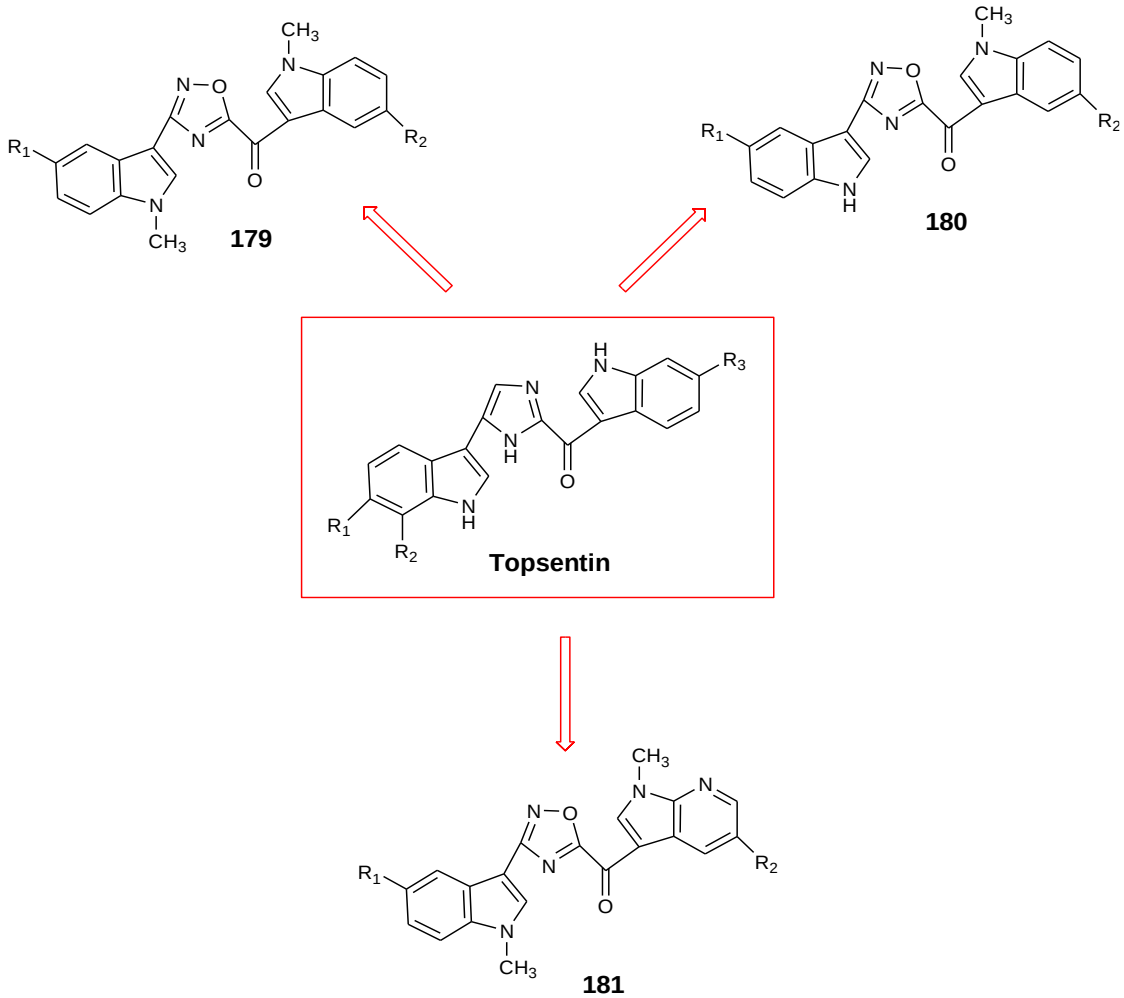

3. CHEMISTRY SECTION

The synthesis of 1,2,4-oxadiazole derivatives **179, 180** was initially planned from *N*-hydroxy-1*H*-indole-3-carboxamidines **182, 183** and (1-methyl-1*H*-indol-3-yl)-oxo-acetyl chlorides **184** (Scheme 1).

Scheme 1.

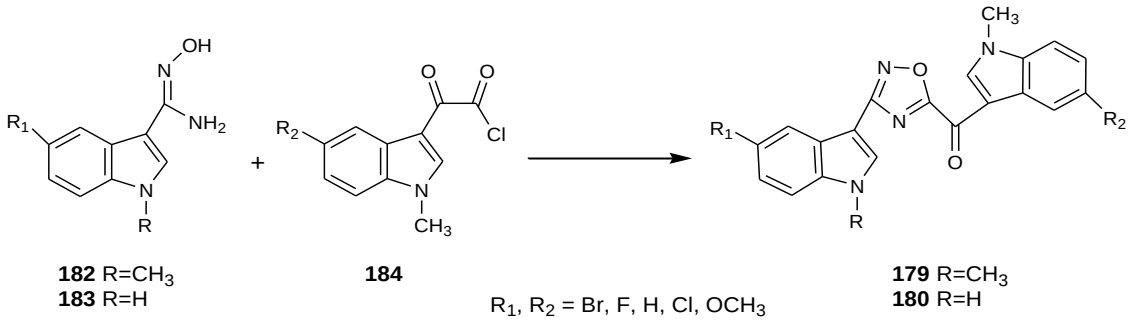

The key carboxamidine intermediates **182, 183** were prepared from the corresponding commercial indoles **185** or methylated indole derivatives **186**. In particular, the methylated derivatives **186a-e** (Table 1) were obtained at room temperature in excellent yields (90-98%), from the commercial indoles **185a-e**, using potassium t-butoxide (*t*-BuOK) as base, tris [2- (2-methoxyethoxy) ethyl] amine (TDA-1) as a phase transfer catalyst and iodomethane (CH_3I) as a methylating agent (Scheme 2).

Scheme 2.

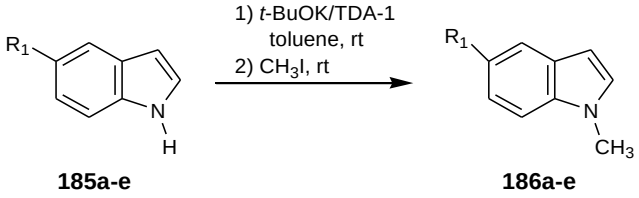

Table 1. 1-Methyl-1*H*-indoles **186a-e**.

Compound	R_1	Yield (%)
186a	Br	96%
186b	F	98%
186c	H	96%
186d	OCH_3	98%
186e	Cl	90%

The commercial indoles **185a-e** or the indole methyl derivatives **186a-e** were reacted with chlorosulfonylisocyanate (CSI) in acetonitrile, to give the corresponding sulphonylchlorides, that after the addition of dimethylformammide (DMF), were transformed into an intermediate that spontaneously rearranges, losing sulfuric anhydride (SO_3), DMF and hydrochloric acid (HCl). The simple reaction, stirred at temperature between 0°C and 5°C afforded the desired compounds **189a-e, 190a-e** in excellent yields (77-98%) (Scheme 3, Table 2).

Scheme 3.

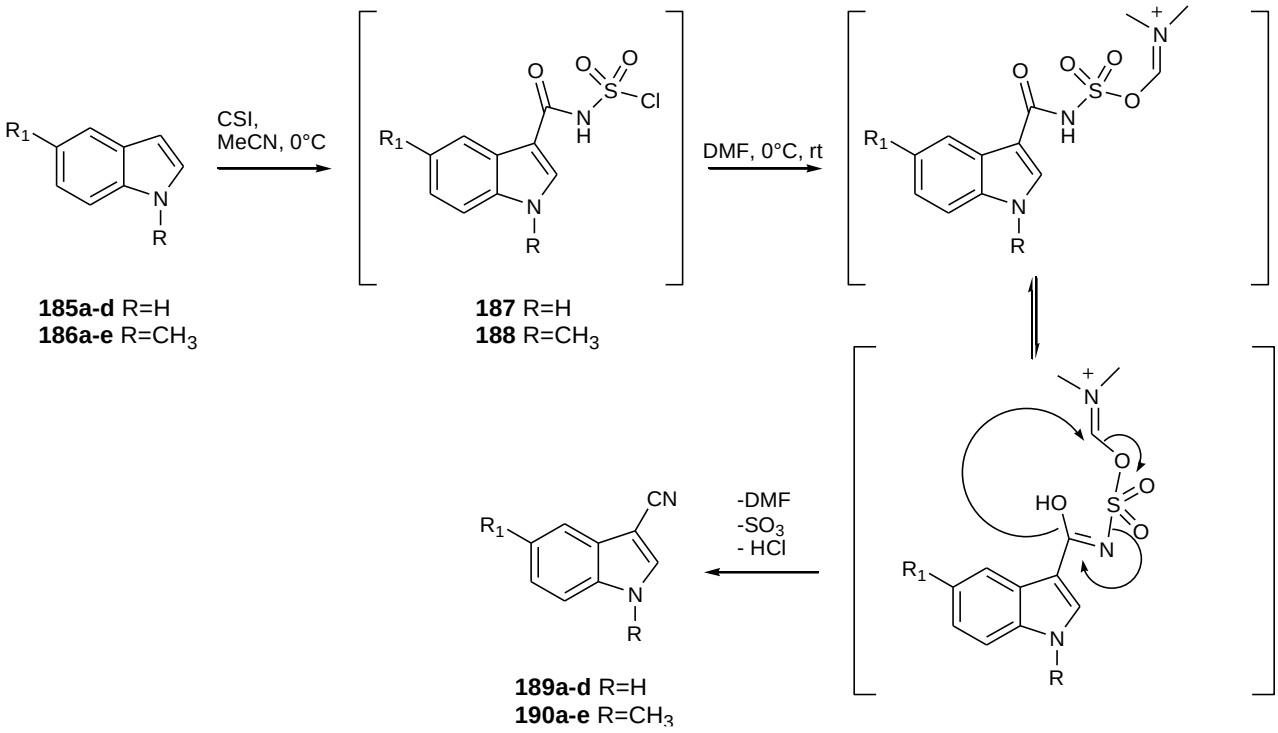

Table 2. 1*H*-indole-3-carbonitriles **189a-d** and 1-methyl-1*H*-indole-3-carbonitriles **190a-e.**

Compound	R	R_1	Yield (%)
189a	H	Br	98%
189b	H	F	90%
189c	H	H	90%
189d	H	OCH_3	90%
190a	CH_3	Br	98%
190b	CH_3	F	80%
190c	CH_3	H	77%
190d	CH_3	OCH_3	80%
190e	CH_3	Cl	79%

The obtained carbonitriles **189a-d, 190a-e** were dissolved in dry ethanol and reacted with *N*,*N*-diisopropylethylamine (DIPEA) and hydroxylamine hydrochloride ($NH_2OH \cdot HCl$). The reaction, heated at 78 °C (reflux temperature), allowed the synthesis of derivatives **182a-e, 183a-d** in good yields (70-82%) (Scheme 4, Table 3).

Scheme 4.

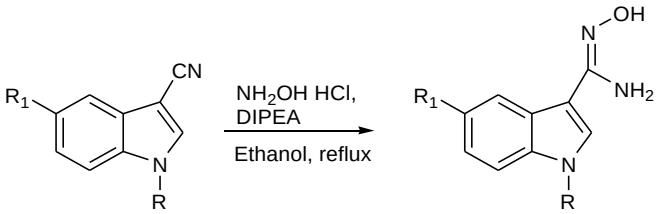

189a-d
190a-e

182a-e
183a-d

Table 3. *N*-Hydroxy-1-methyl-1*H*-indole-3-carboxamidines **182a-e** and *N*-hydroxy-1*H*-indole-3-carboxamidines **183a-d**.

Compound	R	R_1	Yield (%)
182a	CH_3	Br	72%
182b	CH_3	F	70%
182c	CH_3	H	80%
182d	CH_3	OCH_3	75%
182e	CH_3	Cl	82%
183a	H	Br	70%
183b	H	F	68%
183c	H	H	75%
183d	H	OCH_3	60%

The intermediate α-oxo-acetyl chlorides **184a-d** (Table 4) were synthesized in excellent yields (79-96%), from the methyl indole derivatives **186a-d**, obtained as previously reported in scheme 2, by acylation reaction with an excess of oxalyl chloride in diethyl ether, at 0 ° C and under nitrogen atmosphere. This intermediates were used without further purification due to the extreme sensitivity of acetyl chlorides (Scheme 5).

Scheme 5.

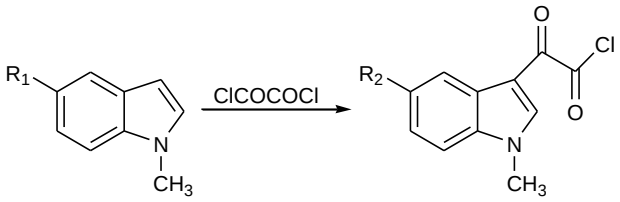

186a-d **184a-d**

Table 4. (1-Methyl-1*H*-indol-3-yl)-oxo-acetyl chlorides **184a-d**.

Compound	R_1	Yield (%)
184a	Br	88%
184b	F	93%
184c	H	79%
184d	OCH_3	80%

Once the key intermediate carboxamidines **182a-e, 183a-d** and α-oxo-acetyl-chlorides **184a-d** were obtained, they were reacted in presence of sodium hydride (NaH) as a base and dry tetrahydrofuran (THF) as reaction solvent. The reaction was heated at reflux for 3 hours.

Unfortunately, the reaction failed as the presence of degradation products, whose formation was probably due to the extreme sensitivity and reactivity of α-oxo-acetyl chlorides or to the excessive strength of the base used (NaH) (Scheme 6).

Scheme 6.

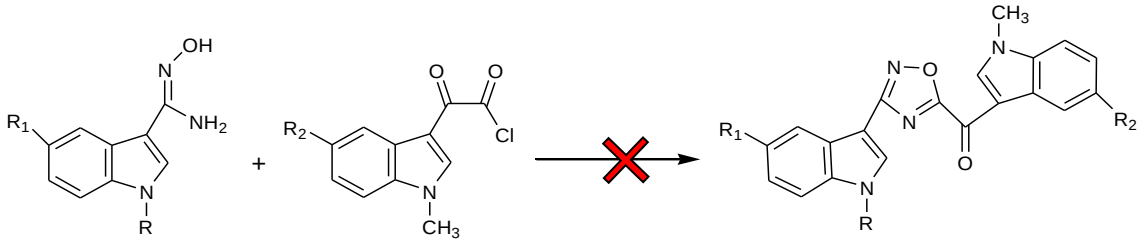

182a-e R=CH_3
183a-d R=H

184a-d

179 R=CH_3
180 R=H

On the basis of the results obtained, the synthetic pathway was changed in order to obtain the oxadiazole derivates **179, 180**, using an alternative intermediate less reactive than α-oxoacetylchloride, such as oxo-acetic acid methyl ester. The two-step synthesis of oxo-acetic acid methyl ester **191** in one-pot was accomplished in good yields (88%), by treating methyl indole precursor **186a** with oxalyl chloride at 0 °C. The α-oxo-acetyl chloride intermediate was cooled to

-65°C and then a sodium methoxide solution, 25 wt. % in methanol was added. The reaction was quenched with brine/water and the resulting precipitate was filtered off, to give the desired product **191** (Scheme 7).

Scheme 7.

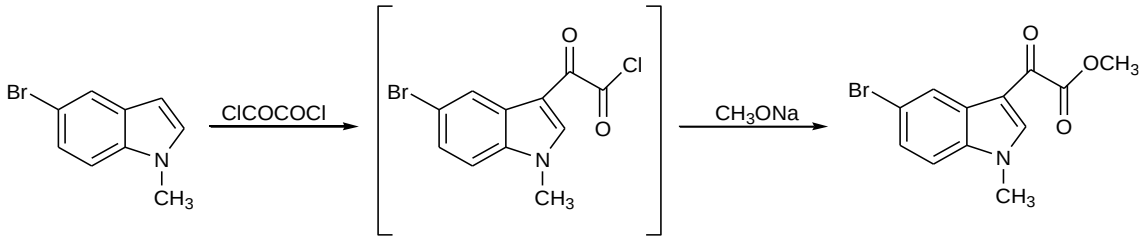

186a **191**

The oxo-acetic acid methyl ester obtained **191** was reacted with carboxamidine **182a**, using NaH as a base and THF as reaction solvent, heating at reflux overnight. Unfortunately the reaction revealed the presence of only starting materials (Scheme 8).

Scheme 8.

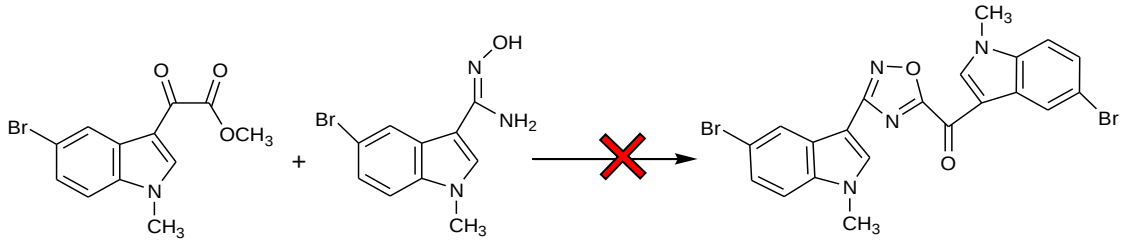

191 **182a** **179**

The same reaction was tried in different solvents such as DMF, ethanol, acetonitrile, toluene, and subsequently a mixture of THF and toluene, in order to decrease the solvation energy and to evaluate how the different reflux temperatures could influence the reaction trend. Even in these cases the outcome of the reactions was negative.

In order to overcome the problems related to the excessive strength of the base (NaH), the reaction was tried with other bases less strength than NaH, such as DIPEA, without tangible improvements.

Considering the difficulties encountered, it was thought to use an alternative method of formation of heterocyclic oxadiazole rings, reacting carboamidine with a suitably activated acid derivative. *N*-hydroxybenzotriazole (HOBt) is largely used for the generation of active esters able to efficiently acylating amino groups, especially carboxamidine.

Attention has converged on the synthesis of (1-methyl-1H-indol-3-yl)-oxo-acetic acids **192a-d**, prepared in good yields (65-90%), from α-oxo-acetyl chlorides **184a-d**, previously synthesized, by nucleophilic substitution reaction with a solution of sodium hydroxide (NaOH) 2M at room temperature (Scheme 9).

Scheme 9.

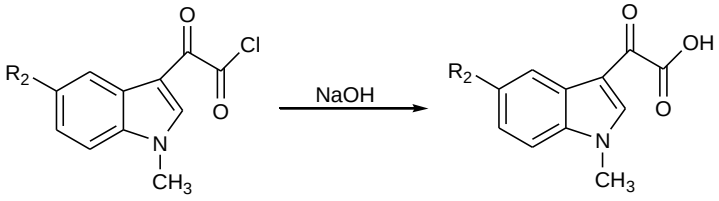

184a-d **192a-d**

Table 5. (1-Methyl-1*H*-indol-3-yl)-oxo-acetic acids **192a-d**.

Compound	R_1	Yield (%)
192a	Br	82%
192b	F	90%
192c	H	65%
192d	OCH_3	70%

The reaction between the key intermediates was performed in dry DMF and in the presence of *N*-(3-dimethylaminopropyl)-N'-ethylcarbodiimide hydrochloride (EDC) and HOBt as the coupling reagents, by following the reaction mechanism below (Scheme 10):

Scheme 10.

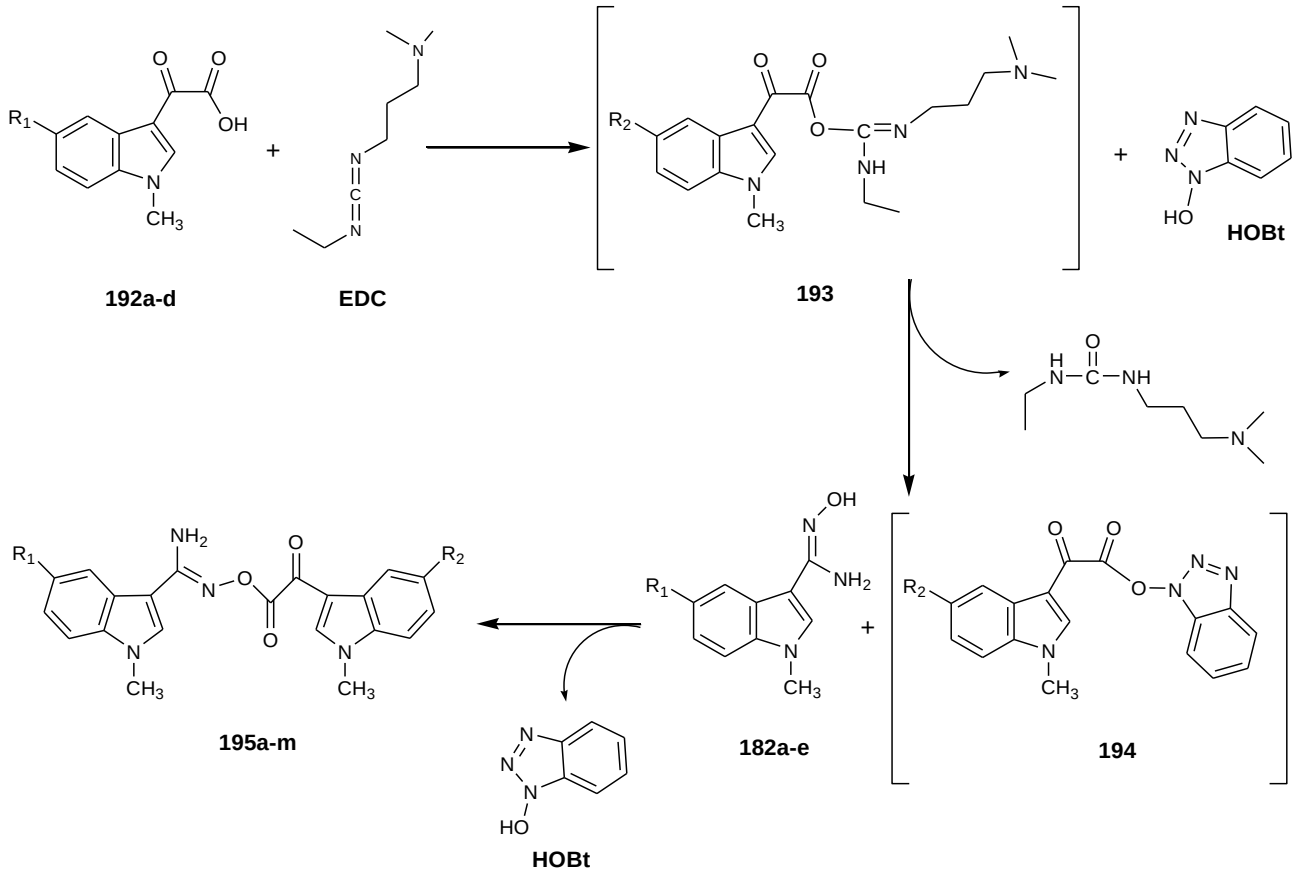

EDC reacts with the carboxylic acid group of derivates **192a-d** to form an active O-acylisourea intermediate **193** that is easily displaced by the nucleophilic attack of HOBt, mediated by its hydroxyl group, leading to the formation of an ester bond with the original carboxyl group and the release of EDC by-product as a soluble urea derivative. The active species in solution is the 1-hydroxybenzotriazole ester **194,** which enhances the reactivity of the ‘‘activated ester’’ by encouraging/stabilising the approach of the carboxamidine via hydrogen bonding.[149] In fact, in the reaction mixture, it undergoes nucleophilic substitution by carboxamidine **182a-e**.

The reaction is, therefore, catalytic in HOBt (nucleophilic catalyst) but stoichiometric in EDC, which is converted to the corresponding urea. The overall stoichiometry of the reaction therefore involves reaction of the acid, carboxamidine, and EDC to produce the derivates **195a-m** (Table 6) and the EDC-derived urea.[150] Addition of HOBt to carbodiimide-based coupling reagents (EDC) form benzotriazole active ester **194** that is less reactive than the O-acylisourea **193** formed from carbodiimides (EDC), thereby avoiding the formation of undesired derivatives.[151]

Table 6. 1-methyl-*N*'-{[(1-methyl-1*H*-indol-3-yl)(oxo)acetyl]oxy}-1*H*-indole-3-carboximidamides **195a-m**.

Compound	R_1	R_2	Yield (%)
195a	H	OCH_3	73%
195b	H	Br	80%
195c	H	H	90%
195d	Br	F	88%
195e	Br	H	87%
195f	Br	OCH_3	95%
195g	F	H	98%
195h	F	F	88%
195i	F	Br	72%
195j	F	OCH_3	70%
195k	Cl	Br	93%
195l	Cl	OCH_3	81%
195m	Cl	H	87%

Once synthesized the derivatives **195a-m**, the latter were subsequently solubilized in acetone and treated with an equimolar aqueous solution of sodium hydroxide (NaOH) 2M. The base-catalyzed cyclodehydration reaction of the key intermediates **195a-m**, performed at room temperature, led to the synthesis of derivatives **179a-m** in good yields (Scheme 11, Table 7).

It was necessary to isolate the intermediates **195a-m** due to their poor stability in the reaction mixture. Furthermore, the unusual choice of using acetone as reaction solvent depends on the solubility characteristics of intermediates **195a-m**. In fact, the reaction, carried out at room temperature and in other different organic solvents, did not provide the desired products due to the lack of solubilization of the intermediates **195a-m**.

Scheme 11.

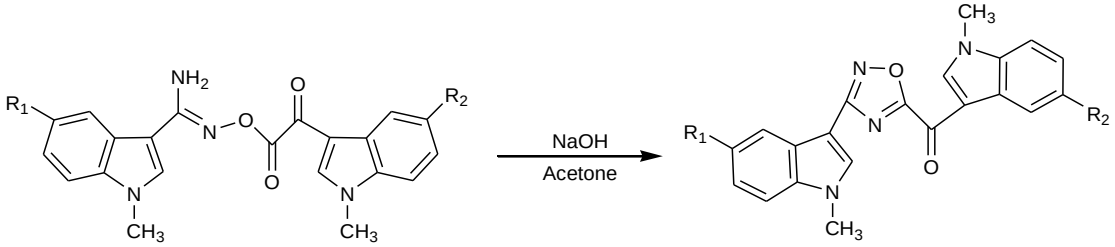

195a-m **179a-m**

Table 7. (1-Methyl-1*H*-indol-3-yl)[3-(1-methyl-1*H*-indol-3-yl)-1,2,4-oxadiazol-5-yl]methanones **179a-m**.

Compound	R_1	R_2	Yield (%)
179a	H	OCH_3	71%
179b	H	Br	63%
179c	H	H	62%
179d	Br	F	70%
179e	Br	H	67%
179f	Br	OCH_3	85%
179g	F	H	68%
179h	F	F	71%
179i	F	Br	71%
179j	F	OCH_3	86%
179k	Cl	Br	65%
179l	Cl	OCH_3	67%
179m	Cl	H	73%

For the preparation of [3-(5-methoxy-1-methyl-1*H*-indol-3-yl)-1,2,4-oxadiazol-5-yl](1-methyl-1*H*-indol-3-yl)methanones **179n-q** and [3-(1*H*-indol-3-yl)-1,2,4-oxadiazol-5-yl](1-methyl-1*H*-indol-3-yl)methanones **180a-p** attention has converged on the synthesis of carboxamidines **182d, 183a-d**, that were reacted with oxo-acetic acids **192a-d**, synthesized as previously reported (Scheme 12).

Due to the formation of a resin as degradation product and, consequently, low yields for derivatives, it was not possible to follow the previously exposed synthetic route for the derivatives **179n-q, 180a-p**.

To obtain these compounds, a different synthetic pathway is proposed. The two-step synthesis of 1,2,4-oxadiazoles **4n-q, 5a-p** in one-pot was accomplished in yields between 20–67%, by treating acid precursors **192a-d** with the corresponding carboxamidine derivatives **182d, 183a-d** in the presence of EDC·HCl and HOBt in DMF, followed by heating to 100 °C for the cyclodehydration step (Scheme 12, Table 8).

Scheme 12.

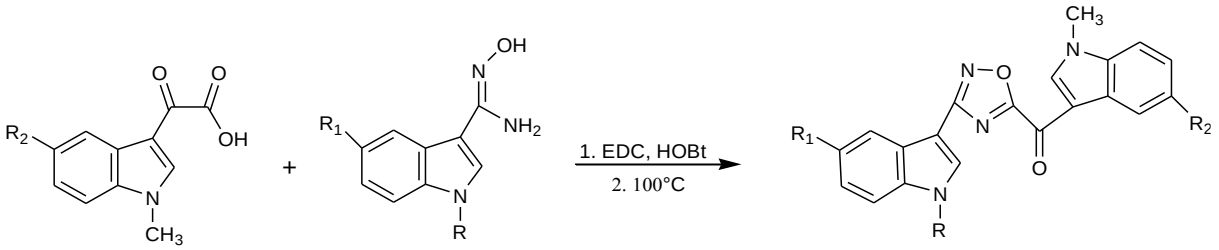

192a-d

182d R=CH_3
183a-d R=H

179n-q R=CH_3
180a-p R=H

Table 8. [3-(5-methoxy-1-methyl-1*H*-indol-3-yl)-1,2,4-oxadiazol-5-yl](1-methyl-1*H*-indol-3-yl)methanones **179n-q** and [3-(1*H*-indol-3-yl)-1,2,4-oxadiazol-5-yl](1-methyl-1*H*-indol-3-yl)methanones **180a-p**.

Compound	R_1	R_2	R	Yield (%)
179n	OCH_3	OCH_3	CH_3	20%
179o	OCH_3	Br	CH_3	30%
179p	OCH_3	F	CH_3	22%
179q	OCH_3	H	CH_3	20%
180a	H	Br	H	21%
180b	H	F	H	30%
180c	H	H	H	33%
180d	H	OCH_3	H	32%
180e	OCH_3	F	H	40%
180f	OCH_3	OCH_3	H	42%
180g	OCH_3	Br	H	35%
180h	OCH_3	H	H	34%
180i	Br	OCH_3	H	67%
180j	Br	H	H	30%
180k	Br	F	H	35%
180l	Br	Br	H	57%
180m	F	H	H	38%
180n	F	F	H	42%
180o	F	OCH_3	H	42%
180p	F	Br	H	38%

In order to increase the water solubility of the compounds and thus facilitate their pharmacological evaluation, it has been considered appropriate to introduce a nitrogen atom in position 7 of a single indole portion, that it can be became protonated at physiological pH. The initial attempt to obtain the 7-azaindolyl-oxadiazole derivates **181**, by reaction between (1-methyl-1*H*-pyrrolo[2,3-*b*]pyridin-3-yl)-oxo-acetic acid **197a-b** and carboxamidines **182a-e**, has not brought the expected results. The reaction was attempted several times, but this method produced unsatisfactory results in my hands, especially in light of the laborious work-up required for the production of oxo-acetic acid and of the low yields (Scheme 13).

Scheme 13.

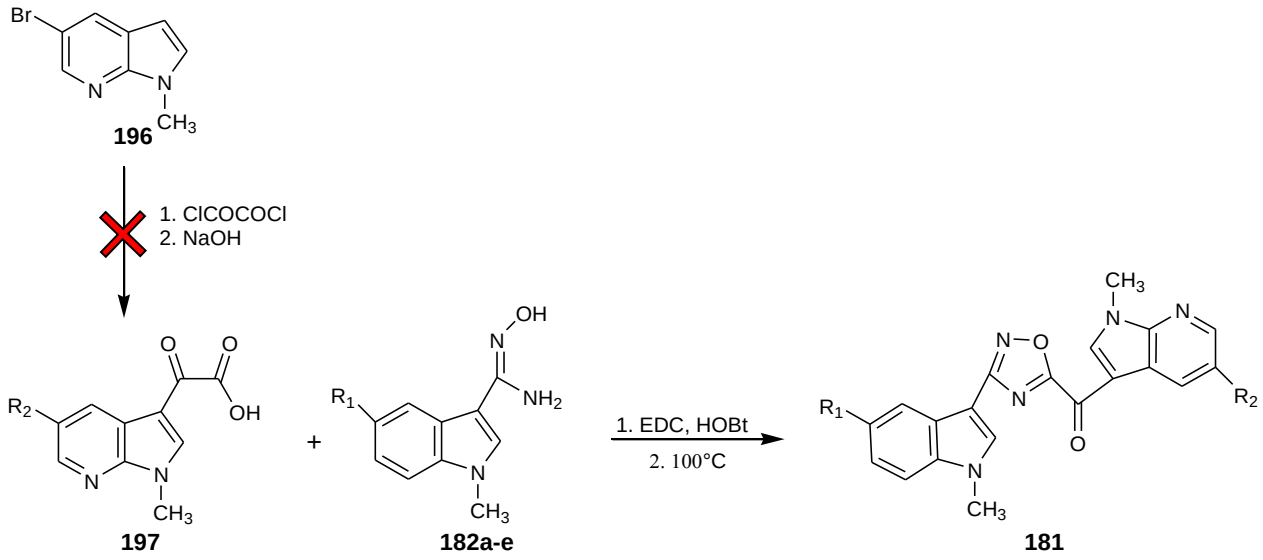

Thereupon, for the preparation of 7-azaindolyl oxadiazole compounds **181** attention has been focused on the synthesis of key intermediates **198a-b** and **182b-d**. The reaction between carboxamidines **182b-d** and (1-methyl-1*H*-pyrrolo[2,3-*b*]pyridin-3-yl)-oxo-acetic acid methyl ester **198a-b** in dimethylsulfoxide (DMSO) at room temperature for 30 minutes-1 hour gave, after purification by chromatography column, the desired 7-azaindolyl oxadiazoles **181a-f** (Scheme 14) in yields ranged from 33% to 62% (Table 9).

Scheme 14.

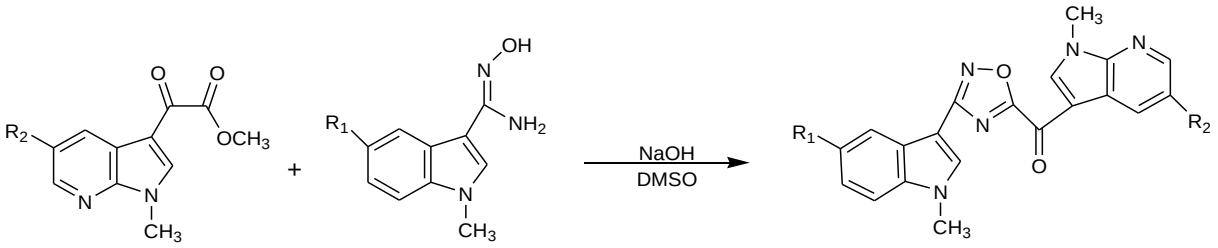

198 **182b-d** **181a-c**

Table 9. (1-Methyl-1*H*-pyrrolo[2,3-*b*]pyridin-3-yl)-[3-(1-methyl-1*H*-indol-3-yl)-[1,2,4]oxadiazol-5-yl]-methanones **181a-f.**

Compound	R_1	R_2	Yield (%)
181a	H	Br	33%
181b	F	Br	40%
181c	OCH_3	Br	62%
181d	H	H	54%
181e	F	H	45%
181f	OCH_3	H	60%

The intermediates (1-methyl-1*H*-pyrrolo[2,3-*b*]pyridin-3-yl)-oxo-acetic acid methyl esters **198a-b** were obtained with the same procedure that led to the synthesis of oxo-acetic acid methyl ester of the type **191**. In this synthetic pathway the methylindole precursor of the type **196** was reacted with an excess of oxalyl chloride and the reaction, conducted at 0°C, led to the synthesis of acetyl chloride intermediate. The latter was cooled to -65°C, using a acetone bath with immersion cooler at atmospheric pressure, and then a sodium methoxide solution, 25 wt. % in methanol was added. The reaction, using appropriate work-up, allowed to obtain the derivatives **198a-b** with yields of 32-42%, respectively. (Table 10, Scheme 15). The derivatives **196a-b** were obtained with a good yield (80-96%) through the methylation of the commercial 5-bromo-7-azaindole **199a** or 7-azaindole **199b** , using *t*- BuOK as a base, TDA-1 as phase transfer catalyst and methyl iodide as methylating agent in toluene at room temperature (Table 11, Scheme 15).

Table 10. (1-Methyl-1*H*-pyrrolo[2,3-*b*]pyridin-3-yl)-oxo-acetic acid methyl ester **198a-b.**

Compound	R_2	Yield (%)
198a	Br	32%
198b	H	42%

Table 11. 1-Methyl-1*H*-pyrrolo[2,3-*b*]pyridines **196a-b.**

Compound	R_2	Yield (%)
196a	Br	80%
196b	H	96%

Scheme 15.

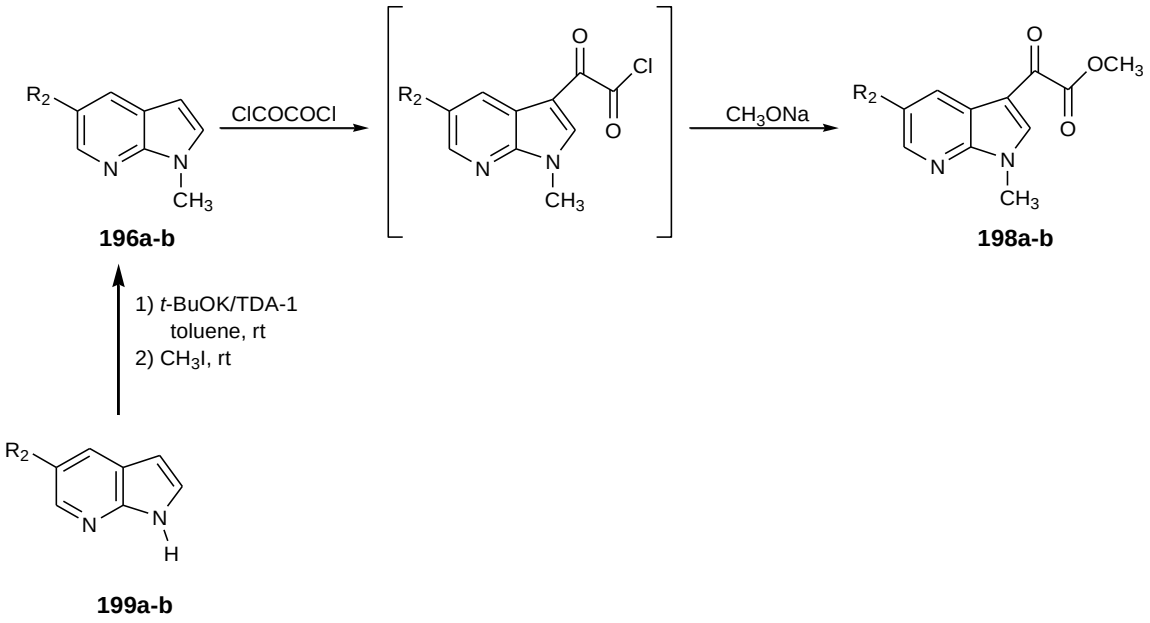

Finally, to overcame the poor water solubility of the compounds and thus facilitate their biological evaluation, it has been considered appropriate to insert a fixed morpholin-ethyl substituent in position 1 of the indole. It was thought to obtain the derivative **201** with the following synthetic strategy, by reacting the oxo-acetic acid **192a** with caboxamidines **200**, in presence of EDC·HCl and HOBt in DMF, followed by NaOH-catalyzed cyclodehydration step (Scheme 16):

Scheme 16.

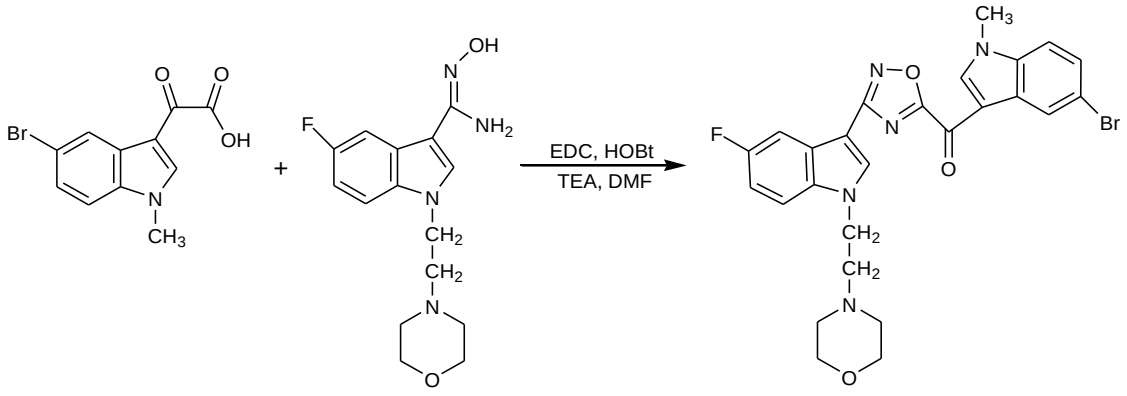

192a **200** **201**

Carboxymidamide of tipe **200** was prepared from the carbonitrile **189b**. The latter was reacted with 4-(2-chloroethyl)morpholine **203**, synthesized from a commercially available compound 4-(2-chloroethyl)morpholine hydrochloride **202**, which was solubilized in distilled water and treated with an aqueous solution of NaOH at 5%. The reaction, stirred at room temperature, allowed the synthesis of compound **203** in excellent yield (98%).[152]

The reaction between the derivates **189b** and **203** was heated to 50 °C, using NaH as the base and DMF as reaction solvent, leading to the synthesis of the intermediate **204**, with excellent yields (95%). The latter was reacted with $NH_2OH \cdot HCl$ and DIPEA (Hünig's base) in ethanol under reflux and using appropriate work-up, was synthesized the key intermediate caboxamidine **200** with yields of 68% (Scheme 17).

Scheme 17.

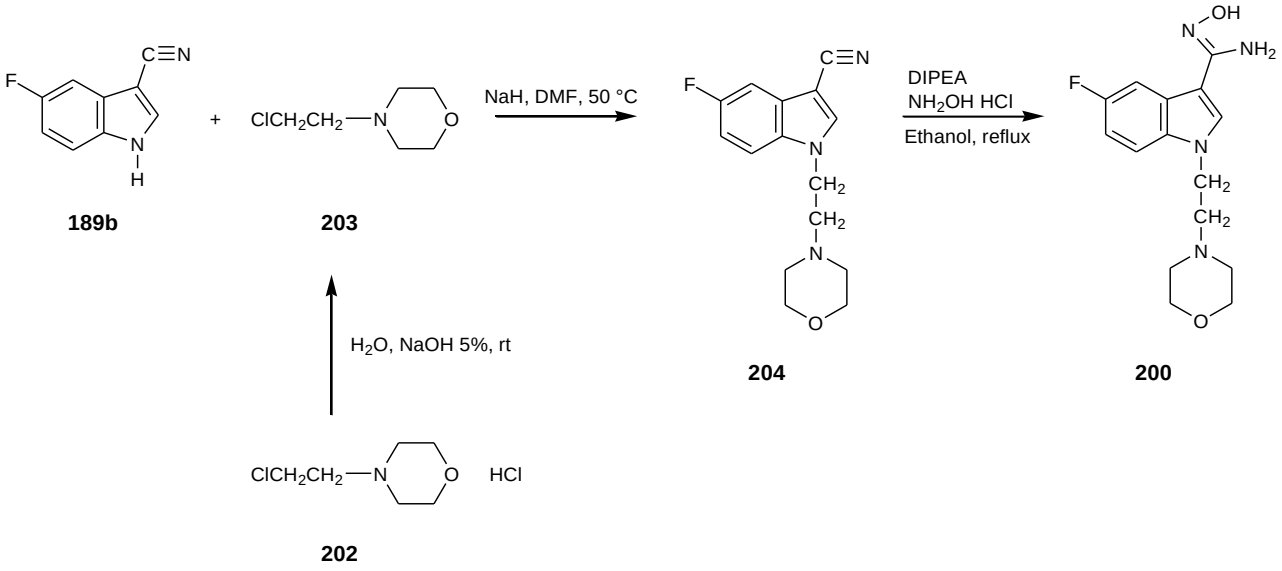

However, due to the poor solubility of the derivative **201** in DMSO-d_6 and in $CDCl_3$ it was not possible to carry out its structural characterization.

So, I decided to abandon the synthesis of this series of compounds.

4. BIOLOGY SECTION

4.1 Anti-biofilm activity

All derivatives of the type **179,180** were tested in order to evaluate their ability to inhibit the biofilm formation of the Gram-positive pathogens *S. aureus* 25923, *S. aureus* 6538 and *S. epidermidis* 12228 and of the Gram-negative pathogens *P. aeruginosa* 15442 and *E. coli* 25922.

All derivates showed a greater selectivity against the Gram-positive pathogen *S. aureus* 25923 and Gram-negative pathogen *P. aeruginosa* 15442, for which the percentages of inhibition of biofilm formation were found between 12.4% and 69.8%.
For the compounds that showed a percentage of inhibition of biofilm formation higher than 20%, the 50% inhibitory concentrations (IC_{50}s) were therefore evaluated. The results obtained are shown in Table 11.

The compounds were particularly active in inhibiting the formation of biofilms of Gram-positive pathogens *S. aureus* 25923, showing IC_{50} between 0.27 μg/mL and 19.1 μg/mL. In particular, the derivatives **179h** and **180n** were able to inhibit the formation of the biofilm reporting, respectively, IC_{50} values of 0.27 and 0.9 μg/mL.
Against Gram-positive pathogen *S. epidermidis* 12228, the compound **180g** showed the best result with IC_{50} value of 9.8 μg/mL.
Conversely, no significant activity was observed against Gram-positive strain *S. aureus* 6538.
Against Gram-negative pathogen *P. aeruginosa* 15442, the most active compounds **179g** and **179j** showed IC_{50} values of 9 μg/mL and 4.7 μg/mL, respectively.
In general, the oxadiazole derivatives of the type **179**, bearing a methyl group at the indole-N-atom, were more active than those of the type **180**, bearing a proton at the indole-N-atom, against Gram-positive biofilm formation. On the other hand, the oxadiazole derivatives of the series **180** were more active than those of the series **179**, in inhibiting Gram-negative biofilm formation. In fact, the highest potency against *E. coli* 25922 was observed for the compounds **180b**, **180l** and **180m**, whose IC_{50} values were 12.6 μg/mL, 13.4 μg/mL and 14.1 μg/mL, respectively.

The increased selectivity found for Gram-positive pathogens and the inhibitory activities toward sortase A (SrtA) of topsentin, the lead compound of these new oxadiazole derivatives, reinforces our hypothesis of an inhibition mechanism that could involve the inhibition of the transpeptidase activity of SrtA.

So, in order to evaluate the potential ability of the most promising anti-staphylococcal compounds to inhibit sortase A, further assays are in progress.

Table 10. Percentages of inhibition of biofilm formation at the screening concentration of 10 µg/mL.

Compound	% of inhibition of biofilm formation at 10µg/mL				
	***S. aureus* 25923**	***S. aureus* 6538**	***S. epidermidis* 12228**	***P. aeruginosa* 15442**	***E. coli* 25922**
179a	51.1	-	26.5	50.6	21.4
179b	41.6	-	-	44.9	28.8
179c	57.4	26.1	-	44.5	23.4
179d	58.6	-	-	-	-
179e	-	-	-	43.6	-
179f	43.5	-	-	-	-
179g	45.9	-	-	53.7	-
179h	60.3	15.6	-	43.8	15.6
179i	45.8	-	32.6	-	25.6
179j	38.8	-	-	53.9	-
179k	44.5	-	-	35.7	-
179l	-	-	-	17.4	-
179m	39.7	-	-	35.0	21.3
179n	69.2	-	-	44.3	-
179o	49.6	15.4	-	34.1	-
179p	60.3	-	-	23.2	-
179q	18.7	-	14.2	34.9	-
180a	54.9	-	-	31.0	-
180b	69.8	-	-	20.1	42.9
180c	36.3	28.8	-	8.6	-
180d	46.9	15.4	27.6	12.3	-
180e	36.1	53.5	-	4.0	68.9
180f	60.5	39.9	-	26.3	73.8
180g	-	-	51.7	36.5	-
180h	-	-	13.7	-	-
180i	50.2	-	-	44.7	-
180j	31.3	29.8	-	13.3	-
180k	3.9	27.8	-	-	-
180l	54.7	-	12.6	40.6	38.1
180m	67.4	25.3	-	22.1	76.4
180n	-	27	-	-	67.7
180o	24.6	43.7	-	-	46.6
180p	36.3	26.1	-	21.4	-

Table 11. Results of the analysis of the half maximal inhibitory concentration (IC_{50}), as a measure of the potency of a substance in inhibiting biofilm formation.

Compound	IC_{50} [µg/mL]				
	***S. aureus* 25923**	***S. aureus* 6538**	***S. epidermidis* 12228**	***P. aeruginosa* 15442**	***E. coli* 25922**
179a	12.8	-	30.5	11.6	21.4
179b	17.2	-	-	17.1	17.1
179c	5.0	19.1	-	13.1	25.7
179d	4.4	-	-	-	-
179e	-	-	-	34.2	-
179f	19.1	-	-	-	-
179g	11.4	-	-	9.0	-
179h	0.27	-	-	19.5	-
179i	13.4	-	18.7	-	20.7
179j	16.0	-	-	4.7	-
179k	13.0	-	-	25.3	-
179l	-	-	-	-	-
179m	18.6	-	-	20.9	23.3
179n	0.9	-	-	31.1	-
179o	8.9	-	-	13.1	-
179p	6.0	-	-	21.1	-
179q	-	-	-	18.3	-
180a	3.8	-	-	20.0	-
180b	6.5	-	-	25.5	12.6
180c	-	-	-	-	-
180d	-	-	22.4	-	-
180e	-	95.1	-	-	72.3
180f	24.0	-	-	-	18.9
180g	-	-	9.8	13.0	-
180h	-	-	-	-	-
180i	8.8	-	-	38.8	-
180j	-	-	-	-	43.6
180k	-	-	-	-	37.8
180l	7.8	-	-	13.4	13.4
180m	40.3	-	-	-	14.1
180n	-	-	-	-	52.7
180o	-	-	-	-	>100
180p	-	-	-	-	-

4.2 Anti-proliferative activity

All synthesized oxadiazoles **179, 180** were submitted to the National Cancer Institute (NCI, Bethesda MD) in order to evaluate their antiproliferative activity.

All derivates were selected, according to the NCI protocol, for the *in vitro* disease-oriented antitumor one dose screening (10^{-5} M) against a panel of about 60 human tumor cell lines derived from 9 human cancer cell types, grouped in disease sub-panels. The full NCI 60 cell panel included five leukemia cell lines, nine non-small cell lung cancer cell lines, seven colon cancer cell lines, six central nervous system cancer cell lines, eight melanoma cell lines, six ovarian cancer cell lines, eight renal cancer cell lines, two prostate cancer cell lines and breast cancer cell lines (including one with P-glycoprotein overexpression).
Initially, the only growth percentages were calculated. The One-dose data was reported as a mean graph of the percent growth of treated cells. The number reported for the One-dose assay is growth relative to the no-compound control, and relative to the time zero number of cells. This allows detection of both growth inhibition (values between 0 and 100) and lethality (values less than 0). For example, a value of 100 means no growth inhibition. A value of 30 would mean 70% growth inhibition. A value of 0 means no growth during the experiment. A negative value means lethality. A value of -100 means all cells are dead.

Among all submitted oxadiazoles, compounds **180b, 180c** and **180l** showed the best results, with mean growth percent values of 38.68%, 61.64% and 68.04%, respectively.
The compounds **180b** and **180l** were selective against the leukemia subpanel, if compared to those obtained for other subpanels, with mean growth percent values of 20.24% and 57.36%, respectively, and significant antiproliferative effect against SR cell line for the compound **180l** (growth percent value of 6.41%) and against HL-60 (TB) cell line for the compound **180b** (growth percent value of -6.73%). Instead, the compound **180c** was selective against the colon cancer subpanel with a mean growth percent value of 41.26%. The most sensitive cell line of this subpanel was KM12, reaching a growth percent value of 21.92%.

The compound **180b** showed significant antiproliferative effect in a wide range of human tumor cell lines. Against non-small cell lung cancer subpanel this compound reported a mean growth percent value of 43.54%. The most sensitive cell line of this subpanel was NCI-H522, showing one of the lower growth percent values (2.36%). Moreover, it resulted significant active against colon cancer subpanel with mean growth percent value of 31.45%. For instance, the compound **180b** reduced *in vitro* the proliferation of HT29 human colorectal cancer cells by 91.2%.

Furthermore, the compound **180b** resulted active against the CNS cancer subpanels (mean growth percent value of 33.39%), showing the best result against SF-295 cell line (growth percent value of 20.74%). This compound has been proven to show cytotoxic effects also toward MDA-MB-435 melanoma cancer cells, for which negative growth percent value was recorded (-19.13%). The % viability of OVCAR-3 (ovarian cancer), A498 (renal carcinoma), PC-3 (prostate cancer), as well as MCF-7 (breast cancer) cells decreased after treatment with **180b**, and these effects ranged from 0.72 to 41.87 percent of growth on all types of cancer cells (Figure 3).

The compound **180c** resulted active against the melanoma cancer subpanels, showing the best growth percent values against MDA-MB-435 (7.96%) and SK-MEL-5 (16.84%) cell lines. This compound has been proven to show cytotoxic effects toward MDA-MB-468 breast cancer cells, for which negative growth percent value was recorded (-4.38%). It showed also activity against human ovarian cancer subpanel; in particular, it resulted significant active against IGROV1 and OVCAR-3 cell lines, with growth percent values of 25.69% and 12.83%, respectively. The compound was active against the leukemia subpanel with significant antiproliferative effects against K-562 (37.87%) and SR (44.12%) cell lines. Among the non-small cell lung cancer subpanel, it showed the best result against NCI-H460 cell line, with a growth percent value of 35.19% (Figure 4).

The compound **180l** showed significant cytotoxic effect in a wide range of human tumor cell lines with different negative growth percent values (e.g. -0.34% for OVCAR-4 of the ovarian cancer subpanel and -2.17% for SW-620 of colon cancer subpanel). Moreover it resulted significant active against prostate cancer subpanel with mean growth percent value of 21.20%. The most sensitive cell line of this subpanel was DU-145, showing the lowest growth percent value (3.08%). However this compound showed also activity against NCI-H460 human non-small cell lung cancer cell line, with mean growth percent value of 12.46% (Figure 5).

Based on the NCI results obtained, it was possible to draw some rational conclusions about structure activity relationships (SAR). In general, the presence of halogen atom in position 5 of the indole ring plays an important role for the cytotoxicity. Compound **180b**, with a fluorine atom in position 5, exhibited an increased activity compared to derivative **180c** without halogen atom. The 5,5'-dibrominated compound **180l** showed a greater anti-proliferative activity than 5'-brominated derivative **180j**. On the other hand, the presence of the methoxyl group in position 5 of one or both indole portions reduced or cancelled the antiproliferative activity. Similarly, the introduction of a methyl group in the indole moiety lead to (*N*-methylindolyl)-oxadiazoles **179** in which we observe a decrease of the activity against most cell lines.

Figure 3. One dose mean graph of **180b**.

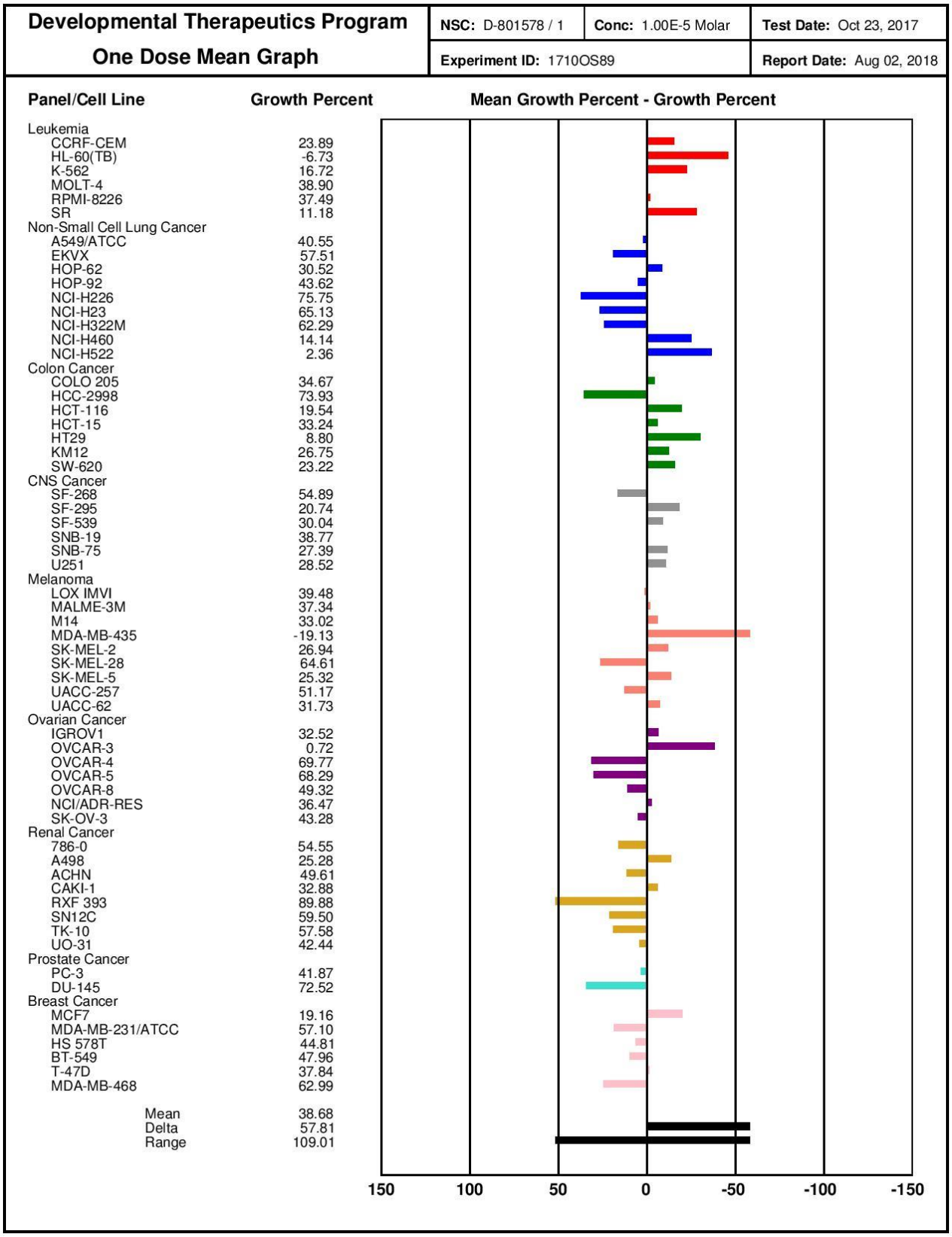

Figure 4. One dose mean graph of **180c**.

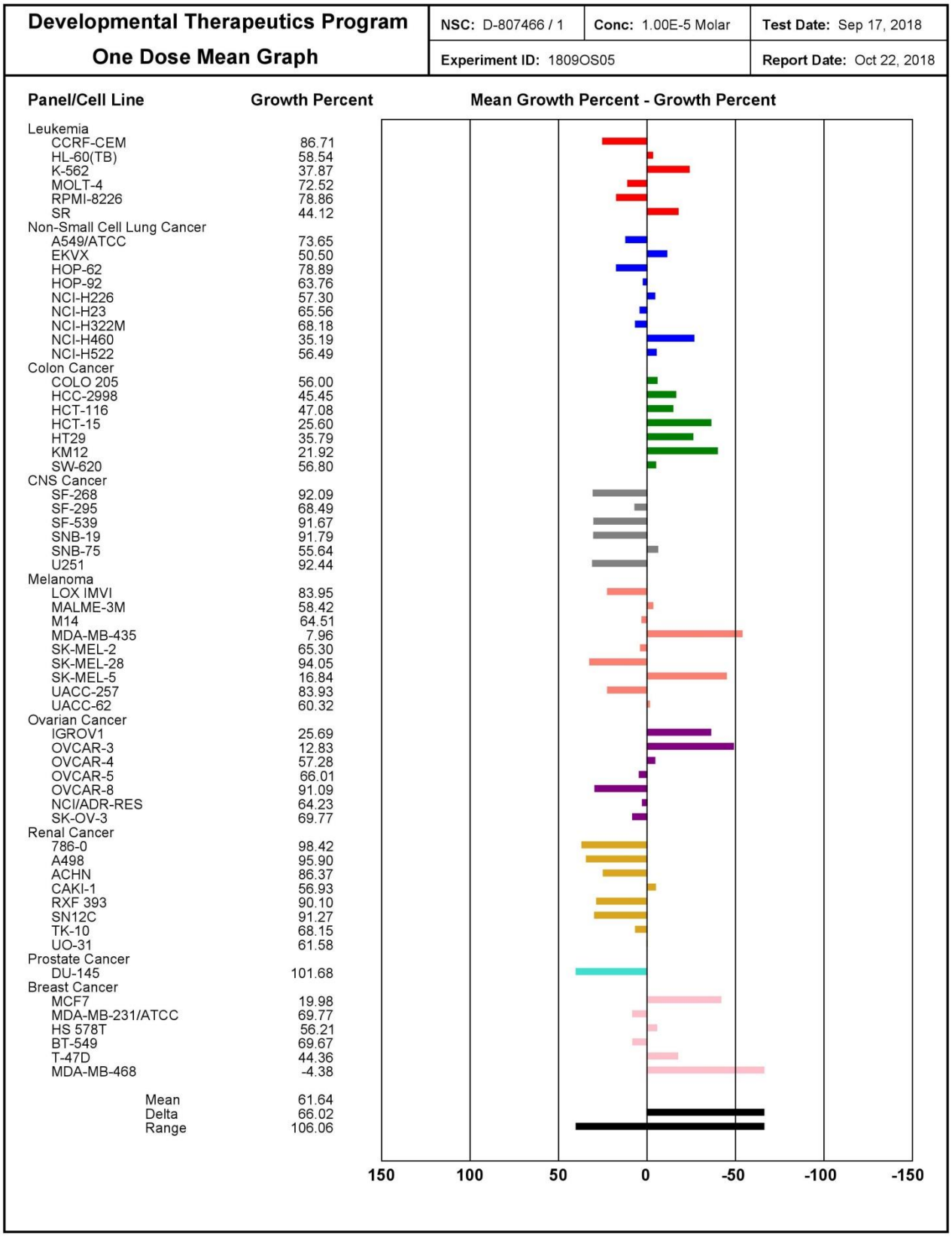

Figure 5. One dose mean graph of **180l**.

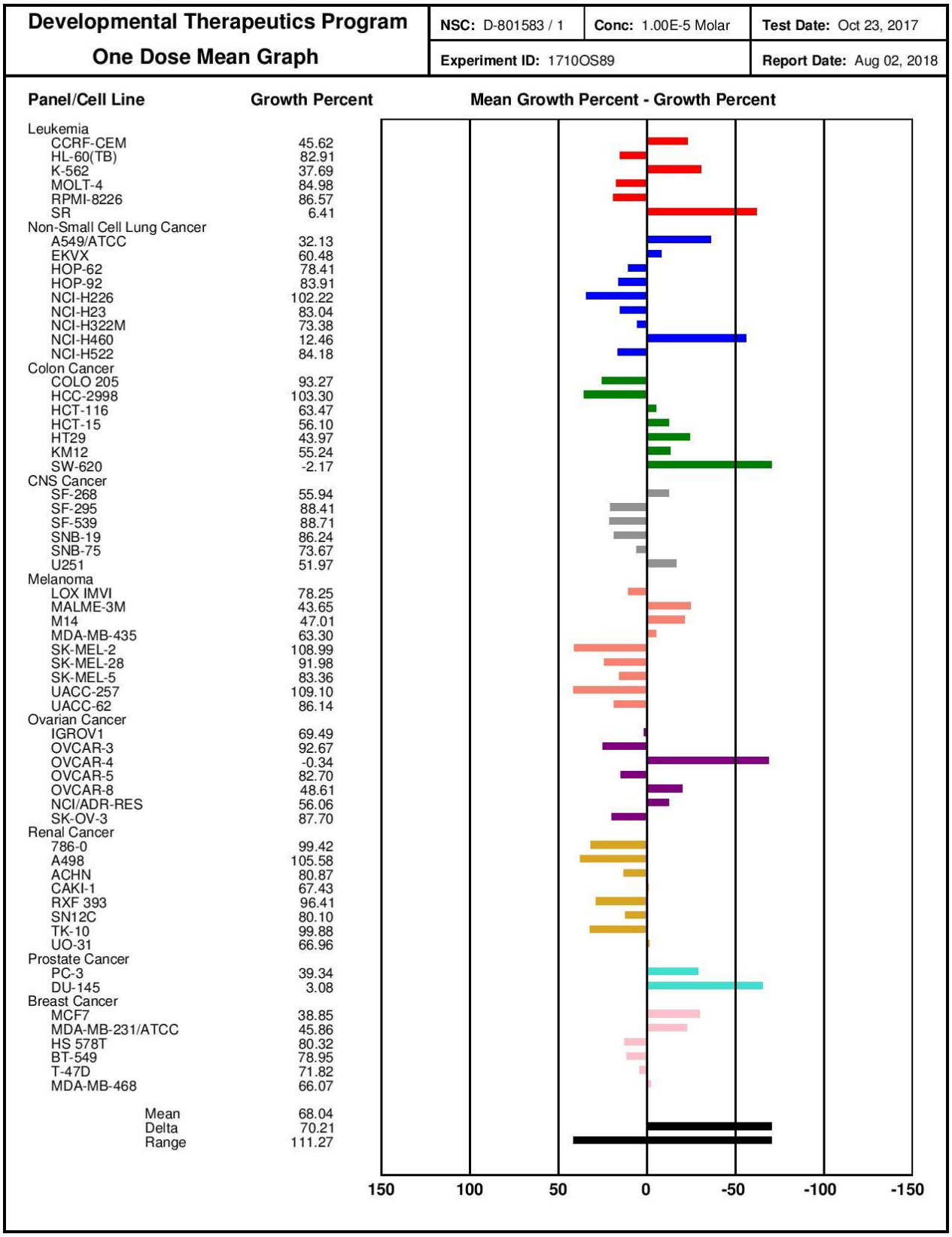

During the third year of my PhD, I spent 3 months at the Cancer Center Amsterdam, under the supervision of Prof. Elisa Giovannetti, where I evaluated the antiproliferative activity of the most promising antitumor compounds, chosen based on the NCI results obtained, using three additional cell lines, SUIT-2, CAPAN-1 and PANC-1, derived from human pancreatic cancer, a tumour type not included in the NCI panel.

SUIT-2 is a cell line derived from a metastatic liver tumour of human pancreatic carcinoma. SUIT-2 cell line produces and releases at least two tumour markers, carcinoembryonic antigen and carbohydrate antigen 19-9.[153] Under an electron microscope, they appear to be morphologically heterogeneous (i.e., both fusiform and polygonal, Figure 6A). Cells were cultured in Roswell Park Memorial Institute (RPMI) supplemented with 10% FBS and 1% Pen/Strep in T-75 flasks.

CAPAN-1 cells are adherent epithelial-like cells derived from a liver metastasis of a pancreatic adenocarcinoma that grown in tissue culture appeared as large epithelial-like mucin-producing cells. They are characterized by large, relatively dark stained nuclei and abundant slightly basophilic, finely granular, reticulated or vacuolated cytoplasm (Figure 6B).[154,155] Cells were cultured in Dulbecco's Modified Eagle Medium (DMEM) supplemented with 10% fetal bovine serum and 20 mM (1%) HEPES in T-75 flasks.

PANC-1 is an epithelioid carcinoma attached cell line, that is commonly used as an *in vitro* model to study pancreatic ductal adenocarcinoma carcinogenesis and tumour therapies, especially in light of the presence of presence of the SSTR2 receptors, prognostic marker in pancreatic cancer.[156,157,155] PANC-1 cells appear to be morphologically heterogeneous (i.e., both cuboid and focally sarcomatoid) and typically display a perinuclear Golgi, scattered or apically localized cytoplasmic vesicles, and a large number of apical plasma membrane microvilli (Figure 6C).[158,159] PANC-1 cells were cultured in Dulbecco's Modified Eagle Medium (DMEM) supplemented with 10% fetal bovine serum and 20 mM (1%) HEPES in T-75 flasks.

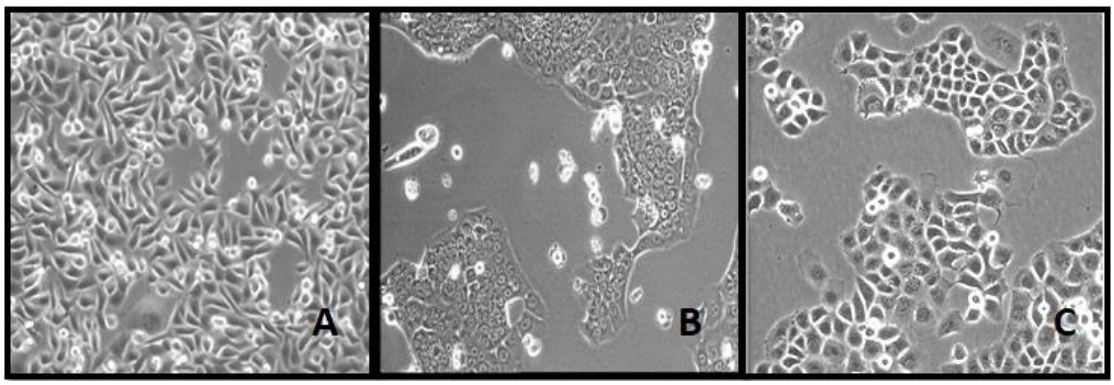

Figure 6. Microscopic observation of SUIT-2 (A), CAPAN-1 (B) and PANC-1 (C) cells.

All the cells were maintained under conditions where they are actively growing and undergoing mitotic division, in a humidified incubator at 37°C with a supply of 5% CO_2/95% air atmosphere and 100% relative humidity.

Each compound was initially dissolved in dimethyl sulfoxide (DMSO), in order to obtain 10 mM stock solution, stored at +4 °C, which was then diluted in complete culture medium immediately before use at the appropriate concentration.

Cells were exposed to three screening concentrations (0.1 μM, 1 μM, 10 μM) of each compound for 72 hours, and the amount of proliferation was then determined by the sulforhodamine B (SRB) chemosensitivity assay.

The sulforhodamine B (SRB), a pink anionic amino xanthene protein dye with two sulfonic groups, has been used to the quantification of cellular proteins content of adherent cultures (Figure 7). Its distribution and its ability to bind biological components, such as cellular proteins, within and between biological cell (histochemistry) is similar to that of related dyes, such as Coomassie brilliant blue[154], naphthol yellow S[154], and bromophenol blue[160], which are widely used as protein stains.

The SRB assay is based on the property of SRB, which binds stoichiometrically, by electrostatic complex formation, to basic amino acid residues of proteins under mild acidic conditions and then can be extracted using basic conditions. This molecule is UV active and the quantification of the dye bound to the cells at 492 nm, provides an estimate of total protein mass, which is related to viable cell number. In other words, the greater the viable cell number, the greater is the amount of dye responsible for more intense colour and greater absorbance.

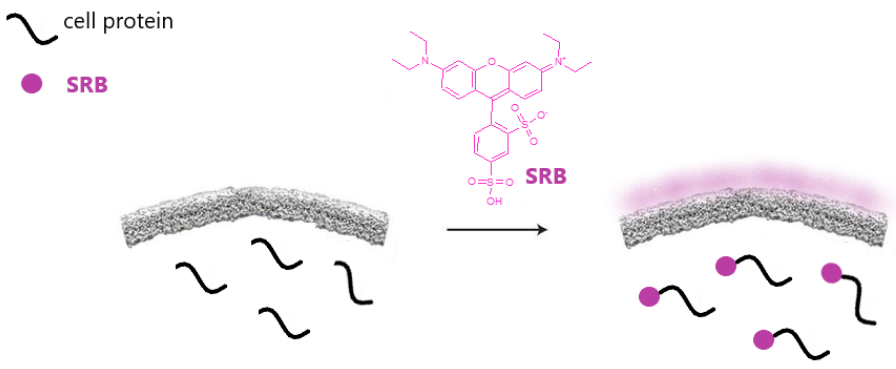

Figure 7. Schematic representation of the chemical structure and key features of SRB as an indicator of cell viability.

Graphs in the figure 8 show the growth inhibition effects of compounds **180b** (A), **180c** (B), **180i** (C), **180j** (D) and **180l** (E), as single agent in PDAC cells. Results showed that only some concentrations of them impaired the growth of both experimental models of pancreatic cancer.

At concentration of 0.1 μM all compounds did not appreciably impair vitality of pancreatic cancer cells, while at concentration of 10 μM all compounds showed antiproliferative activity. In particular, the compound **180b** was selective against the SUIT-2 pancreatic cells, if compared to the other cells, with a mean growth percent value of 18.97%.

The compound **180c** did not determine a noteworthy inhibition of growth in the PANC-1 cell line. However, it resulted significantly active against the SUIT-2 cells, with mean growth percent value of 27.09%. Of note, the compound **180i** has been proven to have cytotoxic effects toward CAPAN-1 pancreatic cancer cells, for which we observed a negative growth percent value (-5.62%).

Our studies demonstrated also that **180j** reduced the proliferation of all pancreatic cells at concentration of 10 μM. Anyway, the most sensitive cell line of our pancreatic panel to this compound was CAPAN-1 in which one of the lowest growth percent value was reached (19.63%).

The % viability of SUIT-2, CAPAN-1 and PANC-1 cells decreased after treatment with the compound **180l** at concentration of 10 μM, and these effects ranged from -0.04 to 34.31 percent of growth (Figure 8).

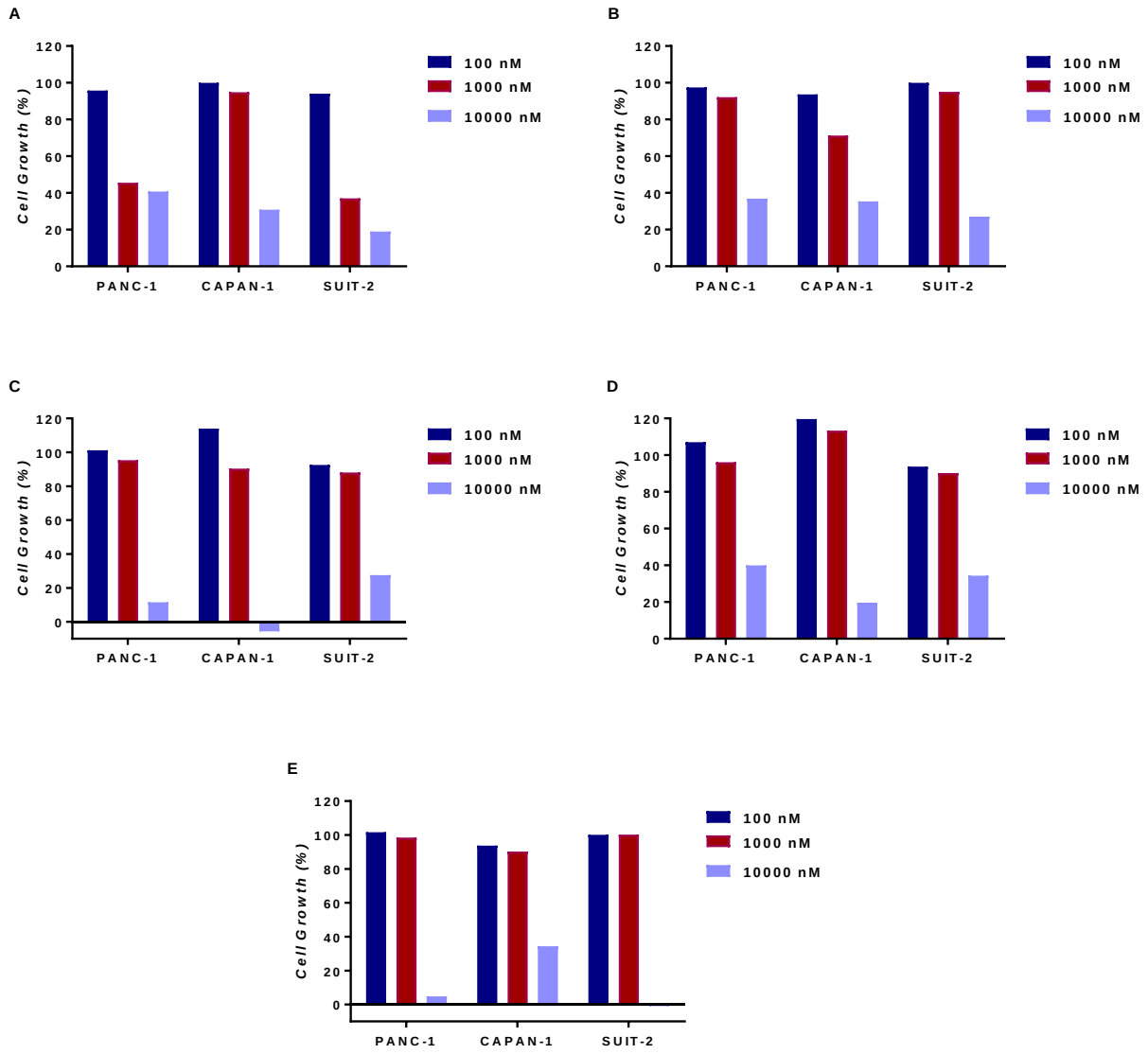

Figure 8. Cell growth data for compounds **180b** (A), 1**80c** (B), **180i** (C), **180j** (D) and **180l** (E) using a panel of pancreatic cancer cell lines, measured by the SRB Assay for 72 h exposure and expressed as percentage of cell growth.

SRB assays have been performed again in order to further verify the EC_{50} values of these five compounds. Cells were exposed to nine increasing concentrations (from 0.1 μM to 40 μM) of each compound for 72 hours. The antitumor activity of compounds was measured, using the EC_{50} value which is defined as the molar concentration of a compound where 50% of its maximal effect is observed. For EC_{50} determination, a dose-response curve between the compounds' concentration and percent growth inhibition has been plotted. EC_{50} values have been derived using a non-linear regression analysis and curve fitting parameter with the analysis software GraphPad Prism. Error bars of dose-response curves represent the standard deviation of three replicates.

Dose-dependent studies revealed that SUIT-2 cells were the cells more sensitive to **180b**; against these pancreatic cancer cells **180b** showed the highest potency with an EC_{50} value below 0.5 μM (0.403 μM). This compound showed antitumor activity also against PANC-1 and CAPAN-1 cells, but with higher EC_{50} values (0.779 and 1.190 μM, respectively, Figure 9).

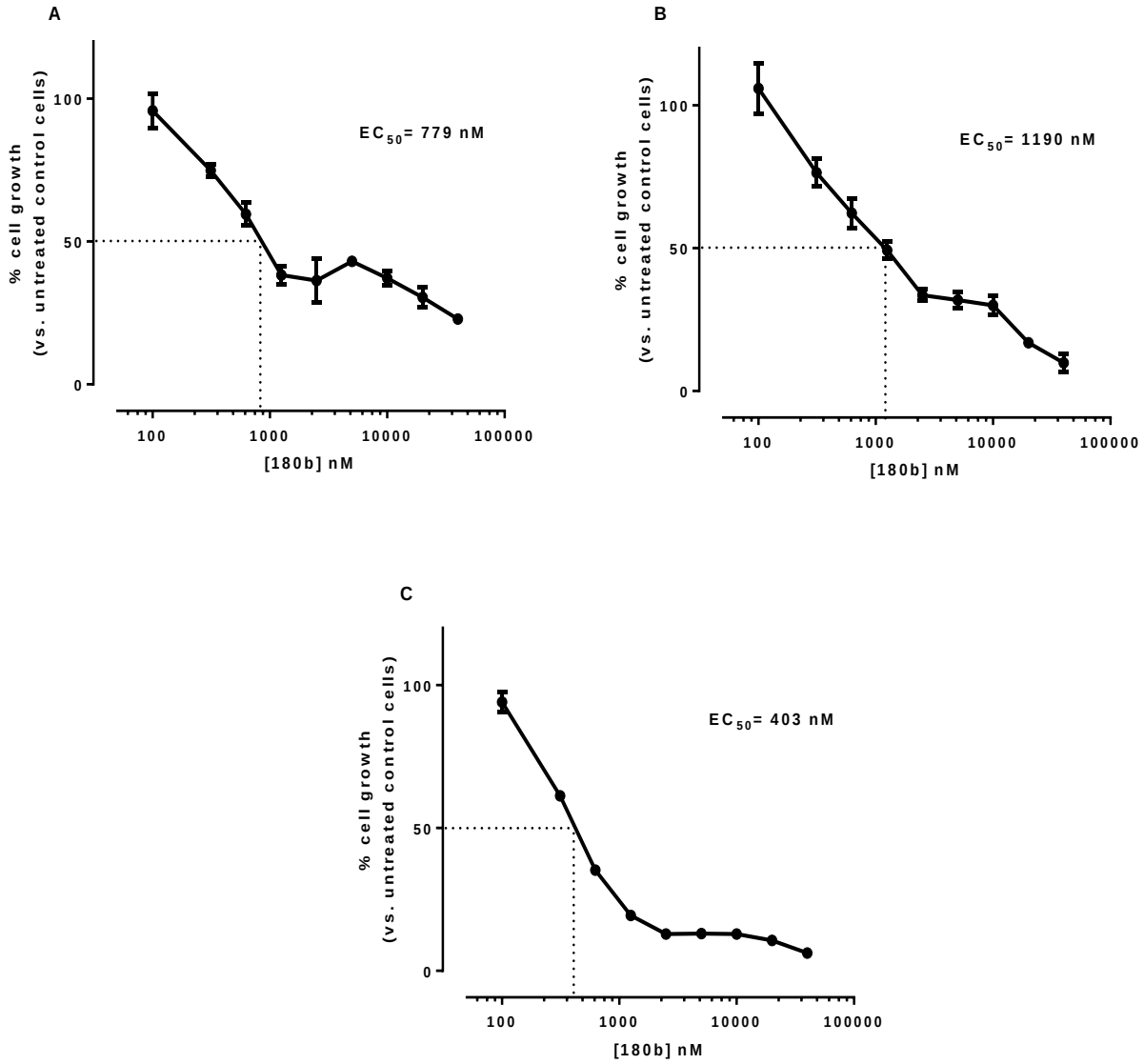

Figure 9. Effect of **180b** on the viability of PANC-1 (A), CAPAN-1 (B) and SUIT-2 (C) pancreatic cell lines. Cells were treated with nine different concentration of the compound and cell survival was measured after 72 h by SRB assay in comparison to untreated control cells. Values are reported as the mean ± SD of three separate experiments in triplicate.

The compound **180c** showed the most notable anti-proliferative activity against CAPAN-1 (EC_{50} = 1.3 μM) and PANC-1 (EC_{50} = 1.6 μM); whereas in SUIT-2 it showed a lower anti-proliferative potency (EC_{50}= 3.2 μM, Figure 10).

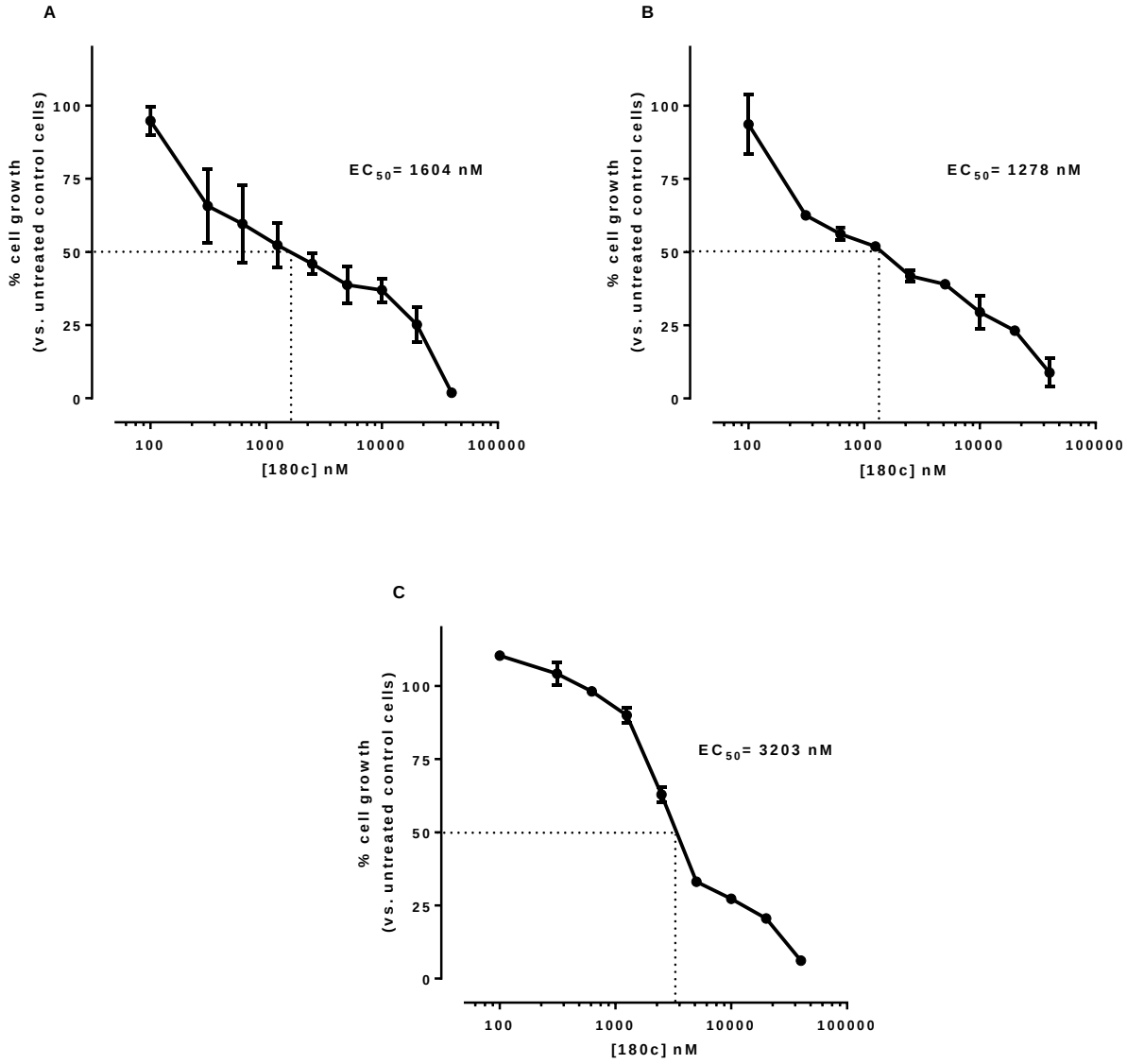

Figure 10. Effect of **180c** on the viability of PANC-1 (A), CAPAN-1 (B) and SUIT-2 (C) pancreatic cell lines. Cells were treated with nine different concentration of the compound and cell survival was measured after 72 h by SRB assay in comparison to untreated control cells. Values are reported as the mean ± SD of three separate experiments in triplicate.

The compound **180i** was reported to be most active against CAPAN-1 and PANC-1 cancer cell lines, with the EC_{50} values ranging from 2.7 to 2.8 μM, while a weak antiproliferative activity was observed against SUIT-2 cell line (EC_{50} = 7.1 μM, Figure 11).

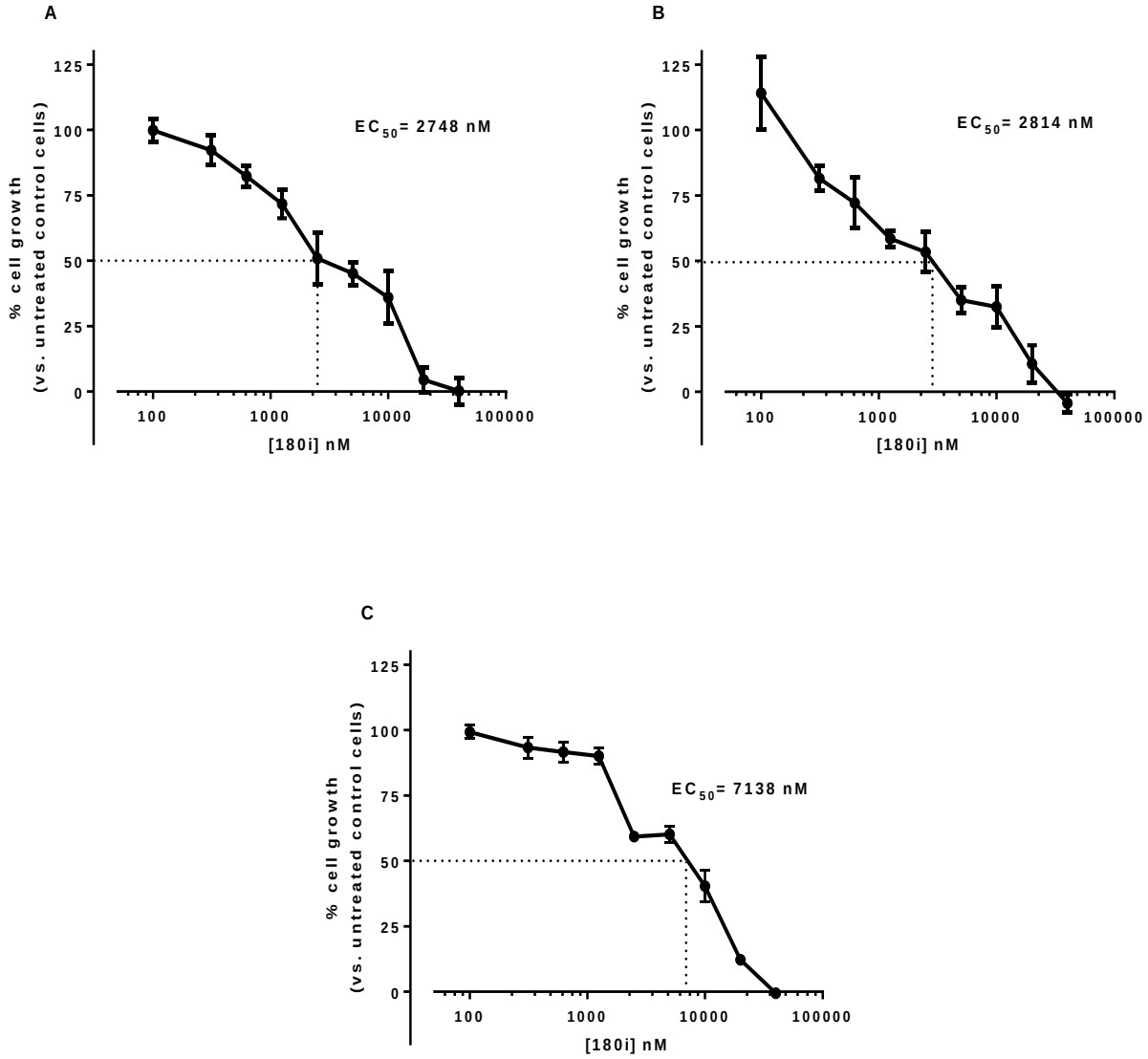

Figure 11. Effect of **180i** on the viability of PANC-1 (A), CAPAN-1 (B) and SUIT-2 (C) pancreatic cell lines. Cells were treated with nine different concentration of the compound and cell survival was measured after 72 h by SRB assay in comparison to untreated control cells. Values are reported as the mean ± SD of three separate experiments in triplicate.

The compound **180j** proved to have a more potent anti-proliferative activity against CAPAN-1 (Figure 12B) than against PANC-1 (Figure 12A) and SUIT-2 (Figure 12C) cell lines. However, this compound had EC_{50} values at higher micromolar levels (EC_{50} values at 72 hours ranging from 5.9 μM to 6.7 μM).

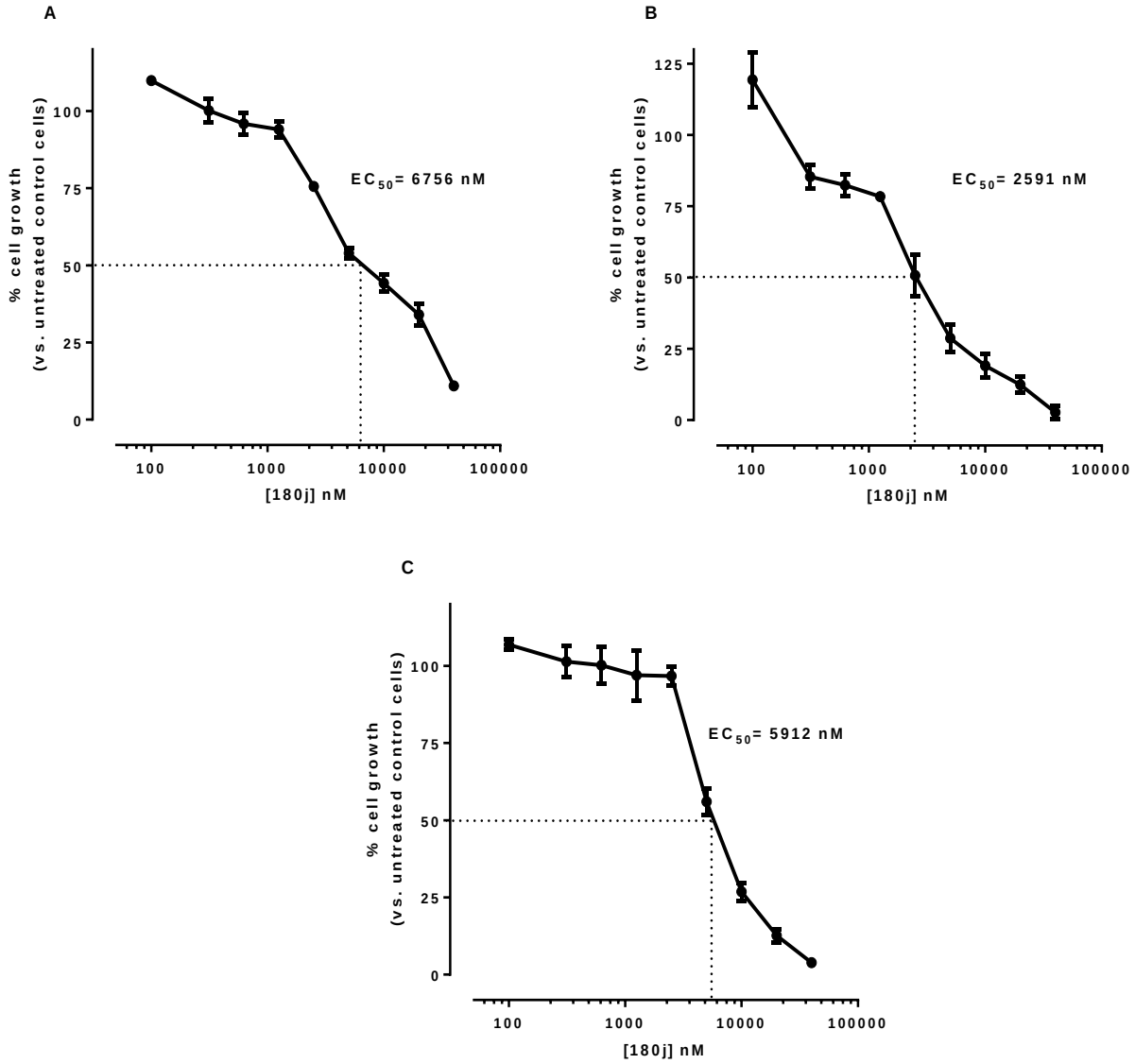

Figure 12. Effect of **180j** on the viability of PANC-1 (A), CAPAN-1 (B) and SUIT-2 (C) pancreatic cell lines. Cells were treated with nine different concentration of the compound and cell survival was measured after 72 h by SRB assay in comparison to untreated control cells. Values are reported as the mean ± SD of three separate experiments in triplicate.

The compound **180l** showed comparable antiproliferative activity against PANC-1, CAPAN-1 and SUIT-2 cells, with EC_{50} values of 1.51 μM, 1.41 μM and 1.91 μM, respectively (Figure 13).

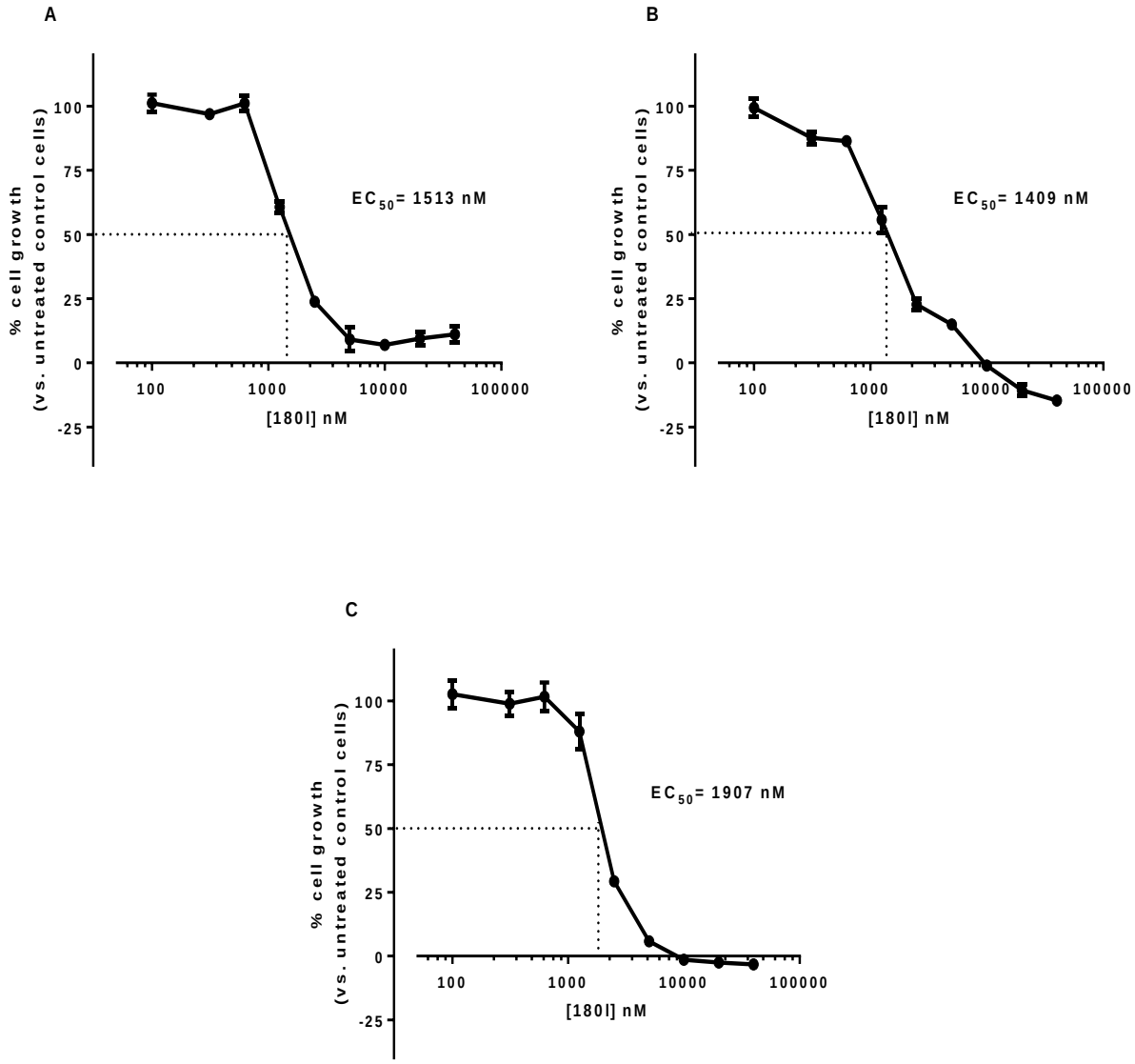

Figure 13. Effect of **180l** on the viability of PANC-1 (A), CAPAN-1 (B) and SUIT-2 (C) pancreatic cell lines. Cells were treated with nine different concentration of the compound and cell survival was measured after 72 h by SRB assay in comparison to untreated control cells. Values are reported as the mean ± SD of three separate experiments in triplicate.

To sum up, an evaluation of the data reported in Table 12 points out that all derivatives resulted active from nanomolar to micromolar concentrations, against all of tested cell lines, as it has been confirmed by the range of EC_{50} values, from 0.4 to 7.14 μM.

Table 12. Summary of the antiproliferative activity of oxadiazole derivatives in pancreatic cancer cells.

Compound	EC_{50} (μM)[a]		
	PANC-1	***CAPAN-1***	***SUIT-2***
180b	0.78	1.19	0.40
180c	1.60	1.28	3.20
180i	2.75	2.81	7.14
180j	6.76	2.59	5.91
180l	1.51	1.41	1.91

(a). Data are reported as EC_{50} values (the molar concentration of a compound where 50% of its maximal effect is observed) determined by the SRB assay after 72 hours of continuous exposure to each compound. Data represent mean values ± SD of at least three independent experiments.

4.3 Effect on cell apoptosis

To prove the inhibitory nature of new oxadiazole compounds against pancreatic cancer cells, the analysis of the cell apoptosis induction of SUIT-2, CAPAN-1 and PANC-1 cells was performed by flow cytometry.

The apoptotic cells are characterized by certain morphologic features, that concern cell shrinkage, the loss of plasma membrane asymmetry and attachment, loss of the interaction with cytoskeleton, condensation of the cytoplasm and nucleus, and double-stranded internucleosomal cleavage of nuclear DNA in fragments of roughly 180 base pairs (bp) and multiples thereof.[161,162,163]
Loss of plasma membrane is one of the earliest sign of apoptosis. Indeed, in apoptotic cells, the membrane phospholipid phosphatidylserine (PS), normally restricted to the inner side (cytoplasmic face) of the plasma membrane, is translocated to the outer leaflet, exposing PS to the outer extracellular environment.[164,165]

To evaluate externalization of plasma membrane phosphatidylserine, a reliable marker of cell apoptosis, flow cytometry analysis of annexin V-FITC and 7-Amino-Actinomycin D (7-AAD) stained cancer cells was carried out.

Annexin V is a 35-36 kDa Ca^{2+} dependent phospholipid-binding protein that has a high affinity for PS, and binds to apoptotic cells with exposed PS. Because of these spectral characteristics, 7-AAD may be conjugated with other fluorochromes excited at 488 nm, such as fluorescein isothiocyanate (FITC). Since externalization of PS occurs in the earlier stages of apoptosis, PE Annexin V staining can identify apoptosis at an earlier stage to apoptotic changes affecting the nucleus. PE Annexin V staining precedes the loss of membrane integrity which accompanies the latest stages of cell death resulting from either apoptotic or necrotic processes. Therefore, staining with PE Annexin V is typically used in conjunction with a vital dye such as 7-AAD. 7-AAD is a fluorescent intercalator, membrane impermeant dye, that is generally excluded from viable cells with intact membrane. It binds to double stranded DNA by intercalating between base pairs in GC regions of DNA, in the same way as nonfluorescent actinomycin. 7-AAD can be excited at 488 nm with an argon laser. It has a relatively large Stokes shift, emitting at a maximum wavelength of 647 nm.

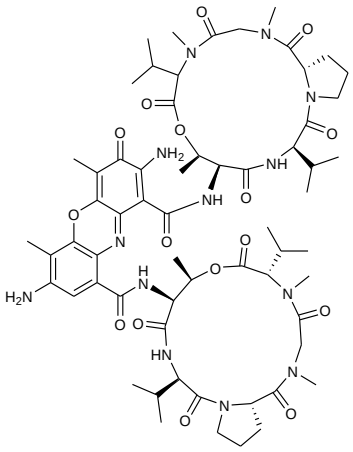

7-AAD

Viable cells with intact membranes (normal cells) exclude 7-AAD, whereas the membranes of dead and damaged cells are permeable to 7-AAD. As a result, the viable cells are Annexin V and 7-AAD negative; the early apoptosis cells, that retain membrane integrity, are Annexin V positive and 7-AAD negative; while, the late apoptosis cells or death cell, with compromised membranes, are both Annexin V and 7-AAD positive. This assay does not distinguish between cells that undergo apoptotic death versus those that die as a result of a necrotic pathway because in either case, the dead cells will stain with both Annexin V and 7-AAD.

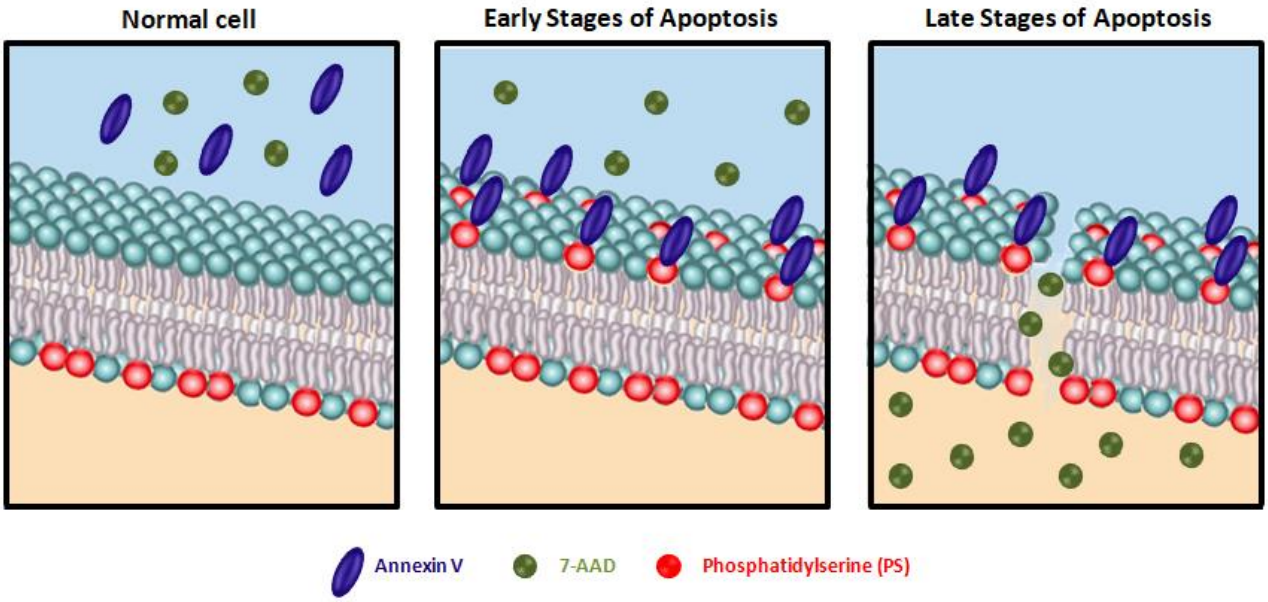

As shown in Figure 14A, the early apoptosis features were detectable after SUIT-2 cells were treated with 5 μM or 10 μM of **180l** for 24 hours. The statistical apoptosis rates of SUIT-2 cells were increased in a concentration-dependent manner. The percentage of apoptotic SUIT-2 cells were 13.6% and 15.9% when compared to the control group (11.9%), when treated with 5 μM and 10 μM of the compound **180l**, respectively (Figure 14A).

In CAPAN-1 cells, only the treatment with **180l** at 5 μM increased the apoptotic rate from 8.1% (control cells) to 9.7% (treated cells) (Figure 14B).

Induction of apoptotic death following treatment with **180b** and **180l** suggests that these compounds may orchestrate a potential axis of autophagy and apoptosis in PANC-1 cells which can, in turn, facilitates cellular destruction. Compared to control cells (13.3%), the compound **180b**, at 2 μM and 5 μM, increased the apoptotic rate to 18.6% and 18.2%, respectively, proving that increase of apoptotic death was not dependent to compound concentration. The same effect has been observed after treatment with **180l** at concentration of 5 μM, that increased the apoptotic rate from 13.3% to 19.2% (Figure 14C).

Of note, the compound **180c** did not appreciably induce apoptotic death in all available pancreatic cancer cells (Figure 14). The representative cell apoptosis spectra are reported in the Supporting Information chapter (7.1).

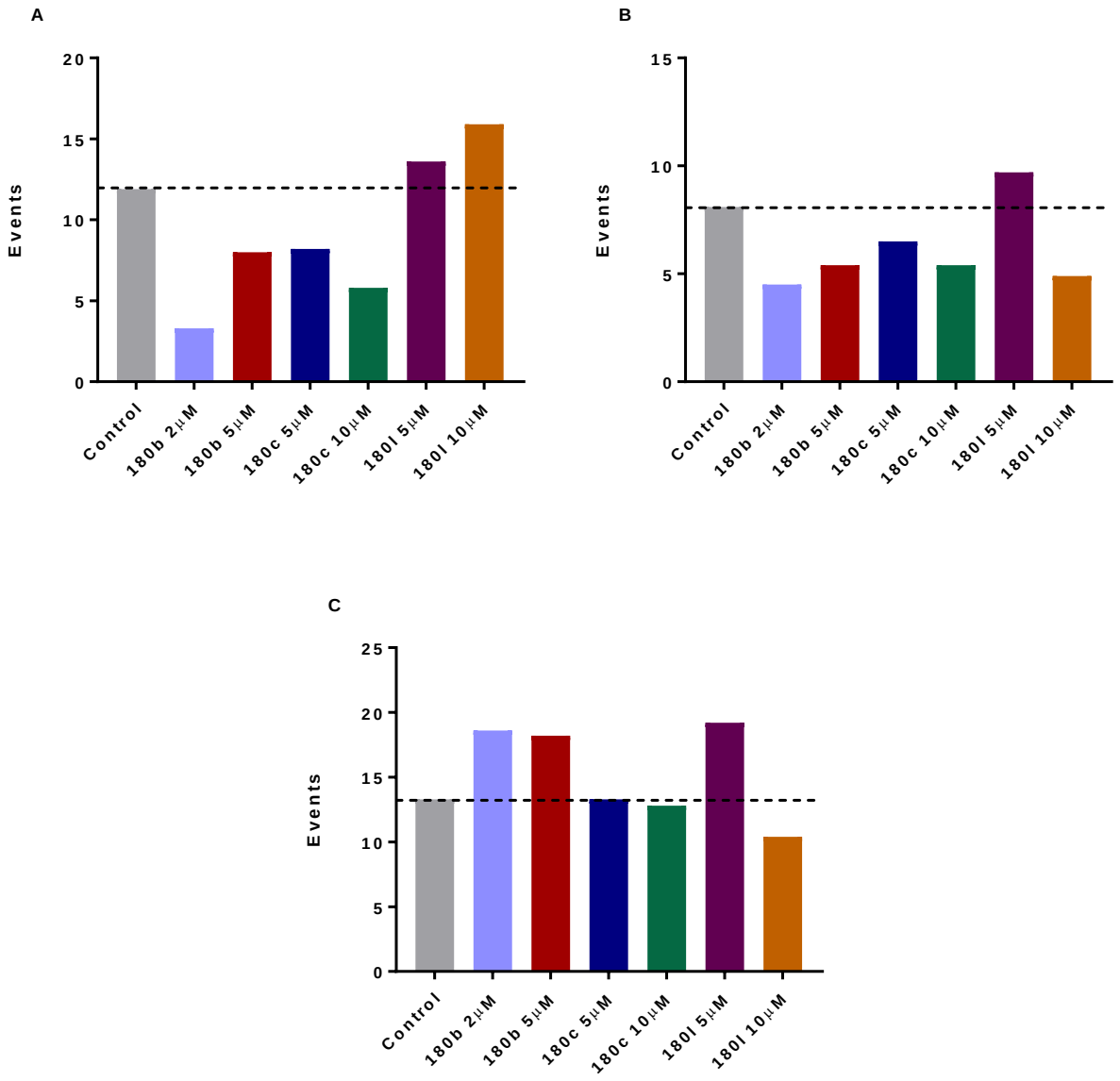

Figure 14. Effect of compounds **180b**, **180c** and **180l** on apoptosis induction in SUIT-2 (A), CAPAN-1 (B) and PANC-1 (C) pancreatic cancer cells. The percentage of cells with apoptotic morphology was assessed by fluorescence microscopy after exposure of cell lines to derivatives **180b**, **180c** and **180l** at 24 hours after treatment.

4.4 Effect on cell cycle

Alterations in the cell cycle caused by the derivatives **180b**, **180c**, **180l** were evaluated in the SUIT-02 pancreatic cancer cell line. Cell cycle progression was analyzed by flow cytofluorimetry, using propidium iodide (3,8-diamino-5-[3-(diethylmethylammonio)propyl]-6phenyl- diiodide, PI) staining solution.

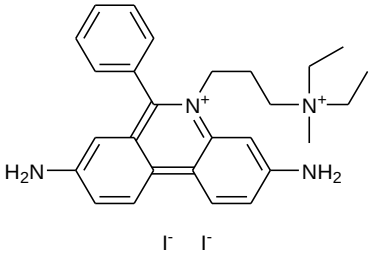

Propidium Iodide

PI is an interlayer that selectively binds nucleic acids. It also acts as a synthetic dye characterized by a low fluorescence (red-orange). The PI is in fact able to establish a stable bond with the DNA, intercalating between two pairs of adjacent bases, with a stoichiometry of one dye per 4–5 base pairs of DNA. Once the dye is bound to nucleic acids, it increases twenty-thirty times, compared to the free dye, its quantum fluorescence efficiency. The PI is therefore an excellent fluorescent "marker" of the double helix nucleic acids, thus providing information on the amount of DNA content in the cells, in relation to the emitted fluorescence intensity (the higher the DNA content the greater the fluorescence). It is known that the DNA content varies according to the phase of the cycle in which a cell is located. In particular, the G2 phase and mitosis (M) have double amount of DNA compared to the G1 phase, while during the DNA synthesis phase (S phase), the cell has a quantity of DNA intermediate between the content in G1 and G2. This technique allows to analyze the percentage of cells in the various phases of the cell cycle (G0/G1, S and G2/M), as well as to evaluate possible blocks, and to detect the occurrence of apoptotic episodes.

In SUIT-2 cells, the compound **180b**, at concentration of 2 μM and 5 μM, decreased the G0/G1 phase from 50.6% to 47.4% and 43.6%, respectively, as well as the S phase from 24.5% to 17.0% and 15.5%. In contrast, the G2/M phase increased from 24.5% to 30.6% and 29.9%. This could be due to the triggering, in at least some cell subpopulations, of different cell survival mechanisms in response to the antiproliferative effect of this compound, eventually leading to an increase in the number of mitosis events. The cells treated with **180l**, at both concentrations, gave results comparable to the ones obtained from the control samples, while all the samples treated with the

compound **180c** at 2 μM and at 5 μM, showed similar results, lowering the percentages of G0/G1 cells from 50.6% to 32.6% and 30.4%, respectively, and increasing S percentages from 24.5% to 30.8% and 33.6%, respectively. Strikingly, the G2/M phase increased after treatment with the compound **180c** at 5 μM and decreased after treatment with 10 μM of the same compound (Figure 15). The cell cycle spectra are reported in the Supporting Information chapter (7.2).

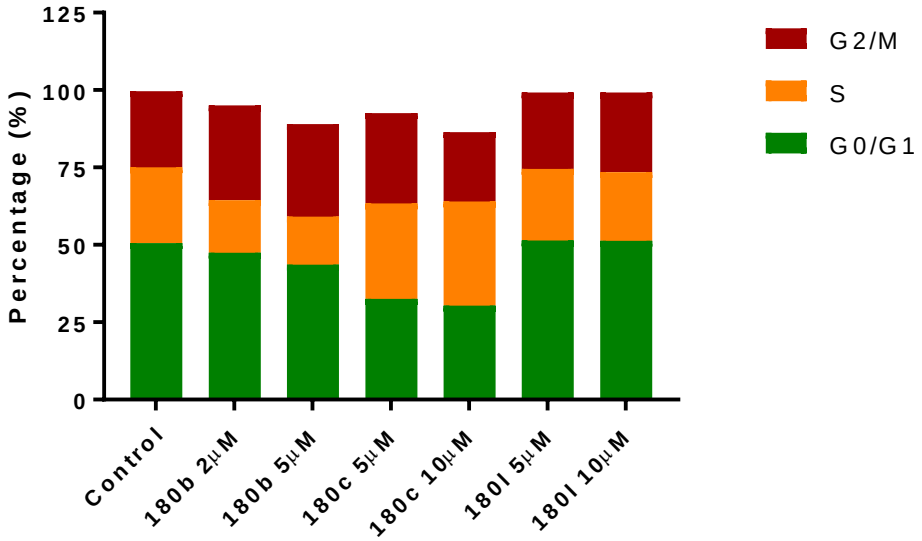

Figure 15. Effect of oxadiazole compounds **180b**, **180c** and **180l** on cell cycle distribution. SUIT-2 cells were exposed to derivatives **180b**, **180c** and **180l** for 24 hours. Stacked bar graphs showing the percentage of cells at various stages of cell cycle, G0/G1 (green), S (orange), and G2/M (red) phase, in untreated control and after treatment with the compounds.

4.5 Anti-migration activity

In order to evaluate the impact of the compounds **180b, 180c, 180i, 180j, 180l**) on cell migration, an important step in the metastatic process, the *in vitro* scratch wound healing assay has been performed on CAPAN-1, PANC-1 and SUIT-2 pancreatic cancer cell lines. Of note, PANC-1 cell line was chosen for anti-migration study due to previous studies showing its highly aggressive and strongly metastatic properties.[166]

The *in vitro* scratch wound healing assay is an easy, economical and well-developed method to study cell migration in vitro. This method is based on the observation that, upon creation of a new artificial space, so called ‘‘scratch’’, on a confluent cell monolayer, the cells on the edge of the newly created gap will move toward the opening to close the “scratch” until new cell–cell contacts are established again. The basic steps involve therefore (1) the creation of a ‘‘scratch’’ on monolayer cells (Figure 16A), (2) the capture of images at the beginning and regular intervals

during cell migration to close the scratch (Figure 16B), and (3) the comparison of the images to determine the rate of cell migration.[167]

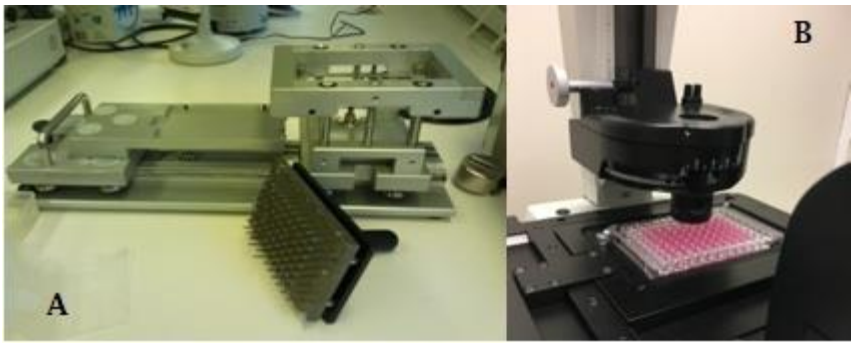

Figure 16. (A) Picture of the 96 pin floating array device used to perform the scratches; (B) Leica microscope equipped with a JAI TMC-1327 camera.

The effects of **180b** on cell migration were examined on SUIT-2, CAPAN-1 and PANC-1 pancreatic cancer cells. The compound was tested at concentrations of 2 μM and 5 μM. The data (Figure 17) showed that this compound sightly inhibited the migration rate of SUIT-2 and PANC-1 cells compared with untreated cells, but only 20 h after the treatment (Figure 17A,B).

On the other hand, treatment with **180b** at both concentrations showed markedly inhibitory effect on cell migration of CAPAN-1 cell line already after 8 h, in a dose-dependent way. The cell migration rate was indeed decreased gradually in correlation with an increase in the compound concentration (Figure 17). As a result, at the concentration of 2 μM, the compound **180b** reduced the cell migration of 33%; while, at 5 μM, the compound **180b** reduced the cell migration of 39% (Figure 17C).

In the Figure 18 and 19 we reported data and images demonstrating that the cell density in the scratch area is reduced after treatment, compared with the control after 20 hours, as is reflected by an higher scratch area in treated wells.

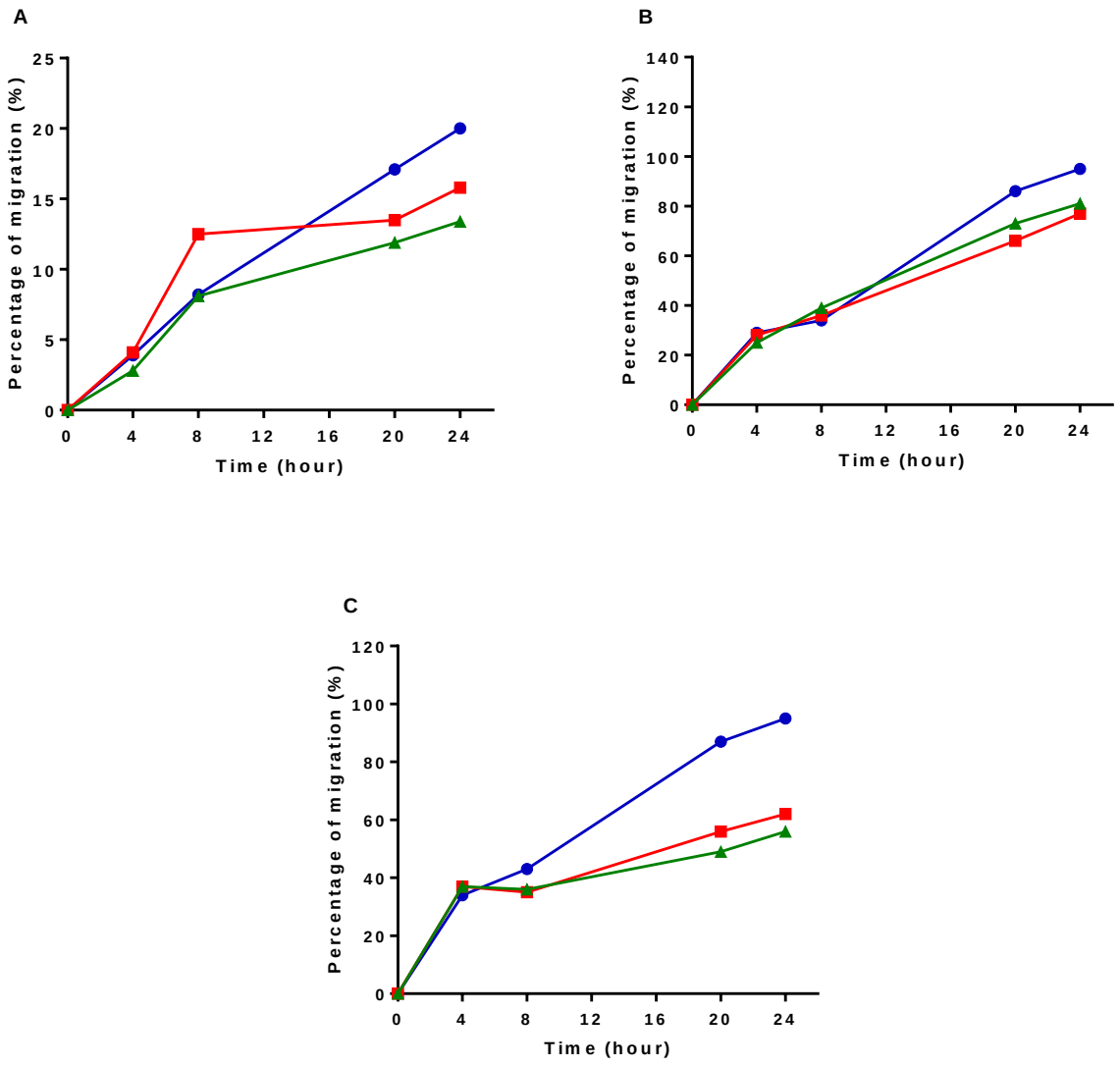

Figure 17. Evaluation of cell migration using the wound healing scratch assay. A scratch was induced after which the cells were treated with **180b** immediately. After 0, 4, 8, 20, 24h, images of scratches were captured and the width of scratches was measured. The percentages of migration were calculated for untreated cells (control, blu line), cells treated with **180b** at concentration of 2 μM (red line) and cells treated with **180b** at concentration of 5 μM (green line). (A) Scratch-wound closure monitored over time in SUIT-2 cells (isolated from a metastatic liver tumour of human pancreatic carcinoma). (B) Scratch-wound closure monitored over time in PANC-1 adherent epithelial-like cells. (C) Scratch-wound closure monitored over time in CAPAN-1 epithelioid carcinoma cells.

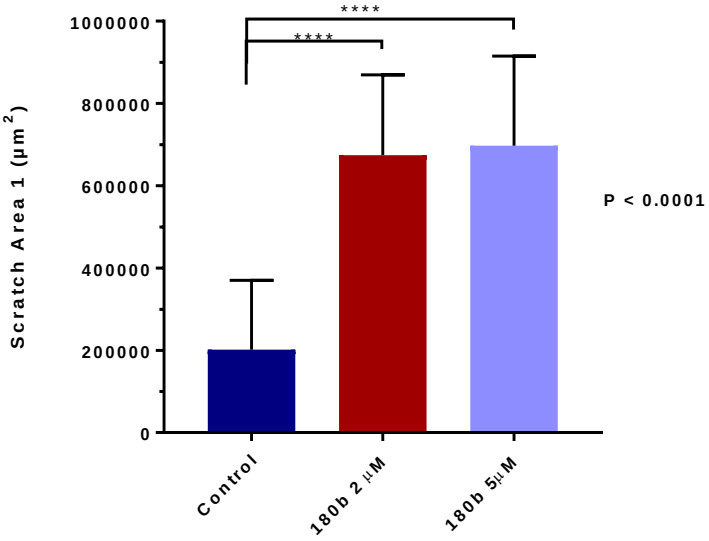

Figure 18. Scratch area values and comparison of the areas of the scratches in CAPAN-1, calculated 20 hours after scratch and treatment with the compound **180b**.

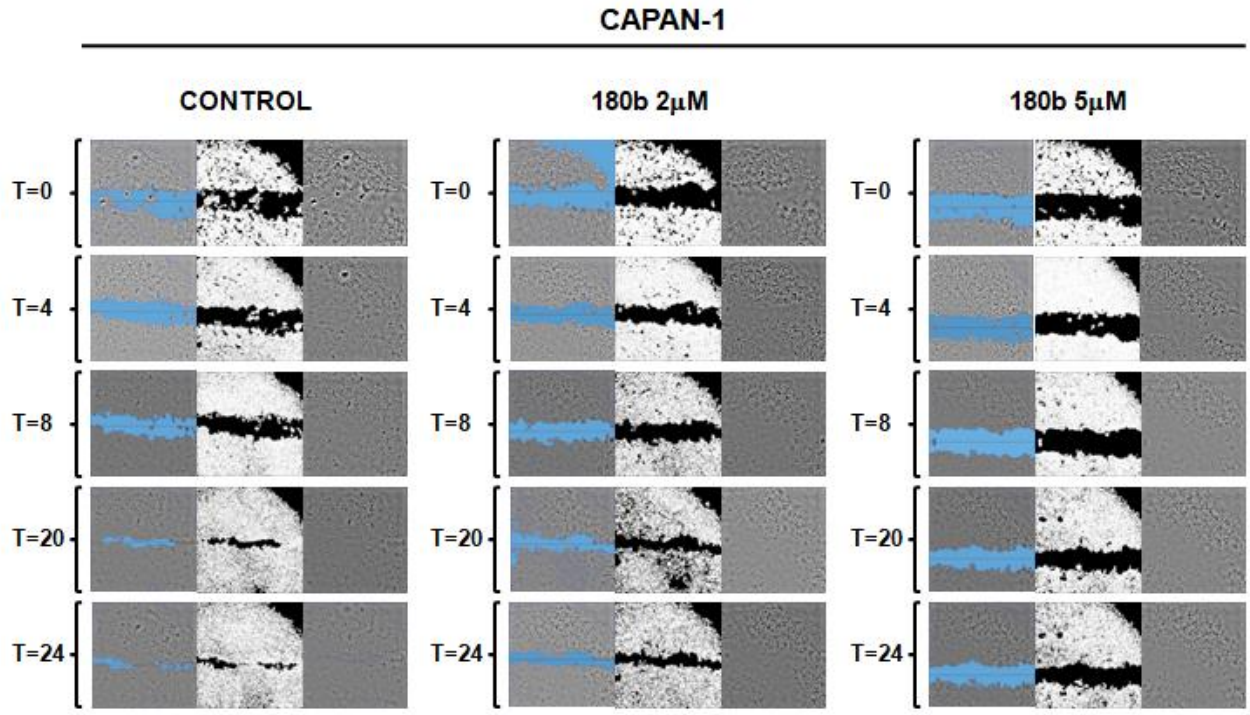

Figure 19. Representative images from wound healing assay of CAPAN-1 cell cultures treated with or without the compound **180b**, at concentration of 2 µM and 5 µM.

SUIT-2 cells treated with the compound **180c** at concentration of 10 µM showed a 10% and 15% decrease in cell migration, at 4 and 8h after the treatment, respectively. Nevertheless, after 8h, the treatment with the compound did not greatly influenced cellular migration (Figure 20A). A 20%

decrease was observed in PANC-1 cells treated with the compound **180c** at both concentrations, between 8 and 20 hours after treatment (Figure 20B). The compound **180c** showed the best results against the CAPAN-1 cell migration, as reflected by a higher scratch area in treated wells (Figure 21). At T = 20h, in the parental cell line, 90% of the scratch was closed. After **180c** treatment at concentration of 2 μM, 68% of the scratch was closed, in contrast to 45% when treated with **180c** at 5 μM (Figure 20C) (Figure 20).

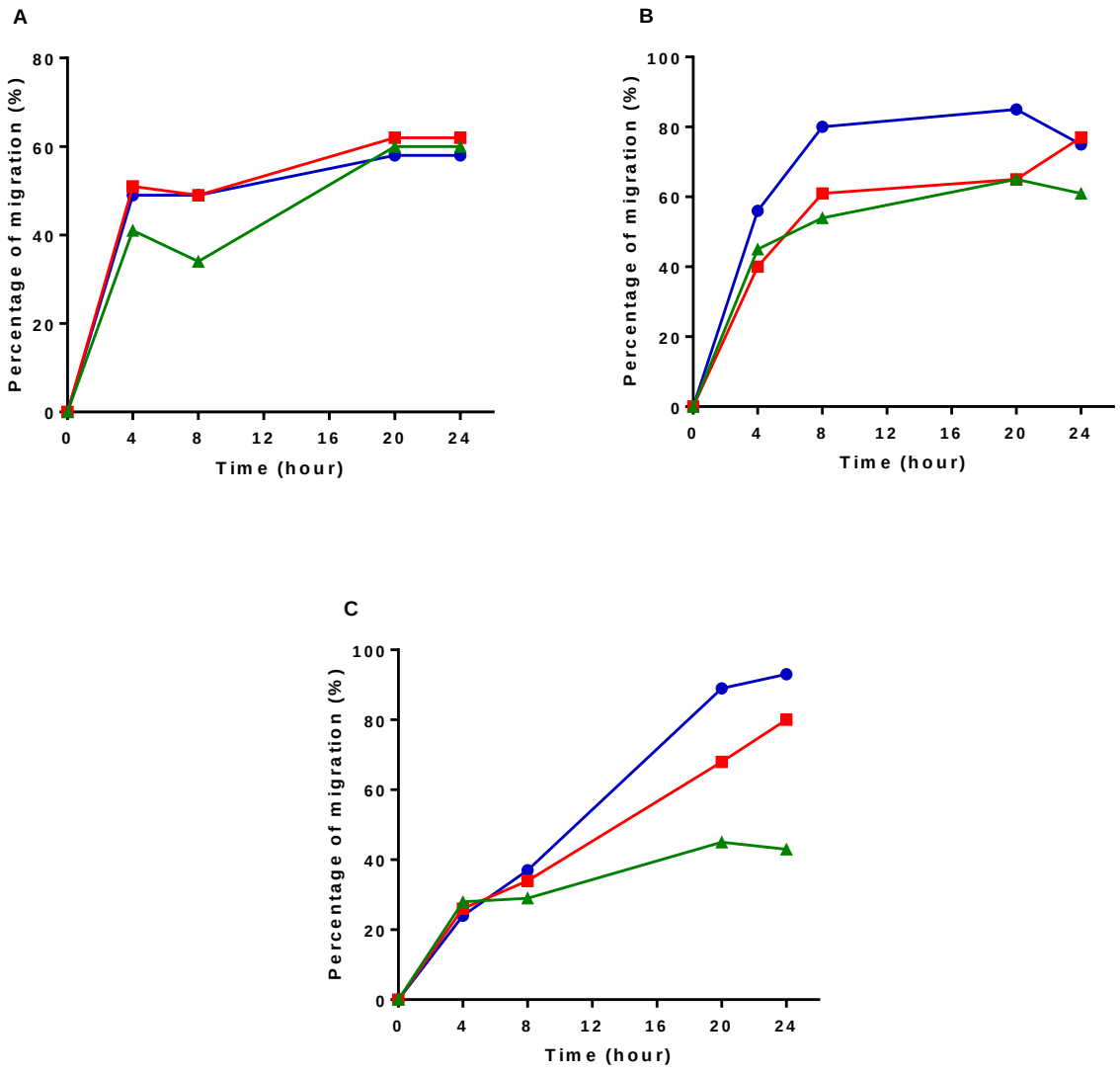

Figure 20. Evaluation of cell migration using the wound healing scratch assay. A scratch was induced after which the cells were treated with **180c**. After 0, 4, 8, 20, 24h, images of scratches were captured and the width of scratches was measured. The percentages of migration were calculated for untreated cells (control, blu line), cells treated with **180c** at minor concentration (red line) and cells treated with **180c** at major concentration (green line). SUIT-02 and PANC-1 cells were treated with 5 μM (red line) and 10 μM (green line) of compound **180c**. While, CAPAN-1 cells were treated with 2 μM (red line) and 5 μM (green line) of compound **180c**. (A) Scratch-wound closure monitored over time in SUIT-2 cells (isolated from a metastatic liver tumour of human pancreatic carcinoma). (B) Scratch-wound closure monitored over time in PANC-1

adherent epithelial-like cells. (C) Scratch-wound closure monitored over time in CAPAN-1 epithelioid carcinoma cells.

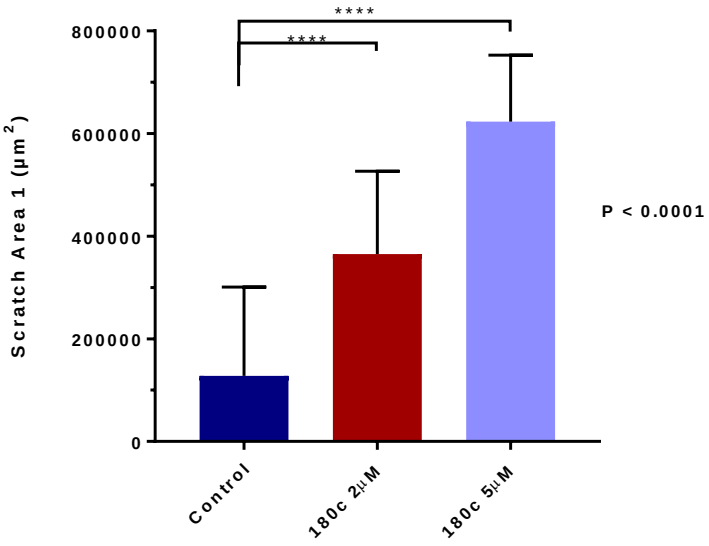

Figure 21. Scratch area values and comparison of the areas of the scratches in CAPAN-1, calculated 20 hours after scratch and treatment with the compound **180c**.

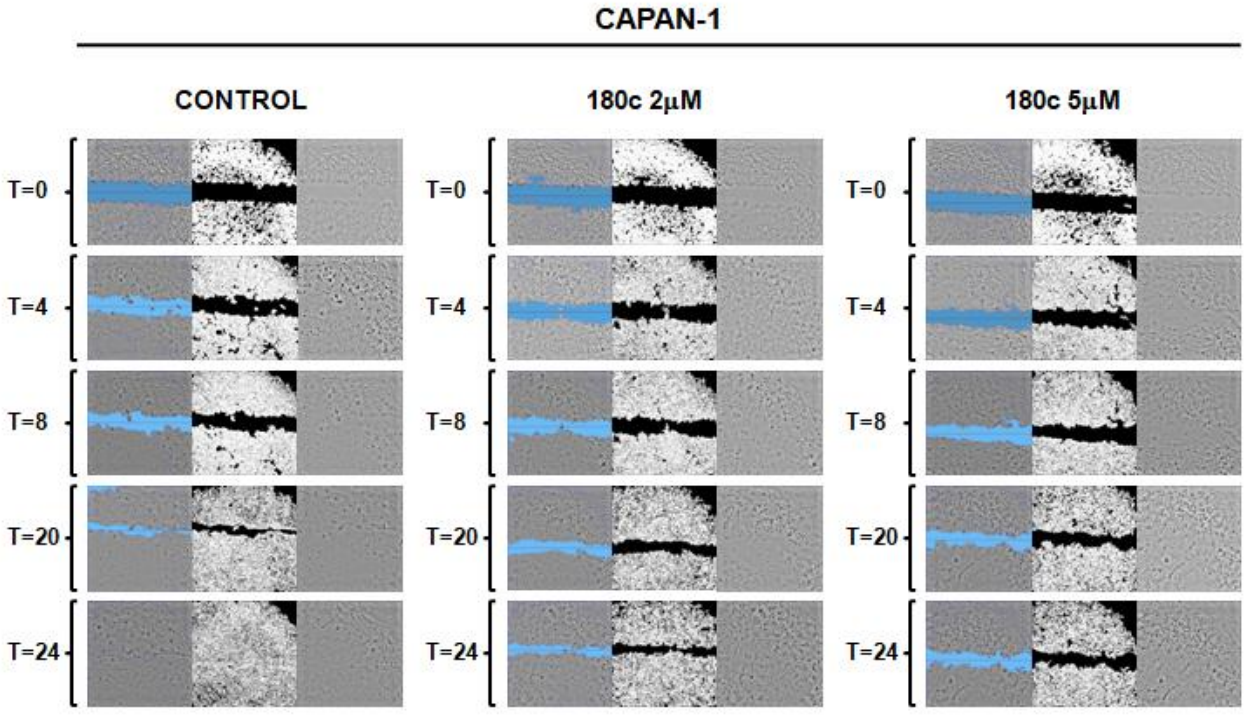

Figure 22. Representative images from wound healing assay of CAPAN-1 cell cultures treated with or without the compound **180c**, at concentration of 2 µM and 5 µM.

The compound **180i** did not exhibit considerable inhibitory effect on cell migration of CAPAN-1 and PANC-1, within 24h (Figure 23B and 23C). Indeed, in PANC-1 cells, the treatment with the compound **180i** resulted in an unexpected increased cell migration, leading to 100% wound closure compared to 60% of control cells wound closure. However, against SUIT-2 pancreatic cancer cells, at concentration of 5 μM and 10 μM, this compound inhibited cell migration, but only in the period between 4 and 16 hours after treatment (Figure 23A).

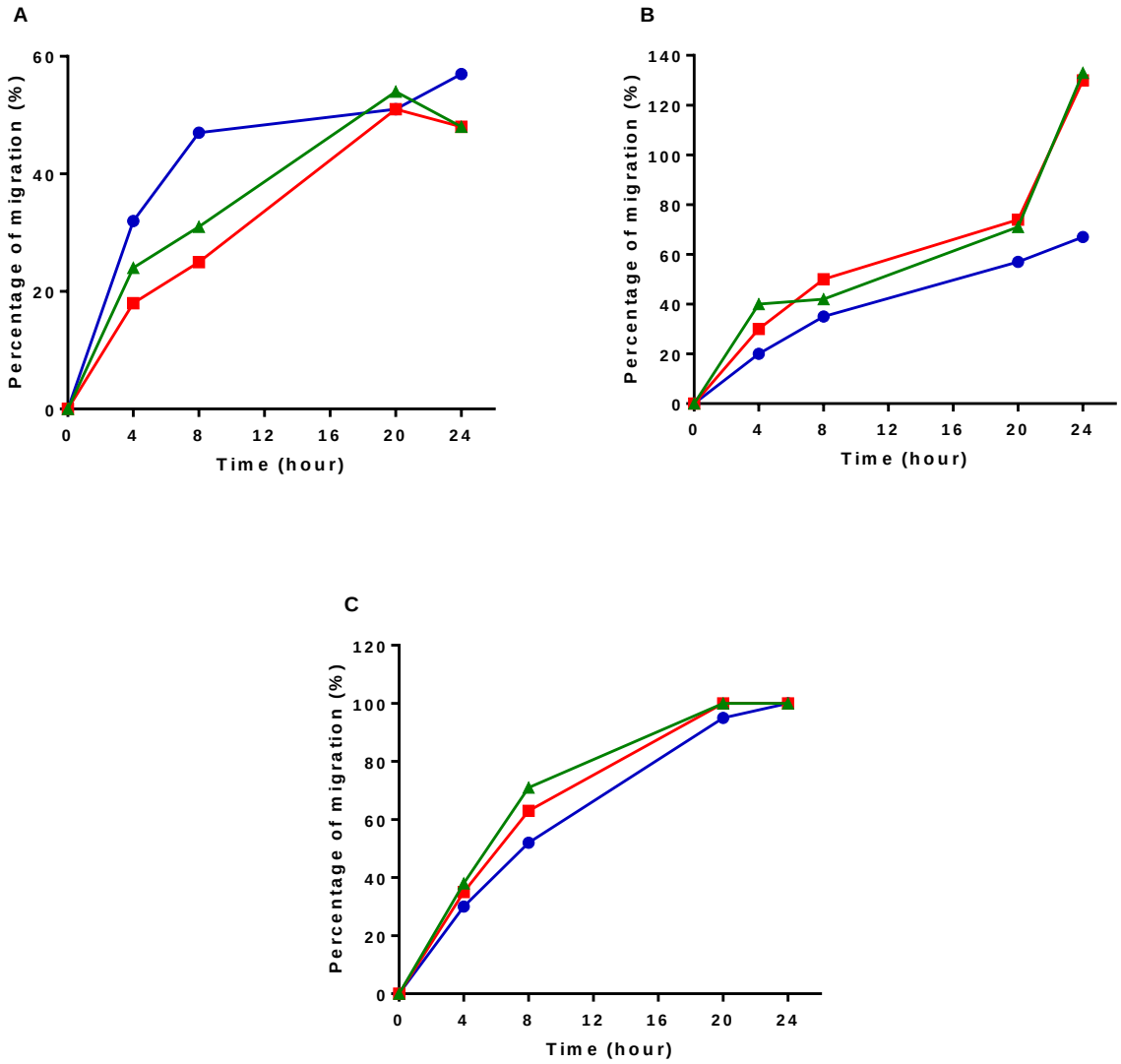

Figure 23. Evaluation of cell migration using the wound healing scratch assay. A scratch was induced after which the cells were treated with **180i**. After 0, 4, 8, 20, 24h, images of scratches were captured and the width of scratches was measured. The percentages of migration were calculated for untreated cells (control, blu line), cells treated with **180i** at minor concentration (red line) and cells treated with **180i** at major concentration (green line). SUIT-02 cells were treated with 5 μM (red line) and 10 μM (green line) of compound **180i**. While, CAPAN-1 and PANC-1 cells were treated with 2 μM (red line) and 5 μM (green line) of compound **180i**. (A) Scratch-wound closure monitored over time in SUIT-2 cells. (B) Scratch-wound closure monitored over time in PANC-1. (C) Scratch-wound closure monitored over time in CAPAN-1 cells.

In the scratch wound-healing assay, the wound closure rate of SUIT-2 cells was notably decreased when treated with 10 μM of compound **180j** at 4h (18.0%) and 8h (27.0%), compared with untreated control SUIT-2 cells (37% and 41%, respectively). However, no significant differences in the levels of cell migration were identified for the cells treated with the compound **180j** at 5 μM (Figure 24A). Besides, the treatment of PANC-1 and CAPAN-1 cells with the same compound did not significantly modify the percent of cell migration with respect to control (Figure 24B and 24C).

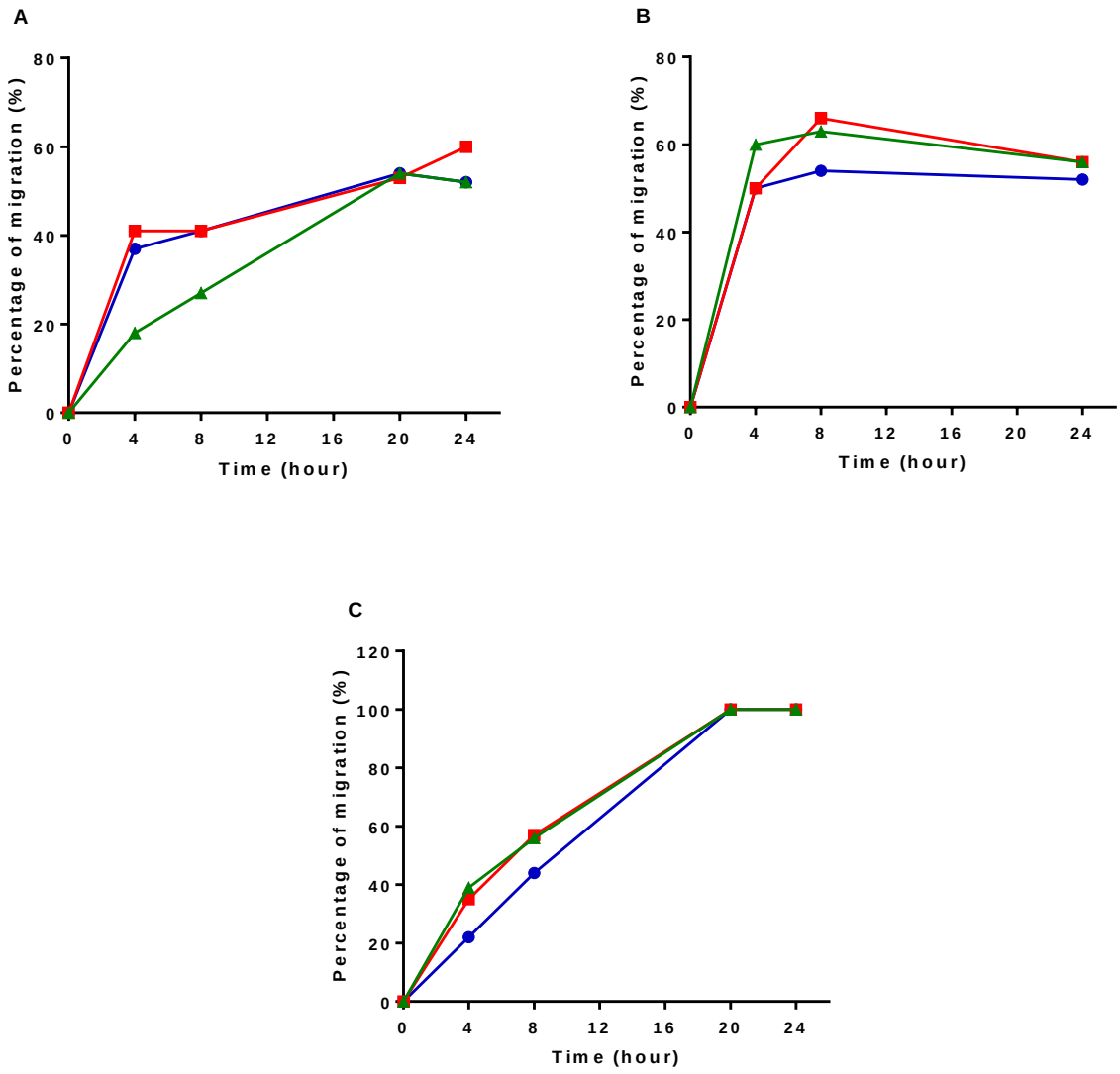

Figure 24. Evaluation of cell migration using the wound healing scratch assay. A scratch was induced after which the cells were treated with **180j**. After 0, 4, 8, 20, 24h, images of scratches were captured and the width of scratches was measured. The percentages of migration were calculated for untreated cells (control, blu line), cells treated with **180j** at concentration of 5 μM (red line) and cells treated with the same compound at concentration of 10 μM (green line). (A) Scratch-wound closure monitored over time in SUIT-2 cells. (B) Scratch-wound closure monitored over time in PANC-1 cells. (C) Scratch-wound closure monitored over time in CAPAN-1 epithelioid carcinoma cells.

The treatment with the compound **180l** at two concentrations (5 μM and 10 μM) in the assays performed on SUIT-2, PANC-1 and CAPAN-1 cells was not able to stop the cells from healing the scratch wound; thus, in the CAPAN-1 (Figure 25B) and in the PANC-1 (Figure 25C) cells, the untreated wells and the wells treated with the compound **180l** (at both concentrations) healed completely within 24 hours. This could be justified by the highly aggressive and strongly metastatic properties of these cell lines and by the lack of anti-migration activity of this compound. No effects were also observed in the SUIT-2 cell line, which conversely in these experiments showed minimal migratory behaviour, as reflected by an average of 20% gap closure after 24h (Figure 25A).

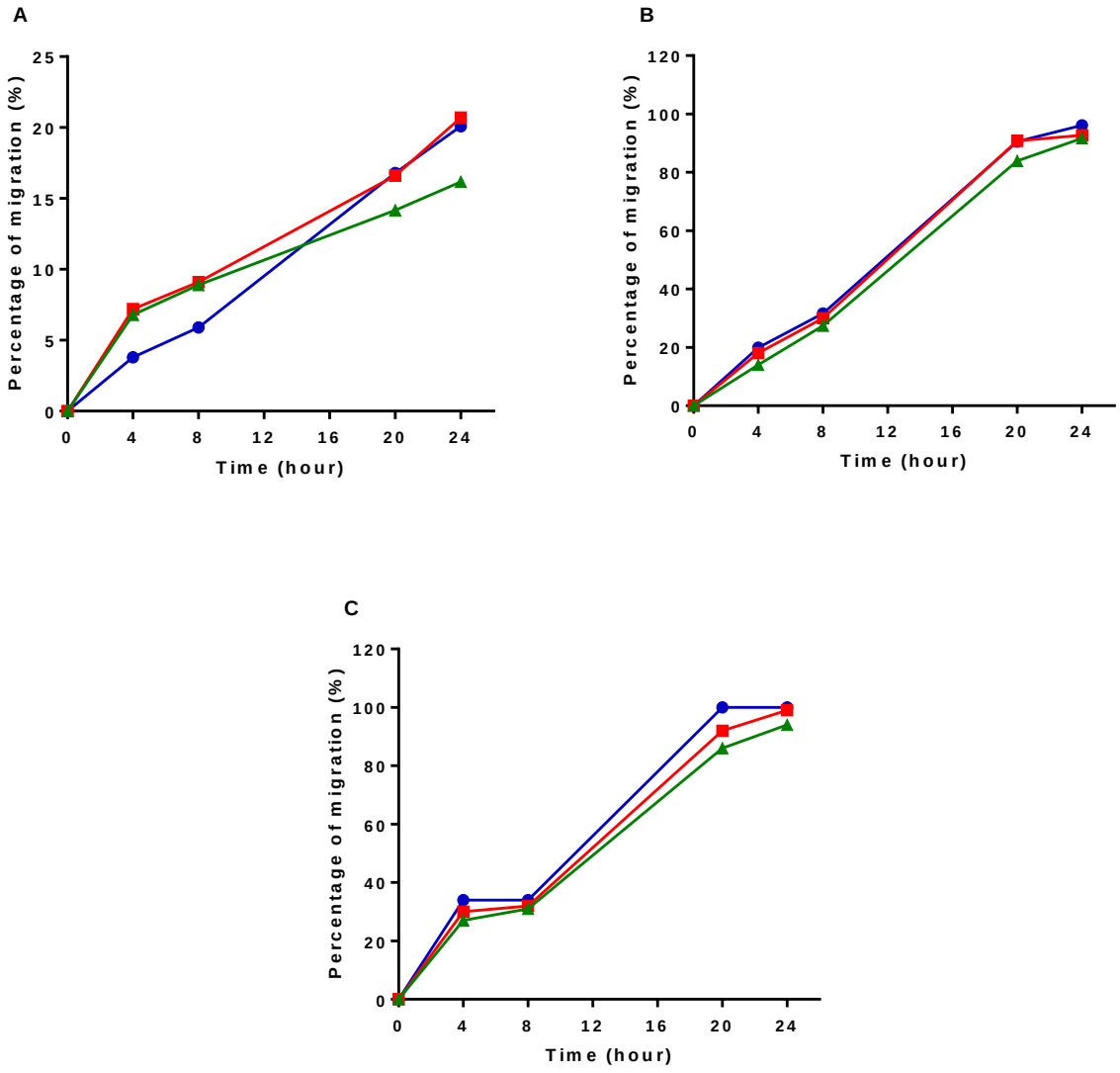

Figure 25. Evaluation of cell migration using the wound healing scratch assay. A scratch was induced after which the cells were treated with the compound **180l** immediately. After 0, 4, 8, 20, 24h, images of scratches were captured and the width of scratches was measured. The percentages of migration were calculated for untreated cells (control, blu line), cells treated with **180l** at concentration of 5 μM (red line) and cells treated with **180l** at concentration of 10 μM (green line). (A) Scratch-wound closure monitored over time in SUIT-2 cells isolated from a metastatic liver tumour of human pancreatic carcinoma. (B) Scratch-wound closure monitored over time in PANC-1 adherent epithelial-like cells. (C) Scratch-wound closure monitored over time in CAPAN-1 epithelioid carcinoma cells.

4.6 Gene expression profiling of epithelial-mesenchymal transition by real-time PCR

Epithelial-Mesenchymal transition (EMT) has been proposed as the critical mechanism for the acquisition of malignant phenotypes by epithelial cancer cells, resulting in tumour invasion and induction of the metastasis process.[168,169]

During EMT, primary site epithelial cells acquire the motile and invasive characteristics of mesenchymal cells, such as motility, invasiveness, and resistance to apoptosis, resulting in secondary tumour formation at another site.[170] Thus, controlling of EMT is considered a promising approach for the inhibition of metastasis.

In order to evaluate the capability of the most promising antitumor compounds **180b** and **180l** to modulate EMT, we performed a preliminary analysis of the effects on EMT critical determinants, such as E-cadherin, N-cadherin, Vimentin. To this goal, a specific Real-Time PCR analysis has been performed on the total mRNA extracted from the PANC-1 and CAPAN-1 pancreatic cancer cell lines previously treated with two different concentrations (2 μM and 5 μM) of these compounds.

In particular, the quantitative Real Time PCR was performed on cDNA obtained through reverse transcription of total RNA extracted from pancreatic cancer cells untreated and treated with the compounds.

The yield and absorbance ratio of total RNA Isolated from PANC-1 and CAPAN-1 untreated or treated with the compounds **180b** and **180l** were reported in Table 13.

Table 13. Yield and Absorbance Ratio of Total RNA Isolated from PANC-1 and CAPAN-1 untreated or treated with the compounds **180b** and **180l**, by Trizol method.

Cell line	Condition	ng/mL[a]	A260	A280	260/280	260/230
PANC-1	Control	221.47	5.537	3.121	1.77	2.25
CAPAN-1	Control	266.99	6.675	3.694	1.81	2.23
PANC-1	180b 2μM	240.59	6.015	3.358	1.79	2.25
PANC-1	180b 5μM	299.54	7.489	4.154	1.80	2.17
PANC-1	180l 2μM	460.51	11.513	6.307	1.83	2.22
PANC-1	180l 5μM	463.20	11.580	6.287	1.84	2.17
CAPAN-1	180b 2μM	285.33	7.133	3.947	1.81	2.26
CAPAN-1	180b 5μM	191.62	4.791	2.659	1.80	2.08
CAPAN-1	180l 2μM	310.17	7.750	4.288	1.81	2.20
CAPAN-1	180l 5μM	351.01	8.775	4.800	1.83	2.09

(a). The concentration of RNA of each sample was calculated by applying the Lambert-Beer law, which draws a direct correlation between absorbance and concentration.

The absorbance at 260 nm has been used as a measure of the amount of nucleic acid extracted. Nucleic acids have maximal absorbance at 260 nm due to the aromatic base moieties within their structure (purines and pyrimidines). The absorbance at 280 nm has been used as a measure of the amount of proteins, phenolic compounds and aromatic amino acid side chains (tryptophan, phenylalanine, tyrosine and histidine), responsible for this absorbance. The 260/280 ratio has been used as a measure of purity in RNA extraction. A ratio of ~1.8 is generally accepted as “pure” for RNA. The 260/230 ratio indicates the presence of organic contaminants, such as phenol and Trizol. A 260/230 ratio of ~2.0 is generally accepted as “pure” RNA without significant amount of these contaminants that might interfere with downstream applications (Figure 26).

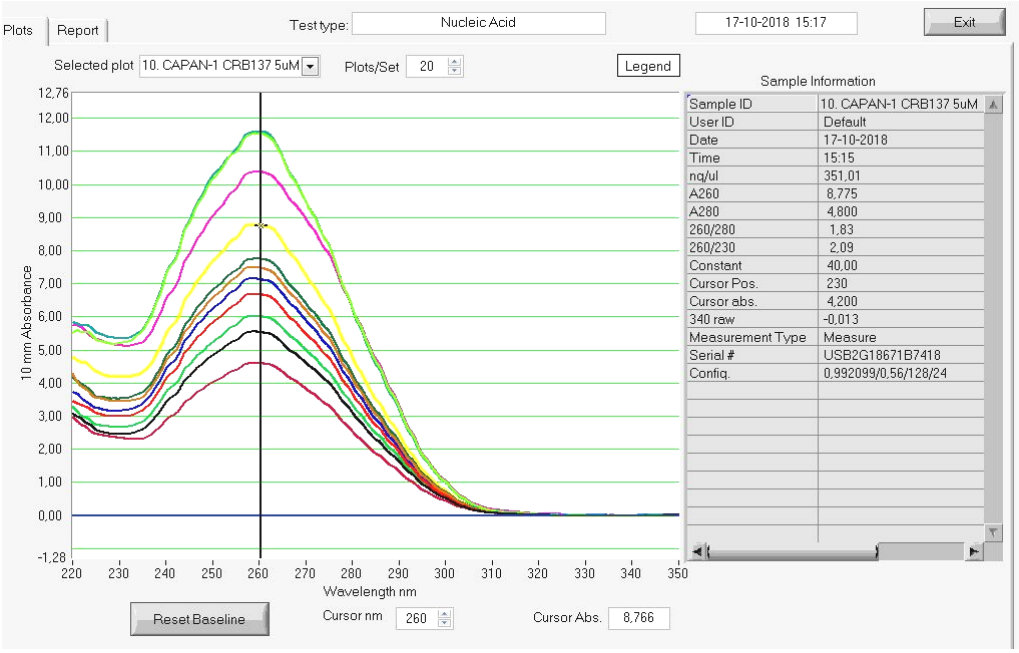

Figure 26. NanoDrop data viewer; the plot shows the absorbance spectra of all samples.

Afterwards, reverse transcription (RT) reactions to produce cDNA from RNA for RT-PCR were conducted using M-MuLV RNAse H^+ reverse transcriptase enzyme, Reverse Transcription buffer 2X, incluging dNTP mix and $MgCl_2$, and random hexamers primer (DyNAmoTM cDNA Synthesis Kit).

Finally, RT-PCR reactions were performed using the commercial kit TaqMan® Universal PCR Master Mix. The method is based on the standard PCR technology and, additionally, uses the 5`-3` nuclease activity of Taq DNA polymerase to cleave a non-extendible hybridization probe during the extension phase of the reaction. The probe is a target-specific nucleotide sequence labeled with two different fluorescent dyes: one serves as a reporter and its emission spectra is quenched by the second fluorescent dye through energy transfer. The nuclease degradation of the probe releases the quenching of the fluorescent dye, resulting in an increase in emission spectrum at 518 nm.

Reactions were carried out in duplicate: one reaction has been performed for the quantification of *SNAIL 1*, *SNAIL 2*, *VIM*, *MMP 9*, *CDH1* and *CDH12* gene expression and the other one for the quantification of *β-actin* or *GAPDH* expression, used as housekeeping genes expressed at relatively constant levels in all cells.

The use of a Sequence Detector System (SDS) allowed to measurement of fluorescent spectra of all 96 wells of the thermal cycle during the PCR amplification and to calculate a value termed ΔRQ, using the following equation:

$$\Delta RQ = (RQ+) - (RQ-)$$

The emission intensity of quencher at any time in a reaction mixture (QR+) was normalized by the emission intensity of quencher measured prior to PCR amplification in that same reaction mixture (QR-).

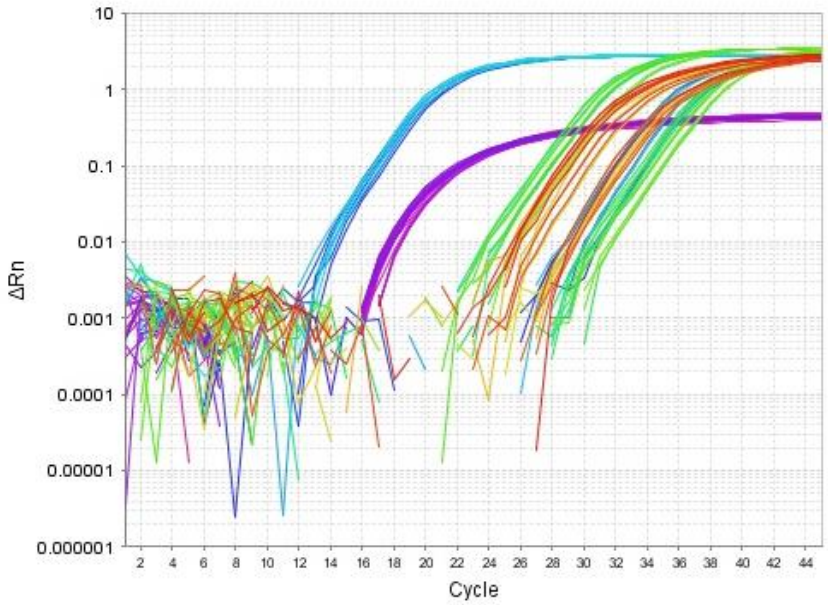

Figure 27. Amplification plot for the RT-qPCR developed to quantify the gene expression levels and to determine mean threshold cycle (C_T) values.

When the ΔRQ values were plotted on the y-axis and time, represented by cycle number, was plotted on the x-axis, it was possible to extrapolate other two values: the threshold line and the C_T value. The threshold line is an arbitrary line, the point at which the reaction reaches a fluorescent intensity above the background level, that is the mean of the baseline emission from cycles 1 to 15. C_T values (cycle threshold) or cycle quantification value represent the PCR cycle in which an increase in fluorescence, over a defined threshold line, first occurred, for each amplification plot.
The Cq value, the PCR cycle number at which each sample reaction curve intersects the threshold line, tells how many cycles it took to detect a real signal from samples (Figure 27).

Output data of the Real-Time PCR experiment (Figure 28) are shown as Ct values and normalized by a standard curve of housekeeping genes of β-actin or GAPDH, in order to obtain quantitative information about gene expression levels, in PANC-1 and CAPAN-1 cells treated with the compounds **180b** and **180l**, at concentrations of 2 μM and 5 μM.
Our correlation analysis indicated an interesting potential influence of the new topsentin analogues treatment on EMT pathways in the PANC-1 and CAPAN-1 pancreatic cancer cell lines. Our results indicated a significant alteration of expression in key EMT marker genes, such as *SNAIL2* and *MMP9*. In PANC-1 pancreatic cancer cells, the compound **180b**, at both concentrations, induced

over-expression of *SNAIL2* and *MMP9* and down-regulation of *SNAIL1*, *VIM* and *CDH2*. In the same pancreatic cancer cells,**180l**, at both concentrations, induced down-expression of *SNAIL1* and over-expression of *SNAIL2*. Not significant alteration in expression of *VIM* was registered after treatment with the compound **180l.** Instead, at concentration of 5 μM, **180l** induced up-regulation of *MMP9* and down-regulation of *CDH1*. The expression of *CDH12* has not been determined in PANC-1 pancreatic cancer line (Figure 28).

In CAPAN-1 pancreatic cancer cells, the compounds **180b** and**180l,** at both concentration, induced over-expression of *SNAIL2*, *CDH2* and *MMP9*. The *VIM* and *SNAIL1* expression was up-regulated under **180b** treatment and down-regulated under **180l** treatment. The higher concentration of both compounds induced down-regulation of *CDH12* gene expression. While, the compound **180b** at concentration of 2 μM induced up-regulation of this gene (Figure 29).

Our studies indicated that, regardless of cell phenotype, the *SNAIL2* was over-expressed after treatment with our analogues. It was hypothesized that, in response to the inhibition of cell growth, *SNAIL2* promoter increased the activity of this promoter in these cells, indicating the existence of a negative feed-back control by the protein SNAIL2, which might be a potential downstream molecular target of these compounds, that can provide cells with the capability of buffering, meaning to stabilize SNAIL levels in spite of small perturbations.[77] Similarly, the gene of MMP-9 was over-expressed after treatment in both cell lines, suggesting a mechanism of anti-migration activity of these compounds, especially for **180b** in CAPAN-1 cells, that causes a decrease of MMP-9 protein levels, and consequently, a negative feed-back mechanism that controls MMP-9 mRNA expression. Further studies on the levels of expression of these proteins, and on the effects of the modulation of these proteins on the anti-proliferative and anti-migratory activity of our novel compounds are needed, to confirm these hypotheses.

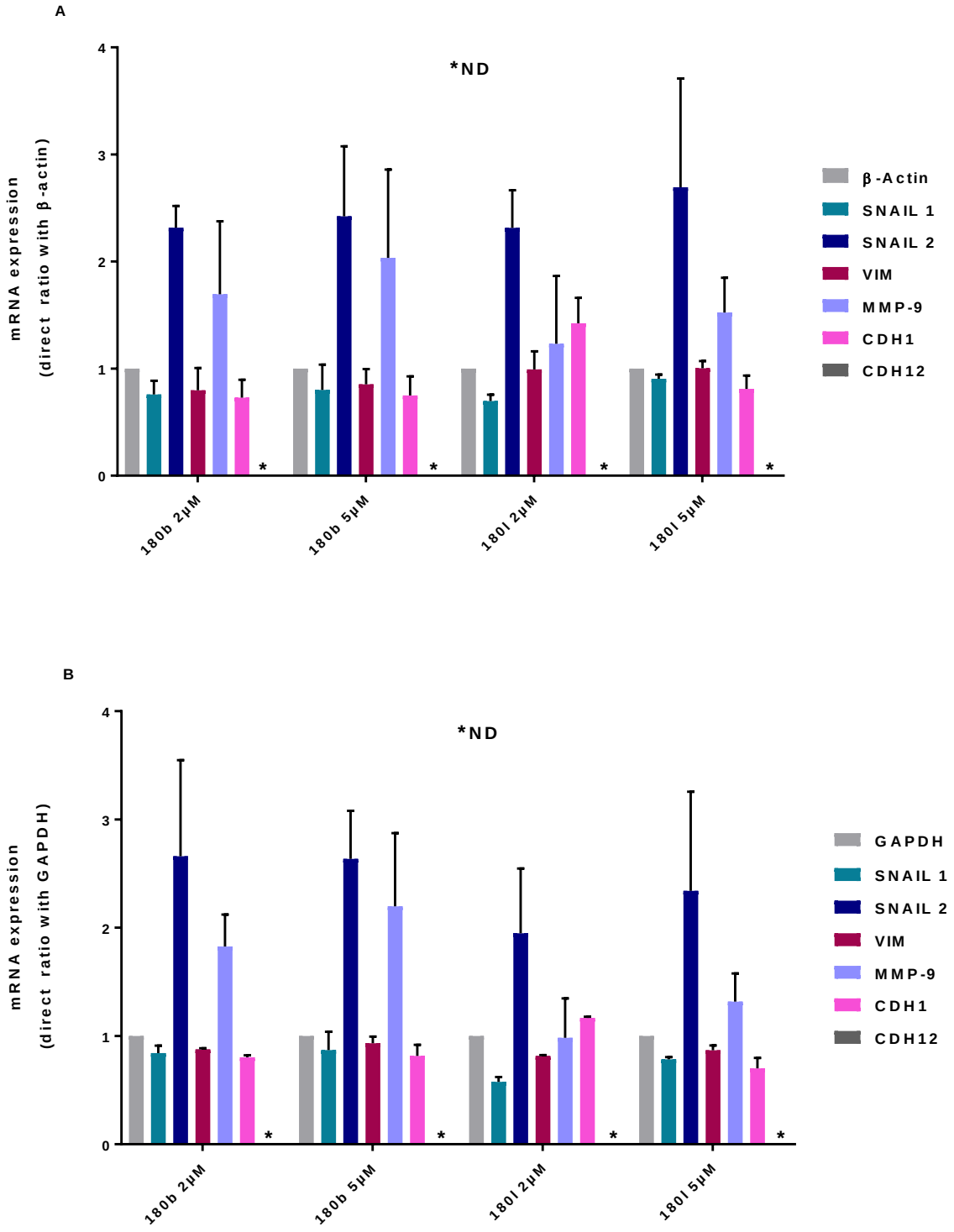

Figure 28. Analysis of the relative levels of *SNAIL 1*, *SNAIL 2*, *VIM*, *MMP 9*, *CDH1* and *CDH12* gene expression by real-time quantitative PCR in PANC-1 pancreatic cancer cells treated with the compounds **180b** and **180l**, at concentration of 2 μM or 5 μM, for 24h. Normalized gene expression levels were given as the ratio between the mean value for the target gene and that of the housekeeping genes β-actin (A) or GAPDH (B) in each sample**.** ND, no detectable.

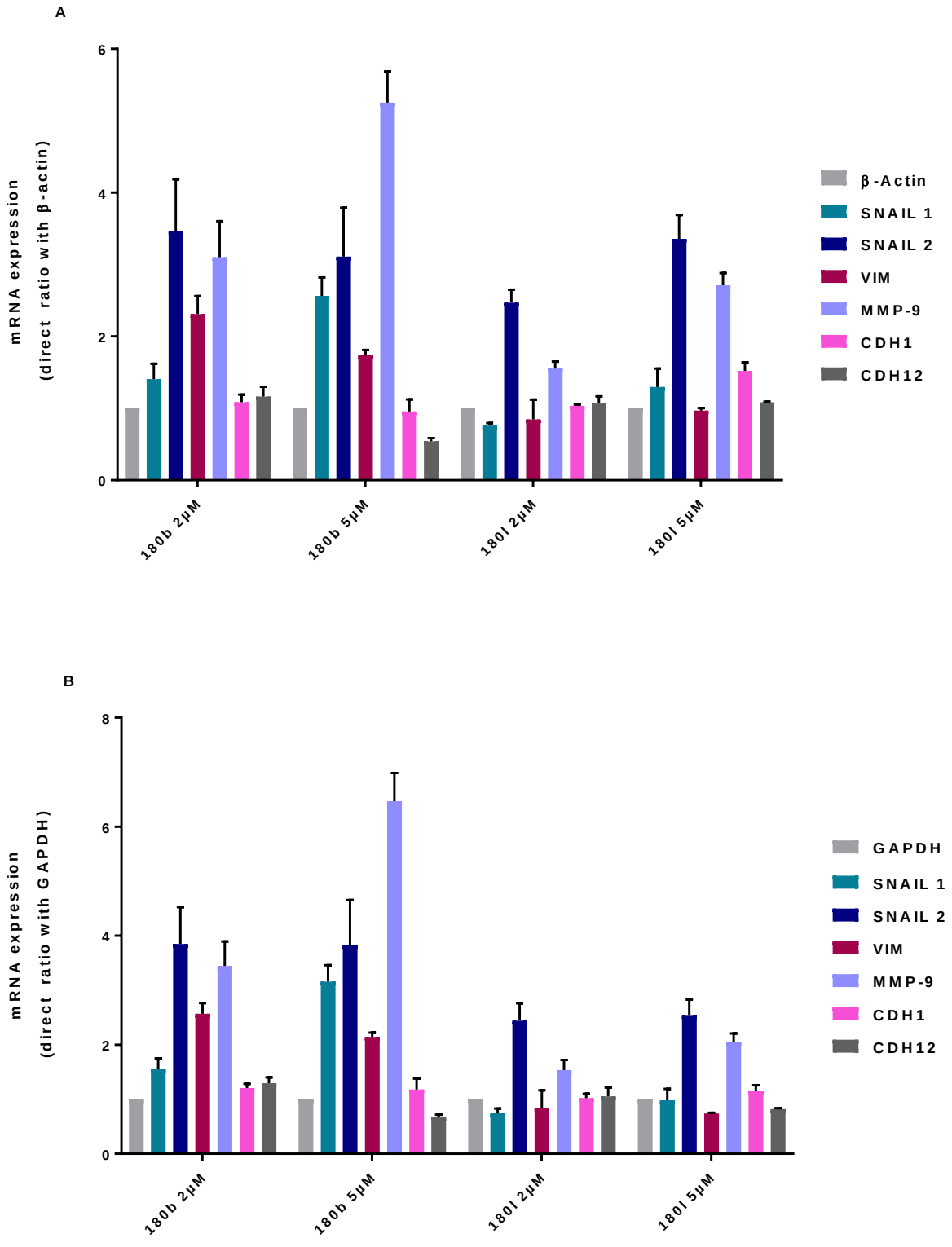

Figure 29. Analysis of the relative levels of *SNAIL 1*, *SNAIL 2*, *VIM*, *MMP 9*, *CDH1* and *CDH12* gene expression by real-time quantitative PCR in CAPAN-1 pancreatic cancer cells treated with the compounds **180b** and **180l**, at concentration of 2 μM or 5 μM, for 24h. Normalized gene expression levels were given as the ratio between the mean value for the target gene and that of the housekeeping genes β-actin (A) or GAPDH (B) in each sample**.**

5. EXPERIMENTAL SECTION

5.1 Chemistry

The dry solvents used for organic synthesis (acetonitrile, dimethylformammide and diethyl ether) and the reagents were purchased from Sigma-Aldrich Co, Alfa Aesar, VWR International and Acros Organics. Other solvents were purified and dried using standard method: toluene was distilled from calcium hydride, ethanol and methanol from iodine and magnesium. All dry solvents were stored over 4 Å molecular sieves. All air- or moisture-sensitive reactions were performed using oven-dried glassware under an inert dry nitrogen atmosphere. Analytical thin layer chromatography (TLC) was performed on silica gel 60 F254 plates (0.25 mm thickness) and the develop plates were examined under ultraviolet (UV) light. All melting points were taken on a Buchi-Tottoly capillary apparatus and were uncorrected. IR spectra were determined in bromoform with a Shimadzu FT / IR 8400S spectrophotometer and peaks were reported in wavenumber (cm^{-1}). ^{1}H and ^{13}C NMR spectra were measured at 200 and 50 MHz, respectively, on DMSO-d_6 or $CDCl_3$ solution, using a Bruker Avance II series 200 MHz spectrometer. Chemical shifts were described in parts per million (δ), coupling constants (J) are expressed in Hertz (Hz), and splitting patterns were reported as singlet (s), doublet (d), triplet (t), quartet (q), multiplet (m), doublet of doublets (dd) and triplet of doublets (td). Chromatography column was performed with MERK silica gel 230-400 mesh ASTM or FLASH40i Biotage chromatography or with Buchi Sepacore chromatography module (prepacked cartridge reference). Elementary analyses (C, H, N) were within ± 0.4% of the theoretical values.

Compounds **195a-m, 179a-b, 179d-f, 179h-q, 181a-f** and **200** were characterized only by ^{1}H NMR spectra, for their poor solubility.

General procedure for the synthesis of 1-methyl-1*H*-indoles (186a-e)

To a cold solution of commercial indole **185a-e** (0.8 g, 5.0 mmol) in anhydrous toluene (50 mL), potassium *t*-butoxide (0.8 g, 6.8 mmol) and tris[2-(2-methoxyethoxy)ethyl]amine (TDA-1) (1–2 drops) were added. After stirring for overnight, methyl iodide (0.3 mL, 5 mmol) was added dropwise to the reaction mixture. Then, the resulting suspension was stirred at room temperature for 1-2 h. After the solvent was removed *in vacuo*, the resulting residue was treated with water (15 mL) and extracted with DCM (3 × 15 mL), dried (Na_2SO_4) and evaporated under reduced pressure. The product obtained was used it was or further purified by column chromatography, using DCM/EtOAc (9/1) as eluent.

5-Bromo-1-methyl-1*H*-indole (186a)

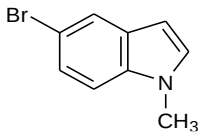

Conditions: room temperature for 1h; work-up: extraction with DCM; yield: 96%; yellow oil; ^{1}H NMR (200 MHz, $CDCl_3$) δ: 3.47 (3H, s, CH_3), 6.29 (1H, d, *J* = 3.1 Hz, H-3), 6.84 (1H, d, *J* = 3.1 Hz, H-2), 6.94 (1H, d, *J* = 8.5 Hz, H-7), 7.17 (1H, dd, *J* = 8.5, 1.7 Hz, H-6), 7.65 (1H, d, *J* = 1.7 Hz, H-4); ^{13}C NMR (50 MHz, $CDCl_3$) δ: 32.6 (q), 100.2 (d), 110.5 (d), 121.2 (s), 122.9 (d), 123.9 (d), 127.6 (s), 129.8 (d), 135.1 (s); *Anal.* Calculated for C_9H_8BrN (MW: 210.07): C, 51.46; H, 3.84; N, 6.67%. Found: C, 51.62; H, 3.78; N, 6.89%.

5-Fluoro-1-methyl-1*H*-indole (186b)

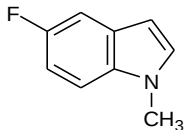

Conditions: room temperature for 1 h; work-up: extraction with DCM; yield: 98%; light yellow oil; ^{1}H NMR (200 MHz, $CDCl_3$) δ: 3.72 (3H, s, CH_3), 6.41 (1H, d, *J* = 3.2 Hz, H-3), 6.89-7.05 (2H, m, H-4 and H-6), 7.15-7.28 (2H, m, H-2 and H-7); ^{13}C NMR (50 MHz, $CDCl_3$) δ: 33.0 (q), 100.7 (d, $J_{C3\text{-}F}$ = 4.9 Hz), 105.4 (d, $J_{C7\text{-}F}$ = 5.6 Hz), 109.6 (d, $J_{C4\text{-}F}$ = 23.3 Hz), 109.9 (d, $J_{C6\text{-}F}$ = 10.8 Hz), 130.3 (d), 130.4 (s x 2), 157.8 (d, $J_{C5\text{-}F}$ = 233.0 Hz); *Anal.* Calculated for C_9H_8FN (MW: 149.16): C, 72.47; H, 5.41; N, 9.39%. Found: C, 72.82; H, 5.21; N, 9.12%.

1-Methyl-1*H*-indole (186c)

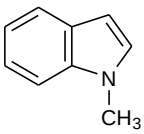

Conditions: room temperature for 1 h; work-up: extraction with DCM; yield: 96%; yellow oil; ^{1}H NMR (200 MHz, $CDCl_3$) δ: 3.86 (3H s, CH_3), 6.67-6.69 (1H, m, H-3), 7.17 (1H, d, *J* = 3.2 Hz, H-2), 7.29-7.35 (1H, m, H-5), 7.39-7.49 (2H, m, H-6 and H-7), 7.83-7.86 (1H, m, H-4); ^{13}C NMR (50

MHz, $CDCl_3$) δ: 32.4 (q), 100.2 (d), 109.6 (d), 118.8 (d), 120.2 (d), 120.9 (d), 128.0 (s), 129.5 (d), 136.3 (s); *Anal.* Calculated for C_9H_9N (MW: 131.17): C, 82.41; H, 6.92; N, 10.68%. Found: C, 82.59; H, 6.80; N, 10.77%.

5-Methoxy-1-methyl-1*H*-indole (186d)

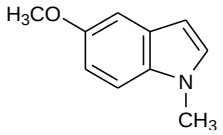

Conditions: room temperature for 2 h; work-up: extraction with DCM; yield: 98%; orange oil; ^1H NMR (200 MHz, $CDCl_3$) δ: 3.67 (3H, s, CH_3), 3.81 (3H, s, OCH_3), 6.38 (1H, d, *J* = 2.9 Hz, H-3), 6.87 (1H, dd, *J* = 8.8, 2.9 Hz, H-6), 6.96 (1H, d, *J* = 2.9 Hz, H4), 7.07 (1H, d, *J* = 2.9 Hz, H-2), 7.17 (1H, d, *J* = 8.8 Hz, H-7); ^{13}C NMR (50 MHz, $CDCl_3$) δ: 32.8 (q), 55.8 (q), 100.3 (d), 102.4 (d), 109.8 (d), 111.8 (d), 128.7 (s), 129.2 (d), 132.1 (s), 153.9 (s); *Anal.* Calculated for $C_{10}H_{11}NO$ (MW: 161.08): C, 74.51; H, 6.88; N, 8.69%. Found: C, 74.76; H, 6.84; N, 8.43%.

5-Cloro-1-methyl-1*H*-indole (186e)

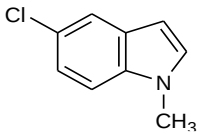

Conditions: room temperature for 1 h; work-up: extraction with DCM; yield: 90%; yellow oil; ^1H NMR (200 MHz, $CDCl_3$) δ: 3.52 (3H, s, CH_3), 6.32 (1H, d, *J* = 3.2 Hz, H-3), 6.89 (1H, d , *J* = 3.2 Hz, H-2), 7.05 (1H, d, *J* = 8.4 Hz, H-7), 7.51 (1H, d, *J* = 8.4 Hz, H-6), 7.65 (1H, s, H-4); ^{13}C NMR (50 MHz, $CDCl_3$) δ: 32.2 (q), 100.2 (d), 110.0 (d), 119.7 (d), 121.3 (d), 124.6 (s), 129.2 (s), 129.9 (d), 134.8 (s); *Anal.* Calculated for C_9H_8ClN (MW: 165.62): C, 65.27; H, 4.87; N, 8.46%. Found: C, 65.54; H, 4.84; N, 8.69%.

General procedure for the synthesis of 1*H*-indole-3-carbonitriles (189a-d) and 1-methyl-1*H*-indole-3-carbonitriles (190a-e)

To a solution of the appropriate indole of the type **185**, **186** (1.0 g, 5.10 mmol) in anhydrous acetonitrile (4.5 mL) at 0 °C chlorosulfonyl isocyanate (CSI) (0.44 ml, 5.10 mmol) was added

dropwise. The reaction mixture was stirred at 0 °C for 2 hours. After that, dimethylformamide anhydrous (DMF) (2.8 mL, 36.39 mmol) was added dropwise and the reaction mixture was stirred at 0 °C for 1 hour and 30 minutes. The mixture was poured into water and ice and the obtained precipitate was filtered off and dried, to give the desired derivatives **189a-d, 190a-e**.

5-Bromo-1*H*-indole-3-carbonitrile (189a)

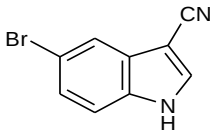

Yield: 98%; white solid; mp: 194-195 °C; IR (cm^{-1}): 3442 (NH), 2221 (CN); ^{1}H NMR (200 MHz, DMSO-d_6) δ: 7.41 (1H, d, J = 8.4 Hz, H-6), 7.54 (1H, d, J = 8.4 Hz, H-7), 7.80 (1H, s, H-4), 8.32 (1H, s, H-2), 12.41(1H, bs, NH); ^{13}C NMR (50 MHz, DMSO-d_6) δ: 83.9 (s), 114.3 (s), 114.9 (d), 115.6 (s), 120.6 (d), 126.0 (d), 128.3 (s), 133.9 (s), 135.8 (d); *Anal*. Calculated for $C_9H_5BrN_2$ (MW: 221.05): C, 48.90; H, 2.28; N, 12.67%. Found: C, 49.23; H, 2.15; N, 12.47%.

5-Fluoro-1*H*-indole-3-carbonitrile (189b)

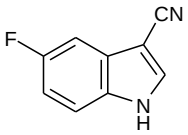

Yield: 90%; light brown solid; mp: 176-177 °C; IR (cm^{-1}): 3443 (NH), 2231 (CN); ^{1}H NMR (200 MHz, DMSO-d_6) δ: 7.15 (1H, td, J = 9.3, 9.2, 2.5 Hz, H-6), 7.42 (1H, dd, J = 9.2, 2.5 Hz, H-7), 7.54-7.61 (1H, m, H-4), 8.33 (1H, d, J = 3.1 Hz, H-2), 12.33 (1H, bs, NH); ^{13}C NMR (50 MHz, DMSO-d_6) δ: 84.5 (d, $J_{C7a\text{-}F}$ = 4.5 Hz), 103.6 (d, $J_{C4\text{-}F}$ = 24.8 Hz), 111.8 (d, $J_{C6\text{-}F}$ = 26.2 Hz), 114.3 (d, $J_{C7\text{-}F}$ = 9.6 Hz), 115.9 (s), 127.2 (d, $J_{C3a\text{-}F}$ = 10.9 Hz), 131.8 (s), 136.2 (d), 158.3 (d, $J_{C5\text{-}F}$ = 236.1 Hz); *Anal*. Calculated for $C_9H_5FN_2$ (MW: 160.15): C, 67.50; H, 3.15; N, 17.49%. Found: C, 67.60; H, 3.25; N, 17.29%.

1*H*-Indole-3-carbonitrile (189c)

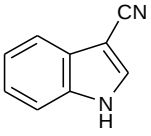

Yield: 90%, light orange solid; mp: 178-179 °C; IR (cm^{-1}): 3442 (NH), 2224 (CN); ^{1}H NMR (200 MHz, DMSO-d_6) δ: 7.20-7.34 (2H, m, H-5 and H-6), 7.52-7.69 (2H, m, H-4 and H-7), 8.26 (1H, d, *J* = 3.0 Hz, H-2), 12.21 (1H, bs, NH); ^{13}C NMR (50 MHz, DMSO-d_6) δ: 84.2 (s), 112.9 (d), 116.5 (s), 118.4 (d), 121.6 (d), 123.3 (d), 126.7 (s), 134.4 (d), 135.2 (s); *Anal*. Calculated for $C_9H_6N_2$ (MW: 142.16): C, 76.04; H, 4.25; N, 19.71%. Found: C, 75.87; H, 4.03; N, 20.10%.

5-Methoxy-1*H*-indole-3-carbonitrile (189d)

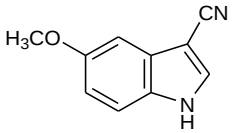

Yield: 90%; light brown solid; mp: 157-158 °C; IR (cm^{-1}): 3427 (NH), 2234 (CN); ^{1}H NMR (200 MHz, DMSO-d_6) δ: 3.81 (3H, s, OCH_3), 6.90 (1H, dd, *J* = 8.5, 2.4 Hz, H-6), 7.08 (1H, d, *J* = 2.4 Hz, H-4), 7.44 (1H, d, *J* = 8.5 Hz, H-7), 8.17 (1H, d, *J* = 3.1 Hz, H-2), 12.07 (1H, bs, NH); ^{13}C NMR (50 MHz, DMSO-d_6) δ: 55.3 (q), 83.9 (s), 99.6 (d), 113.8 (2 × d), 116.6 (s), 127.5 (s), 129.9 (s), 134.3 (d), 155.2 (s); *Anal*. Calculated for $C_{10}H_8N_2O$ (MW: 172.18): C, 69.76; H, 4.68; N, 16.27%. Found: C, 69.47; H, 4.57; N, 16.67%

5-Bromo-1-methyl-1*H*-indole-3-carbonitrile (190a)

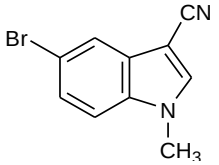

Yield: 98%; light brown solid; mp: 106.2-107.2 °C; IR (cm^{-1}): 2222 (CN); ^{1}H NMR (200 MHz, DMSO-d_6) δ: 3.87 (3H, s, CH_3), 7.48 (1H, dd, *J* = 8.8, 1.9 Hz, H-6), 7.64 (1H, d, *J* = 8.8 Hz, H-7), 7.80 (1H, d, *J* = 1.9 Hz, H-4), 8.31 (1H, s, H-2). ^{13}C NMR (50 MHz, DMSO-d_6) δ: 33.6 (q), 113.6 (d), 114.8 (s),115.3 (s), 120.8 (d), 126.1 (d), 128.6 (s), 134.7 (s), 139.0 (d); *Anal.* Calculated for $C_{10}H_7BrN_2$ (MW: 235.08): C, 51.09; H, 3.00; N, 11.92%. Found: C, 51.15; H, 3.04; N, 11.84%.

5-Fluoro-1-methyl-1*H*-indole-3-carbonitrile (190b)

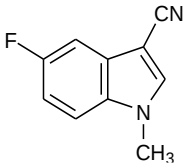

Yield: 80%; white solid; mp: 77.5-76.5 °C; IR (cm^{-1}): 2223 (CN); ^{1}H NMR (200 MHz, DMSO-d_6) δ: 3.88 (3H, s, CH_3); 7.17-7.28 (1H, td, J = 9.3, 9.2, 2.5 Hz, H-6); 7.41-7.47 (1H, m, H-7); 7.65-7.72 (1H, m, H-4); 8.31 (1H, s, H-2); ^{13}C NMR (50 MHz, DMSO-d_6) δ: 33.59 (q), 83.2 (s, $J_{C7a\text{-}F}$ = 4.5 Hz), 103.8 (d, $J_{C4\text{-}F}$ = 24.9 Hz), 111.8 (d, $J_{C6\text{-}F}$ = 26.2 Hz), 113.1 (d, $J_{C7\text{-}F}$ = 9.9 Hz), 115.6 (s), 127.5 (s, $J_{C3a\text{-}F}$ = 11.0 Hz), 132.6 (s), 139.2 (d), 158.5 (d, $J_{C5\text{-}F}$ = 236.6 Hz); *Anal.* Calculated for $C_{10}H_7FN_2$ (MW: 174.17): C, 68.96; H, 4.05; N, 16.08%. Found: C, 68.91; H, 4.15; N, 16.16%.

1-Methyl-1*H*-indole-3-carbonitrile (190c)

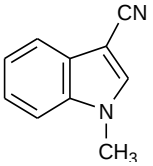

Yield: 77%; yellow oil; IR (cm^{-1}): 2218 (CN); ^{1}H NMR (200 MHz, DMSO-d_6) δ: 3.88 (3H, s, CH_3), 7.25-7.40 (2H, m, H-5 and H-6) 7.63-7.68 (2H, m, H-4 and H-7), 8.27 (1H, s, H-2); ^{13}C NMR (50 MHz, $CDCl_3$) δ: 33.8 (q), 83.0 (s), 111.5 (d), 118.6 (d), 121.9 (d), 123.3 (d), 127.0 (s), 135.8 (d), 137.7 (s). *Anal.* Calculated for $C_{10}H_8N_2$ (MW: 156.18): C, 76.90; H, 5.16; N, 17.94%. Found: C, 76.42; H, 5.35; N 18.30%.

5-Methoxy-1-methyl-1*H*-indole-3-carbonitrile (190d)

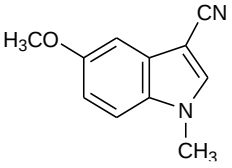

Yield: 80%; white solid; mp: 106.5-107.5 °C; IR (cm^{-1}): 2217 (CN); ^{1}H NMR (200 MHz, DMSO-d_6) δ: 3.83 (6H, m, CH_3 x 2), 7.26–6.82 (2H, m, H-4, H-6), 7.54 (1H, d, J = 9.0 Hz, H-7), 8.16 (1H,

s, H-2); ^{13}C NMR (50 MHz, DMSO-d_6) δ: 33.5 (q), 55.4 (q), 82.6 (s), 99.9 (d), 112.4 (d), 113.7 (d), 116.3 (s), 127.9 (s), 130.8 (s), 137.4 (d), 155.5 (s); *Anal.* Calculated for $C_{11}H_{10}N_2O$ (MW: 186.21): C, 70.95; H, 5.41; N, 15.04%. Found: C, 70.98; H, 5.44; N, 15.14%.

5-Cloro-1-methyl-1*H*-indole-3-carbonitrile (190e)

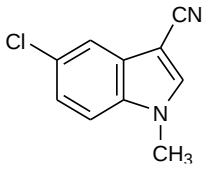

Yield: 79%; light yellow solid; mp: 103.5-104.5 °C; IR (cm^{-1}): 2220 (CN); ^{1}H NMR (200 MHz, $CDCl_3$) δ: 3.85 (3H, s, CH_3), 7.31 (2H, m, H-6 and H-7), 7.58 (1H, s, H-4), 7.73 (1H, d, *J* = 1.2 Hz, H-2); ^{13}C NMR (50 MHz, $CDCl_3$) δ: 33.8 (q), 85.2 (s), 111.4 (d), 115.1 (d), 119.2 (s), 124.4 (d), 128.3 (s), 128.6 (s), 134.4 (s), 136.5 (d); *Anal.* Calculated for $C_{10}H_7ClN_2$ (MW: 190.63): C, 63.01; H, 3.70; N, 14.70%. Found: C, 63.04; H, 3.72, N, 14.64%.

General procedure for the synthesis of *N*-hydroxy-1-methyl-1*H*-indole-3-carboxamidines (182a-e) and *N*-hydroxy-1*H*-indole-3-carboxamidines (183a-d)

To a solution of the appropriate indole carbonitrile **189a-d**, **190a-e** (2.88 mmol) in anhydrous ethanol (50 mL) *N*,*N*-diisopropylethylamine (DIPEA) (1.08 mL) and hydroxylamine hydrochloride ($NH_2OH{\cdot}HCl$) (530 mg, 7.63 mmol) were added in portions. The reaction mixture was heated to vigorous reflux for 1-3 h. The solvent was removed under reduced pressure and the residue was treated with a saturated aqueous solution of sodium hydrogencarbonate ($NaHCO_3$) (10 mL) and then extracted with ethyl acetate (3 × 20 mL), dried (Na_2SO_4), filtered and concentrated under *vacuum*. The product was purified by column chromatography using ethyl acetate as eluent.

5-Bromo-*N*'-hydroxy-1-methyl-1*H*-indole-3-carboxamidine (182a)

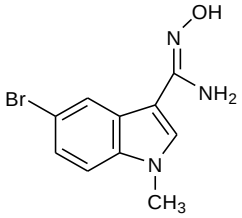

Yield: 72%; mp: 165.9-166.9 °C; IR (cm^{-1}): 3465 (OH), 3360 (NH_2), 1669 (C=N); ^1H NMR (200 MHz, DMSO-d_6) δ: 3.79 (3H, s, CH_3), 5.64 (2H, s, NH_2), 7.30 (1H, d, J = 8.7 Hz, H-6), 7.44 (1H, d, J = 8.7 Hz, H-7), 7.79 (1H, s, H-4), 8.27 (1H, s, H-2), 9.34 (1H, s, OH); ^{13}C NMR (50 MHz, DMSO-d_6) δ: 32.9 (q), 107.8 (s), 111.9 (d), 112.4 (s), 124.0 (d), 124.4 (d), 126.4 (s), 130.0 (d), 135.6 (s), 148.6 (s); *Anal.* Calculated for $C_{10}H_{10}BrN_3O$ (MW: 268.11): C, 44.80; H, 3.76; N, 15.67%. Found: C, 45.11; H, 4.00; N, 15.48%.

5-Fluoro-*N*'-hydroxy-1-methyl-1*H*-indole-3-carboxamidine (182b)

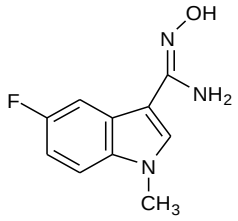

Yield: 70%; mp: 122-123 °C; IR (cm^{-1}): 3465 (OH), 3370 (NH_2), 1640 (C=N); ^1H NMR (200 MHz, DMSO-d_6) δ: 3.79 (3H, s, CH_3), 5.62 (1H, s, NH_2), 6.98- 7.09 (1H, td, J = 9.2, 9.1, 2.5 Hz, H-6), 7.45 (1H, dd, J = 9.1, 4.4 Hz, H-7), 7.74- 7.80 (2H, m, H-4 and H-2), 8.27 (1H, s, OH); ^{13}C NMR (50 MHz, DMSO-d_6) δ: 33.0 (q), 106.7 (d, $J_{C4\text{-}F}$ = 24.8 Hz), 108.5 (s, $J_{C7a\text{-}F}$ = 4.6 Hz), 109.7 (d, $J_{C6\text{-}F}$ = 26.1 Hz), 111.0 (d, $J_{C7\text{-}F}$ = 9.9 Hz), 125.0 (s, $J_{C3a\text{-}F}$ = 11.0 Hz), 130.3 (d), 133.6 (s), 148.8 (s), 157.3 (s, $J_{C5\text{-}F}$ = 231.9 Hz); *Anal*. Calculated for $C_{10}H_{10}FN_3O$ (MW: 207.20): C, 57.97; H, 4.86; N, 20.28%. Found: C, 57.88; H, 4.62; N, 20.31%.

***N*'-Hydroxy-1-methyl-1*H*-indole-3-carboxamidine (182c)**

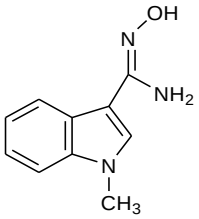

Yield: 80%; yellow oil; IR (cm^{-1}): 3472 (OH), 3387 (NH_2), 1640 (C=N); ^1H NMR (200 MHz, DMSO-d_6) δ: 3.79 (3H, s, CH_3), 5.59 (2H, s, NH_2), 7.03-7.22 (2H, m, H-5 and H-6), 7.43 (1H, d, J = 8.0 Hz, H-7), 7.73 (1H, s, H-2), 8.07 (1H, d, J =7.5 Hz, H-4), 9.27 (1H, s, OH); ^{13}C NMR (50 MHz, DMSO-d_6) δ: 32.6 (q), 108.1 (s), 109.7 (d), 119.6 (d), 121.6 (d), 122.1 (d), 124.8 (s), 128.7

(d), 136.8 (s), 149.1 (s); *Anal.* Calculated for $C_{10}H_{11}N_3O$ (MW: 189.21): C, 63.48; H, 5.86; N, 22.21%. Found: C, 63.48; H, 7.75; N, 22.46%.

5-Methoxy-*N'*-hydroxy-1-methyl-1*H*-indole-3-carboxamidine (182d)

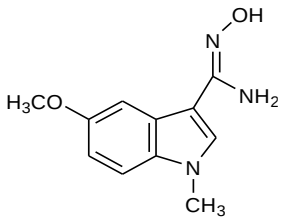

Yield: 75%; mp: 165.9-166.5 °C; IR (cm^{-1}): 3447 (OH), 3356 (NH_2), 1652 (C=N); ^1H NMR (200 MHz, DMSO-d_6) δ: 3.75 (6H, s, CH_3 and OCH_3), 5.58 (2H, s, NH_2), 6.82 (1H, dd, *J* = 8.9, 2.5 Hz, H-6), 7.33 (1H, d, *J* = 8.9 Hz, H-7), 7.59 (1H, d, *J* = 2.4 Hz, H-4), 7.69 (1H, s, H-2), 9.28 (1H, s, OH); ^{13}C NMR (50 MHz, DMSO-d_6) δ: 32.8 (q), 55.2 (q), 103.7 (d), 107.6 (s), 110.5 (d), 111.8 (d), 125.2 (s), 129.1 (d), 132.1 (s), 149.3 (s), 153.9 (s); *Anal.* Calculated for $C_{11}H_{13}N_3O_2$ (MW: 219.24): C, 60.26; H, 5.98; N, 19.17%. Found: C, 60.56; H, 5.68; N, 19.27%.

5-Cloro-*N'*-hydroxy-1-methyl-1*H*-indole-3-carboxamidine (182e)

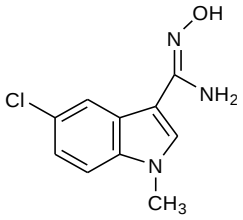

Yield: 82%; mp: 170.7-171.7 °C; IR (cm^{-1}): 3461 (OH), 3364 (NH_2), 1652 (C=N); ^1H NMR (200 MHz, DMSO-d_6) δ: 3.79 (3H, s, CH_3), 5.66 (2H, s, NH_2), 7.19 (1H, dd, *J* = 8.7, 2.2 Hz, H-6), 7.47 (1H, d, *J* = 8.7 Hz, H-7), 7.81 (1H, s, H-2), 8.13 (1H, d, *J* = 2.2 Hz, H-4), 9.35 (1H, s, OH); ^{13}C NMR (50 MHz, DMSO-d_6) δ: 32.9 (q), 107.8 (s), 111.5 (d), 121.3 (d), 121.5 (d) 124.4 (s), 125.8 (s), 130.2 (d), 135.4 (s), 148.6 (s); *Anal.* Calculated for $C_{10}H_{10}ClN_3O$ (MW: 223.66): C, 53.70; H, 4.51; N, 18.79%. Found: C, 53.82; H 4.67; N, 19.00%.

5-Bromo-*N'*-hydroxy-1*H*-indole-3-carboxamidine (183a)

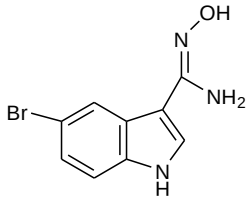

Yield: 70%; mp: 167.6-168.6 °C; IR (cm^{-1}): 3476 (OH), 3382 (NH_2), 3310 (NH), 1653 (C=N); ^1H NMR (200 MHz, DMSO-d_6) δ: 5.70 (2H, s, NH_2), 7.22 (1H, dd, *J* = 8.6, 2.6 Hz, H-6), 7.36 (1H, d, *J* = 8.6 Hz, H-7), 7.84 (1H, d, *J* = 2.6 Hz, H-4), 8.27 (1H, d, *J* = 1.9, H-2), 9.34 (1H, s, OH), 11.47 (1H, s, NH); ^{13}C NMR (50 MHz, DMSO-d_6) δ: 108.6 (s), 112.0 (s), 113.4 (d), 123.9 (d), 124.3 (d), 126.0 (d), 126.2 (s), 135.0 (s), 148.8 (s); *Anal.* Calculated for $C_9H_8BrN_3O$ (MW: 254.08): C, 42.54; H, 3.17; N, 16.54%. Found: C, 42.70; H, 3.38; N, 16.32%.

5-Fluoro-*N'*-hydroxy-1*H*-indole-3-carboxamidine (183b)

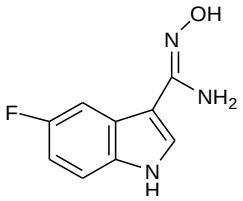

Yield: 68%; mp: 142.7-143.7 °C; IR (cm^{-1}): 3467 (OH), 3359 (NH_2), 3200 (NH), 1630 (C=N); ^1H NMR (200 MHz, DMSO-d_6) δ: 5.64 (2H, s, NH_2), 6.96 (1H, td, *J* = 9.1, 9.1, 2.7 Hz, H-6), 7.37 (1H, dd, *J* = 9.1, 4.7 Hz, H-7), 7.73-7.86 (2H, m, H-4 and H-2), 9.25 (1H, s, OH), 11.36 (1H, s, NH); ^{13}C NMR (50 MHz, DMSO-d_6) δ: 106.5 (d, $J_{C4\text{-}F}$ = 24.4 Hz), 109.1 (s, $J_{C7a\text{-}F}$ = 4.7 Hz), 109.7 (d, $J_{C6\text{-}F}$ = 26.1 Hz), 112.4 (d, $J_{C7\text{-}F}$ = 9.6 Hz), 124.7 (s, $J_{C3a\text{-}F}$ = 11.0 Hz), 126.4 (d), 133.0 (s), 149.1 (s), 157.1 (s, $J_{C5\text{-}F}$ = 231.9 Hz); *Anal.* Calculated for $C_9H_8FN_3O$ (MW: 193.18): C, 55.96; H, 4.17; N, 21.75%. Found: C, 56.02; H, 4.38; N, 21.52%.

***N'*-Hydroxy-1*H*-indole-3-carboxamidine (183c)**

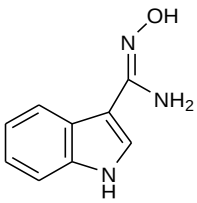

Yield 75%; mp: 147.8-148.8 °C; IR (cm^{-1}): 3607 (OH), 3491 (NH_2), 3392 (NH), 1646 (C=N); ^1H NMR (200 MHz, DMSO-d_6) δ: 5.60 (2H, s, NH_2), 7.01- 7.12 (2H, m, H-5 and H-6), 7.38 (1H, d, *J* = 6.30 Hz, H-7), 7.77 (1H, d, *J* = 2.7 Hz, H-2), 8.07 (1H, d, *J* = 7.5 Hz, H-4), 9.23 (1H, s, OH), 11.25 (1H, s, NH); ^{13}C NMR (50 MHz, DMSO-d_6) δ: 108.9 (s), 111.4 (d), 119.3 (d), 121.5 (d), 122.0 (d), 124.5 (s), 124.6 (d), 136.3 (s), 149.3 (s); *Anal.* Calculated for $C_9H_9N_3O$ (MW: 175.19): C, 61.70; H, 5.18; N, 23.99%. Found: C, 61.80; H, 5.38; N, 24.12%.

5-Metoxy-N'-hydroxy-1*H*-indole-3-carboxamidine (183d)

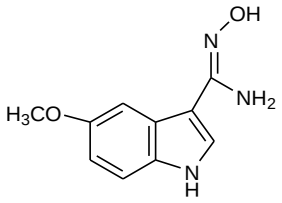

Yield: 60%; mp: 113.2-114.2 °C; IR (cm^{-1}): 3467 (OH), 3364 (NH_2), 3279 (NH), 1634 (C=N); ^1H NMR (200 MHz, DMSO-d_6) δ: 3.74 (3H, s, OCH_3), 5.59 (2H, s, NH_2), 6.75 (1H, dd, *J* = 8.8, 2.5 Hz, H-6), 7.27 (1H, d, *J* = 8.8 Hz, H-7), 7.58 (1H, d, *J* = 2.5 Hz, H-4), 7.73 (1H, s, H-2), 9.23 (1H, s, OH), 11.11 (1H, s, NH); ^{13}C NMR (50 MHz, DMSO-d_6) δ: 55.2 (q), 103.5 (d), 108.7 (s), 111.8 (d), 112.0 (d), 124.9 (s), 125.1 (d), 131.4 (s), 149.6 (s), 153.6 (s); *Anal.* Calculated for $C_{10}H_{11}N_3O_2$ (MW: 205.21): C, 58.53; H, 5.40; N, 20.48%. Found: C, 58.60; H, 5.38; N, 20.32%.

General procedure for the synthesis of (1-methyl-1*H*-indol-3-yl)-oxo-acetyl chlorides (184a-d)

To a solution of the opportune methyl-indole of the type **186** (10 mmol) in anhydrous diethyl ether (20 mL), oxalyl chloride (11.16 mmol, 0.95 mL) was added dropwise at 0 ° C. The reaction mixture was left to stir at 0 ° C for 3 h and then brought to 23 °C for 1 h. The resulting solid product was collected by *vacuum* filtration, washed with cold anhydrous diethyl ether (3 mL) and dried under vacuum for 24 hours. The product was used without further purification.

(5-Bromo-1-methyl-1*H*-indol-3-yl)-oxo-acetyl chloride (184a)

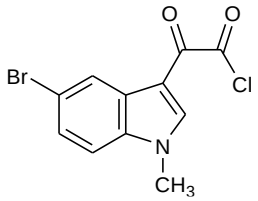

Yield: 88%; yellow solid; mp: 134.4-135.4 °C; IR (cm^{-1}): 1772 (CO), 1613 (CO); ^{1}H NMR (200 MHz, DMSO-d_6) δ: 3.92 (3H, s, CH_3), 7.50 (1H, dd, J = 8.7, 1.9 Hz, H-6), 7.61 (1H, d, J = 8.7 Hz, H-7), 8.31 (1H, d, J = 1.9 Hz, H-4) 8.55 (1H, s, H-2); ^{13}C NMR (50 MHz, DMSO-d_6) δ: 33.6 (q), 110.6 (s), 113.4 (d), 115.9 (s), 123.3 (d), 126.2 (d), 127.7 (s), 136.2 (s), 142.2 (d), 164.6 (s), 179.9 (s); *Anal.* Calculated for $C_{11}H_7BrClNO_2$ (MW: 300.54): C, 43.96; H, 2.35; N, 4.66%. Found: C, 44.14; H, 2.29; N, 4.78%.

(5-Fluoro-1-methyl-1*H*-indol-3-yl)-oxo-acetyl chloride (184b)

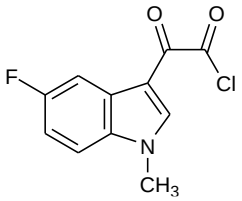

Yield: 93%, yellow solid; mp: 148.6-149.6 °C; IR (cm^{-1}): 1743 (CO), 1642 (CO);^{1}H NMR (200 MHz, DMSO-d_6) δ: 3.93 (3H, s, CH_3), 7.22 (1H, td, J = 9.6, 9.2, 2.6 Hz, H-6), 7.64 (1H, dd, J = 9.2, 4.4 Hz, H-7), 7.86 (1H, dd, J = 9.6, 2.6 Hz, H-4), 8.55 (1H, s, H-2); ^{13}C NMR (50 MHz, DMSO-d_6) δ: 33.7 (q), 106.2 (d, $J_{C4\text{-}F}$ = 24.8 Hz), 111.1 (s, $J_{C7a\text{-}F}$ = 4.4 Hz), 111.7 (d, $J_{C6\text{-}F}$ = 25.7 Hz), 112.7 (d, $J_{C7\text{-}F}$ = 9.8 Hz), 126.7 (s, $J_{C3a\text{–}F}$ = 11.2 Hz), 134.0 (s), 142.4 (d), 159.3 (s, $J_{C5\text{-}F}$ = 234.3 Hz), 166.4 (s), 181.2 (s); *Anal.* Calculated for $C_{11}H_7ClFNO_2$ (MW: 239.63): C, 55.13; H, 2.94; N, 5.85%. Found: C, 54.98; H, 3.01; N, 5.69%.

(1-Methyl-1*H*-indol-3-yl)-oxo-acetyl chloride (184c)

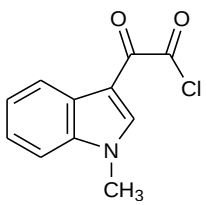

Yield: 79%, yellow solid; mp: 156.4-157.4 °C; IR (cm^{-1}): 1735 (CO); 1604 (CO); ^{1}H NMR (200 MHz, DMSO-d_6) δ: 3.93 (3H, s, CH_3), 7.28-7.41 (2H, m, H-5 and H-6), 7.59-7.64 (1H, m, H-7), 8.18-8.23 (1H, m, H-4), 8.50 (1H, s, H-2); ^{13}C NMR (50 MHz, DMSO-d_6) δ: 33.4 (q), 111.1 (s), 111.2 (d), 121.2 (d), 123.1 (d), 123.7 (d), 126.0 (s), 137.35 (s), 141.3 (d), 165.1 (s), 180.0 (s); *Anal.* Calculated for $C_{11}H_8ClNO_2$ (MW: 221,64): C, 59.61; H, 3.64; N, 6.32%. Found: C, 59.69; H, 3.70; N, 6.18%.

(5-Methoxy-1-methyl-1*H*-indol-3-yl)-oxo-acetyl chloride (184d)

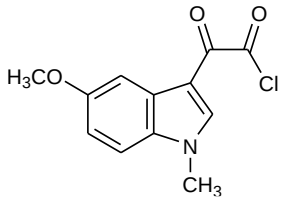

Yield: 80%, orange solid; mp: 132.2-133.2 °C; IR (cm^{-1}): 1779 (CO); 1625 (CO); ^{1}H NMR (200 MHz, DMSO-d_6) δ: 3.82 (3H, s, CH_3), 3.89 (3H, s, OCH_3), 6.98 (1H, dd, J = 8.9, 2.5Hz, H-6), 7.52 (1H, d, J = 8.9 Hz, H-7), 7.70 (1H, d, J = 2.5 Hz, H-4), 8.42 (1H, s, H-2); ^{13}C NMR (50 MHz, DMSO-d_6) δ: 33.5 (q), 55.3 (q), 103.2 (d), 110.9 (s), 112.0 (d), 113.1 (d), 127.0 (s), 132.2 (s), 141.0 (d), 156.4 (d), 165.3 (s), 180.0 (s); *Anal.* Calculated for $C_{12}H_{10}ClNO_3$ (MW: 251.67): C, 57.27; H, 4.01; N, 5.57%. Found: C, 57.19; H, 4.12; N, 5.37%.

General procedure for the synthesis of (1-methyl-1*H*-indol-3-yl)-oxo-acetic acids (192a-d)

To a solution of the suitable acylchloride of the type **184** (10 mmol) in anhydrous THF (20 mL), a solution of sodium hydroxide (NaOH) 2M was added dropwise, until complete alkalization, reaching a pH of 14. The reaction mixture was stirred at room temperature overnight. A solution of hydrochloric acid (HCl) 6M was added up to pH = 1. The resulting solid precipitate was collected by *vacuum* filtration, washed with H_2O and dried under *vacuum* for 24 h.

(5-Bromo-1-methyl-1*H*-indol-3-yl)-oxo-acetic acid (192a)

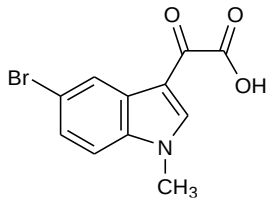

Yield: 82%; yellow solid; mp: 256.6 °C; IR (cm^{-1}): 3273 (OH), 1760 (CO), 1628 (CO); ^{1}H NMR (200 MHz, DMSO-d_6) δ: 3.93 (3H, s, CH_3), 7.50 (1H, dd, J = 8.7, 1.5 Hz , H-6), 7.62 (1H, d, J = 8.7, H-7), 8.31 (1H, d, J = 1.5, H-4), 8.55 (1H, s, H-2), 14.03 (1H, s, OH); ^{13}C NMR (50 MHz, DMSO-d_6) δ: 33.6 (q), 110.6 (s), 113.4 (d), 116.0 (s), 123.3 (d), 126.2 (d), 127.7 (s), 136.2 (s), 142.2 (d), 164.7 (s), 180.0 (s); *Anal.* Calculated for $C_{11}H_8BrNO_3$ (MW: 282.09): C, 46.84; H, 2.86; N, 4.97%. Found: C, 46.54; H, 2.98; N, 5.04%.

(5-Fluoro-1-methyl-1*H*-indol-3-yl)-oxo-acetic acid (192b)

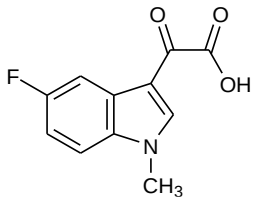

Yield: 90%; yellow solid; mp: 194.5 °C; IR (cm^{-1}): 3216 (OH), 1760 (CO), 1623 (CO); ^{1}H NMR (200 MHz, DMSO-d_6) δ: 3.93 (3H, s, CH_3), 7.23 (1H, td, J = 9.2, 9.1, 2.6 Hz, H-6), 7.66 (1H, dd, J = 9.1, 4.5 Hz, H-7), 7.86 (1H, dd, J = 9.2, 2.6 Hz, H-4), 8.56 (1H, s, H-2), 13.94 (1H, s, OH); ^{13}C NMR (50 MHz, DMSO-d_6) δ: 33.7 (q), 106.2 (d, $J_{C4\text{-}F}$ = 24.8 Hz), 111.1 (s, $J_{C7a\text{-}F}$ = 4.4 Hz), 111.7 (d, $J_{C6\text{-}F}$ = 25.7 Hz), 112.8 (d, $J_{C7\text{-}F}$ = 9.8 Hz,) 126.8 (s, $J_{C3a\text{-}F}$ = 11.2 Hz), 134.0 (s) 142.4 (d) 159.3 (s, $J_{C5\text{-}F}$ = 234.3 Hz), 164.8 (s), 179.9 (s); *Anal.* Calculated for $C_{11}H_8FNO_3$ (MW: 221.18): C, 59.73; H, 3.65; N, 6.33%. Found: C, 59.84; H, 3.71; N, 6.83%.

(1-Methyl-1*H*-indol-3-yl)-oxo-acetic acid (192c)

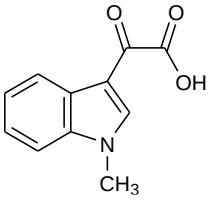

Yield: 65%; yellow solid; mp: 150.6 °C; IR (cm^{-1}): 3261 (OH), 1748 (CO), 1623 (CO); ^{1}H NMR (200 MHz, DMSO-d_6) δ: 3.93 (3H, s, CH_3), 7.28-7.41 (2H, m, H-5 and H-6), 7.62 (1H, dd, *J* = 5.8, 2.3 Hz, H-7), 8.20 (1H, dd, *J* = 6.6, 3.6 Hz, H-4), 8.49 (1H, s, H-2), 13.88 (1H, s, OH); ^{13}C NMR (50 MHz, DMSO-d_6) δ: 33.4 (q), 111.1 (s), 111.2 (d), 121.2 (d), 123.1 (d), 123.7 (d), 126.0 (s), 137.3 (s), 141.3 (d), 165.2 (s), 180.2 (s); *Anal.* Calculated for $C_{11}H_9NO_3$ (MW: 203.19): C, 65.02; H, 4.46; N, 6.89%. Found: C, 65.08; H, 4.36; N, 6.84%.

(5-Methoxy-1-methyl-1*H*-indol-3-yl)-oxo-acetic acid (192d)

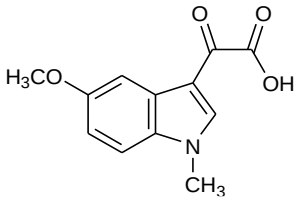

Yield: 70%; Yellow solid; mp: 196.2 °C; IR (cm^{-1}): 3216 (OH), 1765 (CO), 1628 (CO); ^{1}H NMR (200 MHz, DMSO-d_6) δ: 3.82 (3H, s, CH_3), 3.89 (3H, s, OCH_3), 6.98 (1H, dd, *J* = 8.9, 2.5 Hz, H-6), 7.52 (1H, d, *J* = 8,9 Hz, H-7), 7.7 (1H, d, *J* = 2.5 Hz, H-4), 8.41 (1H, s, H-2), 13.89 (1H, s, OH); ^{13}C NMR (50 MHz, DMSO-d_6) δ: 33.5 (q), 55.3 (q) 103.2 (d), 110.9 (s), 112.0 (d), 113.1 (d), 127.0 (s), 132.2 (s), 141.0 (d), 156.4 (d), 165.3 (s), 180.0 (s); *Anal.* Calculated for $C_{12}H_{11}NO_4$ (MW: 233.22): C, 61.80; H, 4.75; N, 6.01%. Found: C, 61.60; H, 4.55; N, 6.21.

General procedure for the synthesis of 1-methyl-*N*'-{[(1-methyl-1*H*-indol-3-yl)(oxo)acetyl]oxy}-1*H*-indole-3-carboximidamides (195a-m)

To a solution of the proper (1-methyl-1*H*-indol-3-yl)-oxo-acetic acid **192a-d** (1.42 mmol) and 1-hydroxybenzotriazole hydrate (HOBt) (230 mg, 1.7 mmol) in anhydrous dimethylformamide (DMF) (2 mL) at 0°C, *N*-ethyl-*N*′-(3-dimethylaminopropyl)carbodiimide hydrochloride (EDC·HCl) (326 mg, 1.7 mmol) was added in portions. After 15 min, a DMF (1 mL) solution of triethylamine (0.2 mL, 1.42 mmol) and appropriate 1-methyl-1*H*-indole-3-carboxamidine **182a-e** (0.71 mmol) was added dropwise at 0°C. The reaction mixture was stirred at 0°C for 15 min. The mixture was poured into water and ice and the obtained precipitate was filtered off and dried, to give the desired derivatives **195a-m.**

_N_'-{[(5-methoxy-1-methyl-1_H_-indol-3-yl)(oxo)acetyl]oxy}-1-methyl-1_H_-indole-3-carboximidamide (195a)

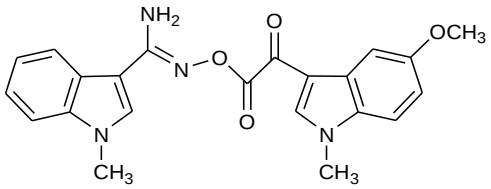

Yield: 73%; yellow solid; mp: 101.5 °C; IR (cm^{-1}): 1612 (CO), 1740 (CO), 3324 (NH_2); ^1H NMR (200 MHz, DMSO-d6) δ: 3.82 (3H, s, CH_3), 3.84 (3H, s, CH_3), 3.90 (3H, s, OCH_3), 6.69 (2H, s, NH_2), 6.97-7.03 (2H, m, H-5 and H-6'), 7.15-7.23 (1H, m, H-6), 7.45-7.57 (2H, m, H-7' and H-4), 7.73 (1H, d, *J* = 2.4 Hz, H-4'), 7.98-8.02 (2H, m, H-4 and H-2), 8.38 (1H, s, H-2'); *Anal.* Calculated for $C_{22}H_{20}N_4O_4$ (MW: 404.42): C, 65.34; H, 4.98; N, 13.85%. Found: C, 65.40; H, 5.00; N, 13.62%.

_N_'-{[(5-bromo-1-methyl-1_H_-indol-3-yl)(oxo)acetyl]oxy}-1-methyl-1_H_-indole-3-carboximidamide (195b)

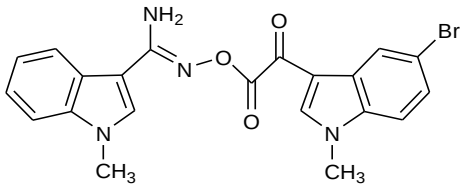

Yield: 80%; yellow solid; mp: 143.6 °C; IR (cm^{-1}): 1624 (CO), 1740 (CO), 3334 (NH_2); ^1H NMR (200 MHz, DMSO-*d6*) δ: 3.82 (3H, s, CH_3), 3.93 (3H, s, CH_3), 6.72 (2H, s, NH_2), 6.91-7.00 (1H, m, H-5), 7.15-7.23 (1H, m, H-6), 7.44-7.49 (1H, m, H-7), 7.54 (1H, dd, *J* = 8.7, 1.9 Hz, H-6'), 7.65 (1H, d, *J* = 8.7 Hz, H-7'), 7.92-7.98 (2H, m, H-4 and H-2), 8.36 (1H, d, *J* = 1.9 Hz, H-4'), 8.52 (1H, s, H-2'); *Anal.* Calculated for $C_{21}H_{17}BrN_4O_3$ (MW: 453.29): C, 55.64; H, 3.78; N, 12.36%. Found: C, 55.72; H, 3.60; N, 12.22%.

1-Methyl-_N_'-{[(1-methyl-1_H_-indol-3-yl)(oxo)acetyl]oxy}-1_H_-indole-3-carboximidamide (195c)

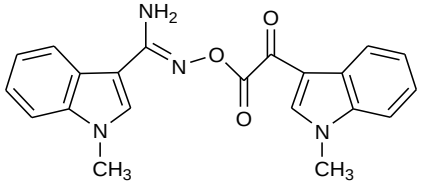

Yield: 95%; Yellow solid; mp: 121.6 °C; IR (cm^{-1}): 1623 (CO), 1748 (CO), 3381 (NH_2); ^1H NMR (200 MHz, DMSO-d_6) δ: 3.81 (3H, s, CH_3), 3.93 (3H, s, CH_3), 6.70 (2H, s, NH_2), 6.95 (1H, t, *J* = 7.4 Hz, H-5), 7.18 (1H, t, *J* = 7.6 Hz, H-5'), 7.36-7.48 (3H, m, H-6, H-6' and H-7), 7.61-7.66 (1H, m, H-7'), 7.96-8.00 (2H, m, H-4 and H-2), 8.22-8.30 (1H, m, H-4), 8.46 (1H, s, H-2'); *Anal.* Calculated for $C_{21}H_{18}N_4O_3$ (MW: 374.39): C, 67.37; H, 4.85; N, 14.96%. Found: C, 67.40; H, 4.90; N, 15.00%.

5-Bromo-*N*'-{[(5-fluoro-1-methyl-1*H*-indol-3-yl)(oxo)acetyl]oxy}-1-methyl-1*H*-indole-3-carboximidamide (195d)

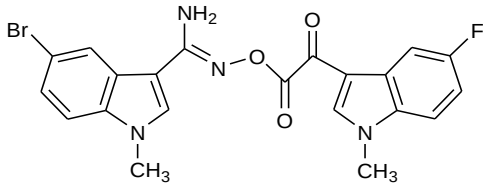

Yield: 88%; yellow solid; mp: 135.8 °C; IR (cm^{-1}): 1612 (CO), 1740 (CO), 3374 (NH_2); ^1H NMR (200 MHz, DMSO-d_6) δ: 3.82 (3H, s, CH_3), 3.95 (3H, s, CH_3), 6.79 (2H, s, NH_2), 7.19-7.34 (2H, m, H-6 and H-6'), 7.47 (1H, d, *J* = 8.7 Hz, H-7'), 7.68 (1H, dd, *J* = 9.0, 4.4 Hz, H-7), 7.90 (1H, dd, *J* = 9.6, 2.5 Hz, H-4), 8.04 (1H, s, H-2'), 8.21 (1H, m, H-4'), 9.09 (1H, s, H-2); *Anal.* Calculated for $C_{21}H_{16}BrFN_4O_3$ (MW: 471.28): C, 53.52; H, 3.42; N, 11.89%. Found: C, 53.70; H, 3.40; N, 11.62%.

5-Bromo-1-methyl-*N*'-{[(1-methyl-1*H*-indol-3-yl)(oxo)acetyl]oxy}-1*H*-indole-3-carboximidamide (195e)

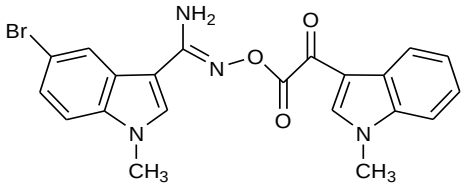

Yield: 87%; yellow solid; mp: 139.8 °C; IR (cm^{-1}): 1621 (CO), 1740 (CO), 3330 (NH_2); ^1H NMR (200 MHz, DMSO-d_6) δ: 3.82 (3H, s, CH_3), 3.94 (3H, s, CH_3), 6.77 (2H, s, NH_2), 7.29-7.39 (3H, m, H-5', H-6' and H-6), 7.48 (1H, d, *J* = 8.8 Hz, H-7), 7.61-7.65 (1H, m, H, H-7'), 8.04 (1H, s, H-2), 8.19-8.28 (2H, m, H-4 and H-4'), 8.49 (1H, s, H-2'); *Anal.* Calculated for $C_{21}H_{17}BrN_4O_3$ (MW: 453.29): C, 55.64; H, 3.78; N, 12.36%. Found: C, 55.55; H, 3.48; N, 12.28%.

5-Bromo-*N*'-{[(5-methoxy-1-methyl-1*H*-indol-3-yl)(oxo)acetyl]oxy}-1-methyl-1*H*-indole-3-carboximidamide (195f)

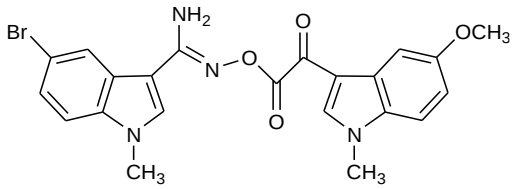

Yield: 95%; yellow solid; mp: 133.1 °C; IR (cm^{-1}): 1622 (CO), 1740 (CO), 3324 (NH_2); ^1H NMR (200 MHz, DMSO-d_6) δ: 3.83 (6H, bs, CH_3 x 2), 3.90 (3H, s, OCH_3), 6.78 (2H, s, NH_2), 6.99 (1H, dd, *J* = 8.9, 2.4 Hz, H-6'), 7.32 (1H, dd, *J* = 8.8, 1.8 Hz, H-6), 7.42-7.56 (2H, m, H-7 and H-7'), 7.72 (1H, d, *J* = 2.4 Hz, H-4'), 8.45 (1H, s, H-2), 8.20-8.27 (1H, m, H-4), 8.41 (1H, s, H-2'); *Anal.* Calculated for $C_{22}H_{19}BrN_4O_4$ (MW: 482.06): C, 54.67; H, 3.96; N, 11.59%. Found: C, 54.82; H, 3.88; N, 11.68%.

5-Fluoro-1-methyl-*N*'-{[(1-methyl-1*H*-indol-3-yl)(oxo)acetyl]oxy}-1*H*-indole-3-carboximidamide (195g)

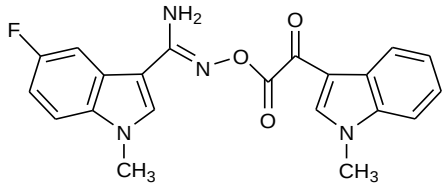

Yield: 98%; yellow solid; mp: 101.1 °C; IR (cm^{-1}): 1637 (CO), 1725 (CO), 3392 (NH_2); ^1H NMR (200 MHz, DMSO-d_6) δ: 3.83 (3H, s, CH_3), 3.94 (3H, s, CH_3), 6.74 (2H, s, NH_2), 7.05 (1H, td, *J* = 9.1, 9.1, 2.6 Hz, H-6), 7.34-7.39 (2H, m, H-5' and H-6'), 7.50 (1H, dd, *J* = 9.1, 4.5 Hz, H-7), 7.61-7.65 (1H, m, H-7'), 7.75 (1H, m, H-4), 8.06 (1H, s, H-2), 8.21-8.25 (1H, m, H-4'), 8.47 (1H, m, H-2'); *Anal.* Calculated for $C_{21}H_{17}FN_4O_3$ (MW: 392.13): C, 64.28; H, 4.37; N, 14.28%. Found: C, 64.55; H, 4.48; N, 14.28%.

5-Fluoro-*N*'-{[(5-fluoro-1-methyl-1*H*-indol-3-yl)(oxo)acetyl]oxy}-1-methyl-1*H*-indole-3-carboximidamide (195h)

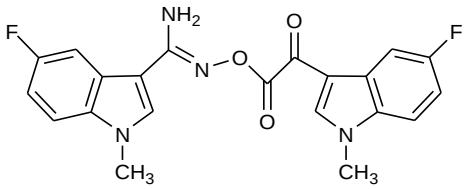

Yield: 88%; yellow solid; mp: 146.3 °C; IR (cm^{-1}): 1628 (CO), 1736 (CO), 3353 (NH_2); ^1H NMR (200 MHz, DMSO-d_6) δ: 3.82 (3H, s, CH_3), 3.94 (3H, s, CH_3), 6.75 (2H, s, NH_2), 7.05 (1H, td, *J* = 9.3, 9.2, 2.5 Hz, H-6), 7.25 (1H, td, *J* = 9.2, 9.1, 2.4 Hz, H-6'), 7.50 (1H, dd, *J* = 9.1, 4.5 Hz, H-7'), 7.64-7.71 (2H, m, H-7 and H-4'), 7.90 (1H, dd, *J* = 9.6, 2.5 Hz, H-4), 8.05 (1H, s, H-2), 8.53 (1H, s, H-2'); *Anal.* Calculated for $C_{21}H_{16}F_2N_4O_3$ (MW: 410.37): C, 61.46; H, 3.93; N, 13.65%. Found: C, 61.50; H, 3.10; N, 13.62%.

***N*'-{[(5-bromo-1-methyl-1*H*-indol-3-yl)(oxo)acetyl]oxy}-5-fluoro-1-methyl-1*H*-indole-3-carboximidamide (195i)**

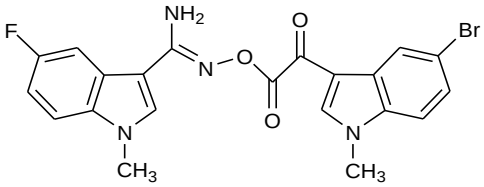

Yield: 72%; Yellow solid; mp: 168.8 °C; IR (cm^{-1}): 1623 (CO), 1735 (CO), 3353 (NH_2); ^1H NMR (200 MHz, DMSO-d_6) δ: 3.82 (3H, s, CH_3), 3.93 (3H, s, CH_3), 6.78 (2H, s, NH_2), 7.05 (1H, td, *J* = 9.1, 9.1, 2.5 Hz, H-6), 7.46-7.55 (2H, m, H-6' and H-7'), 7.61-7.71 (2H, m, H-7 and H-4), 8.06 (1H, s, H-2), 8.35 (1H, d, *J* = 1.7, H-4'), 8.53 (1H, s, H-2'); *Anal.* Calculated for $C_{21}H_{16}BrFN_4O_3$ (MW: 471.28): C, 53.52; H, 3.42; N, 11.89%. Found: C, 53.72; H, 3.30; N, 11.84%.

5-Fluoro-*N*'-{[(5-methoxy-1-methyl-1*H*-indol-3-yl)(oxo)acetyl]oxy}-1-methyl-1*H*-indole-3-carboximidamide (195j)

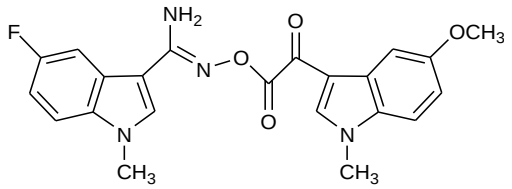

Yield: 70%; yellow solid; mp: 114.8 °C; IR (cm^{-1}): 1637 (CO), 1736 (CO), 3374 (NH_2); ^1H NMR (200 MHz, DMSO-d_6) δ: 3.82-3.83 (6H, m, CH_3 x 2), 3.90 (3H, s, OCH_3), 6.75 (2H, s, NH_2), 6.96-7.11 (2H, m, H-6 and H-6'), 7.45- 7.55 (2H, m, H-7 and H-7'), 7.72-7.78 (2H, m, H-4 and H-4'), 8.05 (1H, s, H-2), 8.35 (1H, s, H-2'); *Anal.* Calculated for $C_{22}H_{19}FN_4O_4$ (MW: 422.41): C, 62.55; H, 4.53; N, 13.26%. Found: C, 62.50; H, 4.31; N, 13.30%.

***N*'-{[(5-bromo-1-methyl-1*H*-indol-3-yl)(oxo)acetyl]oxy}-5-chloro-1-methyl-1*H*-indole-3-carboximidamide (195k)**

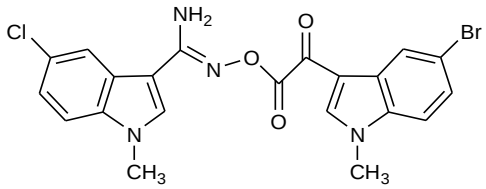

Yield: 93%; yellow solid; mp: 131.3 °C; IR (cm^{-1}): 1628 (CO), 1748 (CO), 3330 (NH_2); ^1H NMR (200 MHz, DMSO-d_6) δ: 3.82 (3H, s, CH_3), 3.93 (3H, s, CH_3), 6.81 (2H, s, NH_2), 7.18 (1H, dd, J = 8.6, 1.9 Hz, H-6'), 7.49-7.54 (2H, m, H-6 and H-7), 7.63 (1H, d, J = 8.6 Hz, H-7'), 7.94-7.95 (1H, m, H-4), 8.05 (1H, s, H-2), 8.36 (1H, d, J = 1.9 Hz, H-4'), 8.53 (1H, s, H-2'); *Anal.* Calculated for $C_{21}H_{16}BrClN_4O_3$ (MW: 487.73): C, 51.71; H, 3.31; N, 11.49%. Found: C, 51.80; H, 3.31; N, 11.50%.

5-Chloro-*N*'-{[(5-methoxy-1-methyl-1*H*-indol-3-yl)(oxo)acetyl]oxy}-1-methyl-1*H*-indole-3-carboximidamide (195l)

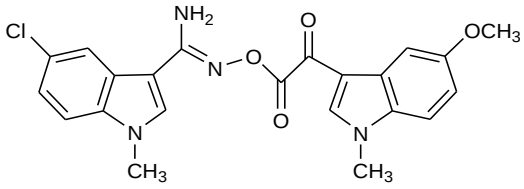

Yield: 81%; yellow solid; mp: 112.2 °C; IR (cm^{-1}): 1629 (CO), 1726 (CO), 3347 (NH_2); ^1H NMR (200 MHz, DMSO-d_6) δ: 3.83 (6H, s, CH_3 x 2), 3.90 (3H, s, OCH_3), 6.77 (2H, s, NH_2), 6.99 (1H, dd, *J* = 8.9, 2.5 Hz, H-6'), 7.21 (1H, dd, *J* = 8.8, 2.1 Hz, H-6), 7.51-7.55 (2H, m, H-7 and H-7'), 7.73 (1H, d, *J* = 2.5 Hz, H-4'), 8.04-8.06 (2H, m, H-4 and H-2), 8.40 (1H, s, H-2'); *Anal.* Calculated for $C_{22}H_{19}ClN_4O_4$ (MW: 438.86): C, 60.21; H, 4.36; N, 12.77%. Found: C, 60.30; H, 4.40; N, 12.72%.

5-Chloro-1-methyl-*N*'-{[(1-methyl-1*H*-indol-3-yl)(oxo)acetyl]oxy}-1-methyl-1*H*-indole-3-carboximidamide (195m)

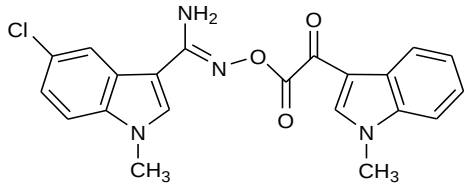

Yield: 87%; yellow solid; mp: 137.3 °C; IR (cm^{-1}): 1625 (CO), 1744 (CO), 3336 (NH_2); ^1H NMR (200 MHz, DMSO-d_6) δ: 3.82 (3H, s, CH_3), 3.94 (3H, s, CH_3), 6.77 (2H, s, NH_2), 7.20 (1H, dd, *J* = 8.7, 2.1 Hz, H-6), 7.33-7.39 (2H, m, H-5' and H-6'), 7.52 (1H, d, *J* = 8.7 Hz, H-7), 7.61-7.65 (1H, m, H-7'), 8.03-8.06 (2H, m, H-4 and H-2), 8.21-8.27 (1H, m, H-4'), 8.48 (1H, s, H-2'); *Anal.* Calculated for $C_{21}H_{17}ClN_4O_3$ (MW: 408.10): C, 61.69; H, 4.19; N, 13.70%. Found: C, 61.70; H, 4.40; N, 13.72%.

General procedure for the synthesis of (1-methyl-1*H*-indol-3-yl)[3-(1-methyl-1*H*-indol-3-yl)-1,2,4-oxadiazol-5-yl]methanones (179a-m)

To a solution of **195a-m** (0.19 mmol) in acetone (15 mL), an equimolar aqueous solution of sodium hydroxide (NaOH) 2M was added and stirred at room temperature for 30 min-1 h. The precipitated solid was filtered off, washed with water and dried under high *vacuum*. The product was purified by column chromatography using dichloromethane as eluent.

(5-Methoxy-1-methyl-1*H*-indol-3-yl)[3-(1-methyl-1*H*-indol-3-yl)-1,2,4-oxadiazol-5-yl]methanone (179a)

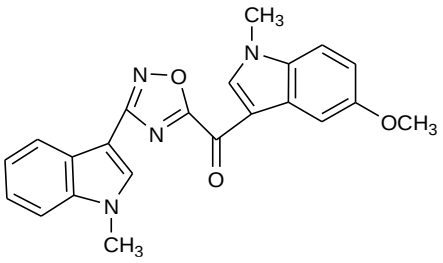

Conditions: 30 min at room temperature; yield: 71%; cream-white solid; mp: 265°C (dec.); IR (cm^{-1}): 1611 (CO); ^{1}H NMR (200 MHz, DMSO-d_6) δ: 3.86 (3H, s, CH_3), 3.96 (3H, s, CH_3), 4.04 (3H, s, OCH_3), 7.04 (1H, dd, *J* = 8.9, 2.5 Hz, H-6), 7.25–7.40 (2H, m, H-5' and H-6'), 7.63 (2H, m, H-7 and H-7'), 7.84 (1H, d, *J* = 2.5 Hz, H-4), 8.11 (1H, m, H-4'), 8.40 (1H, s, H-2'), 8.97 (1H, s, H-2); *Anal.* Calculated for $C_{22}H_{18}N_4O_3$ (MW: 386.40): C, 68.38; H, 4.70; N, 14.50%. Found: C, 68.48; H, 4.62; N, 14.38%.

(5-Bromo-1-methyl-1*H*-indol-3-yl)[3-(1-methyl-1*H*-indol-3-yl)-1,2,4-oxadiazol-5-yl]methanone (179b)

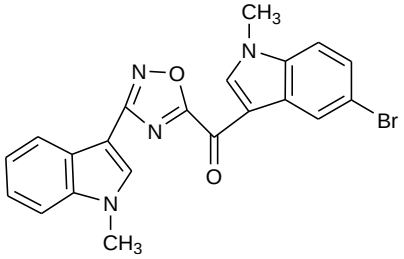

Conditions: 30 min at room temperature; yield: 63%; light yellow solid; mp: 238°C (dec.); IR (cm^{-1}): 1623 (CO); ^{1}H NMR (200 MHz, DMSO-d_6) δ: 3.96 (3H, s, CH_3), 4.04 (3H, s, CH_3), 7.27-7.39 (2H, m, H-5' and H-6'), 7.54- 7.72 (3H, m, H-6, H-7 and H-7'), 8.02-8.12 (1H, m, H-4'), 8.41-8.46 (2H, m, H-4 and H-2'), 9.09 (1H, s, H-2); *Anal.* Calculated for $C_{21}H_{15}BrN_4O_2$ (MW: 435.27): C, 57.95; H, 3.47; N, 12.87%. Found: C, 57.75; H, 3.32; N, 12.66%.

(1-Methyl-1*H*-indol-3-yl)[3-(1-methyl-1*H*-indol-3-yl)-1,2,4-oxadiazol-5-yl]methanone (179c)

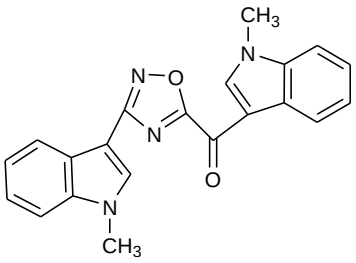

Conditions: 30 min at room temperature; yield: 62%; yellow solid; mp: 246°C (dec.); IR (cm^{-1}): 1634 (CO); ^{1}H NMR (200 MHz, DMSO-d_6) δ: 3.96 (3H, s, CH_3), 4.04 (3H, s, CH_3), 7.27-7.47 (4H, m, H-5, H-5', H-6 and H-6'), 7.62-7.72 (2H, m, H-7 and H-7'), 8.07-8.13 (1H, m, H-4'), 8.32- 8.37 (1H, m, H-4), 8.42 (1H, s, H-2'), 9.06 (1H, s, H-2); ^{13}C NMR (50 MHz, DMSO-d_6) δ: 33.0 (q), 33.7 (q), 100.9 (s), 110.9 (d), 111.5 (d), 112.7 (s), 120.7 (d), 121.4 (d), 121.5 (d), 122.8 (d), 123.6 (d), 124.2 (d), 124.5 (s), 126.3 (s), 133.4 (d), 137.4 (s), 137.5 (s), 142.3 (d), 165.0 (s), 169.7 (s), 170.4 (s); *Anal*. Calculated for $C_{21}H_{16}N_4O_2$ (MW: 356.38): C, 70.77; H, 4.53; N, 15.72%. Found: C, 70.89; H, 4.58; N, 15.54%.

[3-(5-Bromo-1-methyl-1*H*-indol-3-yl)-1,2,4-oxadiazol-5-yl](5-fluoro-1-methyl-1*H*-indol-3-yl)methanone (179d)

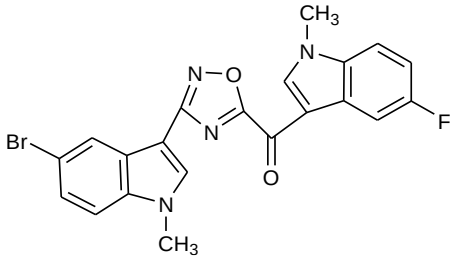

Conditions: 1 h at room temperature; Yield: 70%; Light yellow solid; mp: 256°C (dec.); IR (cm^{-1}): 1610 (CO); ^{1}H NMR (200 MHz, DMSO-d_6) δ: 3.96 (3H, s, CH_3), 4.04 (3H, s, CH_3), 7.29 (1H, td, *J* = 9.2, 9.1, 2.6 Hz, H-6), 7.48 (1H, dd, *J* = 8.8, 1.9 Hz, H-6'), 7.64 (1H, d, *J* = 8.8 Hz, H-7'), 7.74 (1H, dd, *J* = 9.1, 4.4 Hz, H-7), 7.99 (1H, dd, *J* = 9.5, 2.6 Hz, H-4), 8.21 (1H, d, *J* = 1.9 Hz, H-4'), 8.45 (1H, s, H-2'), 9.09 (1H, s, H-2); *Anal.* Calculated for $C_{21}H_{14}BrFN_4O_2$ (MW: 453.26): C, 55.65; H, 3.11; N, 12.36%. Found: C, 55.55; H, 3.31; N, 12.46%.

[3-(5-Bromo-1-methyl-1*H*-indol-3-yl)-1,2,4-oxadiazol-5-yl](1-methyl-1*H*-indol-3-yl)methanone (179e)

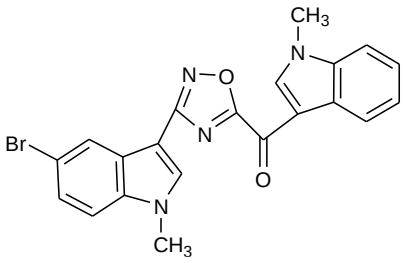

Conditions: 30 min at room temperature; yield: 67%; light yellow solid; mp: 250 °C (dec.); IR (cm^{-1}): 1628 (CO); ^{1}H NMR (200 MHz, DMSO-d_6) δ: 3.97 (3H, s, CH_3), 4.04 (3H, s, CH_3), 7.40-7.52 (3H, m, H-5, H-6 and H-7), 7.64-7.73 (2H, m, H-6' and H-7'), 8.23 (1H, d, *J* = 1.8 Hz, H-4'), 8.32-8.36 (1H, m, H-4), 8.47 (1H, s, H-2'), 9.05 (1H, s, H-2); *Anal.* Calculated for $C_{21}H_{15}BrN_4O_2$ (MW: 435.27): C, 57.95; H, 3.47; N, 12.87%. Found: C, 57.75; H, 3.53; N, 12.66%.

[3-(5-Bromo-1-methyl-1*H*-indol-3-yl)-1,2,4-oxadiazol-5-yl](5-methoxy-1-methyl-1*H*-indol-3-yl)methanone (179f)

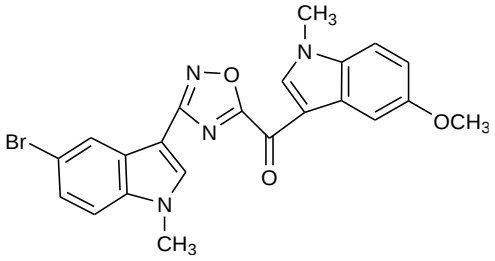

Conditions: 30 min at room temperature; yield: 85%; yellow solid; mp: 255 °C (dec.); IR (cm^{-1}): 1623 (CO); ^{1}H NMR (200 MHz, DMSO-d_6) δ: 3.86 (3H, s, CH_3), 3.96 (3H, s, CH_3), 3.99 (3H, s, OCH_3), 7.04 (1H, dd, *J* = 8.9, 2.5 Hz, H-6), 7.49 (1H, dd, *J* = 8.8, 1.9 Hz, H-6'), 7.58-7.67 (2H, m, H-7' and H-7), 7.83 (1H, d, *J* = 2.5 Hz, H-4), 8.22 (1H, d, *J* = 1.9 Hz, H-4'), 8.45 (1H, s, H-2'), 8.95 (1H, s, H-2); *Anal.* Calculated for $C_{22}H_{17}BrN_4O_3$ (MW: 465.30): C, 56.79; H, 3.68; N, 12.04%. Found: C, 56.85; H, 3.78; N, 12.08%.

[3-(5-Fluoro-1-methyl-1*H*-indol-3-yl)-1,2,4-oxadiazol-5-yl](1-methyl-1*H*-indol-3-yl)methanone (179g)

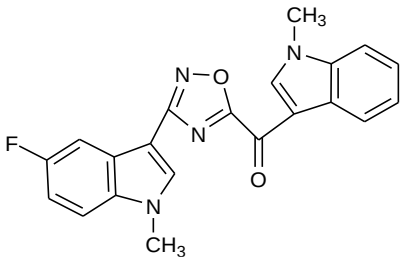

Conditions: 1 h at room temperature; yield: 68%; yellow solid; mp: 242 °C (dec.);IR (cm^{-1}): 1634 (CO); ^{1}H NMR (200 MHz, DMSO-d_6) δ: 3.97 (3H, s, CH_3), 4.03 (3H, s, CH_3), 7.22 (1H, td, J = 9.3, 9.2, 2.6 Hz, H-6'), 7.36-7.47 (2H, m, H-5 and H-6), 7.64- 7.78 (3H, m, H-7, H-7' and H-4'), 8.32-8.36 (1H, m, H-4), 8.47 (1H, s, H-2'), 9.04 (1H, m, H-2); ^{13}C NMR (50 MHz, DMSO-d_6) δ: 33.4 (q), 33.7 (q), 101.0 (s, J_{C7a-F} = 4.2 Hz), 105.5 (d, J_{C4-F} = 24.4 Hz), 111.0 (d, J_{C6-F} = 26.0 Hz), 111.5 (d), 112.4 (d, J_{C7-F} = 9.9 Hz), 112.7 (s), 121.5 (d), 123.6 (d), 124.1 (d), 124.9 (s, J_{C3a-F} = 10.8 Hz), 126.3 (s), 134.1 (s), 134.9 (d), 137.5 (s), 142.3 (d),158.2 (s, J_{C5-F} = 254.9 Hz), 164.7 (s), 169.8 (s), 170.3 (s); *Anal.* Calculated for $C_{21}H_{15}FN_4O_2$ (MW: 374.37): C, 67.37; H, 4.04; N, 14.97%. Found: C, 67.51; H, 3.88; N, 15.08%.

(5-Fluoro-1-methyl-1*H*-indol-3-yl)[3-(5-fluoro-1-methyl-1*H*-indol-3-yl)-1,2,4-oxadiazol-5-yl]methanone (179h)

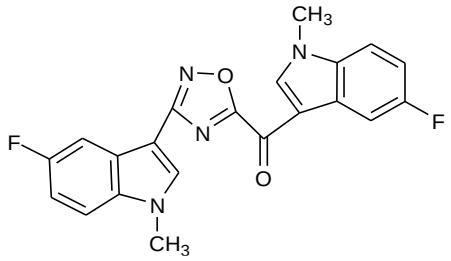

Conditions: 30 min at room temperature; yield: 71%; cream-white solid; mp: 265°C (dec.); IR (cm^{-1}): 1629 (CO); ^{1}H NMR (200 MHz, DMSO-d_6) δ: 3.97 (3H, s, CH_3), 4.04 (3H, s, CH_3), 7.17-7.35 (2H, m, H-6 and H-6'), 7.65-7.78 (3H, m, H-7, H-7' and H-4'), 8.00 (1H, dd, J = 9.6, 2.6 Hz, H-4), 8.47 (1H, s, H-2'), 9.09 (1H, s, H-2); *Anal.* Calculated for $C_{21}H_{14}F_2N_4O_2$ (MW: 392.36): C, 64.28; H, 3.60; N, 14.28%. Found: C, 64.38; H, 3.62; N, 14.38%.

(5-Bromo-1-methyl-1*H*-indol-3-yl)[3-(5-fluoro-1-methyl-1*H*-indol-3-yl)-1,2,4-oxadiazol-5-yl]methanone (179i)

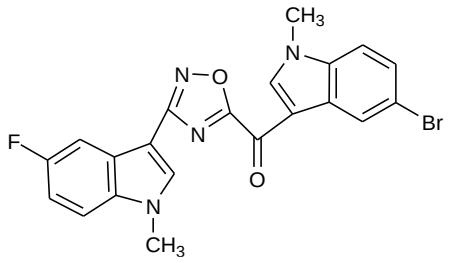

Conditions: 30 min at room temperature; yield: 71%; light yellow solid; mp: 270°C (dec.); IR (cm^{-1}): 1634 (CO); ^{1}H NMR (200 MHz, DMSO-d_6) δ: 3.97 (3H, s, CH_3), 4.04 (3H, s, CH_3), 7.22 (1H, td, *J* = 9.4, 9.3, 2.6 Hz, H-6'), 7.58 (1H, dd, *J* = 8.6, 1.9 Hz, H-6), 7.65-7.69 (1H, m, H-7), 7.72-7.78 (2H, m, H-7'and H-4'), 8.45 (1H, d, *J* = 1.9, H-4), 8.48 (1H, s, H-2'), 9.08 (1H, s, H-2); *Anal.* Calculated for $C_{21}H_{14}BrFN_4O_2$ (MW: 453.26): C, 55.65; H, 3.11; N, 12.36%. Found: C, 55.75; H, 3.22; N, 12.46%.

[3-(5-Fluoro-1-methyl-1*H*-indol-3-yl)-1,2,4-oxadiazol-5-yl](5-methoxy-1-methyl-1*H*-indol-3-yl)methanone (179j)

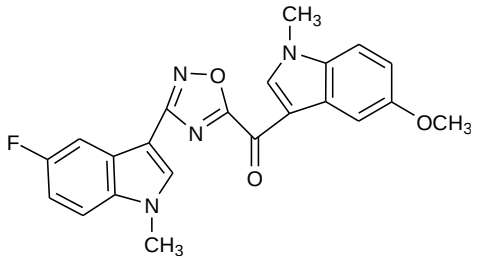

Conditions: 1 h at room temperature; yield: 86%; yellow solid; mp: 250°C (dec.); IR (cm^{-1}): 1617 (CO); ^{1}H NMR (200 MHz, DMSO) δ: 3.86 (3H, s, CH_3), 3.97-4.00 (6H, m, CH_3 and OCH_3), 7.02-7.07 (1H, m, H-6'), 7.17-7.27 (1H, m, H-6), 7.58-7.84 (4H, m, H-7, H-7', H-4 and H-4'), 8.47 (1H, s, H-2'), 8.96 (1H, s, H-2); *Anal* Calculated for $C_{22}H_{17}FN_4O_3$ (MW: 404.39): C, 65.34; H, 4.24; N, 13.85%. Found: C, 65.55; H, 4.31; N, 13.56%.

(5-Bromo-1-methyl-1*H*-indol-3-yl)[3-(5-chloro-1-methyl-1*H*-indol-3-yl)-1,2,4-oxadiazol-5-yl]methanone (179k)

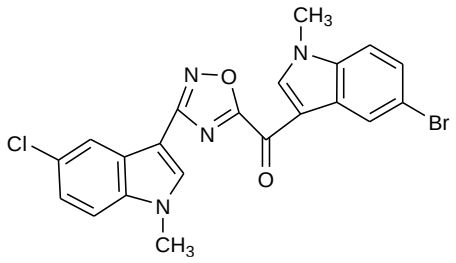

Conditions: 1 h at room temperature; yield: 65%; light yellow solid; mp: 273°C (dec.); IR (cm^{-1}): 1623 (CO); ^{1}H NMR (200 MHz, DMSO-d_6) δ: 3.97 (3H, s, CH_3), 4.04 (3H, s, CH_3), 7.35-7.40 (1H, m, H-6'), 7.55-7.60 (1H, m, H-6), 7.70 (2H, m, H-7' and H-7), 8.06 (1H, s, H-4), 8.45 (1H, s, H-4'), 8.48 (1H, s, H-2'), 9.08 (1H, s, H-2); *Anal.* Calculated for $C_{21}H_{14}BrClN_4O_2$ (MW: 469.72): C, 53.70; H, 3.00; N, 11.93%. Found: C, 53.90; H, 3.20; N, 11.98%.

[3-(5-Chloro-1-methyl-1*H*-indol-3-yl)-1,2,4-oxadiazol-5-yl](5-methoxy-1-methyl-1*H*-indol-3-yl)methanone (179l)

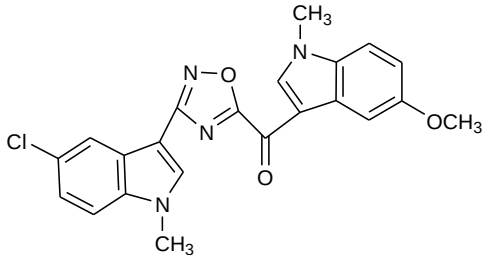

Conditions: 1 h at room temperature; yield: 67%; yellow solid; mp: 254 °C (dec.); IR (cm^{-1}): 1626 (CO); ^{1}H NMR (200 MHz, DMSO-d_6) δ: 3.86 (3H, s, CH_3), 3.97 (3H, s, CH_3), 4.04 (3H, s, OCH_3), 7.04 (1H, dd, *J* = 8.9, 2.5 Hz, H-6), 7.38 (1H, dd, *J* = 8.8, 2.1 Hz, H-6'), 7.61 (1H, d, *J* = 8.9 Hz, H-7), 7.70 (1H, d, *J* = 8.8 Hz, H-7'), 7.84 (1H, d, *J* = 2.5 Hz, H-4), 8.07 (1H, d, *J* = 2.1 Hz, H-4'), 8.48 (1H, s, H-2'), 8.97 (1H, s, H-2); *Anal.* Calculated for $C_{22}H_{17}ClN_4O_3$ (MW: 420.85): C, 62.79; H, 4.07; N, 13.31%. Found: C, 62.82; H, 4.17; N, 13.40%.

[3-(5-Chloro-1-methyl-1*H*-indol-3-yl)-1,2,4-oxadiazol-5-yl](1-methyl-1*H*-indol-3-yl)methanone (179m)

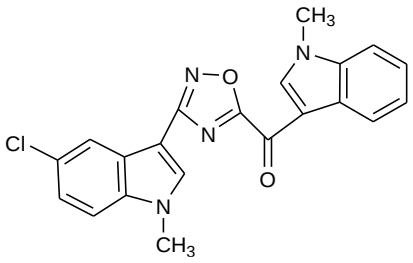

Conditions: 30 min at room temperature; yield: 73%; light yellow solid; mp: 250 °C (dec.); IR (cm^{-1}): 1628 (CO); ^{1}H NMR (200 MHz, DMSO-d_6) δ: 3.97 (3H, s, CH_3), 4.04 (3H, s, CH_3), 7.37-7.44 (3H, m, H-5, H-6 and H-6'), 7.68-7.73 (2H, m, H-7' and H-7), 8.06-8.07 (1H, m, H-4'), 8.31-8.37 (1H, m, H-4), 8.49 (1H, s, H-2'), 9.05 (1H, s, H-2); *Anal.* Calculated for $C_{21}H_{15}ClN_4O_2$ (MW: 390.82): C, 64.54; H, 3.87; N, 14.34%. Found: C, 64.84; H, 3.67; N, 14.14%.

General procedure for the synthesis of [3-(5-methoxy-1-methyl-1*H*-indol-3-yl)-1,2,4-oxadiazol-5-yl](1-methyl-1*H*-indol-3-yl)methanones (179n-q) and [3-(1*H*-indol-3-yl)-1,2,4-oxadiazol-5-yl](1-methyl-1*H*-indol-3-yl)methanones (180a-p)

To a solution of the proper (1-methyl-1*H*-indol-3-yl)-oxo-acetic acid **192a-d (**1.42 mmol) and 1-hydroxybenzotriazole hydrate (HOBt) (230 mg, 1.7 mmol) in anhydrous dimethylformamide (DMF) (2 mL) at 0°C, *N*-ethyl-*N'-(*3-dimethylaminopropyl)carbodiimide hydrochloride (EDC·HCl) (326 mg, 1.7 mmol) was added in portions. After 15 min, a DMF (1 mL) solution of triethylamine (0.2 mL, 1.42 mmol) and appropriate carboxamidine **182d, 183a-d** (0.71 mmol) was added dropwise at 0°C. The reaction mixture was stirred at 0°C for 15 min. After bringing the reaction mixture to room temperature, it was heated at 100°C for 15 min. After cooling, the mixture was poured into water and ice; the obtained precipitate was filtered off and dried under high *vacuum*. The crude was purified on flash chromatography to obtain the desired products **179n-q, 180a-p.**

(5-Methoxy-1-methyl-1*H*-indol-3-yl)[3-(5-methoxy-1-methyl-1*H*-indol-3-yl)-1,2,4-oxadiazol-5-yl]methanone (179n)

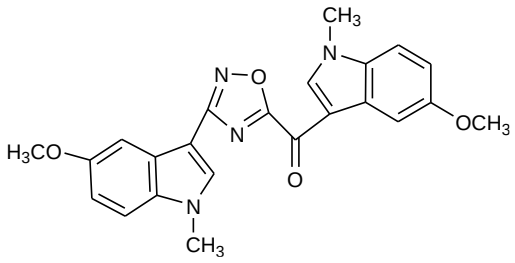

Yield: 20%; light yellow solid; mp: 218°C (dec.); IR (cm^{-1}): 1617 (CO); ^{1}H NMR (200 MHz, DMSO-d_6) δ: 3.86 (6H, bs, CH_3 x 2), 3.93 (3H, s, OCH_3), 4.00 (3H, s, OCH_3), 6.95-7.07 (2H, m, H-6 and H-6'), 7.52-7.63 (3H, m, H-7, H-7' and H-4'), 7.84 (1H, d, *J*= 2.4 Hz, H-4), 8.33 (1H, s, H-2'), 8.98 (1H, s, H-2); *Anal.* Calculated for $C_{23}H_{20}N_4O_4$ (MW: 416.43): C, 66.34; H, 4.84; N, 13.45%. Found: C, 66.55; H, 4.86; N, 13.25%.

(5-Bromo-1-methyl-1*H*-indol-3-yl)[3-(5-methoxy-1-methyl-1*H*-indol-3-yl)-1,2,4-oxadiazol-5-yl]methanone (179o)

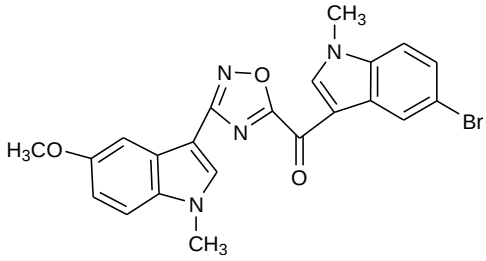

Yield: 30%; yellow solid; mp: 218°C (dec.); IR (cm^{-1}): 1632 (CO); ^{1}H NMR (200 MHz, DMSO-d_6) δ: 3.86 (3H, s, CH_3), 3.93 (3H, s, CH_3), 4.03 (3H, s, OCH_3), 6.98 (1H, dd, *J* = 9.1, 2.4 Hz, H-6'), 7.52-7.60 (3H, m, H-6, H-7 and H-7'), 7.67-7.73 (1H, m, H-4'), 8.34 (1H, s, H-2'), 8.46 (1H, d, *J* = 1.8 Hz, H-4), 9.10 (1H, s, H-2); *Anal.* Calculated for $C_{22}H_{17}BrN_4O_3$ (MW: 465.30): C, 56.79; H, 3.68; N, 12.04%. Found: C, 56.89; H, 3.58; N, 12.24%.

(5-Fluoro-1-methyl-1*H*-indol-3-yl)[3-(5-methoxy-1-methyl-1*H*-indol-3-yl)-1,2,4-oxadiazol-5-yl]methanone (179p)

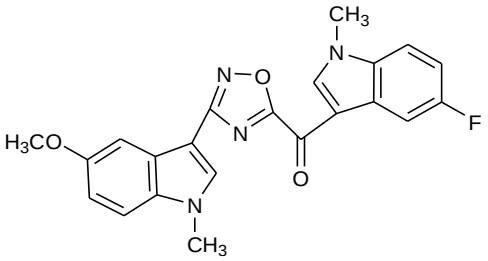

Yield: 22%; yellow solid; mp: 227°C (dec.); IR (cm^{-1}): 1629 (CO); ^{1}H NMR (200 MHz, DMSO-d_6) δ: 3.86 (3H, s, CH_3), 3.92 (3H, s, CH_3), 4.04 (3H, s, OCH_3), 6.98 (1H, dd, *J* = 8.9, 2.4 Hz, H-6'), 7.30 (1H, td, *J* = 9.3, 9.1, 2.5 Hz, H-6), 7.52-7.56 (2H, m, H-7' and H-4'), 7.74 (1H, dd, *J* = 9.1, 4.4 Hz, H-7), 8.00 (1H, dd, *J* = 9.3, 2.5 Hz, H-4), 8.34 (1H, s, H-2'), 9.11 (1H, s, H-2); *Anal.* Calculated for $C_{22}H_{17}FN_4O_3$ (MW: 404.39): C, 65.34; H, 4.25; N, 13.85%. Found: C, 65.49; H, 4.38; N, 13.64%.

[3-(5-Methoxy-1-methyl-1*H*-indol-3-yl)-1,2,4-oxadiazol-5-yl](1-methyl-1*H*-indol-3-yl)methanone (179q)

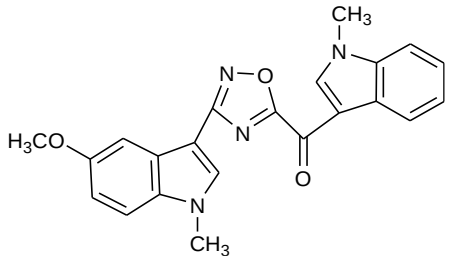

Yield: 20%; yellow solid; mp: 252°C (dec.); IR (cm^{-1}): 1628 (CO); ^{1}H NMR (200 MHz, DMSO-d_6) δ: 3.87 (3H, s, CH_3), 3.93 (3H, s, CH_3), 4.03 (3H, s, OCH_3), 6.98 (1H, dd, *J* = 9.1, 2.7 Hz, H-6'), 7.39-7.47 (2H, m, H-5 and H-6), 7.53-7.57 (2H, m, H-7 and H-7'), 7.68-7.73 (1H, m, H-4'), 8.32-8.37 (2H, m, H-4 and H-2'), 9.07 (1H, s, H-2); *Anal.* Calculated for $C_{22}H_{18}N_4O_3$ (MW: 386.40): C, 68.35; H, 4.70; N, 14.50%. Found: C, 68.49; H, 4.58; N, 14.64%.

(5-Bromo-1-methyl-1*H*-indol-3-yl)[3-(1*H*-indol-3-yl)-1,2,4-oxadiazol-5-yl]methanone (180a)

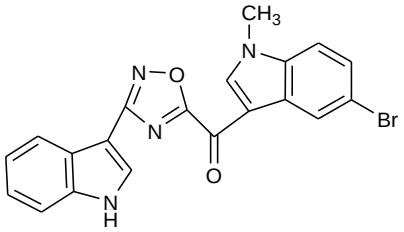

Yield: 21%; yellow solid; mp: 255°C (dec.); IR (cm^{-1}): 1623 (CO); ^{1}H NMR (200 MHz, DMSO-d_6) δ: 4.04 (3H, s, CH_3), 7.22–7.32 (2H, m, H-5' and H-6'), 7.54–7.72 (3H, m, H-6, H-7' and H-7), 8.07- 8.11 (1H, m, H-4'), 8.43–8.46 (2H, m, H-4 and H-2'), 9.16 (1H, s, H-2), 12.07 (1H, s, NH); ^{13}C NMR (50 MHz, DMSO-d_6) δ: 33.92 (q), 101.9 (s), 112.0 (s), 112.4 (d), 113.7 (d), 116.4 (s), 120.5 (d), 121.1 (d), 122.7 (d), 123.6 (d), 124.2 (s), 126.6 (d), 128.1 (s), 129.9 (d), 136.4 (s), 136.8 (s), 143.2 (d), 165.4 (s), 169.2 (s), 170.4 (s); *Anal*. Calculated for $C_{20}H_{13}BrN_4O_2$ (MW: 421.25): C, 57.02; H, 3.11; N, 13.30%. Found: C, 57.10; H, 3.21; N, 13.24%.

(5-Fluoro-1-methyl-1*H*-indol-3-yl)[3-(1*H*-indol-3-yl)-1,2,4-oxadiazol-5-yl]methanone (180b)

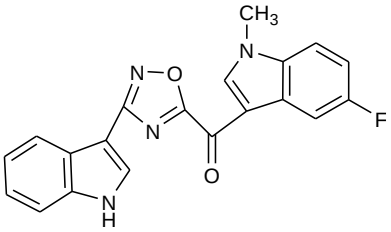

Yield: 30%; yellow solid; mp: 248°C (dec.); IR (cm^{-1}): 3281 (NH), 1617 (CO); ^{1}H NMR (200 MHz, DMSO-d_6) δ: 4.05 (3H, s, CH_3), 7.25–7.32 (3H, m, H-5', H-6' and H-6), 7.55–7.59 (1H, m, H-7'), 7.74 (1H, dd, J = 8.9, 2.4 Hz, H-7), 7.98–8.12 (2H, m, H-4' and H-4), 8.43 (1H, d, J = 2.8 Hz, H-2'), 9.17 (1H, s, H-2), 12.06 (1H, s, NH); ^{13}C NMR (50 MHz, DMSO-d6) δ: 34.01 (q), 99.49 (d), 101.93 (s), 106.6 (d, $J_{C4\text{-}F}$ = 25.4 Hz), 112.1 (d, $J_{C6\text{-}F}$ = 29.2 Hz), 112.6 (s, $J_{C7a\text{-}F}$ = 4.0 Hz), 113.1 (d, $J_{C7\text{-}F}$ = 9.7 Hz), 120.5 (d), 121.1 (d), 122.7 (d), 124.2 (s), 127.2 (s, $J_{C3a\text{-}F}$ = 10.9 Hz), 129.9 (d), 134.2 (s), 136.8 (s), 143.5 (d), 159.6 (s, $J_{C5\text{-}F}$ = 237.3 Hz), 165.4 (s), 169.3 (s), 170.3 (s); *Anal*. Calculated for $C_{20}H_{13}FN_4O_2$ (MW: 360.34): C, 66.66; H, 3.64; N, 15.55%. Found: C, 66.70; H, 3.51; N, 15.34%.

[3-(1*H*-Indol-3-yl)-1,2,4-oxadiazol-5-yl](1-methyl-1*H*-indol-3-yl)methanone (180c)

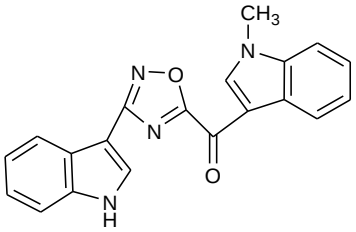

Yield: 33%; yellow solid; mp: 230°C (dec.); IR (cm^{-1}): 3393 (NH), 1617 (CO); ^{1}H NMR (200 MHz, DMSO-d_6) δ: 4.04 (3H, s, CH_3), 7.23-7.33 (2H, m, H-5 and H-5'), 7.40-7.47 (2H, m, H-6 and H-6'), 7.55- 7.60 (1H, m, H-7'), 7.68-7.72 (1H, m, H-7), 8.07-8.13 (1H, m, H-4'), 8.33-8.37 (1H, m, H-4), 8.43 (1H, d, *J* = 2.8 Hz, H-2'), 9.13 (1H, s, H-2), 12.07 (1H, s, NH); ^{13}C NMR (50 MHz, DMSO-d_6) δ: 33.7 (q), 102.0 (s), 111.4 (d), 112.4 (d), 112.7 (s), 120.5 (d), 121.1 (d), 121.5 (d), 122.7 (d), 123.6 (d), 124.1 (d), 124.2 (s), 126.4 (s), 129.8 (d), 136.8 (s), 137.5 (s), 142.5 (d), 165.3 (s), 169.6 (s), 170.4 (s); *Anal.* Calculated for $C_{20}H_{14}N_4O_2$ (MW: 342.35): C, 70.17; H, 4.12; N, 16.37%. Found: C, 70.20; H, 4.30; N, 16.14%.

[3-(1*H*-Indol-3-yl)-1,2,4-oxadiazol-5-yl](5-methoxy-1-methyl-1*H*-indol-3-yl)methanone (180d)

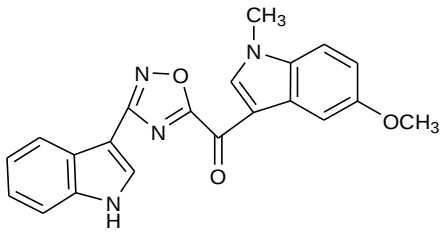

Yield: 32%; yellow solid; mp: 258°C (dec.); IR (cm^{-1}): 3228 (NH), 1617 (CO); ^{1}H NMR (200 MHz, DMSO-d_6) δ: 3.86 (3H, s, CH_3), 4.01 (3H, s, OCH_3), 7.04 (1H, dd, *J* = 8.9, 2.4 Hz, H-6'), 7.23-7.33 (2H, m, H-5 and H-6), 7.55-7.62 (2H, m, H-7' and H-7), 7.85 (1H, d, *J* = 2.4 Hz, H-4'), 8.08-8.13 (1H, m, H-4), 8.42 (1H, d, *J* = 2.4 Hz, H-2'), 9.04 (1H, s, H-2), 12.05 (1H, s, NH); ^{13}C NMR (50 MHz, DMSO-d_6) δ: 33.9 (q), 55.4 (q), 102.0 (s), 103.5 (d), 112.4 (d), 113.4 (d), 120.5 (d), 121.1 (d), 122.7 (d), 124.2 (s), 127.4 (s), 129.5 (d), 129.8 (d), 132.4 (s), 133.5 (s), 136.8 (s), 142.2 (d), 156.8 (s), 165.3 (s), 169.6 (s), 170.2 (s); *Anal.* Calculated for $C_{21}H_{16}N_4O_3$ (MW: 372.38): C, 67.73; H, 4.33; N, 15.05%. Found: C, 67.92; H, 4.12; N, 15.14%.

(5-Fluoro-1-methyl-1*H*-indol-3-yl)[3-(5-methoxy-1*H*-indol-3-yl)-1,2,4-oxadiazol-5-yl]methanone (180e)

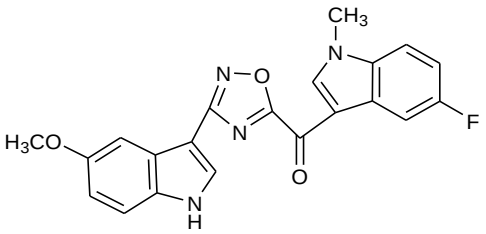

Yield: 40%; yellow solid; mp: 262°C (dec.); IR (cm^{-1}): 3267 (NH), 1623 (CO); ^{1}H NMR (200 MHz, DMSO-d_6) δ: 3.85 (3H, s, CH_3), 4.04 (3H, s, OCH_3), 6.92 (1H, dd, *J* = 8.8, 2.4 Hz, H-6'), 7.29(1H, td, *J* = 9.2, 9.2, 2.6 Hz, H-6), 7.46 (1H, d, *J* = 8.8 Hz, H-7'), 7.56 (1H, d, *J* = 2.4 Hz, H-4'), 7.74 (1H, dd, *J* = 9.2, 4.4 Hz, H-7), 8.01 (1H, dd, *J* = 9.6, 2.6 Hz, H-4), 8.36 (1H, d, *J* = 2.9, H-2'), 9.17 (1H, s, H-2), 11.94 (1H, s, NH); ^{13}C NMR (50 MHz, DMSO-d_6) δ: 34.0 (q), 55.2 (q), 101.7 (s), 102.0 (d), 106.6 (d, $J_{C4\text{-}F}$ = 25.5 Hz), 112.1 (d, $J_{C6\text{-}F}$ = 25.7 Hz), 112.6 (s, $J_{C7a\text{-}F}$ = 4.8 Hz), 112.8 (d), 113.1 (d, $J_{C7\text{-}F}$ = 10.2 Hz), 113.2 (d), 124.8 (s), 127.2 (s, $J_{C3a\text{-}F}$ = 11.4 Hz), 130.0 (d), 131.7 (s), 134.2 (s), 143.4 (d), 154.8 (s), 159.6 (s, $J_{C5\text{-}F}$ = 237.0 Hz), 165.4 (s), 169.3 (s), 170.3 (s); *Anal.* Calculated for $C_{21}H_{15}FN_4O_3$ (MW: 390.37): C, 64.61; H, 3.87; N, 14.35%. Found: C, 64.70; H, 3.61; N, 14.24%.

[3-(5-Methoxy-1*H*-indol-3-yl)-1,2,4-oxadiazol-5-yl](5-methoxy-1-methyl-1*H*-indol-3-yl)methanone (180f)

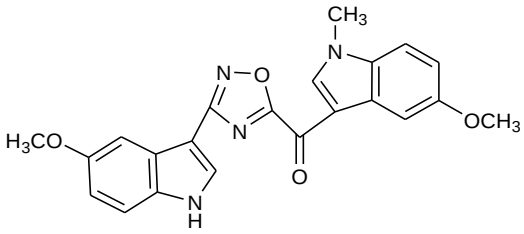

Yield: 42%; yellow solid; mp: 244°C (dec.); IR (cm^{-1}): 3290 (NH), 1627 (CO); ^{1}H NMR (200 MHz, DMSO-d_6) δ: 3.85 (6H, bs, CH_3 and OCH_3), 3.99 (3H, s, OCH_3), 6.92 (1H, dd, *J* = 8.9, 2.3 Hz, H-6'), 7.03 (1H, dd, *J* = 8.9, 2.3 Hz, H-6), 7.46 (1H, d, *J* = 8.9 Hz, H-7), 7.56-7.62 (2H, m, H-7 and H-4), 7.85 (1H, d, *J* = 2.3 Hz, H-4), 8.34 (1H, d, *J* = 2.7, H-2'), 9.03 (1H, s, H-2), 11.93 (1H, s, NH); ^{13}C NMR (50 MHz, DMSO-d_6) δ: 33.83 (q), 55.3 (q), 55.4 (q), 101.7 (s), 102.0 (d), 103.6 (d), 112.3 (d), 112.5 (s), 112.8 (d), 113.2 (d), 113.4 (d), 124.8 (s), 127.4 (s), 129.9 (d), 131.7 (s), 132.4 (s),

142.2 (d), 154.8 (s), 156.8 (s), 165.3 (s), 169.6 (s), 170.2 (s); *Anal.* Calculated for $C_{22}H_{18}N_4O_4$ (MW: 402.40): C, 65.66; H, 4.51; N, 13.92%. Found: C, 65.70; H, 4.61; N, 14.04%.

(5-Bromo-1-methyl-1*H*-indol-3-yl)[3-(5-methoxy-1*H*-indol-3-yl)-1,2,4-oxadiazol-5yl]methanone (180g)

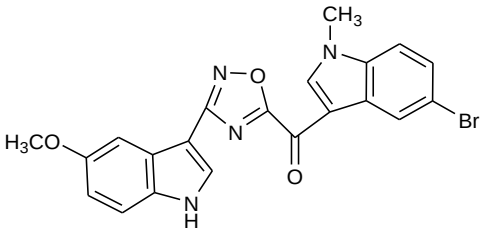

Yield: 35%; yellow solid; mp: 274°C (dec.); IR (cm^{-1}): 3312 (NH), 1623 (CO); ^{1}H NMR (200 MHz, DMSO-d_6) δ: 3.85 (3H, s, CH_3), 4.03 (3H, s, OCH_3), 6.92 (1H, dd, *J* = 8.9, 2.4 Hz, H-6'), 7.46 (1H, d, *J* = 8.9 Hz, H-7'), 7.55- 7.60 (2H, m, H-6 and H-4'), 7.70 (1H, d, *J* = 8.7 Hz, H-7), 8.35 (1H, d, *J* = 2.8, H-2'), 8.46 (1H, d, *J* = 1.6 Hz, H-4), 9.16 (1H, s, H-2), 11.93 (1H, s, NH); ^{13}C NMR (50 MHz, DMSO-d_6) δ: 33.9 (q), 55.2 (q), 101.7 (s), 102.0 (d), 112.4 (s), 112.8 (d), 113.2 (d), 113.6 (d), 116.4 (s), 123.6 (d), 124.8 (s), 126.6 (d), 128.1 (s), 130.0 (d), 131.7 (s), 136.3 (s), 143.2 (d), 154.8 (s), 165.4 (s), 169.2 (s), 170.3 (s); *Anal.* Calculated for $C_{21}H_{15}BrN_4O_3$ (MW: 451.27): C, 55.89; H, 3.35; N, 12.42%. Found: C, 55.70; H, 3.51; N, 12.20%.

[3-(5-Methoxy-1*H*-indol-3-yl)-1,2,4-oxadiazol-5-yl](1-methyl-1*H*-indol-3-yl)methanone (180h)

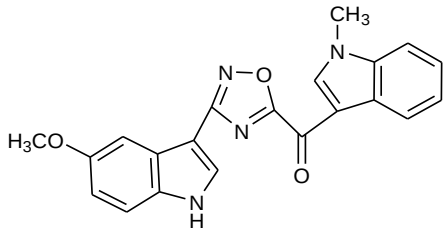

Yield: 34%; yellow solid; mp: 247°C (dec.); IR (cm^{-1}): 3302 (NH), 1616 (CO); ^{1}H NMR (200 MHz, DMSO-d_6) δ: 3.86 (3H, s, CH_3), 4.04 (3H, s, OCH_3), 6.92 (1H, dd, *J* = 8.9, 2.3 Hz, H-6'), 7.36 – 7.49 (3H, m, H-5, H-6 and H-7'), 7.56 (1H, d, *J* = 2.3 Hz, H-4'), 7.67- 7.71 (1H, m, H-7), 8.23 – 8.37 (2H, m, H-4 and H-2'), 9.12 (1H, s, H-2), 11.94 (1H, s, NH); 33.7 (q), 55.2 (q), 101.7 (s), 102.0 (d), 111.4 (d), 112.7 (s), 112.8 (d), 113.2 (d), 121.5 (d), 123.5 (d), 124.1 (d), 124.8 (s), 126.4 (s), 130.0 (d), 131.7 (s), 137.5 (s), 142.4 (d), 154.8 (s), 165.4 (s), 169.5 (s), 170.4 (s); *Anal.*

Calculated for $C_{21}H_{16}N_4O_3$ (MW: 372.38): C, 67.73; H, 4.33; N, 15.05%. Found: C, 67.70; H, 4.51; N, 15.20%.

[3-(5-Bromo-1*H*-indol-3-yl)-1,2,4-oxadiazol-5-yl](5-methoxy-1-methyl-1*H*-indol-3-yl)methanone (180i)

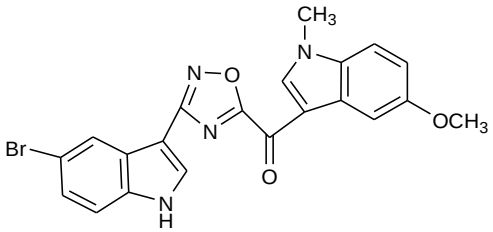

Yield: 67%; yellow solid; mp: 258°C (dec.); IR (cm^{-1}): 3302 (NH), 1610 (CO); ^{1}H NMR (200 MHz, DMSO-d_6) δ: 3.85 (3H, s, CH_3), 4.04 (3H, s, OCH_3), 7.03 (1H, dd, *J* = 8.9, 2.5 Hz, H-6), 7.41 (1H, dd, *J* = 8.6, 1.9 Hz, H-6'), 7.53–7.61 (2H, m, H-7 and H-7'), 7.83 (1H, d, *J* = 2.5 Hz, H-4), 8.21 (1H, d, *J* = 1.9 Hz, H-4'), 8.47 (1H, d, *J* = 2.8 Hz, H-2'), 9.02 (1H, s, H-2), 12.27 (1H, s, NH); ^{13}C NMR (50 MHz, DMSO-d6) δ: 33.9 (q), 55.4 (q), 101.6 (s), 103.5 (d), 112.4 (d), 112.5 (s), 113.4 (d), 113.6 (s), 114.5 (d), 122.6 (d), 125.3 (d), 125.9 (s), 127.4 (s), 131.1 (d), 132.3 (s), 135.6 (s), 142.2 (d), 156.8 (s), 164.9 (s), 169.8 (s), 170.0 (s); *Anal.* Calculated for $C_{21}H_{15}BrN_4O_3$ (MW: 451.27): C, 55.89; H, 3.35; N, 12.42%. Found: C, 55.70; H, 3.51; N, 12.24%.

[3-(5-Bromo-1*H*-indol-3-yl)-1,2,4-oxadiazol-5-yl](1-methyl-1*H*-indol-3-yl)methanone (180j)

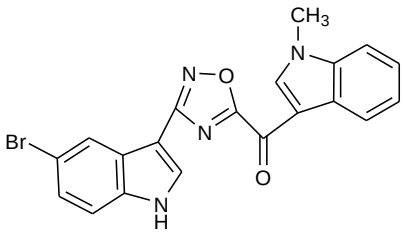

Yield: 30%; yellow solid; mp: 271°C (dec.); IR (cm^{-1}): 3376 (NH), 1618 (CO); ^{1}H NMR (200 MHz, DMSO-d_6) δ: 4.04 (3H, s, CH_3),7.36-7.47 (3H, m, H-5, H-6 and H-6'), 7.56 (1H, d, *J* = 8.6 Hz, H-7'), 7.67- 7.72 (1H, m, H-7), 8.22 (1H, d, *J* = 1.8 Hz, H-4'), 8.32-8.37 (1H, m, H-4), 8.48 (1H, d, *J* = 2.8 Hz, H-2'), 9.11 (1H, s, H-2), 12.27 (1H, s, NH); ^{13}C NMR (50 MHz, DMSO-d_6) δ: 33.7 (q), 101.6 (s), 111.4 (d), 112.7 (s), 113.7 (s), 114.6 (d), 121.5 (d), 122.6 (d), 123.6 (d), 124.1 (d), 125.3 (d), 125.9 (s), 126.4 (s), 131.1 (d), 135.6 (s), 137.5 (s), 142.5 (d), 164.9 (s), 168.8 (s), 170.2 (s);

Anal. Calculated for $C_{20}H_{13}BrN_4O_2$ (MW: 421.25): C, 57.02; H, 3.11; N, 13.30%. Found: C, 56.92; H, 3.02; N, 13.14%.

[3-(5-Bromo-1*H*-indol-3-yl)-1,2,4-oxadiazol-5-yl](5-fluoro-1-methyl-1*H*-indol-3-yl)methanone (180k)

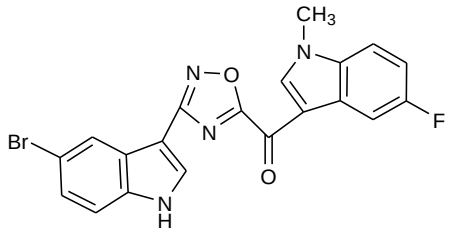

Yield: 35%; yellow solid; mp: 277°C (dec.); IR (cm^{-1}): 3267 (NH), 1615 (CO); ^{1}H NMR (200 MHz, DMSO-d_6) δ: 4.04 (3H, s, CH_3), 7.29 (1H, td, *J* = 9.2, 9.2, 2.6 Hz, H-6), 7.41 (1H, dd, *J* = 8.7, 1.9 Hz, H-6'), 7.55 (1H, d, *J* = 8.7 Hz, H-7'), 7.73 (1H, dd, *J* = 9.2, 4.4 Hz, H-7), 8.00 (1H, dd, *J* = 9.5, 2.6 Hz, H-4), 8.20 (1H, d, *J* = 1.9 Hz, H-4'), 8.48 (1H, d, *J* = 2.1 Hz, H-2'), 9.16 (1H, s, H-2), 12.27 (1H, s, NH); ^{13}C NMR (50 MHz, DMSO-d_6) δ: 34.0 (q), 101.54 (s), 106.6 (d, $J_{C4\text{-}F}$ = 24.9 Hz), 112.1 (d, $J_{C6\text{-}F}$ = 26.4 Hz), 112.5 (s, $J_{C7a\text{-}F}$ = 4.2 Hz), 113.1 (d, $J_{C7\text{-}F}$ = 10.2 Hz), 113.7 (s), 114.6 (d), 122.6 (d), 125.3 (d), 125.9 (s), 127.2 (s, $J_{C3a\text{-}F}$ = 11.3 Hz), 131.1 (d), 134.1 (s), 135.6 (s), 143.6 (d), 159.6 (s, $J_{C5\text{-}F}$ = 236.0 Hz), 164.9 (s), 169.5 (s), 170.1 (s); *Anal.* Calculated for $C_{20}H_{12}BrFN_4O_2$ (MW: 439.24): C, 54.69; H, 2.75; N, 12.76%. Found: C, 54.55; H, 2.60; N, 13.00%.

[3-(5-Bromo-1*H*-indol-3-yl)-1,2,4-oxadiazol-5-yl](5-bromo-1-methyl-1*H*-indol-3-yl)methanone (180l)

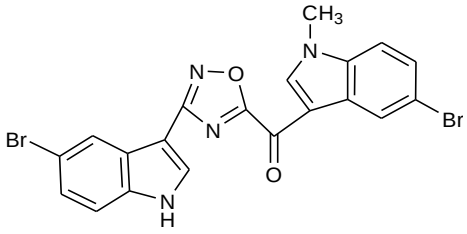

Yield: 57%; yellow solid; mp: 294°C (dec.); IR (cm^{-1}): 3341 (NH), 1617 (CO); ^{1}H NMR (200 MHz, DMSO-d_6) δ: 4.04 (3H, s, CH_3), 7.42 (1H, dd, *J* = 8.6, 1.8 Hz, H-6'), 7.54-7.60 (2H, m, H-6 and H-7), 7.70 (1H, d, *J* = 8.6 Hz, H-7'), 8.21 (1H, d, *J* = 1.8 Hz, H-4'), 8.46 (1H, d, *J* = 1.6 Hz, H-4), 8.49 (1H, s, H-2'), 9.16 (1H, s, H-2), 12.28 (1H, s, NH); ^{13}C NMR (50 MHz, DMSO-d_6) δ:33.9 (q),

101.5 (s), 112.0 (s), 113.7 (d), 114.5 (d), 116.4 (s), 122.6 (d), 123.5 (d), 125.3 (d), 125.9 (s), 126.6 (d), 128.1 (s), 131.2 (d), 135.6 (s), 136.3 (s), 143.2 (d), 158.7 (s), 164.9 (s), 169.4 (s), 170.1 (s); *Anal.* Calculated for $C_{20}H_{12}Br_2N_4O_2$ (MW: 500.14): C, 48.03; H, 2.42; N, 11.20%. Found: C, 48.12; H, 2.60; N, 11.05%.

[3-(5-Fluoro-1*H*-indol-3-yl)-1,2,4-oxadiazol-5-yl](1-methyl-1*H*-indol-3-yl)methanone (180m)

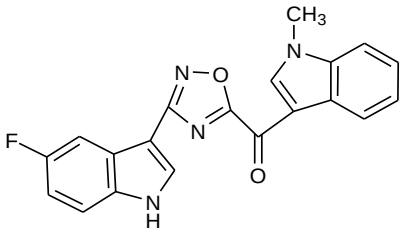

Yield: 38%; yellow solid; mp: 261°C (dec.); IR (cm^{-1}): 3284 (NH), 1623 (CO); ^{1}H NMR (200 MHz, DMSO-d_6) δ: 4.04 (3H, s, CH_3), 7.15 (1H, td, *J* = 9.4, 9.1, 2.4 Hz, H-6'), 7.39-7.43 (2H, m, H-5, H-6), 7.59 (1H, dd, *J* = 9.1, 4.5 Hz, H-7'), 7.67-7.78 (2H, m, H-7 and H-4'), 8.32-8.36 (1H, m, H-4), 8.49 (1H, s, H-2'), 9.11 (1H, s, H-2), 12.18 (1H, s, NH); ^{13}C NMR (50 MHz, DMSO-d_6) δ: 33.7 (q), 102.1 (s, J_{C7a-F} = 4.5 Hz), 105.2 (d, J_{C4-F} = 23.6 Hz), 110.0 (d, J_{C6-F} = 26.0 Hz), 111.4 (d),112.7 (s), 113.7 (d, J_{C7-F} = 12.0 Hz), 121.5 (d), 123.6 (d), 124.1 (d), 124.6 (s, J_{C3a-F} = 11.2 Hz), 126.4 (s), 131.5 (d), 133.5 (s), 137.5 (s), 142.5 (d), 158.0 (s, J_{C5-F} = 234.6 Hz), 165.0 (s), 169.7 (s), 170.3 (s); *Anal.* Calculated for $C_{20}H_{13}FN_4O_2$ (MW: 360.34): C, 66.66; H, 3.64; N, 15.55%. Found: C, 66.70; H, 3.60; N, 15.22%.

[3-(5-Fluoro-1*H*-indol-3-yl)-1,2,4-oxadiazol-5-yl](5-fluoro-1-methyl-1*H*-indol-3-yl)methanone (180n)

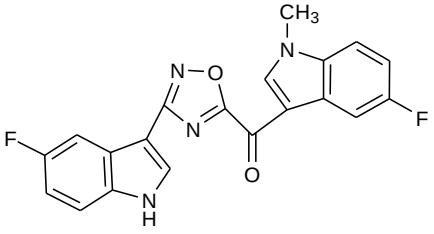

Yield: 42%; yellow solid; mp: 265°C (dec.); IR (cm^{-1}): 3267 (NH), 1615 (CO); ^{1}H NMR (200 MHz, DMSO-d_6) δ: 4.04 (3H, s, CH_3), 7.15 (1H, td, *J* = 9.2, 9.1, 2.6 Hz, H-6'), 7.30 (1H, td, *J* = 9.2, 9.1, 2.6 Hz, H-6), 7.60 (1H, dd, *J* = 9.1, 4.6 Hz, H-7'), 7.71- 7.77 (2H, m, H-7 and H-4'), 8.01 (1H, dd, *J*

= 9.6, 2.6 Hz, H-4), 8.50 (1H, d, *J* = 2.9 Hz, H-2'), 9.16 (1H, s, H-2), 12.19 (1H, s, NH); ^{13}C NMR (50 MHz, DMSO-d_6) δ: 34.0 (q), 102.1 (s, $J_{C7'a-F}$ = 4.3 Hz), 105.2 (d, $J_{C4'-F}$ = 25.1 Hz), 106.6 (d, J_{C4-F} = 24.9 Hz), 111.0 (d, $J_{C6'-F}$ = 26.4 Hz), 112.1 (d, J_{C6-F} = 25.7 Hz), 112.5 (s, J_{C7a-F} = 4.2 Hz), 113.1 (d, J_{C7-F} = 9.5 Hz), 113.7 (d, $J_{C7'-F}$ = 9.7 Hz), 124.6 (s, $J_{C3'a-F}$ = 11.2 Hz), 127.2 (s, J_{C3a-F} = 11.1 Hz), 131.5 (d), 133.4 (s), 134.2 (s), 143.5 (d), 158.0 (s, $J_{C5'-F}$ = 234.1 Hz), 159.6 (s, J_{C5-F} = 235.3 Hz), 165.0 (s), 169.4 (s), 170.1 (s); *Anal.* Calculated for $C_{20}H_{12}F_2N_4O_2$ (MW: 378.33): C, 63.49; H, 3.20; N, 14.81%. Found: C, 63.50; H, 3.30; N, 15.00%.

[3-(5-Fluoro-1*H*-indol-3-yl)-1,2,4-oxadiazol-5-yl](5-methoxy-1-methyl-1*H*-indol-3-yl)methanone (180o)

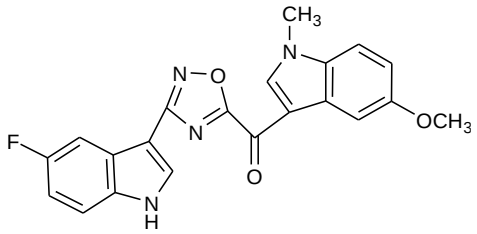

Yield: 42%; yellow solid; mp: 218°C (dec.); IR (cm^{-1}): 3244 (NH), 1618 (CO); ^{1}H NMR (200 MHz, DMSO-d_6) δ: 3.86 (3H, s, CH_3), 4.04 (3H, s, OCH_3), 7.04 (1H, dd, *J* = 8.9, 2.5 Hz, H-6), 7.15 (1H, td, *J* = 9.2, 9.1, 2.6 Hz, H-6'), 7.55-7.62 (2H, m, H-7 and H-7'), 7.74 (1H, dd, *J* = 9.7, 2.6 Hz, H-4'), 7.84 (1H, d, *J* = 2.5 Hz, H-4), 8.48 (1H, d, *J* = 2.7 Hz, H-2'), 9.03 (1H, s, H-2), 12.18 (1H, s, NH); ^{13}C NMR (50 MHz, DMSO-d_6) δ: 33.9 (q), 55.4 (q), 102.1 (s, J_{C7a-F} = 4.5 Hz), 103.5 (d), 105.2 (d, J_{C4-F} = 24.7 Hz), 111.0 (d, J_{C6-F} = 26.1 Hz), 112.4 (d), 112.5 (s), 113.4 (d), 113.7 (d, J_{C7-F} = 9.5 Hz), 124.6 (s, J_{C3a-F} = 11.1 Hz), 127.4 (s), 131.5 (d), 132.3 (s), 133.4 (d), 142.2 (d), 156.8 (s), 158.0 (s, J_{C5-F} = 234.4 Hz), 165.0 (s), 169.8 (s), 170.0 (s); *Anal.* Calculated for $C_{21}H_{15}FN_4O_3$ (MW: 390.37): C, 64.61; H, 3.87; N, 14.35%. Found: C, 64.70; H, 3.70; N, 14.10%.

(5-Bromo-1-methyl-1*H*-indol-3-yl)[3-(5-fluoro-1*H*-indol-3-yl)-1,2,4-oxadiazol-5-yl]methanone (180p)

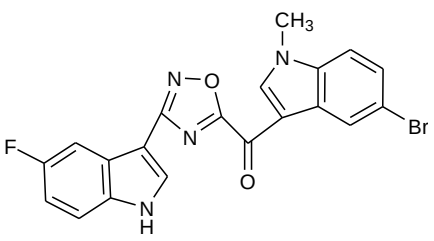

Yield: 38; yellow solid; mp: 280°C (dec.); IR (cm^{-1}): 3310 (NH), 1592 (CO); ^{1}H NMR (200 MHz, DMSO-d_6) δ: 4.03 (3H, s, CH_3), 7.14 (1H, td, J = 9.1, 9.1, 2.6 Hz, H-6'), 7.53-7.76 (4H, m, H-6, H-7, H-7' and H-4'), 8.44-8.49 (2H, m, H-4 and H-2'), 9.13 (1H, s, H-2), 12.18 (1H, s, NH); ^{13}C NMR (50 MHz, DMSO-d_6) δ: 33.9 (q), 99.5 (d), 102.1 (s, J_{C7a-F} = 4.5 Hz), 105.2 (d, J_{C4-F} = 25.1 Hz), 111.0 (d, J_{C6-F} = 26.6 Hz), 112.0 (s), 113.7 (d, J_{C7-F} = 9.2 Hz), 116.4 (s), 123.6 (d), 124.6 (s, J_{C3a-F} = 11.1 Hz), 126.6 (d), 128.1 (s), 131.6 (d), 133.5 (s), 136.3 (s), 143.2 (d), 158.0 (s, J_{C5-F} = 234.4 Hz), 165.1 (s), 169.3 (s), 170.2 (s); *Anal.* Calculated for $C_{20}H_{12}BrFN_4O_2$ (MW: 439.24): C, 54.69; H, 2.75; N, 12.76%. Found: C, 54.80; H, 2.70; N, 12.60%.

General procedure for the synthesis of 1-methyl-1*H*-pyrrolo[2,3-*b*]pyridines (196a-b)

To a cold solution of appropriate 7-azaindoles **199a-b** (2.5 mmol) in anhydrous toluene (25 mL), *t*-BuOK (0.38 g, 3.4 mmol) and TDA-1 (1 or 2 drops) were added at 0 °C. The reaction mixture was stirred at room temperature for 3 h and then methyl iodide (2.5 mmol, 0.2 mL) was added at 0 °C. TLC analysis (ethyl acetate) revealed that methylation was complete after 1 h. The solvent was evaporated under reduced pressure. The residue was treated with water, extracted with DCM (3 × 20 mL), dried (Na_2SO_4), evaporated and purified by column chromatography using DCM/ethyl acetate (9/1) as eluent, to give the desired product.

5-Bromo-1-methyl-1*H*-pyrrolo[2,3-*b*]pyridine (196a)

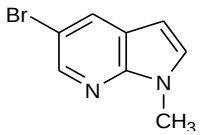

Yield: 85%; brown solid; mp: 62–63 °C; ^{1}H NMR (200 MHz, DMSO-d_6) δ: 3.83 (3H, s, CH_3), 6.44 (1H, d, J = 3.4 Hz, H-3), 7.60 (1H, d, J = 3.4 Hz, H-2), 8.21 (1H, d, J = 2.1 Hz, H-4), 8.33 (1H, d, J = 2.1 Hz, H-6); ^{13}C NMR (50 MHz, DMSO-d_6) δ: 31.0 (q), 98.5 (d), 110.7 (s), 121.7 (s), 130.3 (d), 131.8 (d), 142.2 (d), 145.7 (s); *Anal.* Calculated for $C_8H_7BrN_2$ (MW: 211.06): C, 45.53; H, 3.34; N, 13.27%. Found: C, 45.38; H, 3.24; N, 13.45%.

1-Methyl-1*H*-pyrrolo[2,3-*b*]pyridine (196b)

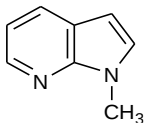

Yield: 96%; yellow oil; ^{1}H NMR (200 MHz, $CDCl_3$) δ: 3.87 (3H, s, CH_3), 6.43 (1H, d, *J* = 3.4 Hz, H-3), 7.03 (1H, dd, *J* = 7.8, 4.8 Hz, H-5), 7.15 (1H, d, *J* = 3.4 Hz, H-2), 7.88 (1H, dd, *J* = 7.8, 1.5 Hz, H-4), 8.33 (1H, d, *J* = 4.8 Hz, H-6); ^{13}C NMR (50 MHz, DMSO-d_6) δ: 31.1 (q), 99.1 (d), 115.3 (s), 120.4 (s), 128.6 (d), 128.9 (d + s), 142.6 (d); *Anal.* Calculated for $C_8H_8N_2$ (MW: 132.16): C, 72.70; H, 6.10; N, 21.20%. Found: C, 72.65; H, 6.24; N, 21.45%.

General Procedure for the synthesis of (1-methyl-1*H*-pyrrolo[2,3-*b*]pyridin-3-yl)-oxo-acetic acid methyl esters (198a-b)

Oxalyl chloride (0.42 mL, 4.8 mmol) was added dropwise to a solution of 1-methyl-1*H*-pyrrolo[2,3-*b*]pyridine **196a-b** (1 g, 4.8 mmol) in dry diethyl ether (8.5 mL) under nitrogen atmosphere at 0 °C. The reaction mixture was stirred overnight at room temperature. The solution was cooled down to -65 °C, using a acetone bath with immersion cooler, before adding a sodium methoxide solution, 25 wt. % in methanol (11 mL, 10.8 mmol, 2.3 eq.) dropwise. The reaction mixture was heated up to room temperature and stirred for 2 h. The reaction was quenched with brine (1 mL) and water (1 mL) and the obtained precipitate was filtered off. Upon filtering, the isolated solid was dried under high *vacuum* overnight.

(5-Bromo-1-methyl-1*H*-pyrrolo[2,3-*b*]pyridin-3-yl)-oxo-acetic acid methyl ester (198a)

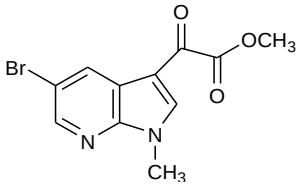

Yield: 42%; light yellow solid; mp: 140.5-141.5 °C; IR (cm^{-1}): 1731 (CO), 1653 (CO); ^{1}H NMR (200 MHz, DMSO-d_6) δ: 3.91 (3H, s, CH_3), 3.92 (3H, s, OCH_3), 8.54 (1H, d, *J* = 2.2 Hz, H-4), 8.57

(1H, d, *J* = 2.2 Hz, H-6), 8.80 (1H, s, H-2); ^{13}C NMR (50 MHz, DMSO-d_6) δ: 32.0 (q), 52.8 (q), 109.2 (s), 114.7 (s), 131.4 (d), 143.0 (d), 145.1 (d), 146.6 (s), 162.6 (s), 176.8 (s), 177.6 (s); *Anal.* Calculated for $C_{11}H_9BrN_2O_3$ (MW: 297.10): C, 44.47; H, 3.05; N, 9.43%. Found: C, 44.38; H, 3.14; N, 9.45%.

(1-Methyl-1*H*-pyrrolo[2,3-b]pyridin-3-yl)-oxo-acetic acid methyl ester (198b)

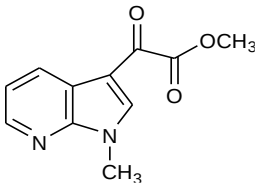

Yield: 42%; white solid; mp: 97.8-98.8 °C; IR (cm^{-1}): 1729 (CO), 1650 (CO); ^{1}H NMR (200 MHz, DMSO-d_6) δ: 3.91 (3H, s, CH_3), 3.93 (3H, s, OCH_3), 7.38 (1H, dd, *J* = 7.8, 4.8 Hz, H-4), 8.44-8.51 (2H, m, H-5 and H-6), 8.74 (1H, s, H-2); ^{13}C NMR (50 MHz, DMSO-d_6) δ: 31.8 (q), 52.7 (q), 109.7 (s), 118.3 (s), 119.3 (d), 129.8 (d), 141.8 (d), 144.9 (d) 148.1 (s), 163.1 (s), 176.8 (s), 178.0 (s); *Anal.* Calculated for $C_{11}H_{10}N_2O_3$ (MW: 218.21): C, 60.55; H, 4.62; N, 12.84%. Found: C, 60.38; H, 4.70; N, 12.85%.

General procedure for the synthesis of (1-methyl-1*H*-pyrrolo[2,3-*b*]pyridin-3-yl)-[3-(1-methyl-1*H*-indol-3-yl)-[1,2,4]oxadiazol-5-yl]-methanones (181a-f)

A fine powder of sodium hydroxide (60 mg, 1.5 mmol) was quickly added to a solution of appropriate (1-methyl-1*H*-pyrrolo[2,3-*b*]pyridin-3-yl)-oxo-acetic acid methyl ester **198a-b** (446 mg, 1.5 mmol) and suitable carboxamidine **182b-d** (190 mg, 1.0 mmol) in dry dimethylsulfoxide (DMSO) (2 mL). The resulting solution was allowed to stir at room temperature for 40 min. Then, water and ice were slowly added and the obtained precipitate was filtered off. The residue was purified by column chromatography using cyclohexane/ethyl acetate (1/1) as eluent.

(5-Bromo-1-methyl-1*H*-pyrrolo[2,3-*b*]pyridin-3-yl)-[3-(1-methyl-1*H*-indol-3-yl)-[1,2,4]oxadiazol-5-yl]-methanone (181a)

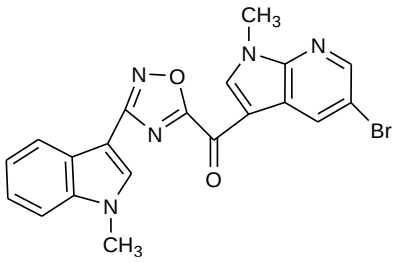

Yield: 33%; yellow solid; mp: 258 °C (dec); IR (cm^{-1}): 1630 (CO); ^{1}H NMR (200 MHz, DMSO-d_6) δ: 3.90 (3H, s, CH_3), 3.98 (3H, s, CH_3), 7.21-7.33 (2H, m, H-5' and H-6'), 7.56-7.60 (1H, m, H-7'), 7.99-8.06 (1H, m, H-4'), 8.37 (1H, s, H-2'), 8.56 (1H, d, *J* = 2.2 Hz, H-4), 8.68 (1H, d, *J* = 2.2 Hz, H-6), 9.24 (1H, s, H-2); *Anal.* Calculated for $C_{20}H_{14}BrN_5O_2$ (MW: 436.26): C, 55.06; H, 3.23; N, 16.05%. Found: C, 55.18; H, 3.14; N, 15.99%.

(5-Bromo-1-methyl-1*H*-pyrrolo[2,3-*b*]pyridin-3-yl)-[3-(5-fluoro-1-methyl-1*H*-indol-3-yl)-[1,2,4]oxadiazol-5-yl]-methanone (181b)

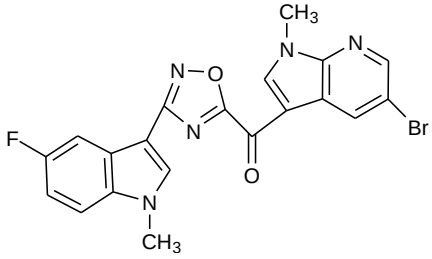

Yield: 40%; yellow solid; mp: 246 °C (dec); IR (cm^{-1}): 1635 (CO); ^{1}H NMR (200 MHz, DMSO-d_6) δ: 3.97 (3H, s, CH_3), 4.04 (3H, s, CH_3), 7.17-7.28 (1H, m, H-6'), 7.65-7.78 (2H, m, H-7' and H-4'), 8.50 (1H, s, H-2'), 8.61 (1H, d, *J* = 1.8 Hz, H-4), 8.73 (1H, d, *J* = 1.8 Hz, H-6), 9.30 (1H, s, H-2); *Anal.* Calculated for $C_{20}H_{13}BrFN_5O_2$ (MW: 454.25): C, 52.88; H, 2.88; N, 15.42%. Found: C, 55.80; H, 3.00; N, 15.50%.

(5-Bromo-1-methyl-1*H*-pyrrolo[2,3-*b*]pyridin-3-yl)-[3-(5-methoxy-1-methyl-1*H*-indol-3-yl)-[1,2,4]oxadiazol-5-yl]-methanone (181c)

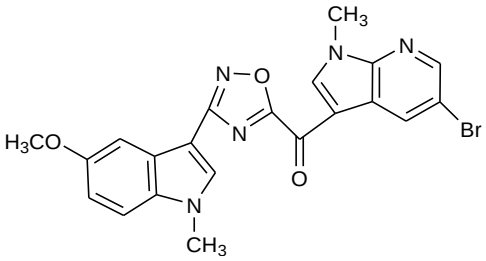

Yield: 62%; yellow solid; mp: 288 °C (dec); IR (cm^{-1}): 1637 (CO); ^{1}H NMR (200 MHz, DMSO-d_6) δ: 3.86 (3H, s, CH_3), 3.92 (3H, s, CH_3), 4.02 (3H, s, OCH_3), 6.95-7.08 (1H, m, H-6'), 7.54-7.55 (2H, m, H-7' and H-4'), 8.35 (1H, s, H-2'), 8.60 (1H, s, H-4), 8.72 (1H, s, H-6), 9.29 (1H, s, H-2); *Anal.* Calculated for $C_{21}H_{16}BrN_5O_3$ (MW: 466.29): C, 54.09; H, 3.46; N, 15.02%. Found: C, 54.18; H, 3.40; N, 15.15%.

(1-Methyl-1*H*-pyrrolo[2,3-*b*]pyridin-3-yl)-[3-(1-methyl-1*H*-indol-3-yl)-[1,2,4]oxadiazol-5-yl]-methanone (181d)

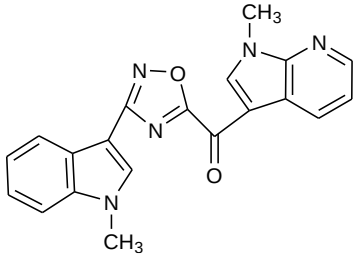

Yield: 54%; yellow solid; mp: 230 °C (dec); IR (cm^{-1}): 1620 (CO); ^{1}H NMR (200 MHz, DMSO-d_6) δ: 3.97 (3H, s, CH_3), 4.05 (3H, s, CH_3), 7.28-7.40 (2H, m, H-5' and H-6'), 7.46 (1H, dd, J = 9.9, 4.8 Hz, H-4), 7.65 (1H, dd, J = 6.5, 2.1 Hz, H-7'), 8.11 (1H, dd, J = 6.2, 2.4 Hz, H-4'), 8.44 (1H, s, H-2'), 8.51 (1H, dd, J = 4.7, 1.3 Hz, H-6), 8.64 (1H, dd, J = 7.9, 1.3 Hz, H-5), 9.27 (1H, s, H-2); *Anal.* Calculated for $C_{20}H_{15}N_5O_2$ (MW: 357.37): C, 67.22; H, 4.23; N, 19.60%. Found: C, 67.18; H, 4.14; N, 19.70%.

(1-Methyl-1*H*-pyrrolo[2,3-*b*]pyridin-3-yl)-[3-(5-fluoro-1-methyl-1*H*-indol-3-yl)-[1,2,4]oxadiazol-5-yl]-methanone (181e)

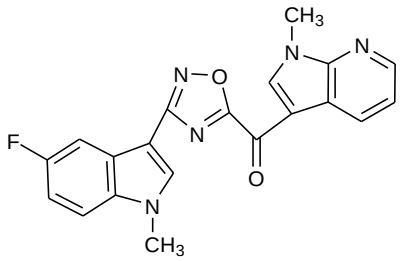

Yield: 45%; yellow solid; mp: 257 °C (dec); IR (cm^{-1}): 1638 (CO); ^{1}H NMR (200 MHz, DMSO-d_6) δ: 3.98 (3H, s, CH_3), 4.05 (3H, s, CH_3), 7.18-7.28 (1H, m, H-6'), 7.42-7.50 (1H, m, H-4), 7.66-7.79 (2H, m, H-7' and H-4'), 8.50 (1H, s, H-2'), 8.52-8.67 (2H, m, H-5 and H-6), 9.26 (1H, s, H-2); *Anal.* Calculated for $C_{20}H_{14}FN_5O_2$ (MW: 375.36): C, 64.00; H, 3.76; N, 18.66%. Found: C, 64.20; H, 3.64; N, 18.50%.

(1-Methyl-1*H*-pyrrolo[2,3-*b*]pyridin-3-yl)-[3-(5-methoxy-1-methyl-1*H*-indol-3-yl)-[1,2,4]oxadiazol-5-yl]-methanone (181f)

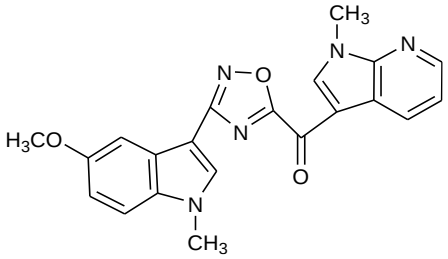

Yield: 60%; yellow solid; mp: 231 °C (dec); IR (cm^{-1}): 1623 (CO); ^{1}H NMR (200 MHz, DMSO-d_6) δ: 3.87 (3H, s, CH_3), 3.92 (3H, s, CH_3), 4.04 (3H, s, OCH_3), 6.95-7.08 (1H, m, H-6'), 7.40-7.63 (3H, m, H-7', H-4' and H-4), 8.31-8.67 (3H, m, H-2', H-5 and H-6), 9.29 (1H, s, H-2); *Anal.* Calculated for $C_{21}H_{17}N_5O_3$ (MW: 387.39): C, 65.11; H, 4.42; N, 18.08%. Found: C, 65.18; H, 4.40; N, 18.15%.

General procedure for the synthesis of 5-fluoro-1-(2-morpholin-4-yl-ethyl)-1*H*-indole-3-carbonitrile (204)

To a solution of the appropriate indole carbonitrile **189b** (0.3 g, 1.35 mmol) in DMF (2 mL), was slowly added at 0-5 °C, sodium hydride 60% dispersion in mineral oil (NaH) (0.05 g, 2.03 mmol) and the reaction mixture was stirred at room temperature for 30 min. After that, it was added dropwise a solution of 4-(2-chloroethyl)morpholine **203** (0.8 g, 5.40 mmol) in DMF (2 mL), and the reaction mixture was stirred at 50 °C for 1 h. After cooling, the mixture was poured into water and ice and the obtained precipitate was filtered off, dried, to give the desired products.

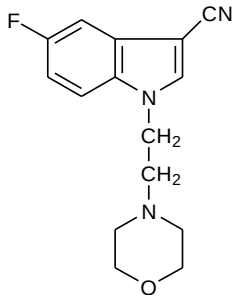

Yield: 95%; brown solid; mp: 86-87 °C; IR (cm^{-1}): 2220 (CN); ^{1}H NMR (200 MHz, DMSO-d_6) δ: 2.41 (4H, t, J = 4.5 Hz, CH_2 × 2), 2.68 (2H, t, J = 6.1 Hz, CH_2), 3.52 (4H, t, J = 4.4 Hz, CH_2 × 2), 4.38 (2H, t, J = 6.2 Hz, CH_2), 7.21 (1H, td, J = 9.3, 9.2, 2.5 Hz, H-6), 7.43 (1H, dd, J = 9.1, 2.4 Hz, H-7), 7.73-7.79 (1H, m, H-4), 8.37 (1H, s, H-2); ^{13}C NMR (50 MHz, DMSO-d_6) δ: 43.6 (t), 53.1 (2 × t), 57.1 (t), 66.1 (2× t), 83.4 (s, $J_{C7a\text{-}F}$ = 4.4 Hz),103.9 (d, $J_{C4\text{-}F}$ = 24.9 Hz), 111.7 (d, $J_{C6\text{-}F}$ = 26.3 Hz), 113.2 (d, $J_{C7\text{-}F}$ = 9.6 Hz), 115.7 (s), 127.5 (d, $J_{C3a\text{-}F}$ = 10.8 Hz), 132.0 (s), 138.9 (d), 158.4(d, $J_{C5\text{-}F}$ = 239.5 Hz); *Anal*. Calculated for $C_{15}H_{16}FN_3O$ (MW: 273.13): C, 65.92; H, 5.90; N, 15.37%. Found: C, 66.20; H, 6.01; N, 14.98%.

General procedure for the synthesis of 5-fluoro *N*-hydroxy-1-(2-morpholin-4-yl-ethyl)-1*H*-indole-3-carboxamidine (200)

To a solution of 5-fluoro-1-(2-morpholin-4-yl-ethyl)-1*H*-indole-3-carbonitrile **204** (2.1 mmol) in anhydrous ethanol (37 mL) *N*,*N*-diisopropylethylamine (DIPEA) (0.8 mL) and hydroxylamine hydrochloride ($NH_2OH{\cdot}HCl$) (400 mg, 5.76 mmol) were added in portions. The reaction mixture was heated under reflux for 7 h. The solvent was removed under reduced pressure and the residue was treated with a saturated aqueous solution of sodium hydrogencarbonate ($NaHCO_3$) (10 mL) and

then extracted with ethyl acetate (3 × 20 mL), dried (Na_2SO_4), filtered and concentrated under *vacuum*. The residue was purified by column chromatography using DCM/MeOH (96:4) as eluent.

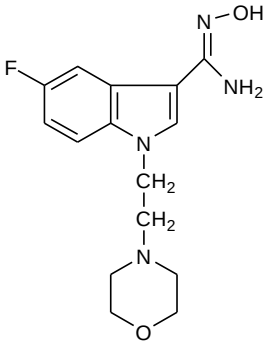

Yield: 68%; white solid; ^{1}H NMR (200 MHz, DMSO-d_6) δ: 2.42 (4H, t, J = 4.5 Hz, 2 × CH_2), 2.66 (2H, t, J = 6.1 Hz, CH_2), 3.54 (4H, t, J = 4.4 Hz, CH_2 × 2), 4.27 (2H, t, J = 6.2 Hz, CH_2), 5.64 (1H, s, NH), 6.96-7.06 (1H, m, H-6), 7.48-7.56 (1H, m, H-7), 7.72-7.79 (1H, m, H-4), 7.88 (1H, s, NH), 8.12 (1H, s, H-2), 9.30 (1H, s, OH); *Anal*. Calculated for $C_{15}H_{19}FN_4O_2$ (MW: 306.15): C, 58.81 H, 6.25; N, 18.29%. Found: C, 58.90; H, 6.11; N, 18.35%.

5.2 Biology

5.2.1 Inhibition of biofilm formation assay

The inhibitory activities toward biofilm formation of new oxadiazole derivatives were determined by the Crystal Violet Method.

Bacteria were grown in tryptic soy broth (TSB, Sigma) containing 2% w/v glucose overnight a 37 °C in a shaking bath. The obtained culture broth was diluted 1:200 to a suspension of 2% w/v of glucose in TSB, with optical density (OD) between 0.020 and 0.040, at 570 nm. 2.5 µl of diluted suspension were added to the wells of polystyrene 96-well tissue culture plates, previously filled with TSB (200 µL) with 2% w/v glucose. In each of these wells, 1µl of stock solution (10 µg / mL) of different compounds were added, in order to obtain the desired concentrations of substance in each well. Each concentration was evaluated in duplicate within the same experiment. The plates were incubated for 24 h at 37 °C. Then, the wells were emptied, washed twice with 1 ml of sterile NaCl 0.9% and stained with 200 µl of 0.1% v/v crystal violet solution for 15 mins at 37 °C. The excess stain was rinsed off by placing the plates under running tap water and then the plates were air dried overnight. Stained biofilms were rinsed with 200 µl of ethanol for each well, and the

optical density (OD) was read at 600 nm, using a microplate reader (GlomaxMultidetection System Promega). Each assay was performed in triplicate and assays were repeated at least twice.

The comparison of the average optical density of the growth in control wells with that in the sample wells allowed to estimate the percentage of inhibition of the biofilm formation at the screening concentration of 10 µg/mL, using the following equation:

$$inhibition\ (\%) = \frac{\mathrm{OD}_{570}\ \text{growth control} - \mathrm{OD}_{570}\ \text{compound}}{\mathrm{OD}_{570}\ \text{growth control}} * 100$$

5.2.2 Viability assay *in vitro*

Cytotoxic activity of the topsentin derivatives **180b**, 1**80c**, **180i**, **180j** and **180l** on differentiated pancreatic cancer cells was determined by the sulforhodamine B (SRB) chemosensitivity assay.

Cells were plated in 96-well flat-bottom plates at a final concentrations ranging from 3000-5000 cells/well in 100 µl of medium. After a 24 hours pre-incubation period, cells were treated with the compounds at nine screening concentrations (from 0.1 µM to 40 µM) in triplicate and incubated at 37°C for 72 hours. After the treatment, cells were fixed with 25 µl of cold 50% trichloroacetic acid (TCA) for each well and incubated at 4 °C for 1 hour. Afterwards plates were washed five times with demiwater and air dried overnight. Then, the plates were stained with 50 µl of 0.4% SRB solution in 1% acetic acid for 15 minutes. The excess stain was rinsed off by placing the plates under running 1% acetic acid and allowed to dry at room temperature for overnight. SRB staining was rinsed with 150 µl tris(hydroxymethyl)aminomethane solution pH= 8.8 (TRIS-base), and the OD (optical density) was read at 492 nm.
Each assay was performed in triplicate and assays were repeated at least three times.
The comparison of the average optical density of the growth in control wells with that in the sample wells allowed estimating the percentage of cell growth, using the following equation:

$$\%\ Cell\ Growth = \frac{\text{mean}\ \mathrm{OD}_{\text{compound}} - \text{mean}\ \mathrm{OD}_{\text{day zero plate}}}{\text{mean}\ \mathrm{OD}_{\text{control cells}} - \text{mean}\ \mathrm{OD}_{\text{day zero plate}}} * 100$$

The results obtained were adjusted by the day zero plate (wells containing cells growing for only 24 hours) and normalized by the control cells (wells with untreated cells) to obtain the rate of viable cells.

5.2.3 Cell apoptosis analysis

The externalization of phosphatidylserine to the cell surface was detected by flow cytometry by double staining with annexin V/7-AAD. Briefly, cells (2.0 x 10^5 cells/flask) were seeded in T-25 cell culture flasks. After an overnight incubation at 37 °C, the cells were treated with compounds **180b, 180c, 180l** at two concentrations (i.e. 2 μM and 5μM for **180b** and 5 μM and 10 μM for **180c** and **180l**) and incubated for another 24 hours. Cells recovered from cultures were trypsinized and resuspended in fresh medium. After treatment with two concentration of each compound for 24 hours, cells were stained with 7AAD and Annexin V. In particular, 2.5 μl of 7-AAD (Calbiochem, San Diego, CA) were added to 100 μl of cell suspension. The samples were incubated in the dark at room temperature for 15 min. Each sample was washed in 3 ml of PBS, supplemented with 0.1% HSA and azide, and pelleted by centrifugation. Staining of apoptotic cells was performed by incubating the cells with Annexin V-FITC in Annexin buffer (1:1000) for 15 min on ice, followed by measuring the Apoptosis- and splicing-associated protein complex (ASAP).

5.2.4 Cell cycle analysis

Cell cycle stage was analyzed by flow cytometry. Cells (2.5 x 10^5 cells/flask) were seeded in cell culture flasks T-25. After an overnight incubation at 37 °C, the cells were treated with the compounds **180b**, **180c**, **180l**, at two concentrations (i.e. 2 μM and 5μM for **180b** and 5 μM and 10 μM for **180c** and **180l**), and incubated for 24 hours. Drug concentrations were chosen on the basis of the respective EC_{50} values. After treatment, the cells were harvested by trypsinization (0.5 ml/flask of trypsine-EDTA), incubated until the cells detached from the bottom of the flask and collected using the same medium used for the culture. The samples were then centrifuged in order to form a pellet (5 min at 1200 rpm). Finally, these pellets were fixed in ice-cold 70% ethanol, washed twice with phosphate-buffered saline (20 mM sodium phosphate pH 7.4, 150 mM NaCl) and incubated for 30 min at 37 °C with 50 μl of RNase (100 μg/ml) followed by incubation with 200 μl of propidium iodide solution (PI, 50 μg/ml). The cycle analysis was performed on the FACS (Fluorescence Activated Cell Sorting) Calibur instrument, to evaluate the effects on the cell cycle distribution and cell viability.

5.2.5 Wound healing assay

Cell migration was assessed using a wound healing assay. A total of 5 x 10^4 cells/well were seeded in a 96-well plate, to form confluent monolayer. Gaps or scratch were created in confluent cell layers using the sterile scratch tool (Figure 16A). The detached cell following scratch induction were removed and new medium was added to the wells. Cells were next treated with two concentrations of each compound (i.e. 2 μM and 5μM for **180b** and 5 μM and 10 μM for **180c** and **180l**). Cells growing in complete medium were maintained at 37 °C with a supply of 5% CO2/95% air atmosphere and 100% relative humidity. The wound closure was monitored by phase-contrast microscopy and photographed at the 0th, 4th, 8th, 20th and 24th hour. Pictures of the plates were taken using the Universal Grab 6.3 software (DCILabs) from a computer connected to a Leica microscope with a JAI TMC-1327 camera.

The percentage of migration was calculated using the following equation:

$$\%\, Migration = \frac{\text{Width of the wound at T} = 0 - \text{Width of the wound at T} = \text{X}}{\text{Width of the wound at T} = 0} * 100$$

5.2.6 Gene expression analysis

In order to evaluate the capability of epithelial to mesenchymal transition (EMT) modulation by the new oxadiazole compounds, we determined the gene expression of key EMT determinants by Real-Time PCR analysis in PANC-1 and CAPAN-1 cells.

Cells (3 x 10^5 cells/well) were seeded in a 6-well plate and treated with compounds for 24 h. Cells were then harvested by 250 μl of Trizol reagent and collected in a new eppendorf tube. Total RNA was extracted by adding 50 μl chloroform to each sample, shaking vigorously and spinning 10 min at 12000 RPM at 4 °C, after 3 min of incubation at room temperature. After obtaining a lysate from each sample, the upper aqueous phase containing RNA was collected and washed with isopropanol and 70% ethanol. The pellet was resuspended in nuclease free water and the amount of nucleic acid was determined through NanoDrop technology.

Afterwards, reverse transcription (RT) reactions to produce cDNA from RNA for RT-PCR were conducted using M-MuLV RNAse H^+ reverse transcriptase enzyme, Reverse Transcription buffer 2X, including dNTP mix and $MgCl_2$, and random hexamers primer (DyNAmoTM cDNA Synthesis Kit). cDNA was synthesised from 7 μl of RNA at concentration of 143 ng/mL in a 13 μl reaction volume (10 μl of RT buffer, 1 μl of random hexamer primer and 2 μl of Reverse Transcriptase).

The cDNA synthesis reactions were initiated with a primer extension step at 25 °C for 10 minutes, followed by cDNA synthesis at 37 °C for 30 minutes, termination at 85 °C for 5 minutes and sample cooling at 4 °C.

Finally, RT-PCR reactions were performed using the commercial kit TaqMan® Universal PCR Master Mix. Amplification mixtures, set up in a final volume of 25 µl, contained 12.5 µl of Universal Master Mix 2X (AmpliTaq Gold DNA Polymerase, dNTPs with dUTP, passive reference, and optimized buffer components), 1 µl of Primers and TaqMan® probe, 6.5 µl of H_2O and 5 µl of cDNA sample. RT-PCR assays were carried out in a GeneAmp 5700 Sequence Detection System programmed to hold at 50 °C for 30 min, to hold at 95 °C for 10 min, and to complete 45 cycles of 95 °C for 15 min and 50°C for 1 min. The gene expression profiling was determined using the Sequence Detection System (SDS) software.

6. REFERENCES

1. Kelecom, A. Secondary metabolites from marine microorganisms. *An. Acad. Bras. Cienc.* **74,** 151–170 (2002).
2. Blunt, J. W., Copp, B. R., Munro, M. H. G., Northcote, P. T. & Prinsep, M. Marine natural products. *Nat. Prod. Rep.* **21,** 1–49 (2004).
3. Blunt, J., Copp, B. R., Herbert, M., Munro, G. & Prinsep, M. Marine natural products. *Nat. Prod. Rep.* **20,** 1–48 (2005).
4. Blunt, J. W., Copp, B. R., Keyzers, R. A. & Munro, H. G. Marine natural products. *Nat. Prod. Rep.* **29,** 144–222 (2012).
5. Ishikura, M., Abe, T., Choshi, T. & Hibino, S. Simple indole alkaloids and those with a nonrearranged monoterpenoid unit. *Nat. Prod. Rep.* **32,** 1389–1471 (2015).
6. Pauletti, P. M. *et al.* Halogenated indole alkaloids from marine invertebrates. *Mar. Drugs.* **8,** 1526–1549 (2010).
7. Berlinck, R. G. S. *et al.* Polycyclic Diamine Alkaloids from Marine Sponges. *Top. Heterocycl. Chem.* **10,** 211–238 (2007).
8. Nahar, L., Sarker, S. D. & Turner, A. B. A review on synthetic and natural steroid dimers: 1997-2006. *Curr. Med. Chem.* **14,** 1349–70 (2007).
9. Civelek, M., Lusis, A. J., Genetics, M. & Angeles, L. The Manzamines as an Example of the Unique Structural Classes Available for the Discovery and Optimization of Infectious Disease Controls Based on Marine Natural Products. *Curr. Pharm. Des.* **13,** 653–660 (2007).
10. Kim, C. K. *et al.* Manzamine Alkaloids from an Acanthostrongylophora sp. Sponge. *J. Nat. Prod.* **80,** 1575–1583 (2017).
11. Kita, M., Ohno, O., Han, C. & Uemura, D. Bioactive secondary metabolites from symbiotic marine dinoflagellates: Symbiodinolide and durinskiols. *Chem. Rec.* **10,** 57–69 (2010).
12. Cao, R., Peng, W., Wang, Z. & Xu, A. beta-Carboline Alkaloids: Biochemical and Pharmacological Functions. *Curr. Med. Chem.* **14,** 479–500 (2007).
13. Cheung, R. C. F., Ng, T. B. & Wong, J. H. Marine Peptides: Bioactivities and Applications. *Mar. Drugs.* **13,** 4006–4043 (2015).
14. Hanson, J. R. Diterpenoids. *Nat. Prod. Rep.* **24,** 1332 (2007).
15. Fraga, B. M. Natural sesquiterpenoids. *Nat. Prod. Rep.* **30,** 1226–1264 (2013).
16. Wang, L., Yang, B., Lin, X. P., Zhou, X. F. & Liu, Y. Sesterterpenoids. *Nat. Prod. Rep.* **30,** 455–473 (2013).
17. González, M. A. Spongiane Diterpenoids. *Curr. Bioact. Compd.* **3,** 1–36 (2007).

18. Chianese, G. *et al.* Antiprotozoal Linear Furanosesterterpenoids from the Marine Sponge Ircinia oros. *J. Nat. Prod.* **80,** 2566–2571 (2017).
19. Kigoshi, H. & Hayakawa, I. Marine cytotoxic macrolides haterumalides and biselides, and related natural products. *Chem. Rec.* **7,** 254–264 (2007).
20. Blunt, J. W., Copp, B. R., Munro, M. H. G., Northcote, P. T. & Prinsep, M. Marine natural products. *Nat. Prod. Rep.* **20,** 1–48 (2003).
21. Porter, J. W. & Targett, N. M. Allelochemical interactions between sponges and corals. *Biol. Bull.* **175,** 230–239 (1988).
22. Davis, A. R., Butler, A. J. & Van Altena, I. Settlement behaviour of ascidian larvae: preliminary evidence for inhibition by sponge allelochemicals. *Mar. Ecol. Prog. Ser.* **72,** 117–123 (1991).
23. Uriz, M. J., Turon, X., Becerro, M. A. & Galera, J. Feeding deterrence in sponges. The role of toxicity, physical defenses, energetic contents, and life-history stage. *J. Exp. Mar. Bio. Ecol.* **205,** 187–204 (1996).
24. Becerro, M. A. Multiple functions for secondary metabolites in encrusting marine invertebrates. *J. Chem. Ecol.* **23,** 1527–1547 (1997).
25. Hay, M. E. Marine chemical ecology: What's known and what's next? *J. Exp. Mar. Biol. Ecol.* **200,** 103–134 (1996).
26. Nastrucci, C., Cesario, A. & Russo, P. Anticancer Drug Discovery from the Marine Environment. *Recent Pat. Anticancer Drug Discov.* **7,** 218–232 (2012).
27. Faulkner, D. J. Highlights of marine natural products chemistry (1972-1999). *Nat. Prod. Rep.* **17,** 1–6 (2000).
28. Fenical, W. Chemical Studies of Marine Bacteria: Developing a New Resource. *Chem. Rev.* **93,** 1673–1683 (1993).
29. Calcabrini, C., Catanzaro, E., Bishayee, A., Turrini, E. & Fimognari, C. Marine Sponge Natural Products with Anticancer Potential : An Updated Review. *Mar. Drugs.* **15,** 1–34 (2017).
30. Sipkema, D., Franssen, M. C. R., Osinga, R. & Tramper, J. Marine Sponges as Pharmacy. *Mar. Biotechnol.* **7,** 142–162 (2005).
31. Anjum, K. *et al.* Marine sponges as a drug treasure. *Biomol. Ther.* **24,** 347–362 (2016).
32. Kumar, D. & Rawat, D. S. Marine natural alkaloids as anticancer agents. *Res. Signpost.* **661,** 213–268 (2011).
33. Sharma, V., Sharma, P. C. & Kumar, V. A mini review on pyridoacridines: Prospective lead compounds in medicinal chemistry. *J. Adv. Res.* **6,** 63–71 (2015).

34. Schmitz, F. J., DeGuzman, F. S., Hossain, M. B. & Van der Helm, D. Cytotoxic Aromatic Alkaloids from the Ascidian Amphicarpa meridiana and Leptoclinides sp.: Meridine and 11-Hydroxyascididemin. *J. Org. Chem.* **56,** 804–808 (1991).
35. Ding, Q., Chichak, K. & Lown, J. W. Pyrroloquinoline and Pyridoacridine Alkaloids from marine sources. *Curr. Med. Chem.* **6,** 1–27 (1999).
36. Delfourne, E. & Bastide, J. Marine pyridoacridine alkaloids and synthetic analogues as antitumor agents. *Med. Res. Rev.* **23,** 234–252 (2003).
37. Molinski, T. F. & Ireland, C. M. Varamines A and B, New Cytotoxic Thioalkaloids from Lissoclinum vareau. *J. Org. Chem.* **54,** 4256–4259 (1989).
38. Bry, D., Banaigs, B., Long, C. & Bontemps, N. New pyridoacridine alkaloids from the purple morph of the ascidian Cystodytes dellechiajei. *Tetrahedron Lett.* **52,** 3041–3044 (2011).
39. Kobayashi, J. *et al.* Cystodytins D-I, new cytotoxic tetracyclic aromatic alkaloids from the okinawan marine tunicate cystodytes dellechiajei. *J. Nat. Prod.* **54,** 1634–1638 (1991).
40. Luedtke, N. W. *et al.* Eilatin Ru (II) complexes display anti-HIV activity and enantiomeric diversity in the binding of RNA. *ChemBioChem.* **3,** 766–771 (2002).
41. Charyulu, G. A., McKee, T. C. & Ireland, C. M. Diplamine, a cytotoxic polyaromatic alkaloid from the tunicate diplosoma sp. *Tetrahedron Lett.* **30,** 4201–4202 (1989).
42. Carroll, A. R. & Scheuer, P. J. Kuanoniamines A, B, C, and D: Pentacyclic Alkaloids from a Tunicate and Its Prosobranch Mollusk Predator Chelynotus semperi. *J. Org. Chem.* **55,** 4426–4431 (1990).
43. Kobayashi, J. *et al.* Cystodytins A, B, and C, novel tetracyclic aromatic alkaloids with potent antineoplastic activity from the Okinawan tunicate Cystodytes dellechiajei. *J. Org. Chem.* **53,** 1800–1804 (1988).
44. McDonald, L. A., Eldredge, G. S., Barrows, L. R. & Ireland, C. M. Inhibition of Topoisomerase II Catalytic Activity by Pyridoacridine Alkaloids from a Cystodytes sp. Ascidian: A Mechanism for the Apparent Intercalator-Induced Inhibition of Topoisomerase II. *J. Med. Chem.* **37,** 3819–3827 (1994).
45. Appleton, D. R., Pearce, A. N., Lambert, G., Babcock, R. C. & Copp, B. R. Isodiplamine, cystodytin K and lissoclinidine: Novel bioactive alkaloids from the New Zealand ascidian Lissoclinum notti. *Tetrahedron.* **58,** 9779–9783 (2002).
46. Charyulu, G. A., Mckee, T. C. & Ireland, C. M. Diplamine, a cytotoxic polyaromatic alkaloid from the tunicate diplosoma sp. *Tetrahedron Lett.* **30,** 4201–4202 (1989).
47. Kobayashi, J., Cheng, J., Nakamura, H. & Ohizumi, Y. Ascididemin, a novel pentacyclic

aromatic alkaloid with potent antileukemic activty from the Okinawan tunicate Didemnum sp. *Tetrahedron Lett.* **29,** 1177–1180 (1988).

48. Delfourne, E. *et al.* Synthesis and in vitro antitumor activity of an isomer of the marine pyridoacridine alkaloid ascididemin and related compounds. *Bioorg. Med. Chem.* **11,** 4351–4356 (2003).
49. Bontemps, N., Bonnard, I., Banaigs, B., Combaut, G. & Francisco, C. Cystodamine, a New Cytotoxic Fused Polyaromatic Alkaloid from the Mediterranean Ascidian Cystodytes delle chiajes. *Tetrahedron Lett.* **35,** 7023–7026 (1994).
50. Rudi, A. & Kashman, Y. Six New Alkaloids from the Purple Red Sea Tunicate Eudistoma sp. *J. Org. Chem.* **54,** 5331–5337 (1989).
51. Carroll, A. R., Cooray, N. M., Poiner, A. & Scheuer, P. J. A second Shermilamine alkaloid from a tunicate trididemnum sp. *J. Org. Chem.* **54,** 4231–4232 (1989).
52. Cooray, N. M., Scheuer, P. J., Parkany, L. & Clardy, J. Shermilamine A: A pentacyclic alkaloid from tunicate. *J. Org. Chem.* **53,** 4619–4620 (1988).
53. Koren-Goldshlager, G., Aknin, M., Gaydou, E. M. & Kashman, Y. Three new alkaloids from the marine tunicate Cystodytes violatinctus. *J. Org. Chem.* **63,** 4601–4603 (1998).
54. Kashman, Y., Koren-Goldshlager, G., Aknin, M. & Garcia Gravalos, D. Cytotoxic pyridoacridine alkaloids. *PCT Int Appl.* WO 99/23099 (1999).
55. Barnes, E. C., Said, N. A. B. M., Williams, E. D., Hooper, J. N. A. & Davis, R. A. Ecionines A and B, two new cytotoxic pyridoacridine alkaloids from the Australian marine sponge, Ecionemia geodides. *Tetrahedron.* **66,** 283–287 (2010).
56. Gunawardana, G. P. *et al.* Pyridoacridine Alkaloids from Deep-Water Marine Sponges of the Family Pachastrellidae: Structure Revision of Dercitin and Related Compounds and Correlation with the Kuanoniamines. *J. Org. Chem.* **57,** 1523–1526 (1992).
57. Agrawal, M. S. & Bowden, B. F. Nordehydrocyclodercitin, a hexacyclic pyridoacridine alkaloid from the marine ascidian, Aplidium sp. *Nat. Prod. Res.* **21,** 782–786 (2007).
58. Bouffier, L., Dinica, R., Debray, J., Dumy, P. & Demeunynck, M. Functionalization of the A ring of pyridoacridine as a route toward greater structural diversity. Synthesis of an octacyclic analogue of eilatin. *Bioorg. Med. Chem. Lett.* **19,** 4836–4838 (2009).
59. Kuramoto, M. *et al.* Cylindradines A and B: Novel Bromopyrrole Alkaloids from the Marine Sponge Axinella cylindratus. *Org. Lett.* **10,** 5465–468 (2008).
60. D'Ambrosio, M. *et al.* The Active Centres of Agelastatin A, a Strongly Cytotoxic Alkaloid of the Coral Sea Axinellid Sponge Agelas dendromorpha, as Determined by Comparative Bioassays with Semisynthetic Derivatives. *Helv. Chim. Acta.* **79,** 727–735 (1996).

61. D'Ambrosio, M. *et al.* Agelastatin A, a new skeleton cytotoxic alkaloid of the oroidin family. Isolation from the axinellid sponge Agelas dendromorpha of the coral sea. *J. Chem. Soc. Chem. Commun.* 1305–1306 (1993).
62. Tilvi, S. *et al.* Agelastatin E , Agelastatin F , and Benzosceptrin C from the Marine Sponge Agelas dendromorpha. *J. Nat. Prod.* **73,** 720–723 (2010).
63. Morales, J. & Rodriguez, A. D. The structure of clathrodin, a novel alkaloid isolated from the Caribbean sea sponge Agelas Clathrodes. *J. Nat. Prod.* **52,** 629–631 (1991).
64. Pettit, G. R. *et al.* Antineoplastic Agents . 362 . Isolation and X-ray Crystal Structure of Dibromophakellstatin from the Indian Ocean Sponge Phakellia mauritiana. *J. Nat. Prod.* **60,** 180–183 (1997).
65. Tsukamoto, S. *et al.* Four new bioactive pyrrole-derived alkaloids from the marine sponge Axinella brevistyla. *J. Nat. Prod.* **64,** 1576–1578 (2001).
66. Utkina, N. K., Makarchenko, A. E., Denisenko, V. A. & Dmitrenok, P. S. Zyzzyanone A, a novel pyrrolo[3,2-f]indole alkaloid from the Australian marine sponge Zyzzya fuliginosa. *Tetrahedron Lett.* **45,** 7491–7494 (2004).
67. Utkina, N. K., Makarchenko, A. E. & Denisenko, V. A. Zyzzyanones B-D, dipyrroloquinones from the marine sponge Zyzzya fuliginosa. *J. Nat. Prod.* **68,** 1424–1427 (2005).
68. Landini, D., Maia, A. & Rampoldi, A. Discorhabdin C, a Highly Cytotoxic Pigment from a Sponge of the Genus Latrunculia. *J. Org. Chem.* **51,** 5476–5478 (1986).
69. Perry, N. B., Blunt, J. W. & Munro, M. H. G. Cytotoxic pigments from new zealand sponges of the genus. *Tetrahedron.* **44,** 1727–1734 (1988).
70. Reyes, F. *et al.* Discorhabdins I and L, Cytotoxic Alkaloids from the Sponge Latrunculia brevis Fernando. *J. Nat. Prod.* **67,** 463 (2004).
71. Lang, G., Pinkert, A., Blunt, J. W. & Munro, M. H. G. Discorhabdin W, the first dimeric discorhabdin. *J. Nat. Prod.* **68,** 1796–1798 (2005).
72. Sun, H. H., Sakemi, S., Burres, N. & McCarthy, P. Isobatzellines A, B, C, and D. Cytotoxic and Antifungal Pyrroloquinoline Alkaloids from the Marine Sponge Batzelh sp. *J. Org. Chem.* **55,** 4964–4966 (1990).
73. Radisky, D. C. *et al.* Novel Cytotoxic Topoisomerase II Inhibiting Pyrroloiminoquinones from Fijian Sponges of the Genus Zyzzya. *J. Am. Chem. Soc.* **115,** 1632–1638 (1993).
74. Carney, J. R., Scheuer, P. J. & Kelly-Borges, M. Makaluvamine G, a cytotoxic pigment from an an Indonesian Sponge Histodermella sp. *Tetrahedron.* **49,** 8483–8486 (1993).
75. Venables, D. A., Concepcion, G. P., Matsumoto, S. S., Barrows, L. R. & Ireland, C. M.

Makaluvamine N: A New Pyrroloiminoquinone from Zyzzya fuliginosa Debra. *J. Nat. Prod.* **60,** 408–410 (1997).

76. Casapullo, A. *et al.* Makaluvamine P, a new cytotoxic pyrroloiminoquinone from Zyzzya cf. fuliginosa. *J. Nat. Prod.* **64,** 1354–1356 (2001).
77. Peirò, S. *et al.* Snail1 transcriptional repressor binds to its own promoter and controls its expression. *Nucleic Acids Res.* **34,** 2077–2084 (2006).
78. Kitamura, A., Tanaka, J., Ohtani, I. I. & Higa, T. Echinoclathrines A-C: A new class of pyridine alkaloids from an Okinawan sponge, Echinoclathria sp. *Tetrahedron.* **55,** 2487–2492 (1999).
79. Tsuda, M., Hirano, K., Kubota, T. & Kobayashi, J. Pyrinodemin A, a cytotoxic pyridine alkaloid with an isoxazolidine moiety from sponge Amphimedon sp. *Tetrahedron Lett.* **40,** 4819–4820 (1999).
80. Hirano, K., Kubota, T., Tsuda, M., Mikami, Y. & Kobayashi, J. Pyrinodermins B-D, potent Cytotoxic bis-pyridine alkaloids from marine sponge Amphimedon sp. *Chem. Pharm. Bull.* **48,** 974–977 (2000).
81. Kariya, Y., Kubota, T., Fromont, J. & Kobayashi, J. Pyrinadines B-G, new bis-pyridine alkaloids with an azoxy moiety from sponge Cribrochalina sp. *Bioorg. Med. Chem.* **14,** 8415–8419 (2006).
82. Takekawa, Y., Matsunaga, S., Van Soest, R. W. M. & Fusetani, N. Amphimedosides, 3-alkylpyridine glycosides from a marine sponge Amphimedon sp. *J. Nat. Prod.* **69,** 1503–1505 (2006).
83. Pettit, R. *et al.* Isolation and structure of cribrostatins 1 and 2 from the blue marine sponge Cribrochalina sp. *Can. J. Chem.* **70,** 1170–1175 (1992).
84. Pettit, G. R. *et al.* Antineoplastic agents 430. Isolation and structure of cribrostatins 3, 4, and 5 from the Republic of Maldives Cribrochalina species. *J. Nat. Prod.* **63,** 793–798 (2000).
85. Kashman, Y. *et al.* Ptilomycalin A: A Novel Polycyclic Guanidine Alkaloid of Marine Origin. *J. Am. Chem. Soc.* **111,** 8925–8926 (1989).
86. Sorek, H. *et al.* Netamines A – G : seven new tricyclic guanidine alkaloids from the marine sponge Biemna laboutei. *Tetrahedron.* **62,** 8838–8843 (2006).
87. Ralifo, P., Tenney, K., Valeriote, F. A. & Crews, P. A distinctive structural twist in the aminoimidazole alkaloids from a calcareous marine sponge: Isolation and characterization of leucosolenamines A and B. *J. Nat. Prod.* **70,** 33–38 (2007).
88. Tsukamoto, S. *et al.* Naamidines H and I , Cytotoxic Imidazole Alkaloids from the Indonesian Marine Sponge Leucetta chagosensis. *J. Nat. Prod.* **70,** 1658–1660 (2007).

89. Guillen, P. O. *et al.* Terrazoanthines, 2-Aminoimidazole Alkaloids from the Tropical Eastern Pacific Zoantharian Terrazoanthus onoi. *Org. Lett.* **19,** 1558–1561 (2017).
90. Williams, D. E. *et al.* Motuporamines , Anti-Invasion and Anti-Angiogenic Alkaloids from the Marine Sponge Xestospongia exigua (Kirkpatrick): Isolation, Structure Elucidation, Analogue Synthesis, and Conformational Analysis. *J. Org. Chem.* **67,** 245–258 (2002).
91. Roskelley, C. D. *et al.* Inhibition of Tumor Cell Invasion and Angiogenesis by Motuporamines. *Cancer Res.* **61,** 6788–6794 (2001).
92. Tohme, R., Darwiche, N. & Gali-Muhtasib, H. A Journey Under the Sea: The Quest for Marine Anti-Cancer Alkaloids. *Molecules.* **16,** 9665–9696 (2011).
93. Borbone, N. *et al.* Minor Steroidal Alkaloids from the Marine Sponge Corticium sp . *J. Nat. Prod.* **65,** 1206–1209 (2002).
94. Ridley, C. P. & Faulkner, D. J. New Cytotoxic Steroidal Alkaloids from the Philippine Sponge Corticium niger. *J. Nat. Prod.* **66,** 1536–1539 (2003).
95. Sunassee, S. N. *et al.* Steroidal Alkaloids from the Marine Sponge Corticium niger That Inhibit Growth of Human Colon Carcinoma Cells. *J. Nat. Prod.* **77,** 2475–2480 (2014).
96. Aoki, S., Watanabe, Y., Tanabe, D. & Setiawan, A. Cortistatins J , K , L , novel abeo-9(10-19)-androstane-type steroidal alkaloids with isoquinoline unit, from marine sponge Corticium simplex. *Tetrahedron Lett.* **48,** 4485–4488 (2007).
97. Nakamura, H., Ohizumi, H. & Hirata, Y. Agelasine-A , -B , -C and -D , novel bicyclic diterpenoids with a 9-methyladeninium unit possessing inhibitory effects on na , K-atpase from the okinawa sea sponge Agelas sp. *Tetrahedron Lett.* **25,** 2989–2992 (1984).
98. Utenova, B. T. & Gundersen, L. L. Synthesis of (+)-agelasine D from (+)-manool. *Tetrahedron Lett.* **45,** 4233–4235. (2004).
99. Dahlstro, M. *et al.* Original Article Antifouling Activity of Bromotyrosine-Derived Sponge Metabolites and Synthetic Analogues. *Mar. Biotechnol.* **9,** 776–785 (2007).
100. Hertiani, T. *et al.* Bioorganic & Medicinal Chemistry From anti-fouling to biofilm inhibition : New cytotoxic secondary metabolites from two Indonesian Agelas sponges. *Bioorg. Med. Chem.* **18,** 1297–1311 (2010).
101. Jiang, B. & Gu, X. H. Syntheses and cytotoxicity evaluation of bis(indolyl)thiazole, bis(indolyl)pyrazinone and bis(indolyl)pyrazine: Analogues of cytotoxic marine bis(indole) alkaloid. *Bioorg. Med. Chem.* **8,** 363–371 (2000).
102. Jiang, B., Smallheer, J. M., Amaral-Ly, C. & Wuonola, M. A. Total Synthesis of (±)-Dragmacidin: A Cytotoxic Bis(indole)alkaloid of Marine Origin. *J. Org. Chem.* **59,** 6823–6827 (1994).

103. Wincent, E., Shirani, H., Bergman, J., Rannug, U. & Janosik, T. Synthesis and biological evaluation of fused thio- and selenopyrans as new indolocarbazole analogues with aryl hydrocarbon receptor affinity. *Bioorg. Med. Chem.* **17,** 1648–1653 (2009).
104. Simoni, D. *et al.* Versatile synthesis of new cytotoxic agents structurally related to hemiasterlins. *Bioorg. Med. Chem. Lett.rg. Med. Chem. Lett.* **20,** 3431–3435 (2010).
105. Bokesch, H. R., Pannell, L. K., McKee, T. C. & Boyd, M. R. Coscinamides A, B and C, three new bis indole alkaloids from the marine sponge Coscinoderma sp. *Tetrahedron Lett.* **41,** 6305–6308 (2000).
106. Bergman, J., Janosik, T. & Johnsson, A.-L. Synthesis of Hyrtiosin B, a Bis-indole Alkaloid from the Okinawan Marine Sponge Hyrtios erecta. *Synthesis (Stuttg).* **1999,** 580–582 (1999).
107. Yamamoto, Y., Kiriyama, N., Shimizu, S. & Koshimura, S. Antitumor activity of Asterriquinone, a metabolic product from Aspergillus Terreus. *Gann.* **67,** 623–624 (1976).
108. Wright, A. E., Pomponi, S. A., Cross, S. S., Mccarthy, P. & Pierce, F. A New Bis (indole) Alkaloid from a Deep-Water Marine Sponge of the Genus Spongosorites. *J. Org. Chem.* **57,** 4772–4775 (1992).
109. Cutignano, A. *et al.* Dragmacidin F : A New Antiviral Bromoindole Alkaloid from the Mediterranean Sponge Halicortex sp . *Tetrahedron.* **56,** 3743–3748 (2000).
110. Wright, A. E. *et al.* Dragmacidin G, a bioactive bis-indole alkaloid from a deep-water sponge of the genus Spongosorites. *Mar. Drugs.* **15,** 1–10 (2017).
111. Morris, S. A. & Andersen, R. J. Brominated Bis(indole) Alkaloids from the marine spongge hexadella sp. *Tetrahedron.* **46,** 715–720 (1990).
112. Fahy, E., Potts, B. C. M. & Faulkner, D. J. 6-Bromotryptamine Derivatives From The Gulf of California tunicate Didemnum Candidum. *J. Nat. Prod.* **54,** 564–569 (1991).
113. Kohmoto, S. *et al.* Dragmacidin, a New Cytotoxic Bis(indole) Alkaloid from a Deep Water Marine Sponge, Dragmacidon sp. *J. Org. Chem.* **53,** 3116–3118 (1988).
114. Murray, L. M., Lim, T. K., Hooperb, J. N. A. & Caponaic, R. J. Isobromotopsentin : a New Bis(indole) Alkaloid from a Deep-Water Marine Sponge Spongosorites sp. *Aust. J. Chem.* **48,** 2053–2058 (1995).
115. Endo, T., Tsuda, M. & Fromont, J. Hyrtinadine A, a Bis-indole Alkaloid from a Marine Sponge. *J. Nat. Prod.* **70,** 423–424 (2007).
116. Gunasekera, S. P., McCarthy, P. J. & Kelly-Borges, M. Hamacanthins a and b, new antifungal bis indole alkaloids from the deep-water marine sponge, hamacantha sp. *J. Nat. Prod.* **57,** 1437–1441 (1994).
117. Gupta, L., Talwar, A. & Chauhan, P. M. S. Bis and tris indole alkaloids from marine

organisms: new leads for drug discovery. *Curr. Med. Chem.* **14,** 1789–803 (2007).

118. Sakemi, S. & Sun, H. H. Nortopsentins A, B, and C. Cytotoxic and Antifungal Imidazolediylbis[indoles] from the Sponge Spongosorites ruetzleri. *J. Org. Chem.* **56,** 4304–4307 (1991).
119. Alvarado, S., Roberts, B. F., Wright, A. E. & Chakrabarti, D. The Bis(Indolyl)Imidazole Alkaloid Nortopsentin A Exhibits Antiplasmodial Activity. *Antimicrob. Agents Chemother.* **57,** 2362–2364 (2013).
120. Diana, P. *et al.* Synthesis and antitumor properties of 2,5-bis(30-indolyl)thiophenes: Analogues of marine alkaloid nortopsentin. *Bioorg. Med. Chem. Lett.* **17,** 2342–2346 (2007).
121. Diana, P. *et al.* 3,5-Bis(3′-indolyl)pyrazoles, analogues of marine alkaloid nortopsentin: Synthesis and antitumor properties. *Bioorg. Med. Chem. Lett.* **17,** 6134–6137 (2007).
122. Diana, P. *et al.* Synthesis and antitumor activity of 2,5-bis(3′-indolyl)-furans and 3,5-bis(3′-indolyl)-isoxazoles, nortopsentin analogues. *Bioorg. Med. Chem.* **18,** 4524–4529 (2010).
123. Carbone, A. *et al.* Synthesis and antiproliferative activity of 2,5-bis(3′-Indolyl)pyrroles, analogues of the marine alkaloid nortopsentin. *Mar. Drugs.* **11,** 643–654 (2013).
124. Gu, X. H., Wan, X. Z. & Jiang, B. Syntheses and biological activities of bis(3-indolyl)thiazoles, analogues of marine bis(indole)alkaloid nortopsentins. *Bioorg. Med. Chem. Lett.* **9,** 569–572 (1999).
125. Carbone, A. *et al.* Synthesis and Antiproliferative Activity of Thiazolyl-bis-pyrrolo[2,3-b]pyridines and Indolyl-thiazolyl-pyrrolo[2,3-c]pyridines, Nortopsentin Analogues. *Mar. Drugs.* **13,** 460–492 (2015).
126. Parrino, B. *et al.* 3-[4-(1H-Indol-3-yl)-1,3-thiazol-2-yl]-1H-pyrrolo[2,3-b]pyridines, Nortopsentin Analogues with Antiproliferative Activity. *Mar. Drugs.* **13,** 1901–1924 (2015).
127. Carbone, A. *et al.* Novel 1H-Pyrrolo[2,3-b]pyridine Derivative Nortopsentin Analogues: Synthesis and Antitumor Activity in Peritoneal Mesothelioma Experimental Models. *J. Med. Chem.* **56,** 7060–7072 (2013).
128. Carbone, A. *et al.* Synthesis and antiproliferative activity of substituted 3 [2-(1H-indol-3-yl)-1,3-thiazol-4-yl]-1H-pyrrolo[3,2-b]pyridines, marine alkaloid nortopsentin analogues. *Curr. Med. Chem.* **21,** 1654 (2014).
129. Parrino, B. *et al.* Synthesis, antitumor acticity and CDK1 inhibition of new thiazole nortopsentin analogues. *Eur. J. Med. Chem.* **138,** 371–383 (2017).
130. Carbone, A. *et al.* New Thiazole Nortopsentin Analogues Inhibit Bacterial Biofilm Formation. *Mar. Drugs.* **16,** 274–289 (2018).
131. Bartik, K., Braekman, J. C., Daloze, D. & Stoller, C. Topsentins, new toxic bis-indole

alkaloids from sponge Topsentia genitrix. *Can. J. Chem.* **65,** 2118–2121 (1987).

132. Murray, L. M., Lim, T. K. & Capon, R. J. Isobromotopsentin:A new bis(indole) alkaloid from a deep-Water marine sponge spongosorites sp. *Aust. J. Chem.* **48,** 2053–2058 (1995).
133. Tsujii, S. *et al.* Topsentin, Bromotopsentin, and Dihydrodeoxybromotopsentin: Antiviral and Antitumor Bis(Indolyl)imidazoles from Caribbean Deep-Sea Sponges of the Family Halichondriidae. Structural and Synthetic Studies. *J. Org. Chem.* **53,** 5446–5453 (1988).
134. Bao, B. *et al.* Cytotoxic bisindole alkaloids from a marine sponge Spongosorites sp. *J. Nat. Prod.* **68,** 711–715 (2005).
135. Casapullo, A., Bifulco, G., Bruno, I. & Riccio, R. New bisindole alkaloids of the topsentin and hamacanthin classes from the Mediterranean marine sponge Rhaphisia lacazei. *J. Nat. Prod.* **63,** 447–451 (2000).
136. Phife, D. W. *et al.* Marine Sponge Bis(indole) Alkaloids that Displace Ligand Binding To alfa1 Adrenergic Recetors. *Bioorg. Med. Chem. Lett.* **6,** 2103–2106 (1996).
137. Morris, S. A. & Andersen, R. J. Nitrogenous metabolites from the deep water sponge Hexadella sp. *Can. J. Chem.* **67,** 677 (1989).
138. Oh, K.-B. *et al.* Antimicrobial Activity and Cytotoxicity of Bis(indole) Alkaloids from the Sponge Spongosorites sp. *Biol. Pharm. Bull.* **29,** 570–573 (2006).
139. Shin, J., Seo, Y., Cho, K. W., Rho, J. R. & Sim, C. J. New bis(indole) alkaloids of the topsentin class from the sponge Spongosorites genitrix. *J. Nat. Prod.* **62,** 647–649 (1999).
140. Oh, K. *et al.* Bis(indole) alkaloids as sortase A inhibitors from the sponge Spongosorites sp. *Bioorg. Med. Chem. Lett.* **15,** 4927–4931 (2005).
141. Zoraghi, R. *et al.* Methicillin-resistant Staphylococcus aureus (MRSA) pyruvate kinase as a target for bis-indole alkaloids with antibacterial activities. *J. Biol. Chem.* **286,** 44716–44725 (2011).
142. Veale, C. G. L. *et al.* Synthetic Analogues of the Marine Bisindole Deoxytopsentin: Potent Selective Inhibitors of MRSA Pyruvate Kinase. *J. Nat. Prod.* **78,** 355–362 (2015).
143. Veale, C. G. L. *et al.* Synthesis and MRSA PK inhibitory activity of thiazole containing deoxytopsentin analogues. *Tetrahedron.* **70,** 7845–7853 (2014).
144. Carbone, A. *et al.* A Facile Synthesis of Deaza-Analogues of the Bisindole Marine Alkaloid Topsentin. *Molecules.* **18,** 2518–2527 (2013).
145. Arshad, M., Khan, T. A. & Khan, M. A. 1,2,4-oxadiazole nucleus with versatile biological applications. *Int. J. Pharm. Sci. Res.* **5,** 303–316 (2014).
146. Musmade Deepak, S., Pattan Shashikant, R. & Manjunath, S. Y. Oxadiazole a nucleus with versatile biological behaviour. *Int. J. Pharm. Chem.* **5,** 11–20 (2015).

147. Pace, A. & Pierro, P. The new era of 1,2,4-oxadiazoles. *Org. Biomol. Chem.* **7,** 4337–4348 (2009).
148. Bora, R. O., Dar, B., Pradhan, V. & Farooqui, M. [1, 2, 4]-Oxadiazoles: Synthesis and Biological Applications. *Mini Rev. Med. Chem.* **13,** 1–15 (2014).
149. Valeur, E. & Bradley, M. Amide bond formation: Beyond the myth of coupling reagents. *Chem. Soc. Rev.* **38,** 606–631 (2009).
150. Chan, L. C. & Cox, B. G. Kinetics of amide formation through carbodiimide/N-hydroxybenzotriazole (HOBt) couplings. *J. Org. Chem.* **72,** 8863–8869 (2007).
151. Joullié, M. M. & Lassen, K. M. Evolution of amide bond formation. *Arkivoc.* **8,** 189–250 (2010).
152. Kurbanova, M. M. N-haloalkylation reaction in the presence of trichloroacetic acid. *Russ. J. Org. Chem.* **41,** 1716–1717 (2005).
153. Ikeda, Y., Ezakv, M., Hayashv, I., Yasuda, D. & Nakayama, K. Establishment and Characterization of Human Pancreatic Cancer Cell Lines in Tissue Culture and in Nude Mice. *Jpn. J. Cancer Res.* **81,** 987–993 (1990).
154. Skehan, P. & Friedman, S. J. A Rapid Naphthol Yellow S Method for Measuring the Cellular Protein Content of Anchorage Cultures. *Vitr. Cell. Dev. Biol.* **21,** 288–290 (2014).
155. Lieber, M., Mazzetta, J., Nelson-Rees, W., Kaplan, M. & Todaro, G. Establishment of a continuous tumor-cell line (PANC-1) from a human carcinoma of the exocrine pancreas. *Int. J. Cancer* **15,** 741–747 (1975).
156. Gradiz, R., Silv, H. C., Carvalho, L. & Botelho, M. F. MIA PaCa-2 and PANC-1 – pancreas ductal adenocarcinoma cell lines with neuroendocrine differentiation and somatostatin receptors. *Sci. Rep.* 1–14 (2016).
157. Pilichowska, M., Kimura, N., Schindler, M. & Kobari, M. Somatostatin Type 2A Receptor Immunoreactivity in Human Pancreatic Adenocarcinomas. *Endocr. Pathol.* **12,** 147–155 (2001).
158. Neureiter, D. *et al.* Different capabilities of morphological pattern formation and its association with the expression of differentiation markers in a xenograft model of human pancreatic cancer cell lines. *Pancreatology* **5,** 387–397 (2005).
159. Madden, M. E. & Sarras, M. P. Morphological and Biochemical Characterization of a Human Pancreatic Ductal Cell Line (PANC-1). *Pancreas.* **3,** 512–528 (1988).
160. Flores, R. A rapid and reproducible assay for quantitative estimation of proteins using bromophenol blue. *Anal. Biochem.* **88,** 605–611 (1978).
161. Kerr, J. F., Wyllie, A. H. & Currie, A. R. Apoptosis: a basic biological phenomenon with

wide-ranging implications in tissue kinetics. *Br. J. Cancer.* **26,** 376–398 (1972).

162. Lane, J. D., Allan, V. J. & Woodman, P. G. Active relocation of chromatin and endoplasmic reticulum into blebs in late apoptotic cells. *J. Cell Sci.* **118,** 4059–4071 (2005).
163. Zhang, Y., Chen, X., Gueydan, C. & Han, J. Plasma membrane changes during programmed cell deaths. *Cell Res.* **28,** 9–21 (2018).
164. Shiratsuchi, A., Osada, S., Kanazawa, S. & Nakanishi, Y. Essential role of phosphatidylserine externalization in apoptosing cell phagocytosis by macrophages. *Biochem. Biophys. Res. Commun.* **246,** 549–555 (1998).
165. Elmore, S. Apoptosis: A Review of Programmed Cell Death Susan. *Toxicol. Pathol.* **35,** 495–516 (2007).
166. Bhagwandin, V. J., Bishop, J. M., Wright, W. E. & Shay, J. W. The metastatic potential and chemoresistance of human pancreatic cancer stem cells. *PLoS ONE.* **11,** 1–16 (2016).
167. Cappiello, F., Casciaro, B. & Mangoni, M. L. A Novel In Vitro Wound Healing Assay to Evaluate Cell Migration. *J. Vis. Exp.* **133,** 10–15 (2018).
168. Lee, G. A., Hwang, K. A. & Choi, K. C. Roles of dietary phytoestrogens on the regulation of epithelial-mesenchymal transition in diverse cancer metastasis. *Toxins.* **8,** 1–17 (2016).
169. Gavert, N. & Ben-Ze'ev, A. Epithelial-mesenchymal transition and the invasive potential of tumors. *Trends Mol. Med.* **14,** 199–209 (2008).
170. Hugo, H. *et al.* Epithelial-Mesenchymal and Mesenchymal-Epithelial Transition in Carcinoma Progression. *J. Cell. Physiol.* **213,** 374–383 (2007).

7. SUPPORTING INFORMATION

7.1 Rappresentative cell apoptosis spectra

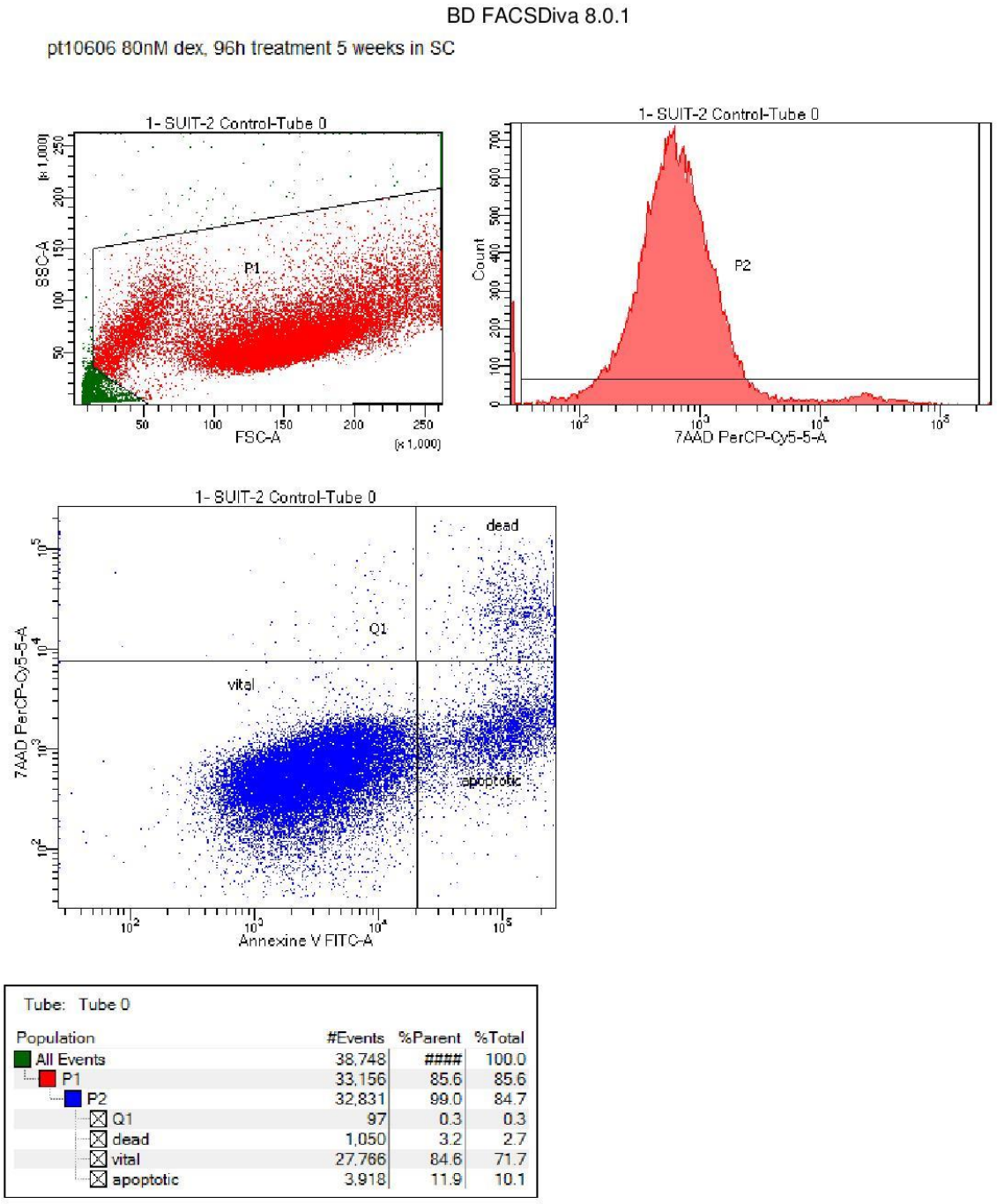

Figure 30. Flow cytometry assessment of apoptosis of SUIT-2 control. P1 events correspond to all the cells monitored by the cytometer during the analysis, while P2 is a sub-category of stained cells, divided in dead cells, vital cells and apoptotic cells. The apoptotic data are expressed as % parent (percentage of parent cells associated with a dye).

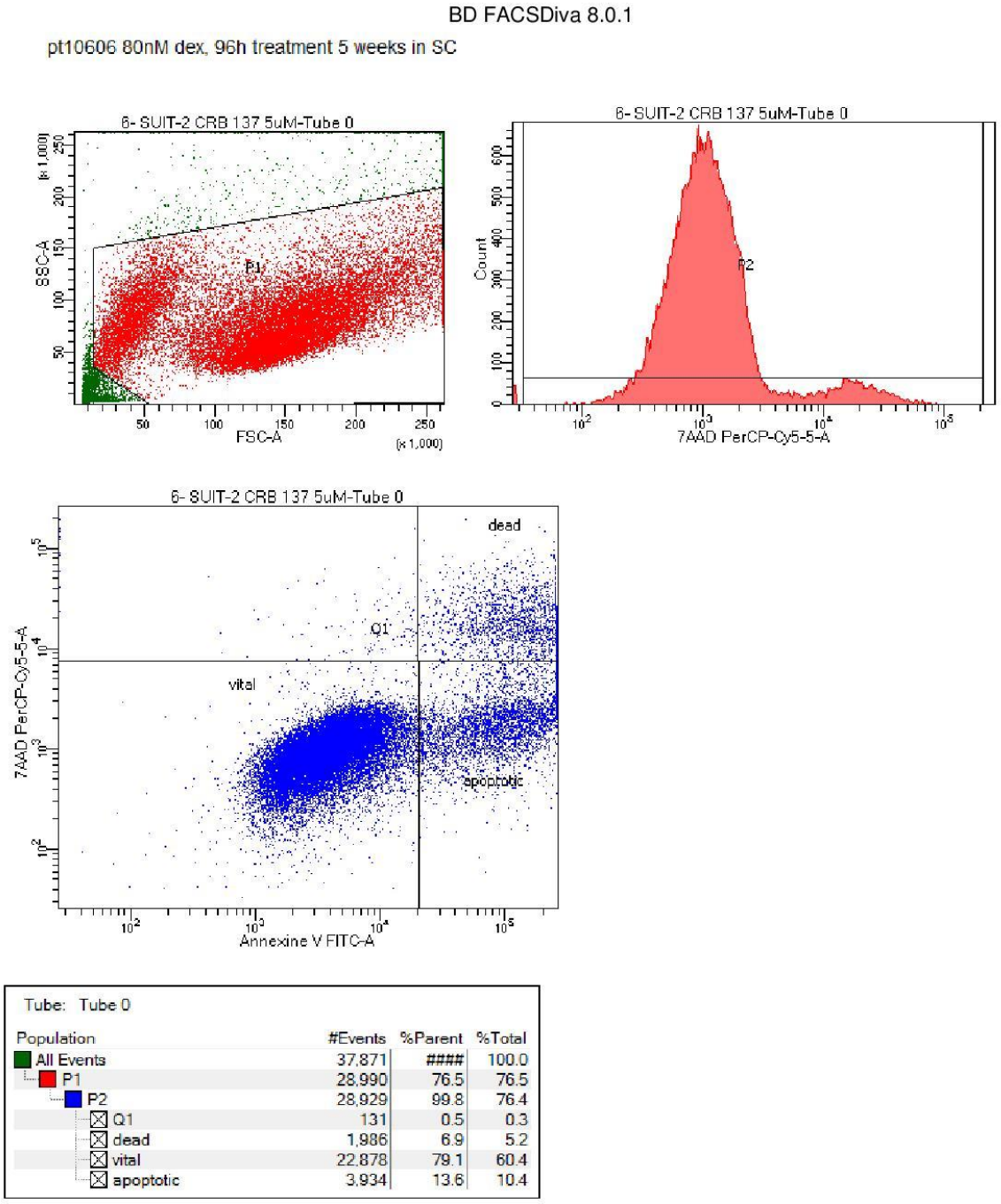

Tube: Tube 0

Population	#Events	%Parent	%Total
All Events	37,871	####	100.0
P1	28,990	76.5	76.5
P2	28,929	99.8	76.4
Q1	131	0.5	0.3
dead	1,986	6.9	5.2
vital	22,878	79.1	60.4
apoptotic	3,934	13.6	10.4

Figure 31. Flow cytometry assessment of apoptosis of SUIT-2 cells after 24h treatment with the compound **180l** at concentration of 5 μM. P1 events correspond to all the cells monitored by the cytometer during the analysis, while P2 is a sub-category of stained cells, divided in dead cells, vital cells and apoptotic cells. The apoptotic data are expressed as % parent (percentage of parent cells associated with a dye).

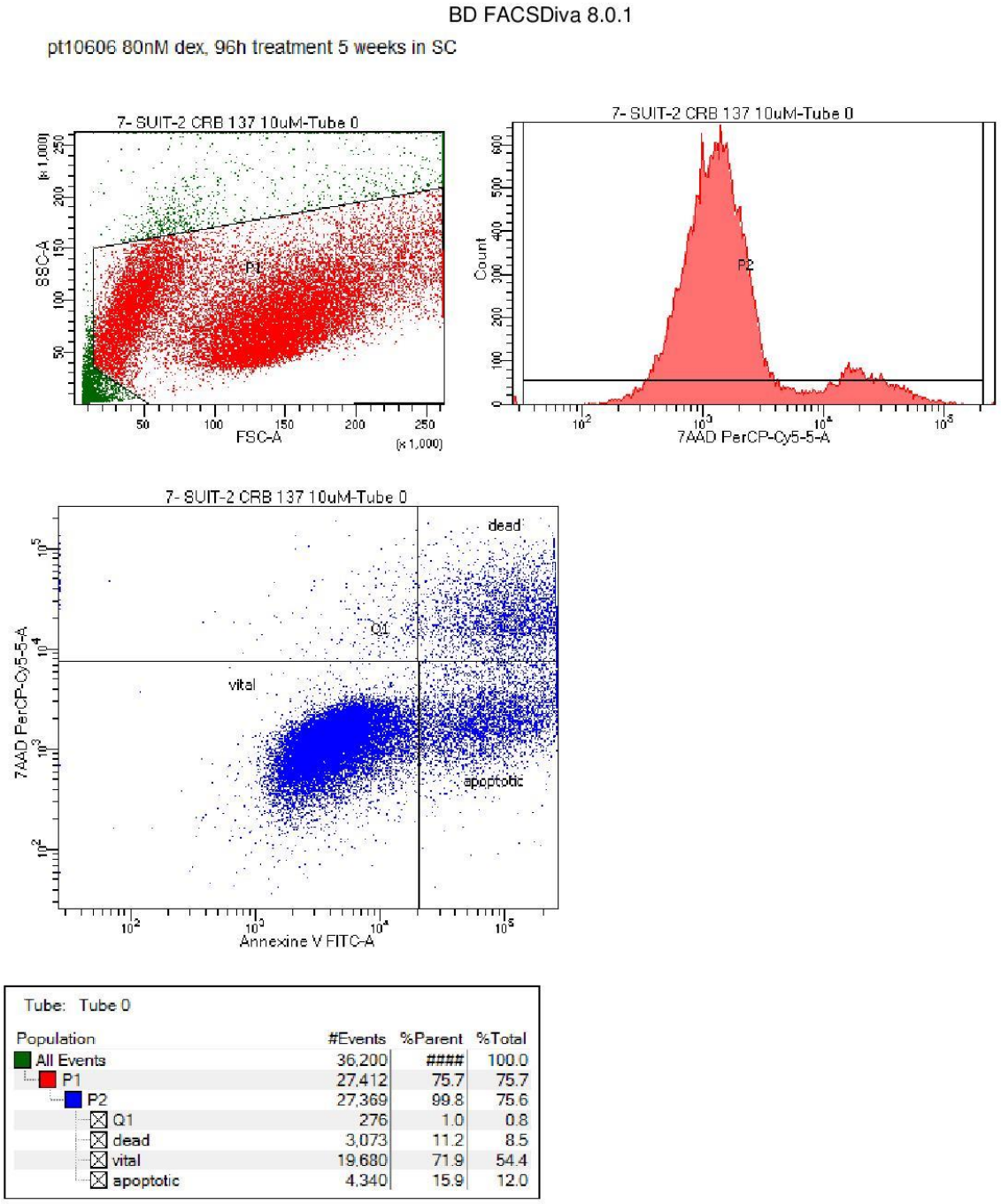

Figure 32. Flow cytometry assessment of apoptosis of SUIT-2 cells after 24h treatment with the compound **180l** at concentration of 10 μM. P1 events correspond to all the cells monitored by the cytometer during the analysis, while P2 is a sub-category of stained cells, divided in dead cells, vital cells and apoptotic cells. The apoptotic data are expressed as % parent (percentage of parent cells associated with a dye).

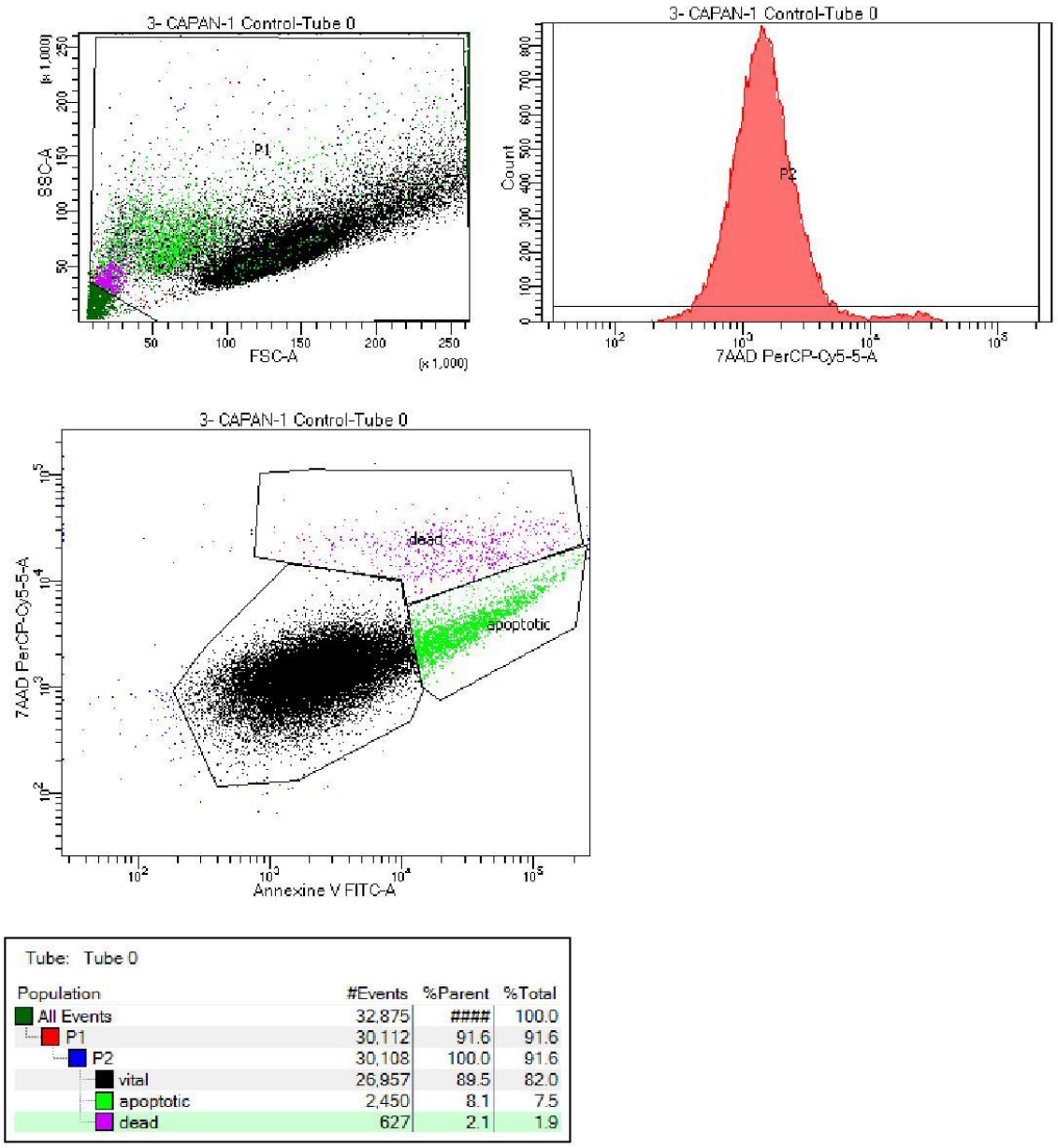

Tube: Tube 0

Population	#Events	%Parent	%Total
All Events	32,875	####	100.0
P1	30,112	91.6	91.6
P2	30,108	100.0	91.6
vital	26,957	89.5	82.0
apoptotic	2,450	8.1	7.5
dead	627	2.1	1.9

Figure 33. Flow cytometry assessment of apoptosis of CAPAN-1 control. P1 events correspond to all the cells monitored by the cytometer during the analysis, while P2 is a sub-category of stained cells, divided in dead cells, vital cells and apoptotic cells. The apoptotic data are expressed as % parent (percentage of parent cells associated with a dye).

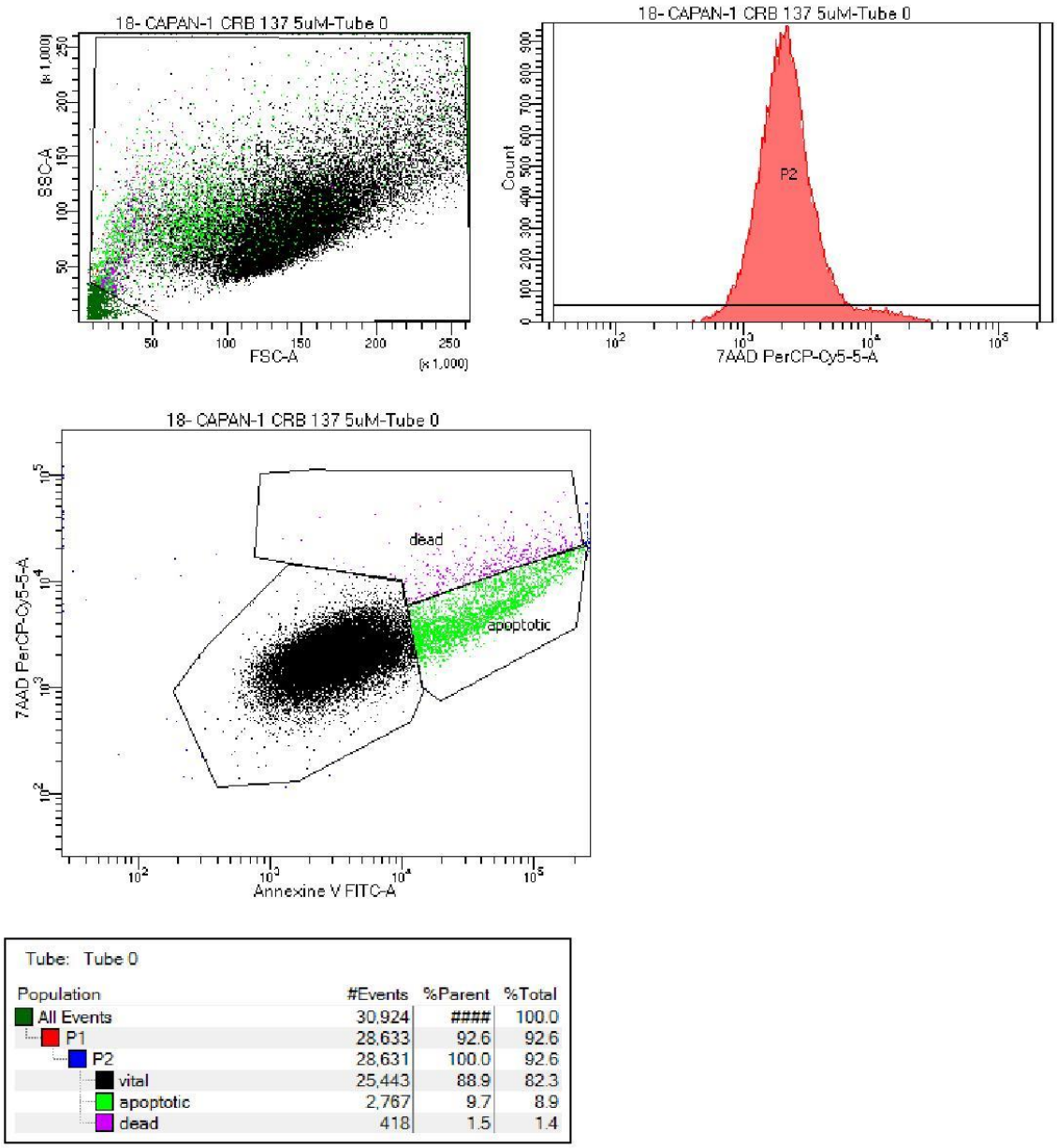

Tube: Tube 0

Population	#Events	%Parent	%Total
All Events	30,924	####	100.0
P1	28,633	92.6	92.6
P2	28,631	100.0	92.6
vital	25,443	88.9	82.3
apoptotic	2,767	9.7	8.9
dead	418	1.5	1.4

Figure 34. Flow cytometry assessment of apoptosis of CAPAN-1 cells after 24h treatment with the compound **180l** at concentration of 5 μM. P1 events correspond to all the cells monitored by the cytometer during the analysis, while P2 is a sub-category of stained cells, divided in dead cells, vital cells and apoptotic cells. The apoptotic data are expressed as % parent (percentage of parent cells associated with a dye).

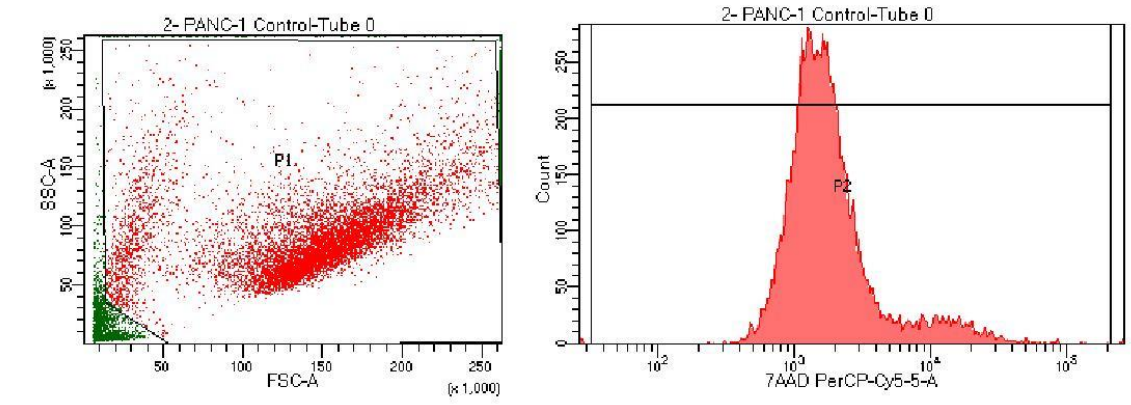

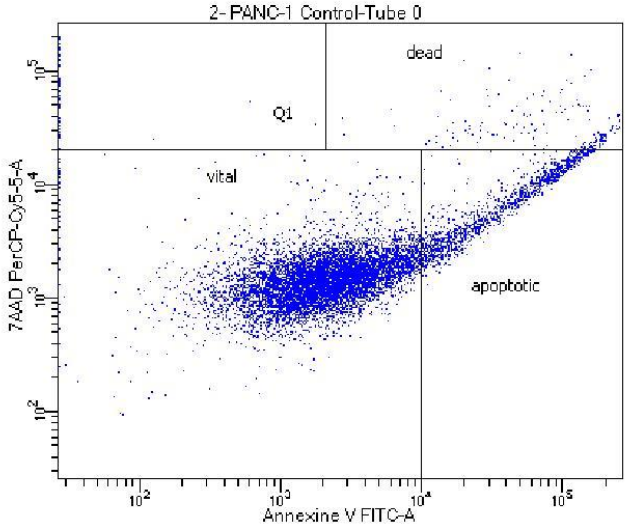

Tube: Tube 0

Population	#Events	%Parent	%Total
All Events	12,316	####	100.0
P1	9,672	78.5	78.5
P2	9,650	99.8	78.4
Q1	55	0.6	0.4
dead	192	2.0	1.6
vital	8,123	84.2	66.0
apoptotic	1,280	13.3	10.4

Figure 35. Flow cytometry assessment of apoptosis of PANC-1 control. P1 events correspond to all the cells monitored by the cytometer during the analysis, while P2 is a sub-category of stained cells, divided in dead cells, vital cells and apoptotic cells. The apoptotic data are expressed as % parent (percentage of parent cells associated with a dye).

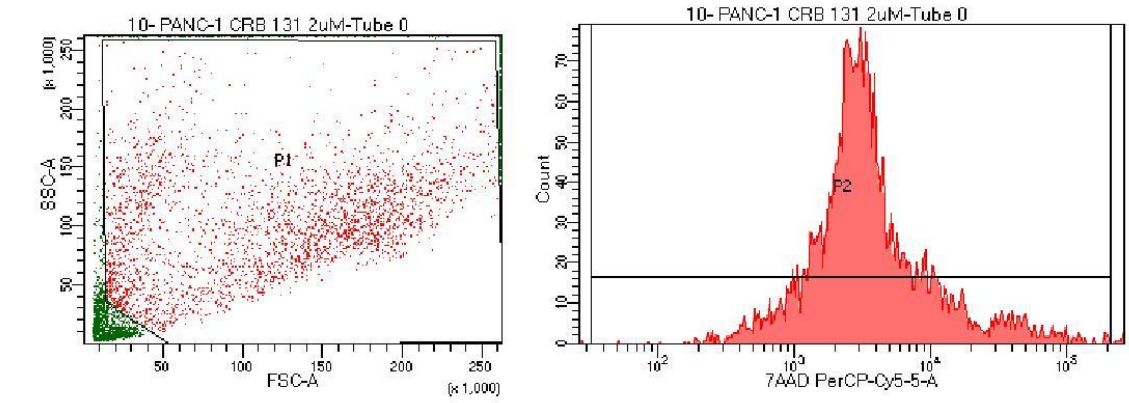

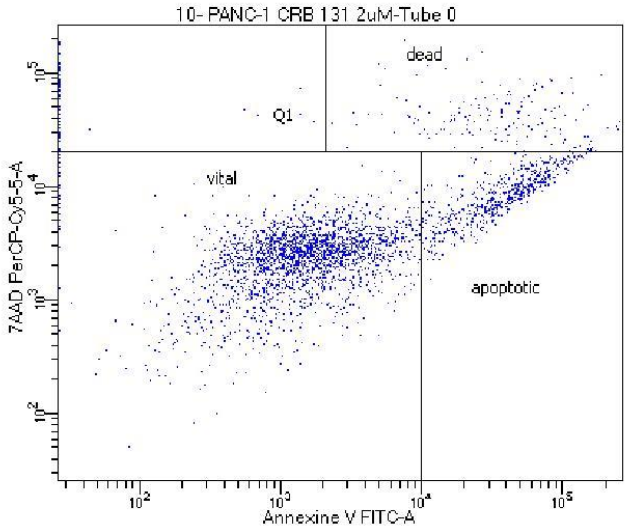

Tube: Tube 0

Population	#Events	%Parent	%Total
All Events	4,890	####	100.0
P1	3,060	62.6	62.6
P2	3,048	99.6	62.3
Q1	56	1.8	1.1
dead	167	5.5	3.4
vital	2,259	74.1	46.2
apoptotic	566	18.6	11.6

Figure 36. Flow cytometry assessment of apoptosis of PANC-1 cells after 24h treatment with the compound **180b** at concentration of 2 μM. P1 events correspond to all the cells monitored by the cytometer during the analysis, while P2 is a sub-category of stained cells, divided in dead cells, vital cells and apoptotic cells. The apoptotic data are expressed as % parent (percentage of parent cells associated with a dye).

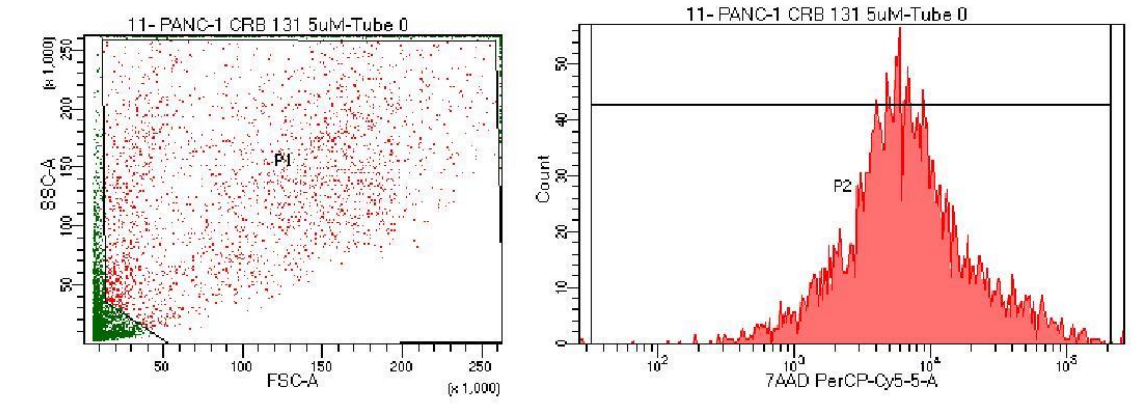

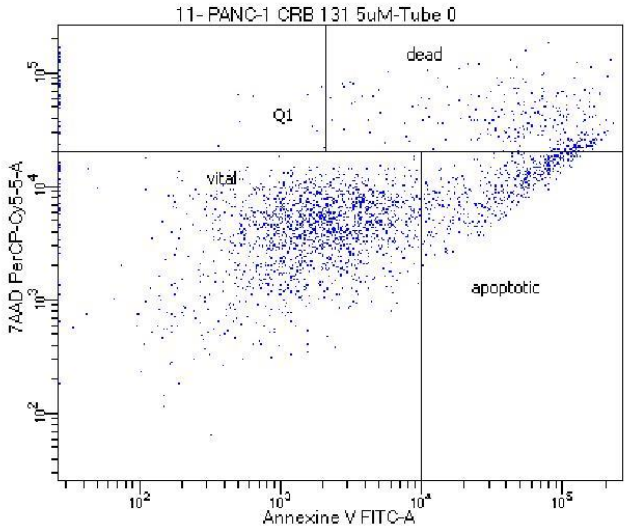

Tube: Tube 0

Population	#Events	%Parent	%Total
All Events	5,583	####	100.0
P1	2,582	46.2	46.2
P2	2,575	99.7	46.1
Q1	43	1.7	0.8
dead	317	12.3	5.7
vital	1,746	67.8	31.3
apoptotic	469	18.2	8.4

Figure 37. Flow cytometry assessment of apoptosis of CAPAN-1 cells after 24h treatment with the compound **180b** at concentration of 5 μM. P1 events correspond to all the cells monitored by the cytometer during the analysis, while P2 is a sub-category of stained cells, divided in dead cells, vital cells and apoptotic cells. The apoptotic data are expressed as % parent (percentage of parent cells associated with a dye).

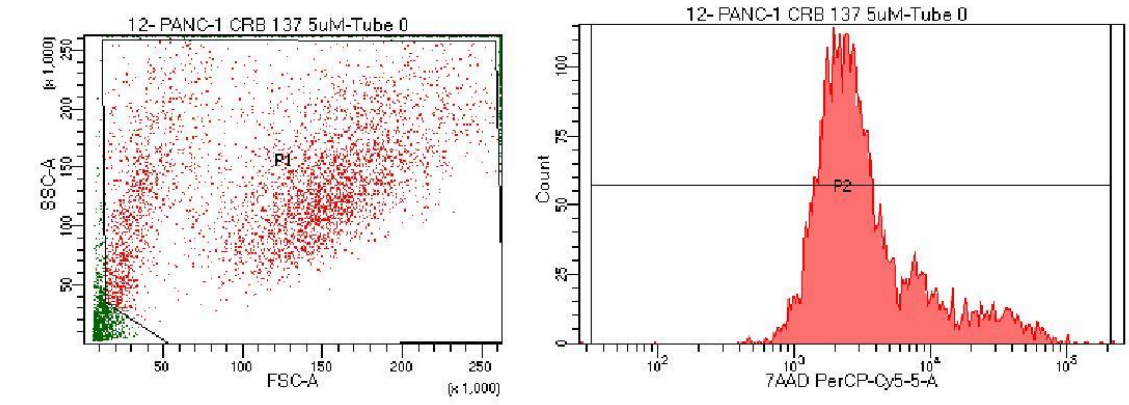

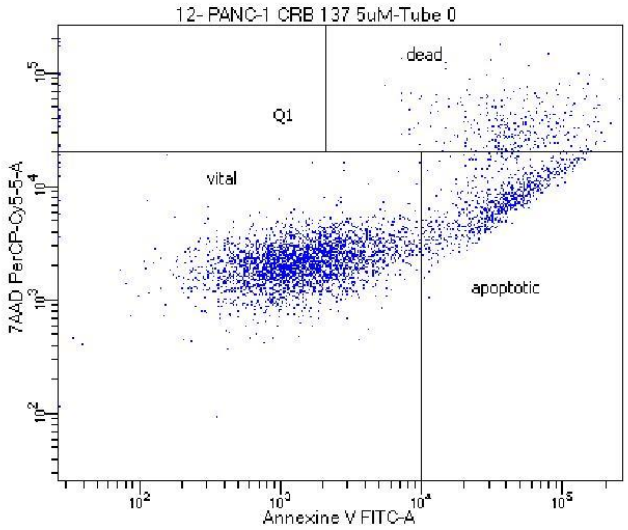

Tube: Tube 0

Population	#Events	%Parent	%Total
All Events	5,944	####	100.0
P1	4,307	72.5	72.5
P2	4,303	99.9	72.4
Q1	19	0.4	0.3
dead	336	7.8	5.7
vital	3,121	72.5	52.5
apoptotic	827	19.2	13.9

Figure 38. Flow cytometry assessment of apoptosis of CAPAN-1 cells after 24h treatment with the compound **180l** at concentration of 5 μM. P1 events correspond to all the cells monitored by the cytometer during the analysis, while P2 is a sub-category of stained cells, divided in dead cells, vital cells and apoptotic cells. The apoptotic data are expressed as % parent (percentage of parent cells associated with a dye).

7.2 Cell cycle spectra

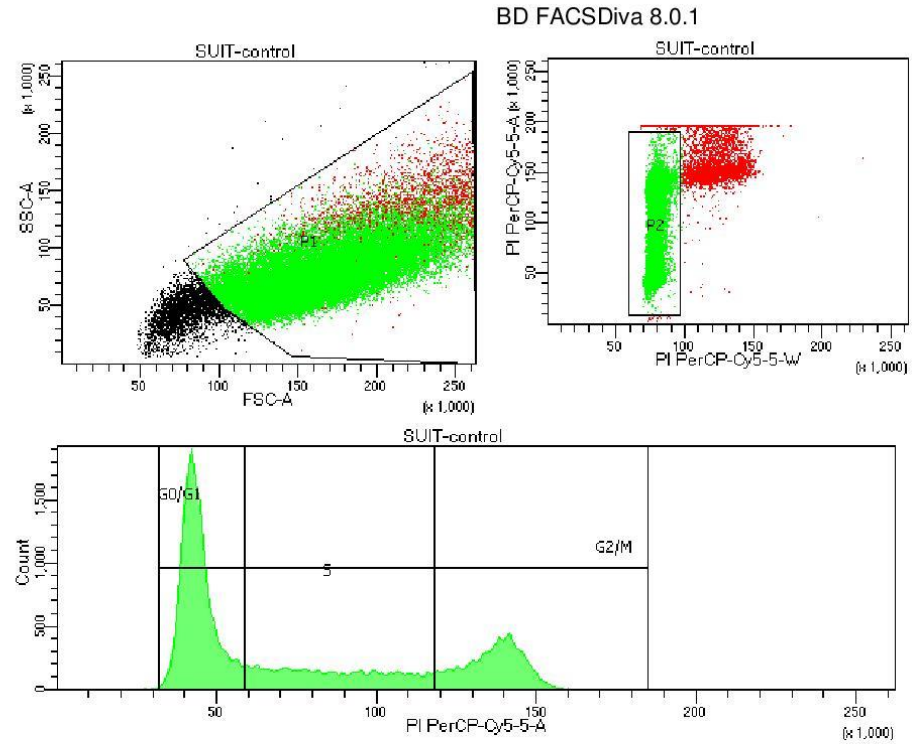

Tube: control

Population	#Events	%Parent	%Total
All Events	51,324	####	100.0
P1	42,306	82.4	82.4
P2	36,246	85.7	70.6
G0/G1	18,331	50.6	35.7
S	8,881	24.5	17.3
G2/M	8,870	24.5	17.3

Experiment Name: Cell cyclus template_001
Specimen Name: SUIT
Tube Name: control
Record Date: Oct 18, 2018 4:38:48 PM

Population	#Events	%Parent	FSC-A Median	SSC-A Median	FITC-A Mean	PI PerCP-Cy5... Mean
P1	42,306	82.4	167,929	78,598	520	90,944
P2	36,246	85.7	160,964	74,136	278	77,118
G0/G1	18,331	50.6	144,418	63,244	-157	43,614
S	8,881	24.5	174,194	80,801	409	86,407
G2/M	8,870	24.5	201,376	97,879	1,049	137,337

Figure 39. Flow cytometry analysis of the cell cycle of SUIT-2 cells. P1 events correspond to all the cells monitored by the cytometer during the analysis, while P2 is a sub-category of stained cells, divided in G0/G1-phase cells, S-phase cells and G2/M-phase cells.

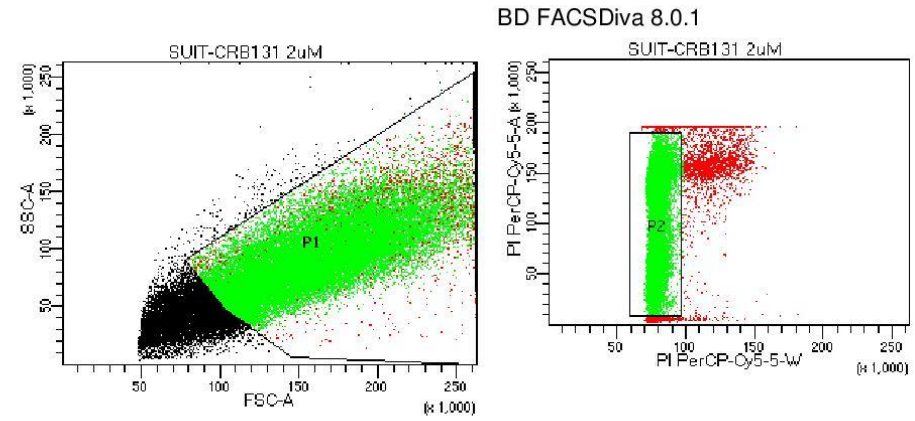

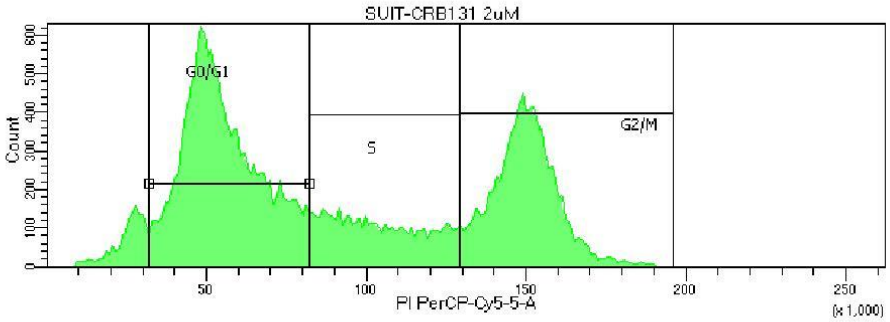

Tube: CRB131 2uM

Population	#Events	%Parent	%Total
All Events	51,914	####	100.0
P1	35,155	67.7	67.7
P2	30,662	87.2	59.1
G0/G1	14,521	47.4	28.0
S	5,214	17.0	10.0
G2/M	9,378	30.6	18.1

Experiment Name: Cell cyclus template_001
Specimen Name: SUIT
Tube Name: CRB131 2uM
Record Date: Oct 18, 2018 4:42:26 PM

Population	#Events	%Parent	FSC-A Median	SSC-A Median	FITC-A Mean	PI PerCP-Cy5... Mean
P1	35,155	67.7	159,560	91,451	671	98,540
P2	30,662	87.2	155,560	88,539	456	90,852
G0/G1	14,521	47.4	137,789	76,050	-11	54,894
S	5,214	17.0	168,967	93,413	622	103,767
G2/M	9,378	30.6	193,273	116,595	1,189	150,178

Figure 40. Flow cytometry analysis of the cell cycle of SUIT-2 cells after treatment with the compound **180b** at concentration of 2 μM. P1 events correspond to all the cells monitored by the cytometer during the analysis, while P2 is a sub-category of stained cells, divided in G0/G1-phase cells, S-phase cells and G2/M-phase cells.

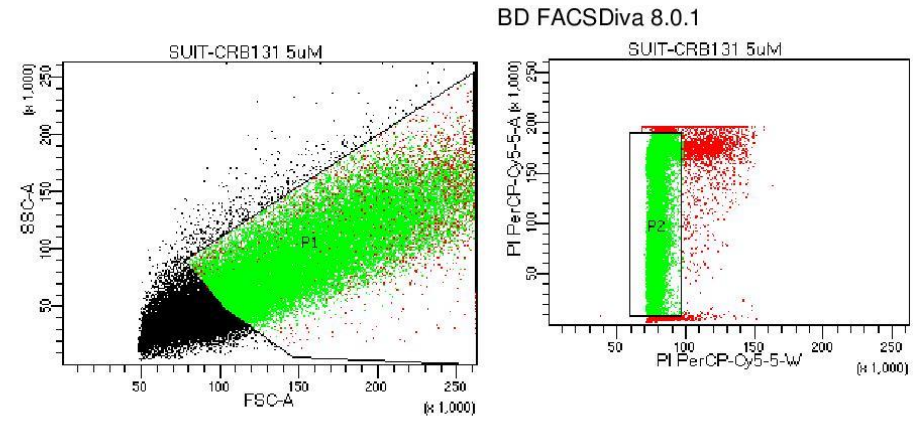

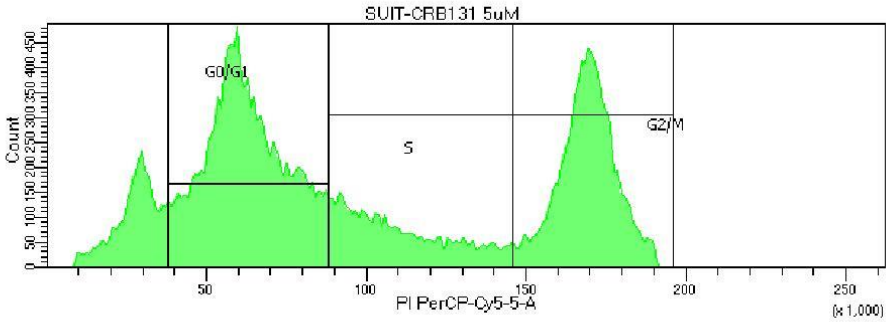

Tube: CRB131 5uM

Population	#Events	%Parent	%Total
All Events	50,912	####	100.0
P1	32,878	64.6	64.6
P2	27,452	83.5	53.9
G0/G1	11,964	43.6	23.5
S	4,256	15.5	8.4
G2/M	8,205	29.9	16.1

Experiment Name: Cell cyclus template_001
Specimen Name: SUIT
Tube Name: CRB131 5uM
Record Date: Oct 18, 2018 4:45:34 PM

Population	#Events	%Parent	FSC-A Median	SSC-A Median	FITC-A Mean	PI PerCP-Cy5... Mean
P1	32,878	64.6	153,583	93,247	898	105,970
P2	27,452	83.5	148,315	89,197	662	97,713
G0/G1	11,964	43.6	134,809	77,445	188	62,217
S	4,256	15.5	157,392	92,695	792	110,502
G2/M	8,205	29.9	195,000	125,521	1,546	168,912

Figure 41. Flow cytometry analysis of the cell cycle of SUIT-2 cells after treatment with the compound **180b** at concentration of 5 μM. P1 events correspond to all the cells monitored by the cytometer during the analysis, while P2 is a sub-category of stained cells, divided in G0/G1-phase cells, S-phase cells and G2/M-phase cells.

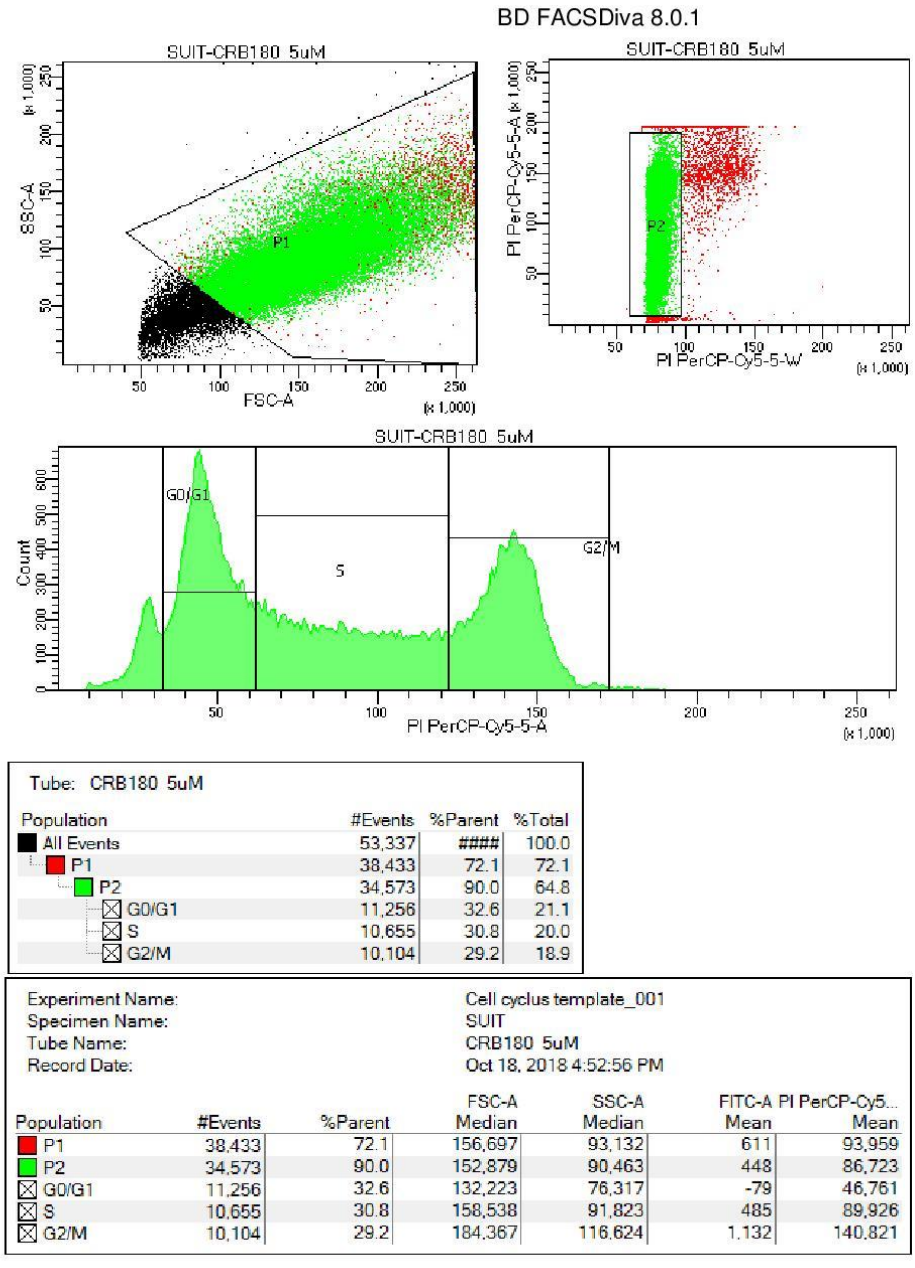

Tube: CRB180 5uM

Population	#Events	%Parent	%Total
All Events	53,337	####	100.0
P1	38,433	72.1	72.1
P2	34,573	90.0	64.8
G0/G1	11,256	32.6	21.1
S	10,655	30.8	20.0
G2/M	10,104	29.2	18.9

Experiment Name: Cell cyclus template_001
Specimen Name: SUIT
Tube Name: CRB180 5uM
Record Date: Oct 18, 2018 4:52:56 PM

Population	#Events	%Parent	FSC-A Median	SSC-A Median	FITC-A Mean	PI PerCP-Cy5... Mean
P1	38,433	72.1	156,697	93,132	611	93,959
P2	34,573	90.0	152,879	90,463	448	86,723
G0/G1	11,256	32.6	132,223	76,317	-79	46,761
S	10,655	30.8	158,538	91,823	485	89,926
G2/M	10,104	29.2	184,367	116,624	1,132	140,821

Figure 42. Flow cytometry analysis of the cell cycle of SUIT-2 cells after treatment with the compound **180c** at concentration of 5 μM. P1 events correspond to all the cells monitored by the cytometer during the analysis, while P2 is a sub-category of stained cells, divided in G0/G1-phase cells, S-phase cells and G2/M-phase cells.

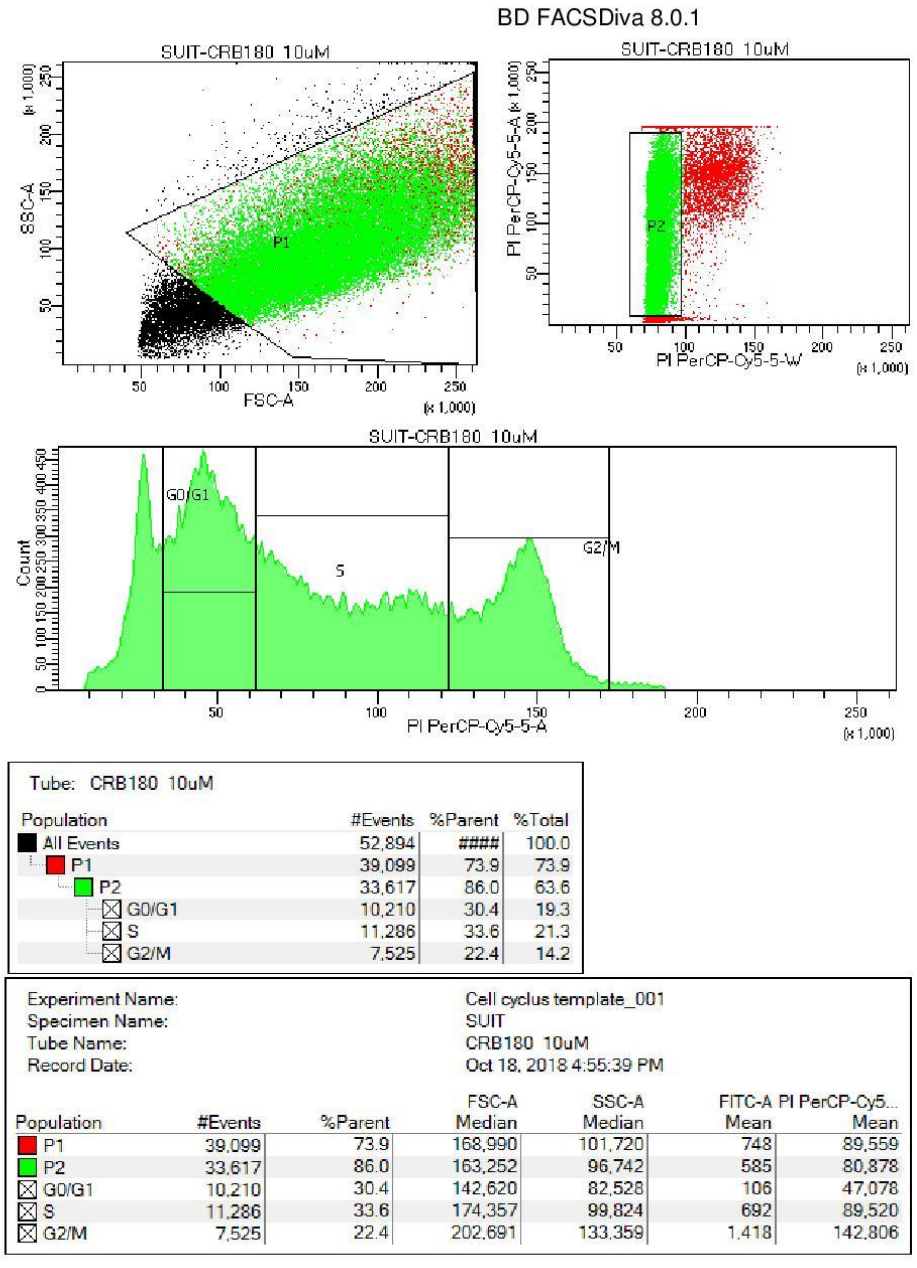

Figure 43. Flow cytometry analysis of the cell cycle of SUIT-2 cells after treatment with the compound **180c** at concentration of 10 μM. P1 events correspond to all the cells monitored by the cytometer during the analysis, while P2 is a sub-category of stained cells, divided in G0/G1-phase cells, S-phase cells and G2/M-phase cells.

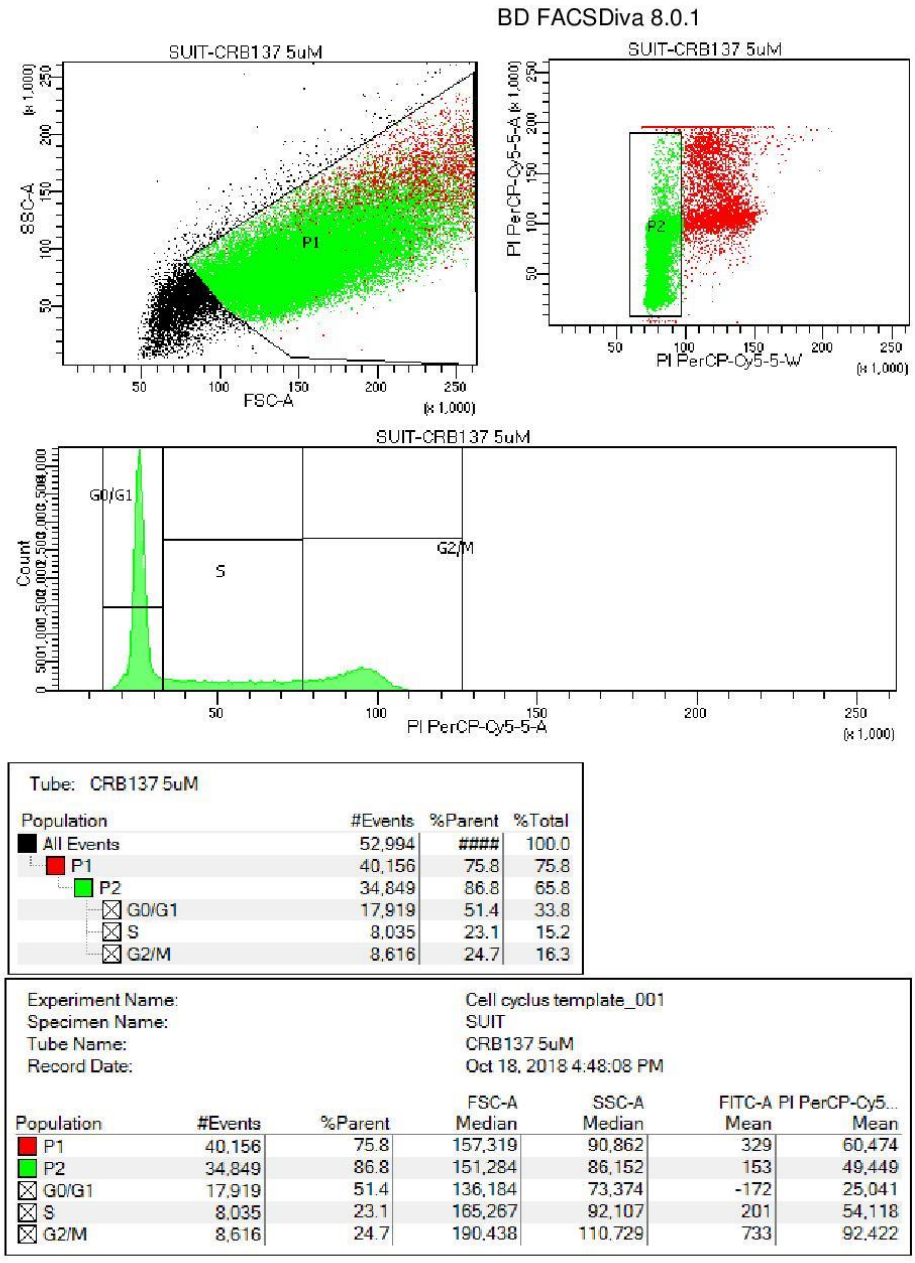

Figure 44. Flow cytometry analysis of the cell cycle of SUIT-2 cells after treatment with the compound **180l** at concentration of 5 μM. P1 events correspond to all the cells monitored by the cytometer during the analysis, while P2 is a sub-category of stained cells, divided in G0/G1-phase cells, S-phase cells and G2/M-phase cells.

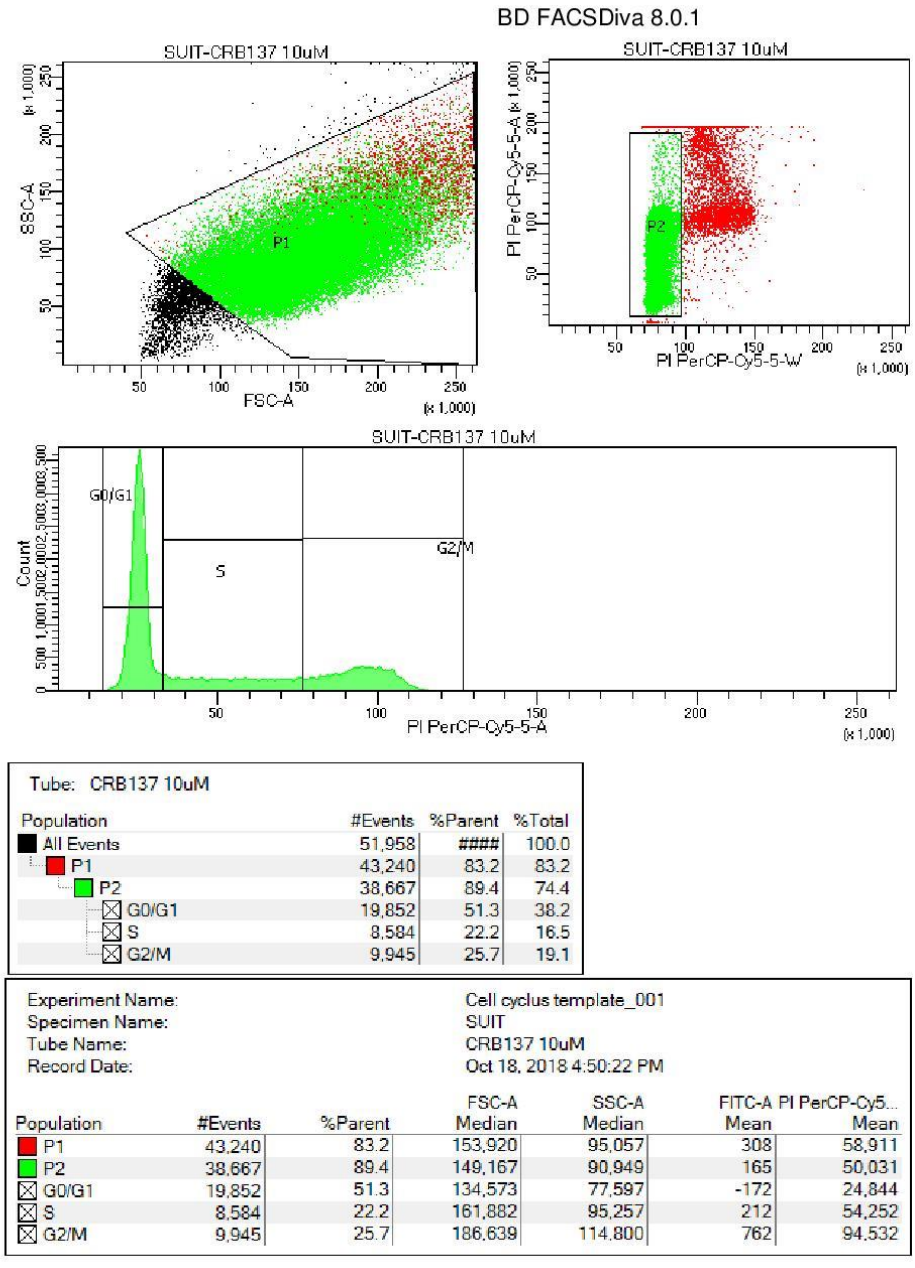

Tube: CRB137 10uM

Population	#Events	%Parent	%Total
All Events	51,958	####	100.0
P1	43,240	83.2	83.2
P2	38,667	89.4	74.4
G0/G1	19,852	51.3	38.2
S	8,584	22.2	16.5
G2/M	9,945	25.7	19.1

Experiment Name: Cell cyclus template_001
Specimen Name: SUIT
Tube Name: CRB137 10uM
Record Date: Oct 18, 2018 4:50:22 PM

Population	#Events	%Parent	FSC-A Median	SSC-A Median	FITC-A Mean	PI PerCP-Cy5... Mean
P1	43,240	83.2	153,920	95,057	308	58,911
P2	38,667	89.4	149,167	90,949	165	50,031
G0/G1	19,852	51.3	134,573	77,597	-172	24,844
S	8,584	22.2	161,882	95,257	212	54,252
G2/M	9,945	25.7	186,639	114,800	762	94,532

Figure 45. Flow cytometry analysis of the cell cycle of SUIT-2 cells after treatment with the compound **180l** at concentration of 10 μM. P1 events correspond to all the cells monitored by the cytometer during the analysis, while P2 is a sub-category of stained cells, divided in G0/G1-phase cells, S-phase cells and G2/M-phase cells.